# THE ROLE OF LIGHT IN ABIOTIC STRESS ACCLIMATION

EDITED BY: Tibor Janda, Éva Hideg and Radomira Vankova

PUBLISHED IN: Frontiers in Plant Science

frontiers Research Topics

# frontiers



ISSN 1664-8714
ISBN 978-2-88963-628-0
DOI 10.3389/978-2-88963-628-0

## About Frontiers

Frontiers is more than just an open-access publisher of scholarly articles: it is a pioneering approach to the world of academia, radically improving the way scholarly research is managed. The grand vision of Frontiers is a world where all people have an equal opportunity to seek, share and generate knowledge. Frontiers provides immediate and permanent online open access to all its publications, but this alone is not enough to realize our grand goals.

## Frontiers Journal Series

The Frontiers Journal Series is a multi-tier and interdisciplinary set of open-access, online journals, promising a paradigm shift from the current review, selection and dissemination processes in academic publishing. All Frontiers journals are driven by researchers for researchers; therefore, they constitute a service to the scholarly community. At the same time, the Frontiers Journal Series operates on a revolutionary invention, the tiered publishing system, initially addressing specific communities of scholars, and gradually climbing up to broader public understanding, thus serving the interests of the lay society, too.

## Dedication to Quality

Each Frontiers article is a landmark of the highest quality, thanks to genuinely collaborative interactions between authors and review editors, who include some of the world's best academicians. Research must be certified by peers before entering a stream of knowledge that may eventually reach the public - and shape society; therefore, Frontiers only applies the most rigorous and unbiased reviews.
Frontiers revolutionizes research publishing by freely delivering the most outstanding research, evaluated with no bias from both the academic and social point of view. By applying the most advanced information technologies, Frontiers is catapulting scholarly publishing into a new generation.

## What are Frontiers Research Topics?

Frontiers Research Topics are very popular trademarks of the Frontiers Journals Series: they are collections of at least ten articles, all centered on a particular subject. With their unique mix of varied contributions from Original Research to Review Articles, Frontiers Research Topics unify the most influential researchers, the latest key findings and historical advances in a hot research area! Find out more on how to host your own Frontiers Research Topic or contribute to one as an author by contacting the Frontiers Editorial Office: researchtopics@frontiersin.org

# THE ROLE OF LIGHT IN ABIOTIC STRESS ACCLIMATION

Topic Editors:
**Tibor Janda,** Centre for Agricultural Research, Hungary
**Éva Hideg,** University of Pécs, Hungary
**Radomira Vankova,** Institute of Experimental Botany of the Czech Academy of Sciences, Czechia

**Citation:** Janda, T., Hideg, É., Vankova, R., eds. (2020). The Role of Light in Abiotic Stress Acclimation. Lausanne: Frontiers Media SA. doi: 10.3389/978-2-88963-628-0

# Table of Contents

frontiers in Plant Science

EDITORIAL
published: 25 February 2020
doi: 10.3389/fpls.2020.00184

# Editorial: The Role of Light in Abiotic Stress Acclimation

*Tibor Janda*[1]*, *Éva Hideg*[2] *and Radomíra Vanková*[3]

[1] Agricultural Institute, Centre for Agricultural Research, Martonvásár, Hungary, [2] Department of Plant Biology, University of Pécs, Pécs, Hungary, [3] Institute of Experimental Botany, Academy of Sciences of the Czech Republic, Prague, Czechia

**Keywords: abiotic stress, carbon balance, crosstalk, drought, light, osmotic stress, photoinhibition, temperature**

**Editorial on the Research Topic**

**The Role of Light in Abiotic Stress Acclimation**

Understanding of mechanisms by which plants perceive environmental signals, transmit them to cellular machinery and activate adaptive responses is of fundamental importance from both theoretical and practical points of view. Mutual interactions among environmental factors are inevitable, and light conditions substantially alter the way plants acclimate to changes in other environmental factors. This Research Topic collected eight articles including one minireview and seven original research papers, which demonstrated that the influence of light on achieving high level of stress tolerance could be as important as the genetic background.

Light as a single stress factor may induce photoinhibition. However, over-excitation of Photosystem II has been shown to induce freezing tolerance in cereals. Results of Szalai et al. suggest that light is essential also for the cold acclimation of chilling sensitive maize plants, and thus photoinhibition can be a necessary evil for the initiation of cold tolerance in plants. The avoidance of the damaging effects of high light intensities is definitely required to protect the photosynthetic apparatus. However, for the protection of the whole plant from a subsequent cold shock, it may be necessary to accept the consequences of light-induced stress-related processes to acquire cold-acclimated plants. Microarray based gene expression study demonstrated the existence of complex regulatory mechanisms and interactions between cold and light signaling processes. Differentially expressed genes were mainly involved, among others, in pathways related to chlorophyll biosynthesis, carboxylic acid metabolism, amino acid, porphyrin or glutathione metabolic processes, ribosome biogenesis and translation (Szalai et al.).

Another example of a positive light effect was reported by Lima-Melo et al. who showed that photoinhibition of photosystem I might protect chloroplasts from oxidative damage in Arabidopsis. Light, on the other hand, is capable of exacerbating low temperature stress. Pérez-Llorca et al. demonstrated that changes in leaf angle acted as the first line of light protection in the Mediterranean semi-deciduous shrub *Cistus albidus* during the winter. Furthermore, these plants enhanced accumulation of α-tocopherol, as a stress sensing and signaling mechanism, to counteract combined high light and low temperature stress when modification of the leaf angle was not sufficient defense. Another interesting example of morphological adaptation was described by Shelef et al. who showed that sub-epidermal air spaces in *Silybum marianum* leaves contribute to elevation of leaf temperature; while white leaf patches provide a microenvironment promoting photosynthesis in cold winter morning periods.

Recent results also suggest that not only light intensity but also its quality is important in the regulation of the acclimation processes. The possible involvement of cryptochromes has been

OPEN ACCESS

***Edited and reviewed by:***
*Rosa M. Rivero,*
*Spanish National Research Council, Spain*

***Correspondence:**
*Tibor Janda*
*janda.tibor@agrar.mta.hu*

***Specialty section:***
*This article was submitted to Plant Abiotic Stress, a section of the journal Frontiers in Plant Science*

***Received:*** *26 January 2020*
***Accepted:*** *07 February 2020*
***Published:*** *25 February 2020*

***Citation:***
*Janda T, Hideg É and Vanková R (2020) Editorial: The Role of Light in Abiotic Stress Acclimation. Front. Plant Sci. 11:184. doi: 10.3389/fpls.2020.00184*

reviewed by D'Amico-Damião and Carvalho. Cryptochromes absorb blue and UV-A light, and evoke a wide range of plant stress responses *via* the regulation of several transcription factors, including HY5 (ELONGATED HYPOCOTYL 5) and PIF4 (PHYTOCHROME INTERACTING FACTOR 4). Cryptochrome mediated stress response genes play key roles in signaling pathways, biosynthesis of plant hormones, regulation of reactive oxygen species, or other stress-related components. However, the exact mode of action of cryptochromes or other photoreceptors is still not fully understood. The interactions between the light-related processes and the acclimation mechanisms to osmotic stressors, such as drought and/or high salinity is also very important from both theoretical and practical points of view. Proline is one of the HY5 inducible protective metabolites responding to several factors, especially to osmotic stress. Kovács et al. demonstrated that light-regulated HY5 activates the *P5CS1* (Δ1-PYRROLINE-5-CARBOXYLATE SYNTHASE 1) gene responsible for proline synthesis, suggesting that HY5 promotes proline biosynthesis through connecting light and stress signals. These authors also showed that the activation of the photosynthetic electron transport also promotes proline accumulation in a yet unknown way.

Study of algae or other lower plants may also reveal important mechanisms, which could be utilized for the improvement of stress tolerance of crop plants. Diatoms, a major group of microalgae, are able to adapt to a broad range of environmental conditions. Reorientation of carbon metabolism may occur under unfavorably changing environment, for example at nutrient deficiency. Heydarizadeh et al. showed that even in conditions of carbon deprivation, diatoms may shift their metabolism toward the production of lipids. Light intensity may also affect the carbon flow among different metabolic pathways. Under low light conditions, accumulation of the storage polysaccharide, chrysolaminarin could be observed. Medium light intensity stimulated predominantly lipid synthesis, while high light resulted in an increase in the amount of proteins (Heydarizadeh et al.).

The effects of different light spectra on the photosynthetic parameters, or the UV light induction of certain ROS-scavenging agents have been widely studied. However, the effect of light quality or light intensity on the changes in the root development is much less known and understood. In a complex physiological study, Klem et al. demonstrated the role of light quality in inducing changes in root and leaf morphology, physiology, and metabolite profile. Interestingly, light quality also affected root length: longer roots could be induced when red light was supplemented with far-red radiation (Klem et al.). Root length can be one of the most critical parameters in adaptation processes, especially to drought conditions. Therefore the investigation of the light-dependent responses of root physiology under stress conditions can be interesting and economically important aim of further studies. The effect of light intensity during the cold acclimation period on certain stress-related processes in the roots have also been demonstrated in young maize plants (Szalai et al.).

In conclusion, there is increasing evidence that light is an important regulator of stress acclimation processes. There are still several open questions concerning molecular mechanisms of the light-regulated signaling processes; and further research is required to address the complex nature of the stress signaling networks, as the direct link between the light perception and the development of stress tolerance is still missing.

## AUTHOR CONTRIBUTIONS

All authors listed, have made substantial, direct, and intellectual contribution to the work, and approved it for publication.

## ACKNOWLEDGMENTS

TJ is supported by a grant from National Research, Development and Innovation Office (grant No. K124430), ÉH is supported by a grant from National Research, Development and Innovation Office (grant No. K124165), and RV is supported by MEYS CR program Inter-Excellence (grant No. LTAUSA17081). We thank all contributors to this Research Topic.

**Conflict of Interest:** The authors declare that the research was conducted in the absence of any commercial or financial relationships that could be construed as a potential conflict of interest.

frontiers in Plant Science

ORIGINAL RESEARCH
published: 19 June 2018
doi: 10.3389/fpls.2018.00850

# Janus-Faced Nature of Light in the Cold Acclimation Processes of Maize

*Gabriella Szalai[1]*, Imre Majláth[1], Magda Pál[1], Orsoly K. Gondor[1], Szabolcs Rudnóy[2], Csilla Oláh[2], Radomíra Vanková[3], Balázs Kalapos[1] and Tibor Janda[1]*

[1] Centre for Agricultural Research, Plant Physiology Department, Agricultural Institute, MTA, Martonvásár, Hungary, [2] Department of Plant Physiology and Plant Molecular Biology, Eötvös Loránd University, Budapest, Hungary, [3] Laboratory of Hormonal Regulations in Plants, Institute of Experimental Botany, Czech Academy of Sciences, Prague, Czechia

Exposure of plants to low temperature in the light may induce photoinhibitory stress symptoms, including oxidative damage. However, it is also known that light is a critical factor for the development of frost hardiness in cold tolerant plants. In the present work the effects of light during the cold acclimation period were studied in chilling-sensitive maize plants. Before exposure to chilling temperature at 5°C, plants were cold acclimated at non-lethal temperature (15°C) under different light conditions. Although exposure to relatively high light intensities during cold acclimation caused various stress symptoms, it also enhanced the effectiveness of acclimation processes to a subsequent severe cold stress. It seems that the photoinhibition induced by low temperature is a necessary evil for cold acclimation processes in plants. Greater accumulations of soluble sugars were also detected during hardening at relatively high light intensity. Certain stress responses were light-dependent not only in the leaves, but also in the roots. The comparison of the gene expression profiles based on a microarray study demonstrated that the light intensity is at least as important a factor as the temperature during the cold acclimation period. Differentially expressed genes were mainly involved in most of assimilation and metabolic pathways, namely photosynthetic light capture via the modification of chlorophyll biosynthesis and the dark reactions, carboxylic acid metabolism, cellular amino acid, porphyrin or glutathione metabolic processes, ribosome biogenesis and translation. Results revealed complex regulation mechanisms and interactions between cold and light signalling processes.

**Keywords: abiotic stress, acclimation, chilling, gene expression, low temperature, photoinhibition, soluble sugars, *Zea mays* L**

OPEN ACCESS

***Edited by:***
*Eric Ruelland, Centre National de la Recherche Scientifique (CNRS), France*

***Reviewed by:***
*Tomas Takac, Palacký University, Czechia*
*Ning Li, Hong Kong University of Science and Technology, Hong Kong*
*Raquel Esteban, University of the Basque Country (UPV/EHU), Spain*

****Correspondence:***
*Gabriella Szalai*
*szalai.gabriella@agrar.mta.hu*

***Specialty section:***
*This article was submitted to Plant Abiotic Stress, a section of the journal Frontiers in Plant Science*

***Received:*** *22 March 2018*
***Accepted:*** *31 May 2018*
***Published:*** *19 June 2018*

***Citation:***
*Szalai G, Majláth I, Pál M, Gondor OK, Rudnóy S, Oláh C, Vanková R, Kalapos B and Janda T (2018) Janus-Faced Nature of Light in the Cold Acclimation Processes of Maize. Front. Plant Sci. 9:850. doi: 10.3389/fpls.2018.00850*

## INTRODUCTION

Low temperature is one of the most important factors limiting the spread and production of plants worldwide. This is especially true for field crops of tropical or subtropical origin. In the case of chilling-sensitive maize plants, temperatures in the 10–15°C range decrease the capacity for biomass production, while the exposure of plants to still lower temperatures for a prolonged period may lead to irreversible damage and the death of the plants (Bredenkamp and Baker, 1994; Greaves, 1996). Efficient early germination and growth at cool temperatures in the spring is a critical part of resistance to low temperature stress in young maize plants. One of the main aims of breeders is to develop cold-tolerant genotypes, which can be sown either earlier in order to extend the vegetation period, or in cooler geographical zones. Although chilling-sensitive plants are generally

considered to lack the ability to develop chilling resistance when exposed to low but non-injurious temperatures, they can also be able to adapt to lower, usually non-freezing temperatures to some extent (Anderson et al., 1994; Prasad, 1996; Janda et al., 1998).

The mechanisms of cold acclimation are mainly studied in overwintering cereals, where a certain period of low, non-freezing temperature is necessary to achieve the maximum level of freezing tolerance even in the case of frost-tolerant winter varieties. This process is generally called frost hardening or cold hardening. Cold hardening is the result of various physical and biochemical processes, including the adjustment of membrane composition and the accumulation of certain protective substances, among them stabilising compounds such as polyamines, osmoprotectants or antioxidants (Winfield et al., 2010; Boldizsár et al., 2016a,b). The synthesis of these compounds and the regulation of acclimation mechanisms are mediated by a complex signal transduction network (Van Buskirk and Thomashow, 2006). However, it has long been known that light is necessary for the development of freezing tolerance as well as low temperature. Without enough light during the cold hardening period even winter cereals with a potentially high level of frost hardiness are incapable of achieving freezing tolerance (Gray et al., 1997; Apostol et al., 2006). Light has been shown to mediate the development of freezing tolerance via several biological processes. These include photosynthesis-related processes, the expression level of stress-related genes and the synthesis of various protective compounds (Janda et al., 2014).

A strong overlap has been shown between factors involved in sensing and transducing light and temperature in plants (Legris et al., 2016, 2017). Acclimation to low temperatures also respond to light and temperature signals (Catalá et al., 2011; Lee and Thomashow, 2012). In hardy plants light is a critical factor during the low temperature hardening period, but in chilling-sensitive plants light often shows another face during exposure to low temperature inducing photoinhibition, which contributes to the development of chilling symptoms in these plants (Gururani et al., 2015). Photoinhibition is a light-induced decline in photochemical activity and occurs when the light energy available exceeds the receptive capacity of the photosynthetic processes and the level that can be neutralised via different protective mechanisms (recently reviewed by Pospíšil, 2016). The mechanisms underlying the development of freezing tolerance during the hardening period of model plants, such as Arabidopsis, or cold-tolerant cereal species, such as wheat or oat, have been widely studied, but these results cannot be generalised for the very chilling-sensitive C4 plants. In recent years several cold-responsive genes have been identified in maize, but these studies were usually focused either on the comparison of genotypes with different levels of chilling tolerance (Sobkowiak et al., 2014, 2016; Li et al., 2016) or on the different phases of cold stress responses (Trzcinska-Danielewicz et al., 2009), and the role of light has not been discussed.

In the present work we hypothesised that light, in spite of its photoinhibitory effects, may also have a similar role in the cold acclimation processes in chilling sensitive plants, similarly as it was found in cold tolerant winter cereals or in *Arabidopsis*. Experiments were designed in order to characterise the contribution of light during the cold acclimation period to the development of a certain level of cold tolerance in maize plants. A detailed microarray study was also carried out, and certain physiological, biochemical and genetic factors contributing to cold tolerance were tested. Results may point out the possible involvement of low temperature-induced photoinhibition in the development of cold tolerance as a signal during the cold acclimation period in chilling sensitive plants.

**Abbreviations:** FC, fold change; GL1, growth light 1 (180 μmol $m^{-2}$ $s^{-1}$); GL2, growth light 2 (387 μmol $m^{-2}$ $s^{-1}$); LL1, low light intensity 1 (46 μmol $m^{-2}$ $s^{-1}$); LL2, low light intensity 2 (14 μmol $m^{-2}$ $s^{-1}$); LL3, low light intensity 3 (283 μmol $m^{-2}$ $s^{-1}$); LL4, low light intensity 4 (107 μmol $m^{-2}$ $s^{-1}$); MDA, malondialdehyde; Y(II), quantum yield of Photosystem 2; Y(NO), non-regulated non-photochemical quenching; Y(NPQ), regulated non-photochemical quenching.

# MATERIALS AND METHODS

## Plant Material and Growth Conditions

In the 1st set of experiments seeds of maize plants (*Zea mays* L. hybrid Norma) were germinated between wet filterpapers for 3 days then grown in a modified Hoagland solution (Pál et al., 2005) for a week at 22/20°C at a photosynthetic photon flux density (PPFD) of 180 μmol $m^{-2}$ $s^{-1}$ (growth light 1; GL1) with 16/8 h light/dark periodicity (control plants). The plants were then hardened at 15/13°C for 3 days under three different light conditions: GL1; low light intensity 1 (LL1): 46 μmol $m^{-2}$ $s^{-1}$; and low light intensity2 (LL2): 14 μmol $m^{-2}$ $s^{-1}$). After this the plants were transferred to 5°C at continuous GL1 for 3 days, and then back to 22/20°C for a 1-day recovery period. Leaf and root samples were collected from treated plants after the acclimation (13 day-old-plants), chilling (16 day-old-plants) and recovery (17 day-old-plants) periods for the estimation of viability and oxidative stress, and for carbohydrate analysis.

In the second set of experiments maize plants were grown for 11 days after 3 days germination at 22/20°C at higher PPFD, (growth light 2, GL2 = 387 μmol $m^{-2}$ $s^{-1}$) with 16/8 h light/dark periodicity (control plants). Some of the plants were then cold acclimated at 15/13°C for 3 days either at GL2 or at moderately low light intensity 3 (LL3): 283 μmol $m^{-2}$ $s^{-1}$; or at moderately low light intensity 4 (LL4): 107 μmol $m^{-2}$ $s^{-1}$. Afterwards all the plants were transferred to 5°C at continuous growth light (GL2) for 3 days, followed by a 7-day recovery period at 22°C. Samples were collected for biochemical analysis from the control plants, and from treated plants after the acclimation (17 day-old-plants), chilling (18 and 20 day-old-plants) and recovery periods (21, 24, and 27 day-old-plants).

## Estimation of Lipid Peroxidation

The lipid peroxidation analysis was based on the measurement of the malondialdehyde (MDA) level according to Gondor et al. (2016a) using 0.5 g of 3rd leaves of the plants. Five replicates were measured from each treatment and at least three leaves were used for one replicate.

## Electrolyte Leakage Test

Two leaf discs (8 mm diameter) cut from the middle part of the 3rd leaves were used for the determination of membrane damage. The measurements were carried out according to Szalai et al. (1996). Ten replicates were measured from each treatment and one leaf was used for one replicate.

## Determination of Chlorophyll Content

The total chlorophyll content was measured on the 3rd leaves using a SPAD-502 chlorophyll meter (Minolta Camera Co., Ltd, Japan) as described by Pál et al. (2011). At least 30 replicates were measured from each treatment and one leaf was used for one replicate.

## Measurement of Chlorophyll-a Fluorescence

Chlorophyll-*a* fluorescence induction was analyzed using a PAM fluorometer with a LED-Array Illumination Unit IMAG-MAX/L ($\lambda = 450$ nm) (Imaging-PAM, Walz, Germany). After 30-min dark adaptation, quenching analysis was carried out on the leaves at laboratory temperature using 250 $\mu$mol $m^{-2}$ $s^{-1}$ actinic light intensity until the steady state level of photosynthesis was reached (15 min). PPFD for the saturation pulses was higher than 2,000 $\mu$mol $m^{-2}$ $s^{-1}$. The fluorescence induction parameters were calculated as described by Klughammer and Schreiber (2008). Ten replicates were measured from each treatment and one leaf was used for one replicate.

## Soluble Sugar Analysis

0.5 g of leaf and root samples were measured according to Gondor et al. (2016b). Five replicates were measured from each treatment and at least three leaves were used for one replicate.

## Microarray Analysis

Three biological replicates each with three technical replicates (each consisting of seven plants) for the microarray analysis were harvested from the 3rd leaves of maize plants. Samples were collected from the control and the cold acclimated plants from the 2nd experiment. Two hundred ng of the total RNA was extracted using an RNEasy Plant Mini Kit (Qiagen, Hilden, Germany) and pooled from the three technical replicates and used for cRNA amplification. The quality of the extracted RNA was examined using the Agilent 2100 Bioanalyzer (Agilent Technologies Inc., Palo Alto, CA). The samples were labelled with Cy3 (Low Input QuickAmp, Agilent), and 1,650 ng cRNA was hybridized to the Agilent Whole Corn Gene Expression Microarray 4 × 44K chip according to the manufacturer's instructions (Agilent). The array was scanned using an Agilent Scanner, Extended Dynamic Range (100% and 10% laser intensities, 5 micron resolution). Signal intensities and normalization processes were detected with the Agilent Feature Extraction (FE 9.5) and GeneSpring (Agilent) Softwares. The fold change (FC) values of the samples were compared for Control vs. GL2, Control vs. LL3, Control vs. LL4, GL2 vs. LL3, GL2 vs. LL4 and LL3 vs. LL4 in a simple loop design. Genes with logFC $> |2|$ and $P < 0.01$ were considered as differentially expressed. The functional annotation of the probe sequences was performed in the *Zea mays* taxon and using the BLASTX with the default settings (Altschul et al., 1997).

## Validation of Microarray Results Using qRT-PCR

The microarray analysis was validated by qRT-PCR, using the same total RNA samples for microarray analysis and cDNA synthesis. cDNA was synthesized from 500 ng RNA with a RevertAid™ First Strand cDNA Synthesis Kit (Thermo Fisher Scientific, Waltham, USA). Seven genes that showed significant changes in the microarray analysis and represented different functional categories in response to cold treatment under different light conditions, namely NM214, LOC285, BT062987, BT060766, BT035304, XM587-2, and LOC531 were chosen for the validation. The gene expression changes were examined using an ABI StepOnePlus Real-Time PCR System (Thermo Fisher Scientific) with Maxima SYBR Green/ROX qPCR Master Mix (Thermo Fisher Scientific). The two internal control genes used for normalizing the variations in cDNA amounts were *actin* and the membrane protein gene *PB1A10.07c* (*MEP*). The geometric mean of the internal control data was applied for normalization. The relative changes in gene expression were compared to the control group and quantified according to the comparative CT method ($2^{-\Delta\Delta CT}$ method, Livak and Schmittgen, 2001). All seven genes showed similar expression patterns with quantitative real-time PCR and microarray analysis, demonstrating the reliability of the microarray results (Figure S1). Although the fold-change values determined by microarray analysis and RT-PCR were slightly different, the microarray values were generally lower than the qRT-PCR data. This might have been due to technical differences in the methods used for analysis and normalization (Liu et al., 2013).

## Venn-Diagram Analysis

Lists of up- and downregulated genes (Control vs. GL2, Control vs. LL3, Control vs. LL4, GL2 vs. LL3, GL2 vs. LL4 and LL3 vs. LL4) with *e*-value $< 1^{-4}$ were compared in order to reveal the uniqueness and overlap of individual genes using the InteractiVenn toolkit (Heberle et al., 2015).

## Principal Component Analysis (PCA)

The similarity of the gene expression data sets for each comparison was analyzed based on the significant logFC values ($P < 0.01$) of array probes using a *var-covar* matrix to principal component analysis (Hammer et al., 2001).

## GO Analysis

The EST hits of the significantly differentially expressed Agilent probes, showing $P < 0.01$, were matched to their Affymetrix IDs using the bioDBnet webtool (Mudunuri et al., 2009) which were used as input of SEA (Singular enrichment analysis) carried out using the agriGO v2.0 web-based toolkit (Tian et al., 2017). The maize locus ID v3.30 (Gramene Release 50) as a reference. Ranking scores between GO nodes, a hypergeometric statistical test was carried out on the *p*-values to correct them for multiple testing errors taking into account the false discovery rate (FDR) (Benjamini and Yekutieli, 2001). GO nodes with $q < 0.05$, where

q means the multiple test adjusted *p*-value, were considered as overrepresented term.

## Metabolic Pathway Analysis

In order to classify and display genes into metabolic pathway groups, MapMan software (Thimm et al., 2004) was used. The maize mapping file was developed as follows. The EST hits of the significantly differentially expressed Agilent probes, showing $P < 0.01$, were matched to their Affymetrix IDs using the bioDBnet webtool (Mudunuri et al., 2009). The maize Affymetrix chromosomal locations was taken as template for mapping the Affymetrix IDs of the treatments to metabolic pathway groups.

## Statistical Analysis

The experiments were repeated 3 times and representative data are shown. The results were the means of at least 5 measurements. The data were statistically evaluated using the standard deviation, ANOVA and *t*-test methods.

# RESULTS

In order to characterise the role of light during the cold acclimation period in maize plants, 2 set of experiments were designed. One with relatively low growth and hardening light intensities, and a 2nd one with relatively higher light conditions, where the possible role of photoinhibition is more dominant.

## 1st Experiment: Cold Hardening at Relatively Low Light Intensity

In the 1st set of experiments maize plants were grown at relatively low light intensity (GL1 = 180 $\mu$mol $m^{-2}$ $s^{-1}$), after which some plants were hardened at even lower light intensity (LL1 or LL2), followed by chilling stress under continuous illumination at GL1. The MDA level was measured to detect the extent of oxidative stress and was found to increase during hardening at GL1 in both leaves (**Figure 1A**) and roots (Figure S2), but did not change at LL1 or LL2. During chilling at GL1 the amount of MDA did not change significantly in the leaves but substantially increased in the roots. In the leaves of plants which were acclimated at low light intensity the chilling-induced increase in the MDA level was more pronounced. Interestingly, the light intensity during the hardening period also affected the chilling-induced MDA levels in the roots, where the lower the PPFD, the lower the MDA level detected (Figure S2). This means that not only the leaves, but also the roots exhibited light-dependent cold responses.

The effect of light during the hardening period was also monitored by estimating the chlorophyll content. The SPAD values showed that although hardening in the light provided protection against subsequent cold-induced oxidative stress in the leaves (**Figure 1B**), the chlorophyll content was slightly higher in plants hardened at lower light intensity.

These results suggest that although light may reduce the chilling-induced oxidative stress in maize, it may also have negative impacts on certain physiological processes indicated by the SPAD and MDA values; and probably photooxidative damage also occurred. Furthermore, loss of photosynthetic pigments may be an adaptive response required to balance the capacity for photosynthetic electron transport with the rate of metabolism. This may also decreased membrane damage in GL1 plants. Therefore the evaluation of the effect of light during cold acclimation in maize was continued by measuring electrolyte leakage. Cold acclimation at GL1 slightly increased the electrolyte leakage from leaf cells (**Figure 1C**). However, after exposure to severe stress at 5°C this increase was more pronounced in plants acclimated at LL1 and LL2.

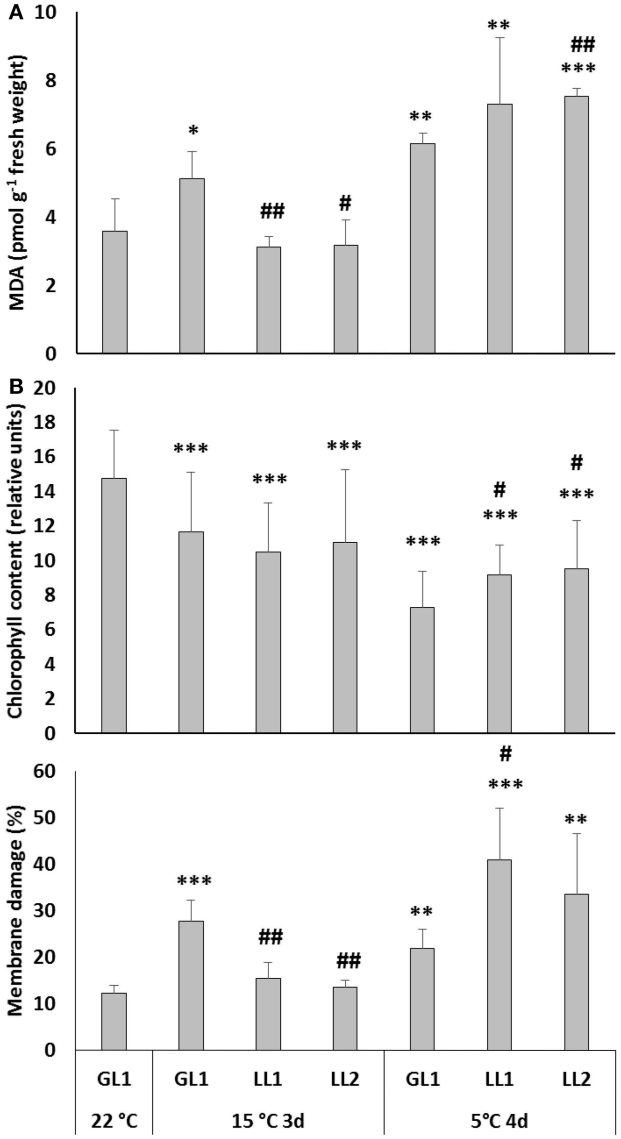


**FIGURE 1 |** MDA levels **(A)** chlorophyll content represented with SPAD-values **(B)** and membrane damage measured as electrolyte leakage **(C)** in the leaves of plants grown at GL1 before and after cold hardening at 15°C at GL1, LL1, or LL2, and after chilling stress at 5°C at GL1. $^{*}$, $^{**}$, $^{***}$Significant differences compared to the GL1 22°C plants at the $p < 0.05$, 0.01, and 0.001 levels, respectively. $^{\#}$, $^{\#\#}$, Significant differences compared to the GL1 plants on the same day at the $p < 0.05$ and 0.01 levels (mean ± SD, $n = 5$ for MDA, and $n = 10$ for SAPD and electrolyte leakage values).

## 2nd Experiment: Cold Hardening Under Medium Light Conditions

Since, despite its beneficial effects during the cold acclimation period, light may also induce secondary stress (photoinhibition), the 2nd set of hardening experiments was performed at higher light intensities. In this set of experiments plants were originally grown at higher PPFD (GL2 = 387 μmol $m^{-2}$ $s^{-1}$) after the germination period. Since plants were generally adapted to this higher light during their growth period, neither cold acclimation nor chilling at 5°C for 3 days caused substantial decrease in the chlorophyll content estimated with SPAD values (data not shown). However, visual analysis showed that the post-chilling symptoms during the recovery period (4 days at 22°C after 3-day cold treatment at 5°C), such as chlorosis in the distal parts of the leaves, were the most pronounced in un-acclimated plants, being less obvious in plants acclimated at higher light intensities (Figure S3).

The chlorophyll-a fluorescence induction technique provides a valuable tool to detect changes in Photosystem 2, especially under photoinhibitory conditions (Foyer et al., 2017). Fv/Fm, which represents the maximum quantum efficiency of Photosystem 2, did not change significantly after growth at hardening temperature. However, it substantially decreased in a light-dependent manner at 5°C in all the plants. Interestingly, this decrease was more pronounced in plants acclimated at higher light intensities. The decrease in Fv/Fm in non-acclimated plants exhibited values intermediate to those of plants acclimated at GL2 and LL (**Figure 2**). It seems that the hardening period preconditioned the plants for the subsequent photoinhibitory effect of low temperature. The recovery of Fv/Fm was relatively fast. The quantum yield of Photosystem 2, Y(II), decreased within 3 days at 15°C at GL2. However, at 5°C Y(II) was not better in the non-hardened plants than in those hardened at GL2, and recovery was also slower than in acclimated plants (**Figure 2**). The negative impact of relatively high light intensity on the quantum yield was still detected during the beginning of the recovery period, but the decrease in this parameter was reversible within 7 days. The most significant changes in the regulated non-photochemical quenching, Y(NPQ), could be found in plants acclimated at GL2, where this parameter slightly increased; however, Y(NPQ) substantially decreased in the same plants after exposure to 5°C for 3 days. This parameter recovered rapidly (within 1 day) at 22°C. Non-regulated non-photochemical quenching, Y(NO), showed a similar pattern but with the opposite trend, substantially increasing in a light-dependent manner at 5°C, especially in plants acclimated at GL2.

In contrast to the 1st set of experiments, where the light intensity was relatively low, the MDA content did not change substantially in the leaves in the 2nd set of experiments (Figure S4). A notable increase could only be detected after 4 days of recovery, probably due to the post-chilling effect. However, as in the previous experiment, MDA showed a light dependent response in the roots, increasing even during the hardening period, especially at higher light intensity. Recovery was also light-dependent.

## Alteration in Gene Expression Profiles at Low Temperature

In order to obtain a better understanding of the molecular mechanisms underlying the role of light during the cold acclimation period in maize, gene expression analysis was performed using the microarray technique. Samples were taken from control plants growing at GL2 at 22°C and from plants hardened for 3 days at 15°C at GL2, LL3, or LL4.

In total, 42,050 transcripts were examined on the Agilent chip. Genes were considered to have significantly different expression with logFC $> |2|$ and the *P*-value was $< 0.01$, which resulted 677, 467, 1,780, 63, 1,317, and 1,240 individual significant array probes in Control vs. GL2, Control vs. LL3, Control vs. LL4, GL2 vs. LL3, GL2 vs. LL4, and LL3 vs. LL4, respectively (Table S1). After the functional annotation of the probe sequences with a *e*-value of $< 1e^{-4}$ cutoff, the results showed that although, as expected, low temperature up- or down-regulated the expression of hundreds of genes, light also substantially altered the expression level of a similar number of genes (Table S1). The Venn diagram comparison can be seen on Figure S5. Selected genes related to photosynthesis with logFC $> |2|$ and known function (*e*-value $< 1^{-4}$) that were differentially expressed in Control vs. GL2 or GL2 vs. LL4 are listed in Table S2.

## Cluster Analysis

To understand the relationships and discrepancy of the effect of cold, light or their combination more comprehensively, cluster analysis was carried out according to log2FC values of significantly differentially expressed genes of all comparisons. The same type of regulations was gathered in clusters with similar gene expression profiles. The cluster of the columns of the heat map is shown in **Figure 3A**. The results indicate that effect of different illuminations clearly distinguished. Low light intensity LL4 induced the expression significantly expressed genes at different levels both at normal and low temperatures. Other light intensities, GL2 and LL3 had altered effect on genes investigated.

## Differential Expression Analysis

Volcano plotscarried out on the significantly expressed microarray probes of each comparisons which either regulated by cold or light or both factors (**Figure 3B**). Genes with log2FC $> |3|$ and $p < 0.0001$ were filtered and considered as the most outlier gene in each regulations. The biological functions were annotated and listed in Table S3. The highest number of genes high log2FC and low *p*-value were found of the effect of LL4 in the cold and most of them were up-regulated, such as the acyclic sesquiterpene synthase which was expressed alone under these conditions. Regarding genes with known function, glutaredoxin-C13 was induced cold under GL2 and repressed by the LL3 and LL4.

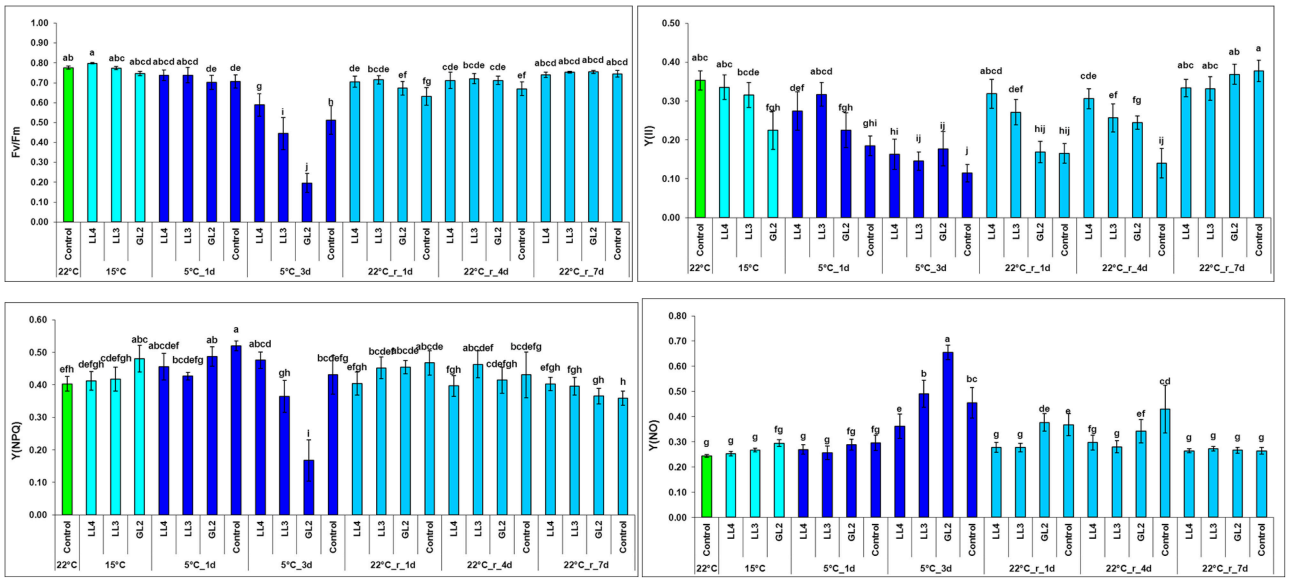


**FIGURE 2 |** Effect of cold hardening in maize at 15°C under different light conditions, followed by chilling stress at 5°C and 7-d recovery on the chlorophyll-a fluorescence induction parameters Fv/Fm, Y(II) (the quantum yield of Photosystem 2 estimated as $\Delta F/Fm'$), Y(NPQ) and Y(NO) (the regulated and non-regulated non-photochemical quenching). Different letters on the bars represent statistically significant differences at $p < 0.05$.

## Principal Component Analysis

A scatter plot diagram and the loadings of the original variables were used to show the similarity between the global gene expression profiles of each comparison (Control vs. GL2, Control vs. LL3, Control vs. LL4, GL2 vs. LL3, GL2 vs. LL4, LL3 vs. LL4) (Figure S6). The biplot representation showed that the Control vs. GL2 and Control vs. LL3 comparisons were similar to each other, but differed from GL2 vs. LL3 in the expression profile along axis 1 (PC 1). The expression pattern of LL3 vs. LL4 was similar to that of GL2 vs. LL4 along axis 2 (PC 2). Control vs. LL4 was quite dissimilar to the other comparisons. The results suggested that illumination levels GL2 and LL3 had a different effect on gene expression than the LL4 illumination level.

## GO Analysis

The microarray output was mapped for gene functions using the GO classification for genes differentially regulated at low temperature under different light conditions (Figures S7–S14). The GO enrichment analysis focused both on the effect of cold under GL2 and how the GL2 acts on global gene expression in contrast to LL4 in the cold.

Low temperature greatly influenced the global gene expression pattern under growth light (GL2) as compared to the control temperature (Figures S7, S8). Most of the genes significantly differentially up-regulated ($q < 0.05$) in the cold are originated from the cytoplasm (GO: 0005737), cytoplasmic membrane-bounded vesicles (GO: 0016023) the plastids (GO: 0009536) or in the mitochondria (GO: 0005739). The result of the ontology analysis of gene functions regulated by cold showed the over-representation of ribosome biogenesis (GO: 0042254), hexose biosynthetic (GO: 0046364) and aspartate and serine family amino acid metabolic processes (GO: 000258, GO: 0009069).

GL2 caused different gene expression as compared to LL4 in the cold in the GL2 vs. LL4 comparison (Figures S9–S11). Genes regulated by GL2 mostly expressed in intracellular membrane-bounded organelles (GO: 0043231) such as plastids (GO: 0009536) and the chloroplast (GO: 0009507). Many genes were also expressed in the cytoplasmic membrane-bounded vesicles (GO: 0016023). The following biological were greatly emphasized under GL2 illumination in the cold, such as chlorophyll biosynthesis (GO: 0015995), cellular nitrogen compound biosynthetic process (GO: 0044271), cellular amino acid biosynthetic process (GO: 0008652), ribosome biogenesis (GO: 0042254). Genes were also associated with the cellular nitrogen compound metabolic process (GO: 0034641) and consequently, cellular amino acid metabolic processes (GO: 0006520). Hexose and galactose biosynthetic processes (GO: 0019319, GO: 0006012) were also significantly over-represented under these conditions. Amongst molecular functions, glutathione transferase activity (GO: 0004364) and rRNA binding (GO: 0019843) were over-represented.

Double factor-regulation, i.e., low light (LL4) illumination in the cold caused higher alterations in the global gene expression than GL2 did that in the cold (Figures S12–S14). Genes functions were significantly over-represented of the effect of LL4 in the following cellular components, namely intracellular membrane-bounded organelles (GO: 0043231) and intracellular membrane-bounded organelles (GO: 0043231), such as mitochondria (GO: 0005739) and plastids (GO: 0009536), as well as cytoplasmic membrane-bounded vesicle (GO: 0016023). Gene functions were highlighted under this light regime are related to the cellular amino acid metabolic processes (GO: 0006520), especially serine amino acid metabolism. On the other hand, gene functions can be mapped to carboxylic acid metabolism (GO: 0019752),

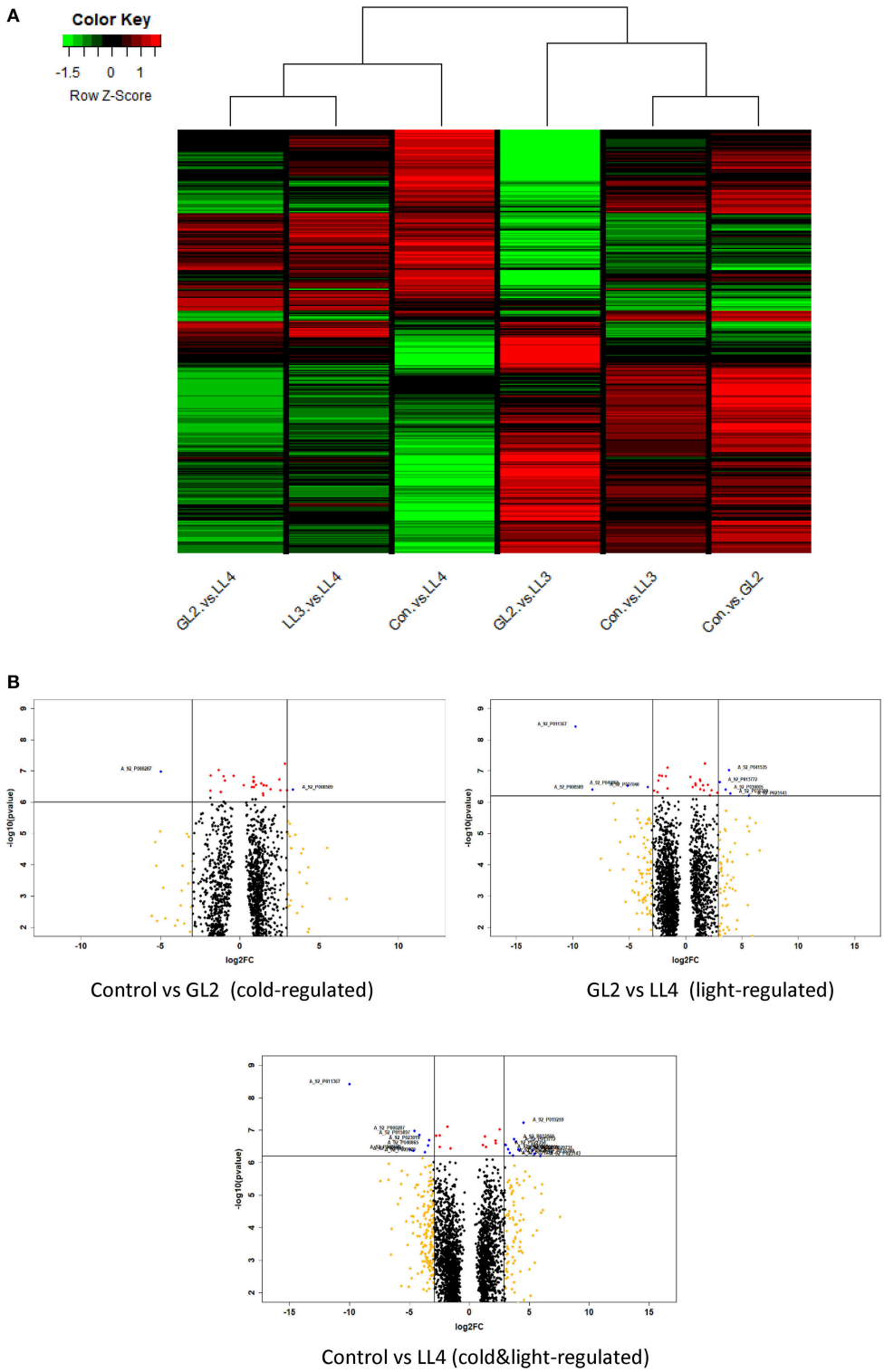


**FIGURE 3 | (A)** Cluster heat map of cold-regulated (Control vs. GL2), Control vs. LL3, Control vs. LL4 (double factor-regulated) and GL2 vs. LL3, GL2 vs. LL4, LL3 vs. LL4 (light-regulated) comparisons with log2FC $< -0.1$ and log2FC $> 0.1$. Red colour represents up-regulated expression and green colour represents down-regulated expression. Each row represents a differentially expressed gene function pathway; **(B)** Volcano plots of three comparisons indicating either cold, light, and their combined regulation. Genes with high level of expression and significance were emphasized (filter red dots indicate if $p < 0.0001$, orange if log2FC $> |3|$ and blue if both).

gluconeogenesis (GO: 0006094) and galactose metabolic process (GO: 0006012). Secondary metabolism (GO: 0019748) and coenzyme metabolism (GO: 0006732) were less affected. In general, most of the important biological processes of the cell were influenced in Control vs. LL4 comparison. The ribosome biogenesis (GO: 0042254) and consequently, the translation (GO: 0006412) and its regulation (GO: 0006417) were affected. Photosynthesis (GO: 0015979) was also affected by LL4 in the cold. Both the process of light capture via the modification of chlorophyll biosynthesis (GO: 0015995) and the dark reactions (GO: 0019685) changed. The amino acid metabolism were significantly affected, such as serine and glutamine metabolism. The genes in the cofactor metabolic processes (GO: 0051186) were also overrepresented, which either belongs to porphyrin (GO: 0006778) or glutathione (GO: 0006749) metabolic processes. Regarding cellular scenes of these versatile processes mostly found in the plastids (GO: 0009536), including the chloroplast (GO: 0009507), mitochondria (GO: 0005739) and cytoplasmic membrane-bounded vesicles (GO: 0016023). Ribosome biogenesis and translation are located in the ribosomes (GO: 0005840) or nuclear transcription factor complexes (GO: 0005667). Similarly to GL2 regulation in the cold, molecular functions such as glutathione transferase activity (GO: 0004364) and rRNA binding (GO: 0019843) were over-represented.

## Pathway Analysis

Differentially regulated genes were classified into metabolic pathway groups using the MapMan software. Amongst numerous metabolic pathways, we found the most informative ones the followings: metabolic overview, transcription and photosynthesis (**Figures 4**–**6**).

The overview of cellular metabolism showed that both cold and light caused a remarkable rearrangement of metabolism. Generally, the effect of LL4 at low temperature caused the up-regulation of the genes, thus, facilitate the metabolism (**Figures 4A**, **5A**, **6A**). Both GL2 and LL4 influenced the tetrapyrrole metabolism in the cold. Similarly, the processes of light utilization on the PSII, carbohydrate metabolism and the ascorbate-glutathione cycle were induced rather at LL4 than at GL2. It can be concluded, that the most processes of assimilation are maintained by LL4 and repressed by cold or GL2.

The distribution of the expression of transcription factors is also affected by cold and light (**Figures 4B**, **5B**, **6B**). One of the most affected transcription protein family is the histones which were repressed at GL2 but not by LL4 in the cold. Both G proteins, bHLH, bZIPs and other putative DNA-binding proteins down-regulated by cold and GL2 and up-regulated by LL4. HSFs, interestingly, remained up-regulated in each treatments.

In a more detailed analysis, gene function of photosynthetic processes were dissected. Higher number of genes functions were classified into the photosynthetic processes at LL4 in the cold compared with control condition. Both light reactions and Calvin cycle were induced rather by LL4 repressed by GL2 (**Figures 4C**, **5C**, **6C**). Results suggest that the expression of genes related to photosynthetic processes is better influenced by light then by the temperature drop.

## Changes in the Amount of Soluble Sugars

Some of the genes whose expression levels were significantly altered by the cold acclimating temperature and/or different light intensities during the hardening period, were involved in the carbohydrate metabolism (**Table 1**). The amounts of fructose, glucose, sucrose and maltose were determined in the leaves and roots after cold acclimation, after chilling treatment and during the recovery period. The highest fructose level was detected in the leaves of GL2 plants during hardening (Figure S15A) but dropped to the control level after three days at 5°C and remained at this level on the first day of recovery. Glucose and sucrose were detected in the highest amount in the leaves (Figures S15B,C). As in the case of fructose, a great increase was detected in the leaves of GL2 plants during hardening, but hardly any change was observed after 3 days at 5°C and only a slight decrease during recovery. A similar change was detected in the amount of maltose during hardening (Figure S15D), but its level increased at 5°C even in unhardened plants although the highest amount was measured in the leaves of GL2 plants. During the recovery period it dropped back to the initial level. Fructose and sucrose increased in the roots in a light-dependent manner during hardening (Figures S16A,C). The fructose content remained at the same level after 3 days at 5°C, but the amount of sucrose increased, particularly in the case of GL2 and LL3. No substantial changes were determined in the levels of glucose and maltose in the roots (Figures S16B,D).

# DISCUSSION

Exposure to low, but non-freezing temperatures is necessary for the development of the maximum level of freezing tolerance in winter cereals, even in the case of the most hardy genotypes, but it has long been known that the development of freezing tolerance is inefficient at low light intensity (Gray et al., 1997). Since it is possible for even chilling-sensitive maize plants to become acclimated to relatively low temperatures (Anderson et al., 1994; Janda et al., 1998), an analogous experiment was carried out to elucidate how light contributes to the development of cold acclimation processes in maize plants. In the first experiment, maize plants were grown at relatively low light intensity (GL1), which was further reduced during the acclimation period. Measurements of electrolyte leakage from the leaves suggested that, similarly to the frost hardening of winter cereals (Gray et al., 1997; Apostol et al., 2006), cold acclimation was less efficient at low light intensity in maize plants. The MDA level in the leaves after exposure to low temperature (5°C) was also higher in plants cold acclimated at low light intensity than at GL1. Interestingly, the chlorophyll content in the leaves showed an opposite pattern to the MDA content in the roots.

These results indicated that although light is necessary during the acclimation period to achieve improved chilling tolerance, it may also have various "side effects." Photoinhibition often occurs under stress conditions, when the photosynthetic processes are impaired or negatively affected by unfavourable

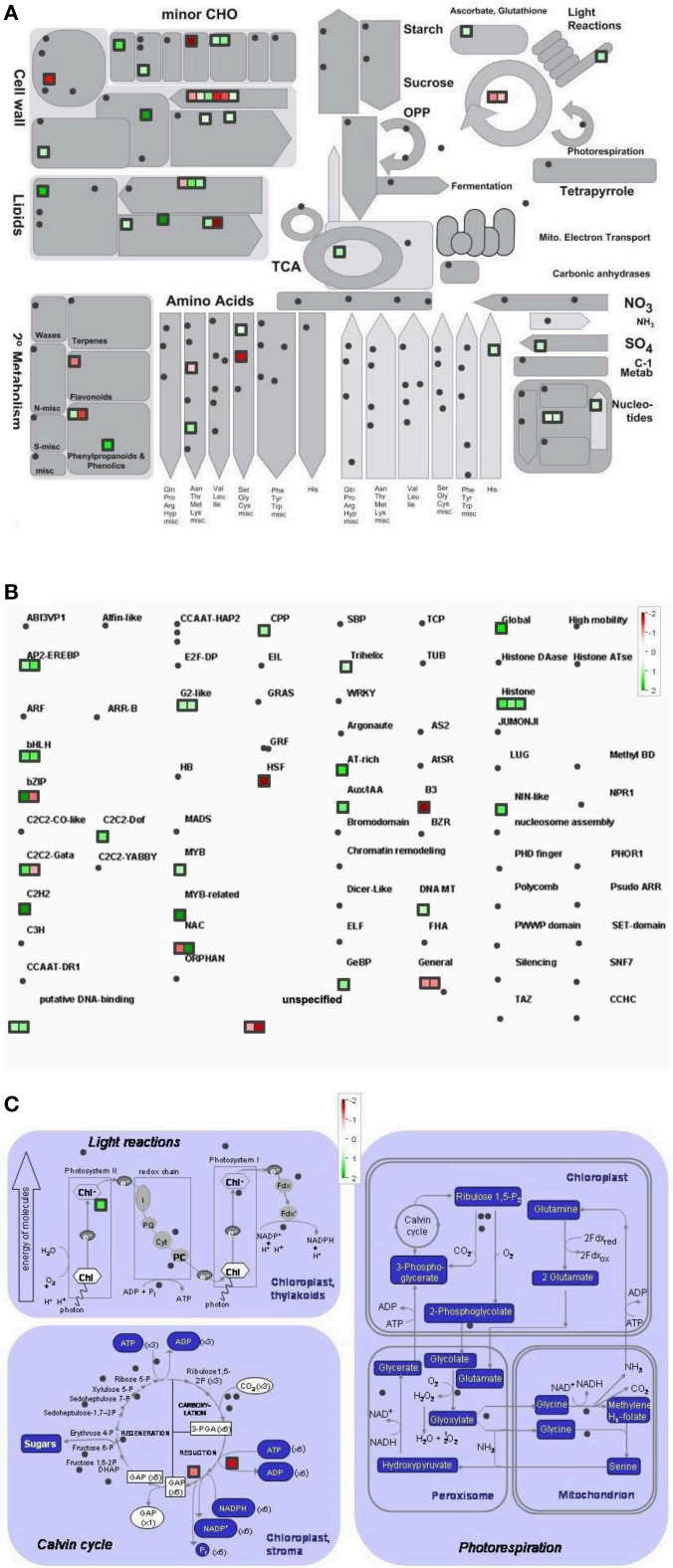


**FIGURE 4 |** Metabolism overview **(A)** distribution of transcription factors **(B)** and genes involved in the photosynthesis **(C)** in Control vs. GL2 (effect of cold). logFC-values of the microarray-based expression were loaded into MapMan to generate the pathway map. Each square represents a logFC > |2| differentially expressed transcript. Genes whose expression does not change are coloured white, and an increasingly large increase or decrease is shown as an increasingly intense green or red colour, respectively. On the log2 scale ranging between 2 or 3 and −2 or −3, green and red colours represent 4, or 8-fold expression.

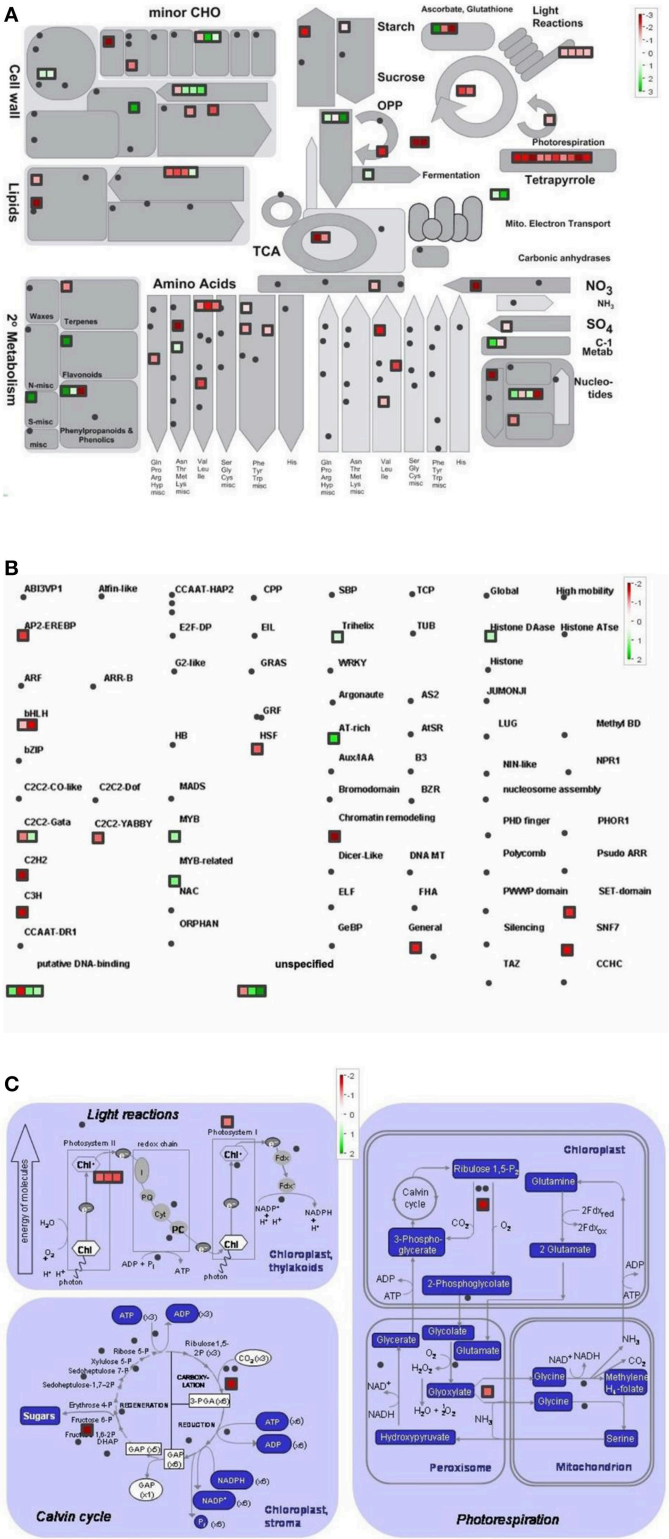


**FIGURE 5 |** Metabolism overview **(A)** distribution of transcription factors **(B)** and genes involved in the photosynthesis **(C)** in GL2 vs. LL4 (effect of light). logFC values of the microarray-based expression were loaded into MapMan to generate the pathway map. Each square represents a logFC > |2| differentially expressed transcript. Genes whose expression does not change are coloured white, and an increasingly large increase or decrease is shown as an increasingly intense green or red colour, respectively. On the log2 scale ranging between 2 or 3 and −2 or −3, green and red colours represent 4, or 8-fold expression.


**FIGURE 6 |** Metabolism overview **(A)** distribution of transcription factors **(B)** and genes involved in the photosynthesis **(C)** in Control vs. LL4 (effect of cold and light). logFC values of the microarray-based expression were loaded into MapMan to generate the pathway map. Each square represents a logFC > |2| differentially expressed transcript. Genes whose expression does not change are coloured white, and an increasingly large increase or decrease is shown as an increasingly intense green or red colour, respectively. On the log2 scale ranging between 2 or 3 and−2 or−3, green and red colours represent 4, or 8-fold expression.

**TABLE 1 |** List of gene functions related to carbohydrate metabolism and regulated by cold, light or both factors.

| Cold-regulated | | | | Light-regulated | | | | Combined regulation | | | |
|---|---|---|---|---|---|---|---|---|---|---|---|
| **Accession number** | **Gene function** | **log2FC** | ***p*-value** | **Accession number** | **Gene function** | **log2FC** | ***p*-value** | **Accession number** | **Gene function** | **log2FC** | ***p*-value** |
| NP_001130108 | Glycerophosphodiester phosphodiesterase | 3.9370346 | 0.002137337 | NP_001151917 | Phosphoenolpyruvate carboxylase kinase 1 | 4.1780014 | 5.85E-04 | AQK60148 | Glucomannan 4-beta-mannosyltransferase 2 | 4.190055 | 5.95E-05 |
| AQK97088 | Phosphoglycerate Mutase family protein | 2.324909 | 0.002300885 | ACG34953 | Glycerol-3-phosphate Acyltransferase 8 | 2.4213006 | 0.003560609 | ONM36349 | Glycerol-3-phosphophosphate Acyltransferase1 | 2.5158112 | 0.003560609 |
| ONM56633 | Bifunctional UDP-glucose 4-epimerase and UDP-xylose 4-epimerase 1 | 1.657018 | 6.30E-04 | ACG28932 | Glycosyltransferase | 2.375742 | 0.002720237 | ONM02814 | Glycerophosphodiester phosphodiesterase GDPDL3 | 2.1040068 | 4.56E-04 |
| ONM60638 | Alpha-galactosidase 3 | 1.4812617 | 0.002564861 | NP_001105047 | Aldehyde dehydrogenase 5 | 2.2098408 | 0.001409359 | ONM10264 | Plastidial pyruvate kinase 1 chloroplastic | 1.807035 | 2.80E-04 |
| AQK87666 | Trehalose-6-phosphate synthase12 | 1.4775023 | 1.85E-04 | ONM30490 | Glycosyltransferase family 61 protein | 2.2052014 | 0.001584862 | NP_001148138 | Glycerol 3-phosphate permease | 1.7980256 | 0.003462655 |
| ACG38167 | Xyloglucan endotransglycosylase/hydrolase protein 8 precursor | 1.2368568 | 2.24E-04 | ONM10098 | Aldehyde oxidase1 | 2.1058974 | 0.00453268 | NP_001105608 | Pyruvate dehydrogenase (lipoamide) kinase 2 | 1.6757569 | 5.62E-05 |
| NP_001105608 | Pyruvate dehydrogenase (lipoamide) kinase 2 | 1.1424388 | 5.62E-05 | NP_001148092 | Aldehyde dehydrogenase, dimeric NADP-preferring | 2.0147645 | 3.71E-05 | ONL96977 | 6-Phosphofructo-2-kinase/fructose-26-bisphosphatase | 1.661703 | 2.06E-04 |
| AQK88045 | Beta-galactosidase 17 | 1.0441507 | 9.79E-04 | ONM02814 | Glycerophosphodiester phosphodiesterase GDPDL3 | 1.6459553 | 4.56E-04 | NP_001137118 | Aldose 1-epimerase precursor | 1.4921634 | 0.00407572 |
| NP_001338725 | Ribulose bisphosphate carboxylase small subunit 2 | −0.9178931 | 5.26E-04 | ONM56302 | Beta-glucosidase 11 | 1.2667857 | 4.08E-04 | ONM22374 | Glucose-6-phosphate isomerase 1 chloroplastic | 1.3741354 | 0.00144248 |
| XP_008675104 | Alpha-amylase 3, chloroplastic | −0.9569126 | 1.05E-05 | XP_008665592 | Pyruvate kinase isozyme A, chloroplastic | 1.1613737 | 2.80E-04 | ONM62564 | Aldehyde dehydrogenase | 1.3029907 | 3.71E-05 |
| ONL97046 | Malonyl CoA-acyl carrier protein transacylase | −1.3121262 | 4.21E-05 | ONL96977 | 6-phosphofructo-2-kinase/fructose-26-bisphosphatase | 0.9451744 | 2.06E-04 | AAN40021 | Putative sugar transporter protein | 1.286771 | 4.21E-06 |
| AQK99444 | Mannose-1-phosphate guanylyltransferase 1 | −1.5589914 | 5.68E-06 | AQK95232 | Phosphoglycerate mutase-like protein AT74H | 0.90894777 | 6.83E-04 | ACG29374 | Sugar carrier protein C | 1.266195 | 0.002126372 |
| XP_008656415 | phosphoglycerate kinase, chloroplastic | −1.664048 | 1.74E-04 | NP_001288421 | Sugar transport protein 6-like | 0.8480516 | 3.54E-04 | AQK95232 | Phosphoglycerate mutase-like protein AT74H | 1.036925 | 6.83E-04 |
| XP_008669175 | probable inactive beta-glucosidase 14 | −2.2985225 | 0.00177892 | NP_001147854 | 6-Phosphofructokinase | 0.7439168 | 5.28E-05 | AAG22094 | Ribulose 1,5-bisphosphate carboxylase/oxygenase activase precursor, partial | −0.99635535 | 2.49E-04 |
| ONM00923 | Alpha/beta-Hydrolases superfamily protein | −2.6030025 | 3.91E-04 | ONM59878 | 4-Alpha-glucanotransferase DPE1 chloroplastic/amyloplastic | −0.80431604 | 4.06E-04 | NP_001104840 | Sucrose transporter 1 | −1.0542811 | 0.004237142 |
| | | | | NP_001142302 | Mannose-1-phosphate guanylyltransferase 1 | −1.0449951 | 5.68E-06 | ONM06244 | Phosphoglycerate kinase | −1.1203326 | 6.00E-05 |
| | | | | NP_001151106 | Fructose-1,6-bisphosphatase, cytosolic | −1.0704721 | 0.003318357 | AQK69130 | Sucrose-phosphate synthase 1 | −1.3283775 | 3.44E-05 |
| | | | | ONM07834 | Phosphoglycerate mutase-like family protein | −1.1184196 | 0.002953377 | NP_001142404 | Phosphoglycerate kinase | −1.4211287 | 0.003085656 |
| | | | | XP_008654210 | trehalose-6-phosphate synthase isoform X1 | −1.2203356 | 1.85E-04 | ONM00332 | Glycerol-3-phosphate acyltransferase chloroplastic | −1.4539771 | 3.02E-04 |
| | | | | ONM00332 | Glycerol-3-phosphate acyltransferase chloroplastic | −1.25687 | 3.02E-04 | AQL07810 | Alpha/beta-Hydrolases superfamily protein, partial | −1.6154816 | 0.002821473 |

*(Continued)*

**TABLE 1** | Continued

| Cold-regulated | | Light-regulated | | | Combined regulation | | | |
|---|---|---|---|---|---|---|---|---|
| | XP_008645148 | phosphoglycerate kinase isoform X1 | −1.2609754 | 6.00E-05 | XP_008673647 | Phosphoenolpyruvate/phosphate translocator 3, chloroplastic | −1.6809244 | 5.76E-05 |
| | AAG22094 | Ribulose bisphosphate carboxylase/oxygenase activase, chloroplastic precursor | −1.3490247 | 0.002121331 | AAX07938 | Phosphoenolpyruvate carboxylase kinase 4 | −1.8123076 | 5.22E-04 |
| | AQK62551 | Ribose-5-phosphate isomerase | −1.3925734 | 0.001351543 | XP_008656415 | phosphoglycerate kinase, chloroplastic | −2.149561 | 1.74E-04 |
| | XP_020403676 | Ribulose bisphosphate carboxylase/oxygenase activase 2, chloroplastic | −1.4514501 | 0.001175892 | XP_020403676 | Ribulose bisphosphate carboxylase/oxygenase activase 2, chloroplastic | −2.1777864 | 0.001175892 |
| | NP_001130532 | Beta-galactosidase Precursor | −1.5497097 | 3.79E-04 | ACF87565 | Unknown | −2.2316277 | 0.001227283 |
| | AQL09362 | Sucrose transport protein SUC3 | −1.5682054 | 1.30E-04 | NP_001147459 | Fructose-1,6-bisphosphatase | −2.2366343 | 0.002749594 |
| | AQK85634 | Mannosylglycoprotein endo-beta-mannosidase | −1.6499152 | 0.003568029 | NP_001108121 | Starch branching enzyme III | −2.3248887 | 4.09E-04 |
| | AQK55931 | Trehalose-6-phosphate synthase10 | −1.6655805 | 8.54E-04 | AQK99444 | Mannose-1-phosphate guanylyltransferase 1 | −2.6039865 | 5.68E-06 |
| | AAX07938 | Phosphoenolpyruvate carboxylase kinase 4 | −1.7103847 | 5.22E-04 | ONM18906 | Pullulanase-type starch debranching enzyme1 | −2.8656135 | 1.51E-05 |
| | XP_020401744 | ruBisCO large subunit-binding protein subunit alpha, chloroplastic | −1.799408 | 2.64E-04 | ONL97046 | Malonyl CoA-acyl carrier protein transacylase | −3.1654654 | 4.21E-05 |
| | ACG30583 | Trehalose-6-phosphate synthase | −1.8578088 | 5.82E-04 | AAC49012 | Xyloglucan endo-transglycosylase homolog; similar to Triticum aestivum endo-xyloglucan transferase, PIR Accession Number E49539 | −3.4923546 | 8.17E-04 |
| | NP_001108121 | Starch branching enzyme III | −1.9227829 | 4.09E-04 | ONM00923 | Alpha/beta-Hydrolases superfamily protein | −3.842009 | 3.91E-04 |
| | XP_008659412 | Alpha-galactosidase 3 | −1.9270322 | 3.29E-05 | | | | |
| | XP_008659412 | Alpha-mannosidase | −1.9270322 | 3.29E-05 | | | | |
| | ONM34741 | Alpha/beta-Hydrolases superfamily protein | −1.9846559 | 2.95E-05 | | | | |
| | NP_001147459 | Fructose-1,6-bisphosphatase | −2.1469374 | 0.002749594 | | | | |
| | ONM29674 | Phosphoenolpyruvate/phosphate translocator 3, chloroplastic | −2.2858033 | 5.76E-05 | | | | |
| | AQK65349 | Starch synthase IIc | −2.3964448 | 0.001227283 | | | | |
| | NP_001104914 | Pyruvate dehydrogenase 2 | −3.0675209 | 4.73E-06 | | | | |
| | NP_001105775 | Alkaline alpha galactosidase 3 | −3.1119506 | 4.45E-05 | | | | |

*Lists were ordered according to the log2FC values (accession number and gene function derived from a BLASTX search in nr database in maize, log2FC and p-value derived from the array image processing).*

environmental factors (Long et al., 1983). Low temperature-induced photoinhibition has been widely studied in a wide range of chilling-sensitive plant species (Janda et al., 1994; Gómez et al., 2015). It has also been shown that upon exposure to low temperature in the light not only photosynthetic processes, but also other stress-related mechanisms are affected, such as the polyamine or free amino acid metabolisms (Szalai et al., 1997). To reveal further details of the effect of light during the cold acclimation period, another experiment was designed with higher light intensities. It has been demonstrated in maize plants that several stress symptoms cannot be detected at low temperature. They only appear in the post-chilling period (Szalai et al., 1996). Fluorescence induction measurements indicated that hardening at higher light intensities reduced the quantum efficiency of Photosystem 2 at low temperatures and also led to the slower recovery of this parameter at normal growth temperature. Interestingly, after exposure to low temperature, plants acclimated at higher light intensities had higher Y(NO), which reflects the fraction of energy that is passively dissipated, and lower Y(NPQ), which represents the regulated non-photochemical quenching, than plants cold acclimated at lower light intensity or not hardened at all. Since the occurrence of high Y(NO) in the light-adapted state is usually thought to indicate the presence of severe stress (Lazár, 2015; Zhang et al., 2017), these results suggest that cold acclimation at high light intensity also stresses plants. However, visual analysis clearly demonstrated that, in spite of the occurrence of photoinhibition, light (GL2) was still beneficial in terms of cold tolerance. These results suggest that the fact that photoinhibition is a possible source of reactive oxygen species may also have useful effects, such as inducing stress acclimation processes in plants (Foyer et al., 2017). Although increasing light intensity itself may also induce cold tolerance to a certain degree, as demonstrated for cereals (Janda et al., 2014), and although it has been shown that the excitation pressure in the photosynthetic electron transport chain is a critical component of the induction of cold tolerance, it cannot be stated that a high level of cold tolerance can be achieved simply through photoinhibitory treatment. It occurs under various type of stress conditions, such as drought, heat, etc. (whenever carbon fixation is limited), but the plants do not necessarily become cold-tolerant (although cross-tolerance effects have been reported in some cases). Nevertheless, it seems that photoinhibition may function as a signal not only for the development of cold hardiness in cereals but also, as suggested by the present results, for the development of cold acclimation in maize.

In efforts to understand the genetic basis of cold sensitivity in maize, several genes responding to low temperature have been identified. The recently published results of microarray-based genomic analysis indicated that hundreds of genes were affected by chilling treatment of various durations (Trzcinska-Danielewicz et al., 2009). Earlier studies showed changes in the expression of various specific genes in maize plants exposed to low-temperature stress. Cold-regulated genes have several functions, influencing transcription factors and genes related to DNA methylation, carbohydrate and secondary metabolism, etc. (Marocco et al., 2005). Among the transcripts present at higher levels in maize seedlings after cold acclimation were those corresponding to chilling acclimation-responsive genes encoding maize mitochondrial catalase isozymes (Anderson et al., 1994). In the cold tolerant Arabidopsis plants it has been shown that the levels an Arabidopsis bZIP transcription factor HY5, which has a pivotal role in light signalling are also regulated by low temperature transcriptionally, via a C-repeat binding factor- and abscisic acid-independent pathway, and post-translationally, via protein stabilization through nuclear depletion of a crucial repressor of light signalling CONSTITUTIVE PHOTOMORPHOGENIC 1 (COP1). HY5 also positively regulated the cold-induced gene expression through certain cis-acting elements, ensuring the complete development of cold acclimation (Catalá et al., 2011).

Recent analyses on the chilling sensitive maize plants indicated three main mechanisms that could be responsible for cold tolerance: the modification of the photosynthetic apparatus, cell wall properties and developmental processes (Sobkowiak et al., 2016). The regulation of the amount of reactive oxygen species and of redox homeostasis have been demonstrated to be important for cold acclimation processes in various plant species (Fracheboud et al., 2004; Gill and Tuteja, 2010; Kocsy, 2015; Boldizsár et al., 2016a). In the present work the comparison of the gene expression profiles in control and acclimated plants demonstrated that the light intensity is at least as important factor as the temperature during the cold acclimation period. The analysis of gene classes with a significant response to the treatments revealed complex regulation mechanisms and interactions between cold and light signalling processes. These results highlight the significance of numerous significantly differentially expressed genes, which are involved in most of assimilation and metabolic pathways, namely photosynthetic light capture via the modification of chlorophyll biosynthesis and the dark reactions, carboxylic acid metabolism, cellular amino acid metabolic processes, such as serine, threonine and glutamine metabolism, cofactor, porphyrin or glutathione metabolic processes as well as ribosome biogenesis and translation. It suggests that light intensity has a fundamental influence on the whole assimilation and metabolism at suboptimal temperature in maize.

In the present study detailed analysis was carried out focusing on the separate effects of cold and light, with special regard to Control vs. GL2 and GL2 vs. LL4 and Control vs. LL4 comparisons. The pathway analysis of gene functions suggests that both light reactions and Calvin cycle were induced by LL4 and repressed by GL2 at low temperature. It is known, that temperature, including chilling and heat, and light prominently influence chloroplast development and chlorophyll biosynthesis, which affect photosynthesis efficiency. Most enzymes involved in the tetrapyrrole pathway significantly differentially expressed in the present experiment. Our results show that the chlorophyll biosynthetic processes were repressed both by the low temperature and GL2. At low light intensity (LL4), however, these genes were up-regulated. In accordance to our findings, chlorophyll biosynthesis was also found to be greatly light-dependent in wheat and cucumber due to a lower activation some key enzymes of tetrapyrrole biosynthesis

in the light at suboptimal temperatures (Mohanty et al., 2006).

Photosynthesis is in a strong relation with amino acid biosynthesis. Chloroplasts are able to reduce nitrite to ammonia, and synthesize a number of amino acids (Wallsgrove et al., 1983). Not surprisingly, amino acid metabolism is also promoted by low light and not by normal growth light in the cold. The pathway analysis of the gene functions classified into transcription factor families showed that more genes were silenced by GL2 than LL4. This can be related to the higher number of active assimilation processes acting under low light during the cold period.

In contrast to the amino acid metabolism, besides many pivotal and secondary biological processes, the translation and ribosome biogenesis, the most important influence of cold was found on the cellular carbohydrate metabolism, particularly hexose biosynthetic process. Beside other processes, GL2 had also significant effect on the hexose biosynthesis in the cold. Literature data also show, that cold acclimation is often associated with the accumulation of compatible solutes (sugars, proline, etc.) (Thomashow, 1999). The present work also focused on the involvement of changes in soluble sugars in osmotic regulation. Soluble sugars may function as osmoprotectants, buffering the harmful effect of low temperatures. The accumulation of soluble sugars was found to be correlated with enhanced freezing tolerance in *Arabidopsis* leaves (Wanner and Junttila, 1999). An elevated level of sugars was also detected during cold acclimation in tomato plants (Song et al., 2015). The shoots of a freezing-tolerant pea genotype accumulated three times more sucrose than the shoots of a freezing-sensitive genotype at low but non-freezing temperature (Grimaud et al., 2013), suggesting that the exposure of tolerant pea plants to low temperatures activates the gluconeogenesis pathway, leading to the accumulation of soluble sugars. In a similar manner, the highest soluble sugar accumulation during the hardening of plants was detected at relatively high light intensity in the present work. This rise in sugar content may also contribute to the better chilling tolerance of maize plants. Chilling at night also caused a significant increase in the soluble sugar content in *Hevea brasiliensis* (Tian et al., 2016). The present results showed that while acclimation at moderately low temperature (15°C) and low light intensity reduced the level of glucose and sucrose, chilling at 5°C increased the levels of soluble sugars. At gene expression level, the effect of light was more emphasized than the cold itself. In both cases, greater number of down-regulated genes involved in the carbohydrate metabolism were found. There was no overlap found between carbohydrate-related genes induced either by cold or light. On the other hand, the gene expression of alpha/beta-hydrolases and the alpha-galactosidase 3 was silenced both at low temperature and under LL4. Similarly, the alpha-galactosidase proteins from barley and *Arabidopsis* were described with an important during dark induced senescence and has roles in leaf development by functioning in cell wall loosening and cell wall expansion (Chrost et al., 2007). The alpha/beta hydrolase superfamily proteins have versatile interactions of G-protein signalling under stress conditions (Khatri and Mudgil, 2015).

## CONCLUSIONS

The light intensity during the cold acclimation period may significantly affect cold acclimation processes in chilling-sensitive maize plants. Although photoinhibition may be dominant even at relatively high light intensity, light nevertheless contributes to the development of cold acclimation in maize. Interestingly, certain stress responses are light-dependent not only in the leaves, which sense the light directly, but also in the roots. As found earlier in frost-tolerant plants, light influences various light-related cold acclimation processes not directly, but at the gene expression and metabolomics levels. The results suggest that the photoinhibition induced by low temperature can be a necessary evil for cold acclimation processes in plants. The avoidance of exposure to high light intensity, especially at low temperature would appear to be required to protect the photosynthetic apparatus, but if the whole plant is to be protected from a subsequent cold shock, it may be necessary to accept the consequences of photodamage in the interests of acquiring cold-acclimated plants.

## AUTHOR CONTRIBUTIONS

GS designed the experiment, measured the sugars, and supervised the work. IM measured the chlorophyll-a fluorescence and made the bioinformatic analyses. MP and OG measured the lipid peroxidation, the electrolyte leakage, and the chlorophyll content. SR and CO made the validation of microarray. IM and BK carried out the annotation of microarray. TJ, IM, RV, and GS wrote the article.

## ACKNOWLEDGMENTS

Thanks are due to Tímea Oláh for her technical assistance. The authors wish to thank Dr. Viktória Kovács for the preparation of the RNA samples for microarray analysis. Thanks are also due to Barbara Hooper for revising the manuscript linguistically. This work was funded by grant K124430 from the National Research, Development and Innovation Office, Hungary.

## SUPPLEMENTARY MATERIAL

The Supplementary Material for this article can be found online at: https://www.frontiersin.org/articles/10.3389/fpls.2018.00850/full#supplementary-material

## REFERENCES

Altschul, S. F., Madden, T. L., Schäffer, A. A., Zhang, J., Zhang, Z., Miller, W., et al. (1997). Gapped BLAST and PSI-BLAST: a new generation of protein database search programs. *Nucl. Acids Res.* 25, 3389–3402. doi: 10.1093/nar/25.17.3389

Anderson, M. D., Prasad, T. K., Martin, B. A., and Stewart, C. R. (1994). Differential gene expression in chilling-acclimated maize seedlings and evidence for the involvement of abscisic acid in chilling tolerance. *Plant Physiol.* 105, 331–339. doi: 10.1104/pp.105.1.331

Apostol, S., Szalai, G., Sujbert, L., Popova, L. P., and Janda, T. (2006). Non-invasive monitoring of the light-induced cyclic photosynthetic electron flow during cold hardening in wheat leaves. *Z. Nat. C.* 61, 734–740. doi: 10.1515/znc-2006-9-1021

Benjamini, Y., and Yekutieli, D. (2001). The control of the false discovery rate in multiple testing under dependency. *Ann. Stat.* 29, 1165–1188. doi: 10.1214/aos/1013699998

Boldizsár, Á., Carrera, D. Á., Gulyás, Z., Vashegyi, I., Novák, A., Kalapos, B., et al. (2016a). Comparison of redox and gene expression changes during the vegetative/generative transition in crowns and leaves of wheat chromosome 5A substitution lines at low temperature. *J. Appl. Gen.* 57, 1–13. doi: 10.1007/s13353-015-0297-2

Boldizsár, Á., Vankova, R., Novák, A., Kalapos, B., Gulyás, Z., Pál, M., et al. (2016b). The mvp2 mutation affects the generative transition through the modification of transcriptome pattern, salicylic acid and cytokinin metabolism in *Triticum monococcum*. *J. Plant Physiol.* 202, 21–33. doi: 10.1016/j.jplph.2016.07.005

Bredenkamp, G. J., and Baker, N. R. (1994). Temperature-sensitivity of D1 protein metabolism in isolated *Zea mays* chloroplasts. *Plant Cell Environ.* 17, 205–210. doi: 10.1111/j.1365-3040.1994.tb00284.x

Catalá, R., Medina, J., and Salinas, J. (2011). Integration of low temperature and light signaling during cold acclimation response in *Arabidopsis*. *Proc. Natl. Acad. Sci. U.S.A.* 108, 16475–16480. doi: 10.1073/pnas.1107161108

Chrost, B., Kolukisaoglu, U., Schulz, B., and Krupinska, K. (2007). An alpha-galactosidase with an essential function during leaf development. *Planta* 225, 311–320. doi: 10.1007/s00425-006-0350-9

Foyer, C. H., Ruban, A. V., and Noctor, G. (2017). Viewing oxidative stress through the lens of oxidative signalling rather than damage. *Biochem. J.* 474, 877–883. doi: 10.1042/BCJ20160814

Fracheboud, Y., Jompuk, C., Ribaut, J.-M., Stamp, P., and Leipner, J. (2004). Genetic analysis of cold-tolerance of photosynthesis in maize. *Plant Mol. Biol.* 56, 241–253. doi: 10.1007/s11103-004-3353-6

Gill, S. S., and Tuteja, N. (2010). Reactive oxygen species and antioxidant machinery in abiotic stress tolerance in crop plants. *Plant Physiol. Biochem.* 48, 909–930. doi: 10.1016/j.plaphy.2010.08.016

Gómez, M., González, A., Sáez, C. A., Morales, B., and Moenne, A. (2015). Copper-induced activation of TRP channels promotes extracellular calcium entry, activation of CaMs and CDPKs, copper entry and membrane depolarization in *Ulva compressa*. *Front. Plant Sci.* 6:182. doi: 10.3389/fpls.2015.00182

Gondor, O. K., Janda, T., Soós, V., Pál, M., Majláth, I., Adak, M. K., et al. (2016a). Salicylic acid induction of flavonoid biosynthesis pathways in wheat varies by treatment. *Front. Plant Sci.* 7:1447. doi: 10.3389/fpls.2016.01447

Gondor, O. K., Szalai, G., Kovács, V., Janda, T., and Pál, M. (2016b). Relationship between polyamines and other cold-induced response mechanisms in different cereal species. *J. Agr. Crop Sci.* 202, 217–230. doi: 10.1111/jac.12144

Gray, G. R., Chauvin, L. P., Sarhan, F., and Huner, N. (1997). Cold acclimation and freezing tolerance (a complex interaction of light and temperature). *Plant Physiol.* 114, 467–474. doi: 10.1104/pp.114.2.467

Greaves, J. A. (1996). Improving suboptimal temperature tolerance in maize - the search for variation. *J. Exp. Bot.* 47, 307–323. doi: 10.1093/jxb/47.3.307

Grimaud, F., Renaut, J., Dumont, E., Sergeant, K., Lucau-Danila, A., Blervacq, A. S., et al. (2013). Exploring chloroplastic changes related to chilling and freezing tolerance during cold acclimation of pea (*Pisum sativum* L.). *J. Prot.* 80, 145–159. doi: 10.1016/j.jprot.2012.12.030

Gururani, M. A., Venkatesh, J., and Tran, L. S. P. (2015). Regulation of photosynthesis during abiotic stress-induced photoinhibition. *Mol. Plant* 8, 1304–1320. doi: 10.1016/j.molp.2015.05.005

Hammer, R., Harper, D. A. T., and Ryan, P. D. (2001). PAST: paleontological statistics software package for education and data analysis. *Pal. Electr.* 4, 1–9.

Heberle, H., Meirelles, G. V., da Silva, F. R., Telles, G. P., and Minghim, R. (2015). InteractiVenn: a web-based tool for the analysis of sets through Venn diagrams. *BMC Bioinformatics* 16:169. doi: 10.1186/s12859-015-0611-3

Janda, T., Majláth, I., and Szalai, G. (2014). Interaction of temperature and light in the development of freezing tolerance in plants. *J. Plant Growth Regul.* 33, 460–469. doi: 10.1007/s00344-013-9381-1

Janda, T., Szalai, G., Ducruet, J.-M., and Páldi, E. (1998). Changes in photosynthesis in inbred maize lines with different degrees of chilling tolerance grown at optimum and suboptimum temperatures. *Photosynthetica* 35, 205–212. doi: 10.1023/A:1006954605631

Janda, T., Szalai, G., Kissimon, J., Páldi, E., Marton, C., and Szigeti, Z. (1994). Role of irradiance in the chilling injury of young maize plants studied by chlorophyll fluorescence induction measurements. *Photosynthetica* 30, 293–299.

Khatri, N., and Mudgil, Y. (2015). Hypothesis: NDL proteins function in stress responses by regulating microtubule organization. *Front. Plant Sci.* 6:947. doi: 10.3389/fpls.2015.00947

Klughammer, C., and Schreiber, U. (2008). Saturation pulse method for assessment of energy conversion in PS I. *PAM Appl. Notes* 1, 11–14.

Kocsy, G. (2015). Die or survive? Redox changes as seed viability markers. *Plant Cell Environ.* 38, 1008–1010. doi: 10.1111/pce.12515

Lazár, D. (2015). Parameters of photosynthetic energy partitioning. *J. Plant Physiol.* 175, 131–147. doi: 10.1016/j.jplph.2014.10.021

Lee, C. M., and Thomashow, M. F. (2012). Photoperiodic regulation of the C-repeat binding factor (CBF) cold acclimation pathway and freezing tolerance in *Arabidopsis thaliana*. *Proc. Natl. Acad. Sci. U.S.A.* 109, 15054–15059. doi: 10.1073/pnas.1211295109

Legris, M., Klose, C., Costigliolo, C., Burgie, E., Neme, M., Hiltbrunner, A., et al. (2016). Phytochrome B integrates light and temperature signals in *Arabidopsis*. *Science* 354, 897–900. doi: 10.1126/science.aaf5656

Legris, M., Nieto, C., Sellaro, R., Prat, S., and Casal, J. J. (2017). Perception and signalling of light and temperature cues in plants. *Plant J.* 90, 683–697. doi: 10.1111/tpj.13467

Li, Z., Hu, G., Liu, X., Zhou, Y., Li, Y., Zhang, X., et al. (2016). Transcriptome sequencing identified genes and gene ontologies associated with early freezing tolerance in maize. *Front. Plant Sci.* 7:1477. doi: 10.3389/fpls.2016.01477

Liu, Y., Ji, X., Zheng, L., Nie, X., and Wang, Y. (2013). Microarray analysis of transcriptional responses to abscisic acid and salt stress in *Arabidopsis thaliana*. *Int. J. Mol. Sci.* 14, 9979–9998. doi: 10.3390/ijms14059979

Livak, K. J., and Schmittgen, T. D. (2001). Analysis of relative gene expression data using real-time quantitative PCR and the $2^{(-\Delta\Delta CT)}$ method. *Methods* 25, 402–408. doi: 10.1006/meth.2001.1262

Long, S. P., East, T. M., and Baker, N. R. (1983). Chilling damage to photosynthesis in young *Zea mays* I. effects of light and temperature variation on photosynthetic CO2 assimilation. *J. Exp. Bot.* 34, 177–188. doi: 10.1093/jxb/34.2.177

Marocco, A., Lorenzoni, C., and Fracheboud, Y. (2005). Chilling stress in maize. *Maydica* 50, 571–580.

Mohanty, S., Grimm, B., and Tripathy, B. C. (2006). Light and dark modulation of chlorophyll biosynthetic genes in response to temperature. *Planta* 224, 692–699. doi: 10.1007/s00425-006-0248-6

Mudunuri, U., Che, A., Yi, M., and Stephens, R. M. (2009). bioDBnet: the biological database network. *Bioinformatics* 25, 555–556. doi: 10.1093/bioinformatics/btn654

Pál, M., Horváth, E., Janda, T., Páldi, E., and Szalai, G. (2005). Cadmium stimulates the accumulation of salicylic acid and its putative precursors in maize (*Zea mays* L.) plants. *Physiol. Plant.* 125, 356–364. doi: 10.1111/j.1399-3054.2005.00545.x

Pál, M., Janda, T., and Szalai, G. (2011). Abscisic acid may alter the salicylic acid-related abiotic stress response in maize. *J. Agr. Crop Sci.* 197, 368–377. doi: 10.1111/j.1439-037X.2011.00474.x

Pospíšil, P. (2016). Production of reactive oxygen species by Photosystem II as a response to light and temperature stress. *Front. Plant Sci.* 7:1950. doi: 10.3389/fpls.2016.01950

Prasad, T. K. (1996). Mechanisms of chilling-induced oxidative stress injury and tolerance in developing maize seedlings: changes in antioxidant system, oxidation of proteins and lipids, and protease activity. *Plant J.* 10, 1017–1026. doi: 10.1046/j.1365-313X.1996.10061017.x

Sobkowiak, A., Jónczyk, M., Adamczyk, J., Solecka, D., Kuciara, I., Hetmanczyk, K., et al. (2016). Molecular foundations of chilling-tolerance of modern maize. *BMC Genomics* 17:125. doi: 10.1186/s12864-016-2453-4

Sobkowiak, A., Jonczyk, M., Jarochowska, E., Biecek, P., Trzcinska-Danielewicz, J., Leipner, J., et al. (2014). Genome-wide transcriptomic analysis of response to low temperature reveals candidate genes determining divergent cold-sensitivity of maize inbred lines. *Plant Mol. Biol.* 85, 317–331. doi: 10.1007/s11103-014-0187-8

Song, Y., Diao, Q., and Qi, H. (2015). Polyamine metabolism and biosynthetic genes expression in tomato (*Lycopersicon esculentum* Mill.) seedlings during cold acclimation. *Plant Growth Regul.* 75, 21–32. doi: 10.1007/s10725-014-9928-6

Szalai, G., Janda, T., Bartók, T., and Páldi, E. (1997). Role of light in changes in free amino acid and polyamine contents at chilling temperature in maize (*Zea mays* L.). *Physiol. Plant.* 101, 434–438.

Szalai, G., Janda, T., Páldi, E., and Szigeti, Z. (1996). Role of light in the development of post-chilling symptoms in maize. *J. Plant Physiol.* 148, 378–383. doi: 10.1016/S0176-1617(96)80269-0

Thimm, O., Blasing, O., Gibon, Y., Nagel, A., Meyer, S., Kruger, P., et al. (2004). MAPMAN: a user-driven tool to display genomics data sets onto diagrams of metabolic pathways and other biological processes. *Plant J.* 37, 914–939. doi: 10.1111/j.1365-313X.2004.02016.x

Thomashow, M. F. (1999). Plant cold acclimation. *Ann. Rev. Plant Physiol. Plant Mol. Biol.* 50, 571–599. doi: 10.1146/annurev.arplant.50.1.571

Tian, Y.-H., Yuan, H.-F., Xie, J., Deng, J.-W., Dao, X.-S., and Zheng, Y.-L. (2016). Effect of diurnal irradiance on night-chilling tolerance of six rubber cultivars. *Photosynthetica* 54, 374–380. doi: 10.1007/s11099-016-0192-z

Tian, T., Liu, Y., Yan, H., You, Q., Yi, X., Du, Z., et al. (2017). agriGO v2.0: a GO analysis toolkit for the agricultural community, 2017 update. *Nucleic Acids Res.* 45, W122–W129. doi: 10.1093/nar/gkx382

Trzcinska-Danielewicz, J., Bilska, A., Fronk, J., Zielenkiewicz, P., Jarochowska, E., Roszczyk, M., et al. (2009). Global analysis of gene expression in maize leaves treated with low temperature I. moderate chilling (14 °C). *Plant Sci.* 177, 648–658. doi: 10.1016/j.plantsci.2009.09.001

Van Buskirk, H. A., and Thomashow, M. F. (2006). *Arabidopsis* transcription factors regulating cold acclimation. *Physiol. Plant.* 126, 72–80. doi: 10.1111/j.1399-3054.2006.00625.x

Wallsgrove, R. M., Keys, A. J., Lea, P. J., and Miflin, B. J. (1983). Photosynthesis, photorespiration and nitrogen metabolism. *Plant Cell Environ.* 6, 310–309.

Wanner, L. A., and Junttila, O. (1999). Cold-induced freezing tolerance in *Arabidopsis*. *Plant Physiol.* 120, 391–400. doi: 10.1104/pp.120.2.391

Winfield, M. O., Lu, C., Wilson, I. D., Coghill, J. A., and Edwards, K. J. (2010). Plant responses to cold: transcriptome analysis of wheat. *Plant Biotech. J.* 8, 749–771. doi: 10.1111/j.1467-7652.2010.00536.x

Zhang, L., Xiao, S., Chen,Y. J., Xu, H., Li, Y. G., Zhang, Y.W., et al. (2017). Ozone sensitivity of four Pakchoi cultivars with different leaf colors: physiological and biochemical mechanisms. *Photosynthetica* 55, 478–490. doi: 10.1007/s11099-016-0661-4

**Conflict of Interest Statement:** The authors declare that the research was conducted in the absence of any commercial or financial relationships that could be construed as a potential conflict of interest.

frontiers in Plant Science

MINI REVIEW
published: 19 December 2018
doi: 10.3389/fpls.2018.01897

# Cryptochrome-Related Abiotic Stress Responses in Plants

*Victor D'Amico-Damião† and Rogério Falleiros Carvalho**

*Department of Biology Applied to Agriculture, São Paulo State University, São Paulo, Brazil*

It is well known that light is a crucial environmental factor that has a fundamental role in plant growth and development from seed germination to fruiting. For this process, plants contain versatile and multifaceted photoreceptor systems to sense variations in the light spectrum and to acclimate to a range of ambient conditions. Five main groups of photoreceptors have been found in higher plants, cryptochromes, phototropins, UVR8, zeitlupes, and phytochromes, but the last one red/far red wavelengths photoreceptor is the most characterized. Among the many responses modulated by phytochromes, these molecules play an important role in biotic and abiotic stress responses, which is one of the most active research topics in plant biology, especially their effect on agronomic traits. However, regarding the light spectrum, it is not surprising to consider that other photoreceptors are also part of the stress response modulated by light. In fact, it has become increasingly evident that cryptochromes, which mainly absorb in the blue light region, also act as key regulators of a range of plant stress responses, such as drought, salinity, heat, and high radiation. However, this information is rarely evidenced in photomorphogenetic studies. Therefore, the scope of the present review is to compile and discuss the evidence on the abiotic stress responses in plants that are modulated by cryptochromes.

**Keywords: abiotic stress acclimation, blue-light photoreceptor, cryptochromes, drought, heat, high light, salinity**

OPEN ACCESS

***Edited by:***
*Éva Hideg,*
*University of Pécs, Hungary*

***Reviewed by:***
*Andrew O'Hara,*
*Örebro University, Sweden*
*Laszlo Kozma-Bognar,*
*Hungarian Academy of Sciences, Hungary*

****Correspondence:***
*Rogério Falleiros Carvalho*
*rogerio.f.carvalho@unesp.br*
*orcid.org/0000-0003-1270-7372*
*†orcid.org/0000-0001-9497-7063*

***Specialty section:***
*This article was submitted to Plant Abiotic Stress, a section of the journal Frontiers in Plant Science*

***Received:*** *17 October 2018*
***Accepted:*** *06 December 2018*
***Published:*** *19 December 2018*

***Citation:***
*D'Amico-Damião V and Carvalho RF (2018) Cryptochrome-Related Abiotic Stress Responses in Plants. Front. Plant Sci. 9:1897. doi: 10.3389/fpls.2018.01897*

## INTRODUCTION

Sunlight is the most essential environmental signal for plant growth and development. Interestingly, its influence is not restricted to the photosynthesis process because light also plays a key role in transferring essential information, such as quality, quantity, periodicity, and direction, that ensures plant survival under environmental fluctuations (Kami et al., 2010; Demarsy et al., 2018). For this reason, photomorphogenesis has been well elucidated by modulating a plethora of plant processes from seed germination to fruiting (Kendrick and Kronenberg, 1994; Kami et al., 2010). In plants, several of these photomorphogenic responses are largely governed by the visible light spectrum (400–700 nm). In fact, variations in light are sensed by photoreceptors, which are photoreversible proteins with a prosthetic group/cofactor or an intrinsic amino acid (tryptophan) as a chromophore. Currently, five photoreceptor systems have been identified in higher plants: phytochromes (phys), which absorb wavelengths of red (600–700 nm) and far-red light (700–750 nm); blue light (BL)/ultraviolet (UV)-A photoreceptors (315–500 nm), which are represented by cryptochromes (crys), phototropins (phots) and zeitlupes (ZTL, FKF1, and LKP2); and UV Resistance Locus 8 (UVR8) photoreceptor, which operate through UV-B light (280–315 nm) (Chen and Chory, 2011; Christie et al., 2012; Ito et al., 2012; Jenkins, 2014; Christie et al., 2015; Mishra and Khurana, 2017).

Although there are several classes of plant photoreceptors, phytochromes were the first type of photoreceptor discovered and are the most characterized. These molecules are dimeric apoproteins (∼130 KDa) covalently linked to phytochromobilin, which is a linear tetrapyrrole that functions as a chromophore. The interconvertible forms of phytochromes allow their activation via the absorption of red light, as well as their inactivation via the absorption of far-red light (Chen and Chory, 2011). Thus, this sensor triggers the light-dependent signal transduction cascade to regulate the expression of numerous genes that result in specific physiological responses (Viczián et al., 2017). Furthermore, various reports have shown that the plant signaling pathways involved in the responses to abiotic and biotic stresses, including insect herbivory, salinity, drought, hot or cold temperatures, and UV-B radiation, are modulated by phytochromes (Donohue et al., 2008; Ballaré, 2009; Carvalho et al., 2011; D'Amico-Damião et al., 2015; Gavassi et al., 2017). However, these responses remain unclear due to the complex light signaling pathways that are operated by other photoreceptors along the light spectrum (Kami et al., 2010; Fiorucci and Fankhauser, 2017; Demarsy et al., 2018). Thus, regarding the intricate photomorphogenic organization, it is important to remember that, in addition to phytochromes, other molecules, such as crys, have also increasingly received attention with regard to light signaling.

Increasingly, crys have been shown to modulate plant responses from germination to fruiting, especially through wavelengths of blue, green, and UV-A light (Cashmore et al., 1999; Chaves et al., 2011). Crys are present from bacteria to humans, in plants, these photoreceptors are basically an apoprotein with two prosthetic groups (**Figure 1A**), the N-terminal photolyase homology-related (PHR) domain and a cryptochrome C-terminal extension (CCE) domain. The PHR domain contains the non-covalent binding site for 5, 10-methenyl tetrahydrofolate (MTHF) and flavin adenine dinucleotide (FAD), the two chromophores. FAD is a chromophore for BL that triggers photomorphogenesis, and the MTHF chromophore is a derivative of pterine that acts in the UV-A region, transferring excitation energy to FAD, which is a catalytic cofactor (Mishra and Khurana, 2017). In the model plant *Arabidopsis thaliana*, three crys were identified (cry1, cry2, and cry3). Cry1 and cry2 are located predominantly in the nucleus (Cashmore et al., 1999; Kleiner et al., 1999) and play a multifaceted role in various aspects of plant growth and development. For instance, cry1 primarily regulates photomorphogenic responses related to the inhibition of hypocotyl elongation, anthocyanin accumulation and cotyledon expansion, while cry2 plays a role in the hypocotyl inhibition, circadian clock and photoperiod-dependent flowering (Yu et al., 2010). However, cry3 is a DASH protein located in chloroplasts and mitochondria (Kleine et al., 2003), which works to repair UV-damaged DNA in a light-dependent manner (Mishra and Khurana, 2017). Overall, cryptochrome-dependent signaling pathways remain unclear because these physiological responses change with BL intensity (Kami et al., 2010) as well as with the plant species in question (Yang et al., 2017).

In addition to the variety of mechanisms orchestrated by crys, the modes of action by which these extraordinary photoreceptors work are very dynamic. For example, recent studies have revealed the role of crys in BL-dependent biosynthesis of reactive oxygen species (ROS) (Consentino et al., 2015; Jourdan et al., 2015; El-Esawi et al., 2017), which is a key signaling pathway for genes, such as those related to biotic and abiotic stresses, that have ROS-dependent transcription (Suzuki and Katano, 2018). In fact, these new findings contribute to the already established knowledge regarding the acclimation responses to biotic and abiotic stress mediated by crys, such as drought, salinity, heat, freezing, high radiation, UV-B light, and pathogen attack (Mao et al., 2005; Catalá et al., 2011; Ma et al., 2016; Zhou et al., 2017, 2018; Demarsy et al., 2018). However, although this information is mixed throughout few research studies already performed in the literature, here we discuss the evidence on cryptochrome-controlled plant acclimation responses under stressful environments and how these responses may occur (**Table 1**). Furthermore, the present review has compiled the most classic and current advances inherent to cry defense mechanisms against abiotic stress conditions.

## OSMOTIC STRESS ACCLIMATION: HOW DO CRYPTOCHROMES REGULATE THIS RESPONSE?

### Drought Stress

Drought is one of the most critical factors of plant production in agricultural systems (Lesk et al., 2016; González-Villagra et al., 2017; Sseremba et al., 2018). Given the evidence regarding the mechanisms that control plant responses to drought stress (Bechtold, 2018; Hussain et al., 2018; Meng, 2018), we would not be surprised that crys are an important part of these responses (Mishra and Khurana, 2017). Previous studies have demonstrated that crys play an interesting role in Arabidopsis drought stress tolerance (Mao et al., 2005). The authors found that Arabidopsis double mutant *cry1cry2* plants were clearly more drought-tolerant than the wild type (WT) after irrigation was suspended for 1 week. However, transgenic *CRY1-ovx* plants, which overexpress the CRY1 protein, exhibited excessive water loss, which was a response mainly associated with the enhanced stomatal aperture of the transgenic plants. This response seems to be strongly related to crys, particularly through their interaction with the downstream signaling protein CONSTITUTIVELY PHOTOMORPHOGENIC 1 (COP1) (Kang et al., 2009); COP1 represses stomatal opening (Delgado et al., 2012). However, the mechanisms by which crys modulate water loss under drought stress are still very unclear because this event is dependent on many factors, including hormones, mainly abscisic acid (ABA) (Miller et al., 2010; Saradadevi et al., 2017), and interactions with other BL photoreceptors, such as phototropins (Mao et al., 2005).

Regarding ABA, some evidence shows that this hormone is part of cry signaling during water stress. For example, transgenic lines of Arabidopsis overexpressing *TaCRY1*a and *TaCRY2* from monocot wheat (*Triticum aestivum*) exhibited a lower tolerance than did WT lines to osmotic stress (300 mM mannitol) and an ABA exogenous treatment (0.3 or 10 μM ABA)

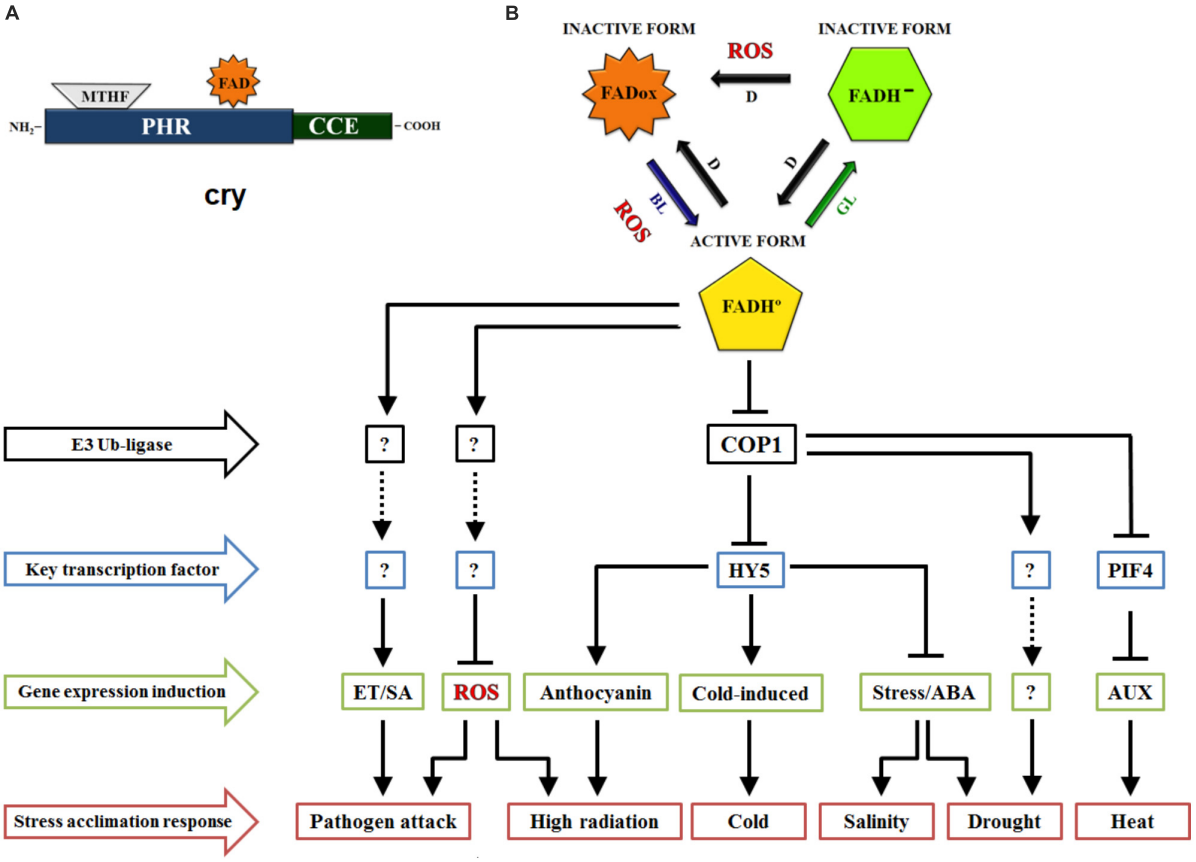


**FIGURE 1 |** Schematic view of cryptochromes (cry) role in stress acclimation responses. **(A)** Domain structure of cry consists of Photolyase-Homologous Region (PHR) domain and CRY C-terminal extension (CCE) domain. The cry chromophores methenyltetrahydrofolate (MTHF) and FAD are binding to PHR, a light perception domain. **(B)** FAD chromophore redox states of cry. FAD is oxidized (FADox) in the darkness (D), with the absorption peak in blue light (BL). On light exposure, FADox changes to the neutral semireduced state (FADH°), which allows the biological activity of cry in the plant cell. With the absorption peak in green light (GL), FADH° is induced to change to the totally reduced form (FAD-). An unclear subject around the reoxidation of FAD is the production of reactive oxygen species (ROS) during the process. Stress signaling pathway regulated by cryptochromes. From the blue light signaling, cry coordinate the negative regulation of COP1-dependent degradation of HY5 and PIF4 transcription factors, triggering changes in stress response target genes expression. Note that these are key pathways in the induction of genes related to signaling and/or biosynthesis of hormones, ROS and stress components. Although the complex signaling of cry in stress acclimation still involves some unknown components, certainly this photoreceptor play a crucial role in BL-dependent stress responses. Arrows means downregulation, T-bars indicate upregulation and dotted lines indicate unknown (?) signaling routes. E3 ubiquitin-ligase; COP1, constitutive photomorphogenic 1; HY5, long hypocotyl 5; PIF4, phytochrome interacting factor 4; ET, ethylene; SA, salicylic acid; ABA, abscisic acid; AUX, auxin.

throughout germination and postgermination development (Xu et al., 2009). Furthermore, these authors also showed the differential expression of *responsive to desiccation 29A* (*RD29A)* and *alcohol dehydrogenase 1* (*ADH1)*, two ABA/stress-responsive genes, in the transgenic lines. In fact, the plants overexpressing *TaCRY1a* showed a strong reduction in *RD29A* expression and a lower induction of *ADH1* under osmotic stress in comparison to plants overexpressing *TaCRY2*; the plants overexpressing *CRY1a* were also more sensitive to osmotic stress. In addition, *NAD(P)-binding Rossmann-fold superfamily protein* (*ABA2)*, which is a gene involved in adjusting ABA biosynthesis, was downregulated in *TaCRY1a-GFP* transgenic lines under ABA treatment and was downregulated in either *TaCRY1a-GFP* or *TaCRY2-GFP* transgenic lines under mannitol treatment, showing how crys coordinate molecular responses under drought via interactions with this stress hormone (Xu and Ma, 2009).

Although crys have been widely investigated in the Arabidopsis plant model (Liu et al., 2018a), recent molecular evidence in *Brassica napus*, an agriculturally important crop, has shown an interaction between cry1 and drought stress-related genes (Sharma et al., 2014). Moreover, *B. napus* cry1 overexpression (*OE-BnCRY1*) resulted in plants that were very sensitive to stress induced by a low osmotic potential (mannitol) when compared to WT, whereas the plants that were transformed with the antisense for cry1 (*AS-BnCRY1*) were more tolerant. Interestingly, cry1 overexpression reduced the transcript levels of genes related to the responses induced by water deficits (e.g., *late embryogenesis abundant protein 4-1*, *LEA4-1*; *dehydrin family protein*, *RAB18*; *nitrate reductase 1*, *NIA1*; *ascorbate peroxidase 1*, *APX1*; and *NAC domain containing protein 60*, *NAC060*). Indeed, these observations show us the involvement of crys in the drought stress acclimation responses. However, several

**TABLE 1 |** General description of stress responses controlled by cryptochromes in plants.

| Species | Type of stress | Cryptochrome | Stress response | Reference |
|---|---|---|---|---|
| *Arabidopsis thaliana* | Drought | cry1, cry2 | COP1, a repressor of stomatal opening is downregulates by crys | Mao et al., 2005 |
| | Drought and Salinity | cry1, cry2 | Cryptochromes-induced altered expression of stress/ABA-responsive genes | Xu and Ma, 2009; Xu et al., 2009 |
| | Salinity | cry1 | Overexpression of *SbCRY1a* confers oversensitive to salt stress | Zhou et al., 2018 |
| | High-light | cry1, cry2 | Cryptochromes inaffects chloroplast light-harvesting complex and redox equilibrium of photosynthetic apparatus | Walters et al., 1999; Weston et al., 2000 |
| | | cry1, cry2 | Cryptochromes promotes the transcription of ROS-responsive genes | Chen et al., 2013 |
| | | cry1 | Singlet oxygen–related programmed cell death is coordinated by cry1 | Danon et al., 2006 |
| | | cry1, cry2 | SIG5 modulates chloroplast transcripts in a cryptochromes-dependent manner | Belbin et al., 2017 |
| | | cry1 | Cry1 promote the photoprotective genes expression under excessive radiation | Kleine et al., 2007; Shaikhali et al., 2012 |
| | Heat | cry1 | PIF4 interact with cry1 controlling hypocotyl elongation under high temperature | Ma et al., 2016 |
| | Cold | – | Cryptochromes share transcription factors with cold acclimatization mechanisms | Catalá et al., 2011 |
| | Biotic | cry1 | Cry1 play a role in plant defense against pathogen attack | Zhou et al., 2017 |
| *Brassica napus* | Drought and Salinity | cry1 | Several osmotic stress responsive genes are downregulates by cry1 | Sharma et al., 2014 |
| *Solanum lycopersicum* | High-light | cry1, cry2 | Cryptochromes modulates a classic high-light stress response, the anthocyanin biosynthesis | Giliberto et al., 2005; Liu et al., 2018b |

questions, such as those related to cry stress response cascades and crosstalk mechanisms in many plant species under water deficit conditions, illuminate a new path for future research. Thus, molecular manipulation of plant crys or their signaling components, through the photoreceptor engineering, could potentially play a key role in improving drought tolerance traits.

## Salt Stress

In addition to the fact that drought and salt stress can share a common signaling pathway mainly due to their osmotic effects (Chaves et al., 2009), it was also shown that crys are part of the salt stress response via an ionic effect. Xu et al. (2009) observed that transgenic lines of Arabidopsis overexpressing *TaCRY1*a and *TaCRY2* (from *T. aestivum*) were more highly sensitive to high salt stress (120 mM NaCl) when compared with the watered control. Although salt stress impaired WT germination, this effect was more harmful to the transgenic lines than to the WT. However, the plants overexpressing *TaCRY1a* were more salt-sensitive than the plants overexpressing *TaCRY2*. In addition, real-time PCR revealed a remarkable increase in *TaCRY2* transcripts in Arabidopsis roots treated with salt stress (250 mM NaCl) after 12 h of stress induction for a 28 h period. Interestingly, the authors found that transcription of TaCRY1a was induced by salt stress after 24 h of exposure to the stressor agent.

An additional molecular event that supports the role of crys in salt stress responses comes from the overexpression of the *SbCRY1a* gene of sweet sorghum (*Sorghum bicolor*) in Arabidopsis under salinity conditions, in which a wide range of stress-responsive genes were modified (Zhou et al., 2018). Notably, the *cry1* mutant had a greater germination and seedling survival rate than the WT plants in response to ABA and salt conditions, showing more tolerance to salinity. On the other hand, the transgenic line *SbCRY1a* was oversensitive to salt stress. These mechanisms are likely regulated through the "LONG HYPOCOTYL 5-ABA INSENSITIVE 5" (HY5-ABI5) regulon, which triggers the differentiated expression of ABA/stress-responsive transcripts (*RD29A* and *RD22*), as speculated by the authors. Indeed, cry1 has been shown to control salt stress responses by ABA-dependent signaling pathways (Sharma et al., 2014). Obviously, these results allow researchers to provide more evidence on how cry signal transduction affects plant acclimation in salinity environments.

# BLUE LIGHT MEDIATES LIGHT STRESS RESPONSES THROUGH CRYPTOCHROMES

The metabolic adjustment of plants in stressful environments of excess or limited light depends on complex mechanisms that are already well established (Demmig-Adams and Adams, 1992; Demarsy et al., 2018). For instance, responsive molecules have important roles in plant photoprotection

against high radiation, including anthocyanin accumulation (Petrussa et al., 2013). Notably, BL modulation of anthocyanin accumulation in Arabidopsis seedlings is cry-dependent because *cry1* C-terminal mutant alleles are known to have altered anthocyanin levels (El-Esawi et al., 2017). In addition, leaf anthocyanin accumulation increased with the overexpression of *CRY1a* in tomato (*Solanum lycopersicum* L.) (Liu et al., 2018b). These authors showed that anthocyanin accumulation was related to variations in the mRNA and protein levels of the LONG HYPOCOTYL 5 (HY5) transcription factor, which interacts with the promoters of genes for anthocyanin biosynthesis (*dihydroflavonol 4—reductase*, *chalcone synthase 1* and *2*) (**Figure 1B**). Similarly, it was also reported that *CRY2* overexpression (*OE-LeCRY2*) in seedlings and leaves of tomato resulted in plants with an abundant accumulation of anthocyanins (Giliberto et al., 2005), indicating the pivotal role of crys on anthocyanin accumulation, even though light stress was not directly associated with the pigments in the above works.

Nevertheless, numerous studies have highlighted the participation of crys in other high light acclimation responses, such as the regulation of redox equilibrium of photosynthetic electron transport chain under high light stress (Walters et al., 1999). Moreover, Weston et al. (2000) observed that crys modulate key photoprotective components, even the chlorophyll a/b ratio and light-harvesting complex of photosystem II (LHCB), in high white light. WT Arabidopsis and its background *cry1* and *cry2* mutants and *cry1cry2* double mutant were submitted to continuous white light under a high (600 μmol $m^{-2}$ $s^{-1}$) or low (60 μmol $m^{-2}$ $s^{-1}$) intensity. In this context, the double mutant *cry1cry2* showed a strong decrease in LHCB accumulation and in the chlorophyll a/b ratio. Currently, strong evidence shows that crys can be part of the response to a light-induced redox imbalance through their interaction with the oxidative stress system (Danon et al., 2006) and specifically through their function in ROS production (Consentino et al., 2015), including the modifications of transcript levels of *ascorbate peroxidase 2* (*APX2*), *salt tolerance zinc finger* (*ZAT10*), sigma factor binding protein 1 (*SIB1*), *ethylene responsive element binding factor 4* (*ERF4*), and *NAD(P)H dehydrogenase B2* (*NDB2*) in Arabidopsis (Chen et al., 2013; **Figure 1B**). More recently, it was shown that the circadian regulation of sigma factor SIG5 transcription, which is a part of the chloroplast signaling pathway in response to light stress adaptation, is predominantly dependent on BL and crys (Belbin et al., 2017). Certainly, nuclear gene expression is severely damaged when light intensities are greater than the maximum potential of the chloroplast electron capacity (Demarsy et al., 2018; Foyer, 2018). In relation to this evidence, Shaikhali et al. (2012) identified two zinc finger GATA-type transcription factors as essential regulators of the photoprotective mechanisms orchestrated by crys. Through cry1 coordination, "ZINC FINGER PROTEIN EXPRESSED IN INFLORESCENCE MERISTEM LIKE1" (ZML1) and "ZML2" play a fundamental role in ROS scavenger responses to excess light. In another way, some discussions have been considered about ROS biosynthesis during crys inactivation (Consentino et al., 2015; Jourdan et al., 2015; El-Esawi et al., 2017). However, the link between the ROS produced under light and dark conditions merits further investigation (**Figure 1B**).

Regarding specific short-wavelength light signaling, such as UV-B, it has also been speculated that crys are part of these responses (Fortunato et al., 2015). In general, it is well known that UV-B light causes photodamage to DNA polymers and affects the electron balance in photosystem II (Czégény et al., 2016; Dotto and Casati, 2017), and it has been shown that cry-DASH homologs participate in restoring the photosynthetic efficiency of the photosystem II reaction center complexes in photosynthetic organisms (Vass et al., 2014). However, it is still hard to understand the mechanisms in which crys are part of high light stress response because a large system of photoprotective mechanisms is triggered under this condition, besides the fact that BL induces UV-B stress tolerance (Adamse et al., 1994; Hoffmann et al., 2015), and numerous high light-responsive genes are modulated by cry1 in Arabidopsis (Kleine et al., 2007). Therefore, there are potential opportunities for future studies about how cry signal transduction is involved in light stress responses to ambient fluctuations.

## WHAT CAN CRYPTOCHROMES REVEAL ABOUT OTHER PLANT STRESSES?

### Temperature Stress

Temperature stress triggers a large amount of metabolic damage in plants with well-known effects on protein stability and enzymatic reactions (Szymańska et al., 2017). In addition, the changes between the regulatory mechanisms of ROS and multiple pathways under heat stress have been recently reviewed, showing that downstream heat shock protein (HSP) is largely associated with these responses (Chen et al., 2018; Suzuki and Katano, 2018). In view of this, the HSP transcription profile is strongly regulated by crys (Facella et al., 2008; Yang et al., 2008), allowing a new perspectives on this BL photoreceptor in high temperature responses. A previous study demonstrated that cry1 repressed auxin biosynthesis to acclimate to heat stress, resulting in morphological changes in Arabidopsis seedlings (Ma et al., 2016). In addition, cry1 interacted with promoters such as *flavin-binding monooxygenase family protein* (*YUC8*), *indole-3-acetic acid inducible 19* (*IAA19*), and *indole-3-acetic acid inducible 29* (*IAA29*) under high temperature in a PHYTOCHROME-INTERACTING FACTOR 4 (PIF4)-dependent manner, which is an important part of BL-dependent signal transduction. On the other hand, the mechanisms of plant acclimation to cold stress in Arabidopsis include HY5, COP1, and Z-box, which are involved in these responses (Catalá et al., 2011); Z-box is a regulatory *cis*-element located in the promoter of responsive genes, such as HY5 transcription factor (Yadav et al., 2005). Coincidentally, these key regulators of light signaling are known to be mediated by crys through various interactions with other photoreceptors and signaling molecules (Mishra and Khurana, 2017), causing speculation that these BL photoreceptors have a role in a part of low temperature tolerance. However, as can be observed in this topic, temperature response modulated by crys in plants is

still uncommon, but intensive research on this subject should be considered.

## EPILOGUE

The role of crys in several events related to plant growth and development has been well established, including biotic stress response (Jeong et al., 2010; Wu and Yang, 2010; Zhou et al., 2017). However, few papers consider the participation of these photoreceptors in one of the most scientifically explored topics, abiotic stress in plants. Although much still needs to be revealed and understood about the subject, this review aimed to address and discuss different insights in the key function of BL in the acclimation to abiotic stresses via cry regulation. Thus, in this paper, we focus on compiling the responses to abiotic stress mediated by crys, although biotic stress is an interesting matter that may need to be intensively addressed (**Table 1**). In fact, since large changes in agronomically desirable traits have been shown in mutants and transgenic lines of important crops (Mawphlang and Kharshiing, 2017), regarding stress tolerance, potential future perspectives could be generated for agriculture on the manipulation of this multifaceted photoreceptor. However, we are aware that the subject is complex because it involves the interaction of crys with other photoreceptors as well as with the signaling of other important stress-modulating molecules (**Figure 1B**), such as plant hormones (Casal, 2000; Warpeha and Montgomery, 2016; Xu et al., 2018). Therefore, we encourage new investigations that clarify the underlying mechanisms of cry-related stress responses in different plant species. Certainly, these efforts will contribute to revealing other crys functions in the acclimation to stressful environmental conditions. Overall, exploring the molecular mechanisms by which crys mediate abiotic stress responses are issues that deserve further investigation.

## AUTHOR CONTRIBUTIONS

VD-D and RC designed this review, wrote the manuscript, and approved it for publication.

## FUNDING

Ph.D. fellowship granted to VD-D was financed by the Coordination for the Improvement of Higher Education Personnel – Brazil (CAPES) (Finance Code 001) and São Paulo Research Foundation (FAPESP) (grant number 2017/26130-9).

## ACKNOWLEDGMENTS

We apologize to those researchers whose work could not be discussed due to space limitations.

## REFERENCES

Adamse, P., Britz, S. J., and Caldwell, C. R. (1994). Amelioration of UV-B damage under high irradiance. II: role of blue light photoreceptors. *Photochem. Photobiol.* 60, 110–115. doi: 10.1111/j.1751-1097.1994.tb05075.x

Ballaré, C. L. (2009). Illuminated behaviour: phytochrome as a key regulator of light foraging and plant anti-herbivore defence. *Plant Cell Environ.* 32, 713–725. doi: 10.1111/j.1365-3040.2009.01958.x

Bechtold, U. (2018). Plant life in extreme environments: how do you improve drought tolerance? *Front. Plant Sci.* 9:543. doi: 10.3389/fpls.2018.00543

Belbin, F. E., Noordally, Z. B., Wetherill, S. J., Atkins, K. A., Franklin, K. A., and Dodd, A. N. (2017). Integration of light and circadian signals that regulate chloroplast transcription by a nuclear-encoded sigma factor. *New Phytol.* 213, 727–738. doi: 10.1111/nph.14176

Carvalho, R. F., Campos, M. L., and Azevedo, R. A. (2011). The role of phytochromes in stress tolerance. *J. Integr. Plant Biol.* 53, 920–929. doi: 10.1007/978-1-4614-6108-1_12

Casal, J. J. (2000). Phytochromes, cryptochromes, phototropin: photoreceptor interactions in plants. *Photochem. Photobiol.* 71, 1–11. doi: 10.1562/0031-8655200007100 1PCPPII2.0.CO2

Cashmore, A. R., Jarillo, J. A., Wu, Y. J., and Liu, D. (1999). Cryptochromes: blue light receptors for plants and animals. *Science* 284, 760–765. doi: 10.1126/science.284.5415.760

Catalá, R., Medina, J., and Salinas, J. (2011). Integration of low temperature and light signaling during cold acclimation response in *Arabidopsis*. *Proc. Natl. Acad. Sci. U.S.A.* 108, 16475–16480. doi: 10.1073/pnas.1107161108

Chaves, I., Pokorny, R., Byrdin, M., Hoang, N., Ritz, T., Brettel, K., et al. (2011). The cryptochromes: blue light photoreceptors in plants and animals. *Annu. Rev. Plant Biol.* 62, 335–364. doi: 10.1146/annurev-arplant-042110-103759

Chaves, M. M., Flexas, J., and Pinheiro, C. (2009). Photosynthesis under drought and salt stress: regulation mechanisms from whole plant to cell. *Ann. Bot.* 103, 551–560. doi: 10.1093/aob/mcn125

Chen, B., Feder, M. E., and Kang, L. (2018). Evolution of heat-shock protein expression underlying adaptive responses to environmental stress. *Mol. Ecol.* 27, 3040–3054. doi: 10.1111/mec.14769

Chen, D., Xu, G., Tang, W., Jing, Y., Ji, Q., Fei, Z., et al. (2013). Antagonistic basic helix-loop-helix/bZIP transcription factors form transcriptional modules that integrate light and reactive oxygen species signaling in *Arabidopsis*. *Plant Cell* 25, 1657–1673. doi: 10.1105/tpc.112.104869

Chen, M., and Chory, J. (2011). Phytochrome signaling mechanisms and the control of plant development. *Trends Cell Biol.* 21, 664–671. doi: 10.1016/j.tcb.2011.07.002

Christie, J. M., Arvai, A. S., Baxter, K. J., Heilmann, M., Pratt, A. J., O'Hara, A., et al. (2012). Plant UVR8 photoreceptor senses UV-B by tryptophan-mediated disruption of cross-dimer salt bridges. *Science* 335, 1492–1496. doi: 10.1126/science.1218091

Christie, J. M., Blackwood, L., Petersen, J., and Sullivan, S. (2015). Plant flavoprotein photoreceptors. *Plant Cell Physiol.* 56, 401–413. doi: 10.1093/pcp/pcu196

Consentino, L., Lambert, S., Martino, C., Jourdan, N., Bouchet, P. E., Witczak, J., et al. (2015). Blue-light dependent reactive oxygen species formation by *Arabidopsis* cryptochrome may define a novel evolutionarily conserved signaling mechanism. *New Phytol.* 206, 1450–1462. doi: 10.1111/nph.13341

Czégény, G., Mátai, A., and Hideg, É. (2016). UV-B effects on leaves—Oxidative stress and acclimation in controlled environments. *Plant Sci.* 248, 57–63. doi: 10.1016/j.plantsci.2016.04.013

D'Amico-Damião, V., Cruz, F. J. R., Gavassi, M. A., Santos, D. M. M., Melo, H. C., and Carvalho, R. F. (2015). Photomorphogenic modulation of water stress in tomato (*Solanum lycopersicum* L.): the role of phytochromes A, B1, and B2. *J. Hortic. Sci. Biotechnol.* 90, 25–30. doi: 10.1080/14620316.2015.11513149

Danon, A., Coll, N. S., and Apel, K. (2006). Cryptochrome-1-dependent execution of programmed cell death induced by singlet oxygen in *Arabidopsis thaliana*. *Proc. Natl. Acad. Sci. U.S.A.* 103, 17036–17041. doi: 10.1073/pnas.0608139103

Delgado, D., Ballesteros, I., Torres-Contreras, J., Mena, M., and Fenoll, C. (2012). Dynamic analysis of epidermal cell divisions identifies specific roles for COP10

in *Arabidopsis* stomatal lineage development. *Planta* 236, 447–461. doi: 10.1007/s00425-012-1617-y

Demarsy, E., Goldschmidt-Clermont, M., and Ulm, R. (2018). Coping with 'dark sides of the sun' through photoreceptor signaling. *Trends Plant Sci.* 23, 260–271. doi: 10.1016/j.tplants.2017.11.007

Demmig-Adams, B., and Adams, III, W. W. (1992). Photoprotection and other responses of plants to high light stress. *Annu. Rev. Plant Biol.* 43, 599–626. doi: 10.1146/annurev.pp.43.060192.003123

Donohue, K., Heschel, M. S., Butler, C. M., Barua, D., Sharrock, R. A., Whitelam, G. C., et al. (2008). Diversification of phytochrome contributions to germination as a function of seed-maturation environment. *New Phytol.* 177, 367–379. doi: 10.1111/j.1469-8137.2007.02281.x

Dotto, M., and Casati, P. (2017). Developmental reprogramming by UV-B radiation in plants. *Plant Sci.* 264, 96–101. doi: 10.1016/j.plantsci.2017.09.006

El-Esawi, M., Arthaut, L. D., Jourdan, N., d'Harlingue, A., Link, J., Martino, C. F., et al. (2017). Blue-light induced biosynthesis of ROS contributes to the signaling mechanism of *Arabidopsis* cryptochrome. *Sci. Rep.* 7:13875. doi: 10.1038/s41598-017-13832-z

Facella, P., Lopez, L., Carbone, F., Galbraith, D. W., Giuliano, G., and Perrotta, G. (2008). Diurnal and circadian rhythms in the tomato transcriptome and their modulation by cryptochrome photoreceptors. *PLoS One* 3:e2798. doi: 10.1371/journal.pone.0002798

Fiorucci, A. S., and Fankhauser, C. (2017). Plant strategies for enhancing access to sunlight. *Curr. Biol.* 27, R931–R940. doi: 10.1016/j.cub.2017.05.085

Fortunato, A. E., Annunziata, R., Jaubert, M., Bouly, J. P., and Falciatore, A. (2015). Dealing with light: the widespread and multitasking cryptochrome/photolyase family in photosynthetic organisms. *J. Plant Physiol.* 172, 42–54. doi: 10.1016/j.jplph.2014.06.011

Foyer, C. H. (2018). Reactive oxygen species, oxidative signaling and the regulation of photosynthesis. *Environ. Exp. Bot.* 154, 134–142. doi: 10.1016/j.envexpbot.2018.05.003

Gavassi, M. A., Monteiro, C. C., Campos, M. L., Melo, H. C., and Carvalho, R. F. (2017). Phytochromes are key regulators of abiotic stress responses in tomato. *Sci. Hortic.* 222, 126–135. doi: 10.1016/j.scienta.2017.04.035

Giliberto, L., Perrotta, G., Pallara, P., Weller, J. L., Fraser, P. D., Bramley, P. M., et al. (2005). Manipulation of the blue light photoreceptor cryptochrome 2 in tomato affects vegetative development, flowering time, and fruit antioxidant content. *Plant Physiol.* 137, 199–208. doi: 10.1104/pp.104.051987

González-Villagra, J., Kurepin, L. V., and Reyes-Díaz, M. M. (2017). Evaluating the involvement and interaction of abscisic acid and miRNA156 in the induction of anthocyanin biosynthesis in drought-stressed plants. *Planta* 246, 299–312. doi: 10.1007/s00425-017-2711-y

Hoffmann, A. M., Noga, G., and Hunsche, M. (2015). High blue light improves acclimation and photosynthetic recovery of pepper plants exposed to UV stress. *Environ. Exp. Bot.* 109, 254–263. doi: 10.1016/j.envexpbot.2014.06.017

Hussain, H. A., Hussain, S., Khaliq, A., Ashraf, U., Anjum, S. A., Men, S., et al. (2018). Chilling and drought stresses in crop plants: implications, cross talk, and potential management opportunities. *Front. Plant Sci.* 9:393. doi: 10.3389/fpls.2018.00393

Ito, S., Song, Y. H., and Imaizumi, T. (2012). LOV domain-containing f-box proteins: light-dependent protein degradation modules in *Arabidopsis*. *Mol. Plant* 5, 47–56. doi: 10.1093/mp/sss013

Jenkins, G. I. (2014). The UV-B photoreceptor UVR8: from structure to physiology. *Plant Cell* 26, 21–37. doi: 10.1105/tpc.113.119446

Jeong, R. D., Chandra-Shekara, A. C., Barman, S. R., Navarre, D., Klessig, D. F., Kachroo, A., et al. (2010). Cryptochrome 2 and phototropin 2 regulate resistance protein-mediated viral defense by negatively regulating an E3 ubiquitin ligase. *Proc. Natl. Acad. Sci. U.S.A.* 107, 13538–13543. doi: 10.1073/pnas.1004529107

Jourdan, N., Martino, C., El-Esawi, M., Witczak, J., Bouchet, P. E., d'Harlingue, A., et al. (2015). Blue-light dependent ROS formation by *Arabidopsis* cryptochrome-2 may contribute toward its signaling role. *Plant Signal. Behav.* 10:e1042647. doi: 10.1080/15592324.2015.1042647

Kami, C., Lorrain, S., Hornitschek, P., and Fankhauser, C. (2010). Light-regulated plant growth and development. *Curr. Top. Dev. Biol.* 91, 29–66. doi: 10.1016/S0070-2153(10)91002-8

Kang, C. Y., Lian, H. L., Wang, F. F., Huang, J. R., and Yang, H. Q. (2009). Cryptochromes, phytochromes, and COP1 regulate light-controlled stomatal development in *Arabidopsis*. *Plant Cell* 21, 2624–2641. doi: 10.1105/tpc.109.069765

Kendrick, R. E., and Kronenberg, G. H. M. (1994). *Photomorphogenesis in Plants*. Dordrecht: Kluwer Academic Publishers. doi: 10.1007/978-94-011-1884-2

Kleine, T., Kindgren, P., Benedict, C., Hendrickson, L., and Strand, Å (2007). Genome-wide gene expression analysis reveals a critical role for CRYPTOCHROME1 in the response of *Arabidopsis* to high irradiance. *Plant Physiol.* 144, 1391–1406. doi: 10.1104/pp.107.098293

Kleine, T., Lockhart, P., and Batschauer, A. (2003). An *Arabidopsis* protein closely related to *Synechocystis* cryptochrome is targeted to organelles. *Plant J.* 35, 93–103. doi: 10.1046/j.1365-313X.2003.01787.x

Kleiner, O., Kircher, S., Harter, K., and Batschauer, A. (1999). Nuclear localization of the *Arabidopsis* blue light receptor cryptochrome 2. *Plant J.* 19, 289–296. doi: 10.1046/j.1365-313X.1999.00535.x

Lesk, C., Rowhani, P., and Ramankutty, N. (2016). Influence of extreme weather disasters on global crop production. *Nature* 529, 84–87. doi: 10.1038/nature16467

Liu, C. C., Ahammed, G. J., Wang, G. T., Xu, C. J., Chen, K. S., Zhou, Y. H., et al. (2018a). Tomato CRY1a plays a critical role in the regulation of phytohormone homeostasis, plant development, and carotenoid metabolism in fruits. *Plant Cell Environ.* 41, 354–366. doi: 10.1111/pce.13092

Liu, C. C., Chi, C., Jin, L. J., Zhu, J., Yu, J. Q., and Zhou, Y. H. (2018b). The bZip transcription factor HY5 mediates CRY1a-induced anthocyanin biosynthesis in tomato. *Plant Cell Environ.* 41, 1762–1775. doi: 10.1111/pce.13171

Ma, D., Li, X., Guo, Y., Chu, J., Fang, S., Yan, C., et al. (2016). Cryptochrome 1 interacts with PIF4 to regulate high temperature-mediated hypocotyl elongation in response to blue light. *Proc. Natl. Acad. Sci. U.S.A.* 113, 224–229. doi: 10.1073/pnas.1511437113

Mao, J., Zhang, Y. C., Sang, Y., Li, Q. H., and Yang, H. Q. (2005). A role for *Arabidopsis* cryptochromes and COP1 in the regulation of stomatal opening. *Proc. Natl. Acad. Sci. U.S.A.* 102, 12270–12275. doi: 10.1073/pnas.0501011102

Mawphlang, O. I., and Kharshiing, E. V. (2017). Photoreceptor mediated plant growth responses: implications for photoreceptor engineering toward improved performance in crops. *Front. Plant Sci.* 8:1181. doi: 10.3389/fpls.2017.01181

Meng, L. S. (2018). Compound synthesis or growth and development of roots/stomata regulate plant drought tolerance or water use efficiency/water uptake efficiency. *J. Agric. Food Chem.* 66, 3595–3604. doi: 10.1021/acs.jafc.7b05990

Miller, G., Suzuki, N., Ciftci-Yilmaz, S., and Mittler, R. (2010). Reactive oxygen species homeostasis and signalling during drought and salinity stresses. *Plant Cell Environ.* 33, 453–467. doi: 10.1111/j.1365-3040.2009.02041.x

Mishra, S., and Khurana, J. P. (2017). Emerging roles and new paradigms in signaling mechanisms of plant cryptochromes. *Crit. Rev. Plant Sci.* 36, 89–115. doi: 10.1080/07352689.2017.1348725

Petrussa, E., Braidot, E., Zancani, M., Peresson, C., Bertolini, A., Patui, S., et al. (2013). Plant flavonoids—biosynthesis, transport and involvement in stress responses. *Int. J. Mol. Sci.* 14, 14950–14973. doi: 10.3390/ijms140714950

Saradadevi, R., Palta, J. A., and Siddique, K. H. (2017). ABA-mediated stomatal response in regulating water use during the development of terminal drought in wheat. *Front. Plant Sci.* 8:1251. doi: 10.3389/fpls.2017.01251

Shaikhali, J., Barajas-Lopéz, J., Östvös, K., Kremnev, D., Sánchez Garcia, A., Srivastava, V., et al. (2012). The CRYPTOCHROME1-dependent response to excess light is mediated through the transcriptional activators ZINC FINGER PROTEIN EXPRESSED IN INFLORESCENCE MERISTEM LIKE1 and ZML2 in *Arabidopsis*. *Plant Cell* 24, 3009–3025. doi: 10.1105/tpc.112.100099

Sharma, P., Chatterjee, M., Burman, N., and Khurana, J. P. (2014). Cryptochrome 1 regulates growth and development in *Brassica* through alteration in the expression of genes involved in light, phytohormone and stress signalling. *Plant Cell Environ.* 37, 961–977. doi: 10.1111/pce.12212

Sseremba, G., Tongoona, P., Eleblu, J., Danquah, E. Y., and Kizito, E. B. (2018). Heritability of drought resistance in *Solanum aethiopicum* Shum group and combining ability of genotypes for drought tolerance and recovery. *Sci. Hortic.* 240, 213–220. doi: 10.1016/j.scienta.2018.06.028

Suzuki, N., and Katano, K. (2018). Coordination between ROS regulatory systems and other pathways under heat stress and pathogen attack. *Front. Plant Sci.* 9:490. doi: 10.3389/fpls.2018.00490

Szymańska, R., Ślesak, I., Orzechowska, A., and Kruk, J. (2017). Physiological and biochemical responses to high light and temperature stress in plants. *Environ. Exp. Bot.* 139, 165–177. doi: 10.1016/j.envexpbot.2017.05.002

Vass, I. Z., Kós, P. B., Knoppová, J., Komenda, J., and Vass, I. (2014). The cry-DASH cryptochrome encoded by the sll1629 gene in the cyanobacterium *Synechocystis* PCC 6803 is required for photosystem II repair. *J. Photochem. Photobiol. B Biol.* 130, 318–326. doi: 10.1016/j.jphotobiol.2013.12.006

Viczián, A., Klose, C., Ádám, É, and Nagy, F. (2017). New insights of red light-induced development. *Plant Cell Environ.* 40, 2457–2468. doi: 10.1111/pce.12880

Walters, R. G., Rogers, J. J., Shephard, F., and Horton, P. (1999). Acclimation of *Arabidopsis thaliana* to the light environment: the role of photoreceptors. *Planta* 209, 517–527. doi: 10.1007/s004250050756

Warpeha, K. M., and Montgomery, B. L. (2016). Light and hormone interactions in the seed-to-seedling transition. *Environ. Exp. Bot.* 121, 56–65. doi: 10.1016/j.envexpbot.2015.05.004

Weston, E., Thorogood, K., Vinti, G., and López-Juez, E. (2000). Light quantity controls leaf-cell and chloroplast development in *Arabidopsis thaliana* wild type and blue-light-perception mutants. *Planta* 211, 807–815. doi: 10.1007/s004250000392

Wu, L., and Yang, H. Q. (2010). CRYPTOCHROME 1 is implicated in promoting R protein-mediated plant resistance to *Pseudomonas syringae* in *Arabidopsis*. *Mol. Plant* 3, 539–548. doi: 10.1093/mp/ssp107

Xu, F., He, S., Zhang, J., Mao, Z., Wang, W., Li, T., et al. (2018). Photoactivated CRY1 and phyB interact directly with AUX/IAA proteins to inhibit auxin signaling in *Arabidopsis*. *Mol. Plant* 11, 523–541. doi: 10.1016/j.molp.2017.12.003

Xu, P., and Ma, Z. (2009). Plant cryptochromes employ complicated mechanisms for subcellular localization and are involved in pathways apart from photomorphogenesis. *Plant Signal. Behav.* 4, 200–201. doi: 10.4161/psb.4.3.7756

Xu, P., Xiang, Y., Zhu, H., Xu, H., Zhang, Z., Zhang, C., et al. (2009). Wheat cryptochromes: subcellular localization and involvement in photomorphogenesis and osmotic stress responses. *Plant Physiol.* 149, 760–774. doi: 10.1104/pp.108.132217

Yadav, V., Mallappa, C., Gangappa, S. N., Bhatia, S., and Chattopadhyay, S. (2005). A basic helix-loop-helix transcription factor in *Arabidopsis*, MYC2, acts as a repressor of blue light–mediated photomorphogenic growth. *Plant Cell* 17, 1953–1966. doi: 10.1105/tpc.105.032060

Yang, Y., Li, Y., Li, X., Guo, X., Xiao, X., Tang, D., et al. (2008). Comparative proteomics analysis of light responses in cryptochrome1-304 and columbia wild-type 4 of *Arabidopsis thaliana*. *Acta Biochim. Biophys. Sin.* 40, 27–37. doi: 10.1111/j.1745-7270.2008.00367.x

Yang, Z., Liu, B., Su, J., Liao, J., Lin, C., and Oka, Y. (2017). Cryptochromes orchestrate transcription regulation of diverse blue light responses in plants. *Photochem. Photobiol.* 93, 112–127. doi: 10.1111/php.12663

Yu, X., Liu, H., Klejnot, J., and Lin, C. (2010). The cryptochrome blue light receptors. *Arabidopsis Book* 8:e0135. doi: 10.1199/tab.0135

Zhou, T., Meng, L., Ma, Y., Liu, Q., Zhang, Y., Yang, Z., et al. (2018). Overexpression of sweet sorghum cryptochrome 1a confers hypersensitivity to blue light, abscisic acid and salinity in *Arabidopsis*. *Plant Cell Rep.* 37, 251–264. doi: 10.1007/s00299-017-2227-8

Zhou, X., Zhu, T., Zhu, L. S., Luo, S. S., Deng, X. G., Lin, H. H., et al. (2017). The role of photoreceptors in response to cucumber mosaic virus in *Arabidopsis thaliana*. *J. Plant Growth Regul.* 36, 257–270. doi: 10.1007/s00344-016-9635-9

**Conflict of Interest Statement:** The authors declare that the research was conducted in the absence of any commercial or financial relationships that could be construed as a potential conflict of interest.

frontiers in Plant Science

ORIGINAL RESEARCH
published: 16 April 2019
doi: 10.3389/fpls.2019.00471

# Carbon Orientation in the Diatom *Phaeodactylum tricornutum*: The Effects of Carbon Limitation and Photon Flux Density

*Parisa Heydarizadeh[1], Brigitte Veidl[1], Bing Huang[1], Ewa Lukomska[2], Gaëtane Wielgosz-Collin[3], Aurélie Couzinet-Mossion[3], Gaël Bougaran[2], Justine Marchand[1] and Benoît Schoefs[1]**

[1] Metabolism, Bioengineering of Microalgal Molecules and Applications, Mer Molécule Santé, Le Mans University, IUML FR 3473 CNRS, Le Mans, France, [2] Physiology and Biotechnology of Algae Laboratory, IFREMER, Nantes, France, [3] Mer Molécule Santé, University of Nantes, IUML FR 3473 CNRS, Nantes, France

OPEN ACCESS

**Edited by:**
Tibor Janda,
Centre for Agricultural Research (MTA), Hungary

**Reviewed by:**
Inna Khozin-Goldberg,
Ben-Gurion University of the Negev, Israel
Tore Brembu,
Norwegian University of Science and Technology, Norway

***Correspondence:**
Benoît Schoefs
benoit.schoefs@univ-lemans.fr

**Specialty section:**
This article was submitted to Plant Abiotic Stress, a section of the journal Frontiers in Plant Science

**Received:** 08 January 2019
**Accepted:** 28 March 2019
**Published:** 16 April 2019

**Citation:**
Heydarizadeh P, Veidl B, Huang B, Lukomska E, Wielgosz-Collin G, Couzinet-Mossion A, Bougaran G, Marchand J and Schoefs B (2019) Carbon Orientation in the Diatom *Phaeodactylum tricornutum*: The Effects of Carbon Limitation and Photon Flux Density. Front. Plant Sci. 10:471. doi: 10.3389/fpls.2019.00471

Diatoms adapt to changing environmental conditions in very efficient ways. Among the mechanisms that can be activated, the reorientation of carbon metabolism is crucial because it allows the storage of energy into energy-dense molecules, typically lipids. Beside their roles in physiology, lipids are commercially interesting compounds. Therefore studies dealing with this topic are relevant for both basic and applied science. Although the molecular mechanisms involved in the reorientation of carbon metabolism as a response to a deficiency in nutrients such as nitrogen or phosphorus has been partially elucidated, the impacts of carbon availability on the implementation of the reorientation mechanisms remain unclear. Indeed, it has not been determined if the same types of mechanisms are activated under carbon and other nutrient deficiencies or limitations. The first aim of this work was to get insights into the physiological, biological and molecular processes triggered by progressive carbon starvation in the model diatom *Phaeodactylum tricornutum*. The second aim was to investigate the effects of the growth light intensity on these processes. For such a purpose three different photon flux densities 30, 300, and 1000 μmol photons $m^{-2}$ $s^{-1}$ were used. The results presented here demonstrate that under carbon limitation, diatom cells still reorient carbon metabolism toward either phospho*enol*pyruvate or pyruvate, which serves as a hub for the production of more complex molecules. The distribution of carbon atoms between the different pathways was partially affected by the growth photon flux density because low light (LL) provides conditions for the accumulation of chrysolaminarin, while medium light mostly stimulated lipid synthesis. A significant increase in the amount of proteins was observed under high light (HL).

**Keywords: diatom, carbon deficiency, carbon metabolism, stress, light intensity, regulation, biotechnology, phospho*enol*pyruvate**

## INTRODUCTION

Diatoms constitute the most abundant group of marine eukaryotic organisms with more than 200 genera and approximately 100,000 species and most have still to be discovered (e.g., Heydarizadeh et al., 2014; Bork et al., 2015; Vinayak et al., 2015; Beauger et al., 2019). It is well established that diatoms are able to adapt to a broad range of environmental conditions including light irradiances and nutrient concentrations through adjustment of their physiology and biochemical activity (e.g., Schoefs et al., 2017) while maintaining high growth rates and a high efficiency of carbon incorporation into different organic metabolites (Nymark et al., 2009). Yet, excessive or insufficient incident photon flux density constrains diatom optimal performance in terms of biomass and metabolite composition (Goldman, 1980; Vidoudez and Pohnert, 2008; Barofsky et al., 2009, 2010; Carvalho et al., 2011). These metabolites are generated along a network of biochemical pathways, the core of which being occupied by the central carbon metabolism. Many stress conditions result in the reorientation of the carbon metabolism toward the accumulation of energy-dense molecules such as lipids (for reviews, see Sayanova et al., 2017; Zulu et al., 2018). The accumulation of these energy-dense molecules is only possible when a source of carbon is available (Parupudi et al., 2016; Heydarizadeh et al., 2017). The fact that most of the stress conditions trigger the same type of response let us hypothesize that the reorientation of carbon metabolism toward the accumulation of energy-dense molecules could constitute a default response mechanism of diatoms to a stress. At first glance, testing this hypothesis seems important only from the academic point of view but a more careful examination of the question reveals its broad interest. In natural conditions, the weak $CO_2$ solubilization in water forces algae to use carbon concentration mechanism(s) (CCM) to acquire more carbon, the amount of which being still limiting for biomass production. On the other hand, our calculations predict that even with 100% utilization of industrial $CO_2$ waste for lipid production, there is not enough atmospheric $CO_2$ to be converted for feeding all transport now (Vinayak et al., 2015). Also, the costs of $CO_2$ used in industrial setups are prohibitive. Altogether, it seems that $CO_2$-limitation could be a limiting factor for the development of an efficient algal biotechnological process as it is already for algae living in the natural environment.

The metabolic reorientation of carbon can be tightly regulated by light (Dron et al., 2012). Recently, Heydarizadeh et al. (2017) showed that under carbon-limited conditions, a sudden transition in the growth light intensity impacts the use of pyruvate/phospho*enol*pyruvate for the production of building blocks: organic acids under low light (LL) and lipids and proteins under high light (HL). Little is still known about carbon flux direction inside the cell, partition between the different pathways, transporters and molecular mechanisms behind light acclimation in diatoms (e.g., Marchand et al., 2018). One way to follow these mechanisms consists in exploring genes encoding proteins associated with the pathways because the level of gene expression may affect enzyme amount and, thus, flux distribution (Depauw et al., 2012; Heydarizadeh et al., 2014).

The experiments presented here have been performed on clonal populations of the marine diatom *Phaeodactylum tricornutum* because the completion of its genome sequencing (Bowler et al., 2008) made it a "model" diatom for genomic, biochemical and physiological studies (Thiriet-Rupert et al., 2016; Gruber and Kroth, 2017; Kroth et al., 2017, 2018).

## MATERIALS AND METHODS

### Experimental Strategy, Growth Rate, and Sampling

Pt4-type *Phaeodactylum tricornutum* Bohlin (UTEX 646) was grown according to Heydarizadeh et al. (2017). Approximately $10^5$ cells $mL^{-1}$ of an axenic culture in exponential phase of *P. tricornutum* were batch cultured in 200 mL of f/2 prepared with artificial seawater (Guillard and Ryther, 1962) in three biological replications. The growth medium was supplemented with $NaHCO_3$ (8%) at the initiation of the culture. The growth photon flux densities of 30, 300, and 1000 μmol photons PAR $m^{-2}$ $s^{-1}$ were used as low light (LL), optimal (ML) and high (HL) photon flux densities, respectively, using cool-white fluorescent tubes (Philips Master TL-D 90 DE luxe 58W/965 and Osram L58/77 FLUORA). These levels of irradiance were chosen according to the light saturation index value ($E_k$) parameters obtained for *P. tricornutum* grown under 300 μmol photons PAR $m^{-2}$ $s^{-1}$ (Heydarizadeh et al., 2017).

Cell counting was carried out regularly using a Neubauer hemocytometer. Growth rate was obtained after fitting growth kinetics with the sigmoid equation using the software CurveExpert Basic[1]. For short time intervals, the daily division rate ($\mu_{ddr}$) was estimated using (Equation 1):

$$\mu_{ddr}(\text{cell d}^{-1}) = [\ln N_t - \ln N_{t-1}]/\Delta t \quad (1)$$

where $N_t$ and $N_{t-1}$ are the number of cells at time t and t-1.

Because cell physiology is dependent on the growth conditions, the elucidation of the underlying mechanisms requires us to compare samples that are in closely similar physiological states (Heydarizadeh et al., 2014). To fulfill this condition, the time-course of the daily division rate ($\mu_{ddr}$) (Equation 1) along the growth period was calculated for each photon flux density (data not shown). Regardless of the light intensity, the time-courses present a bell-shape curve peaking at the middle of the exponential phase and zeroing in lag and plateau phases (data not shown). Sampling times were chosen when the time-course of $\mu_{ddr}$ was reaching its maximum or was close to zero, defining the three sampling times used for each lighting condition. Three biological replicates were conducted.

The photon flux densities were measured using a 4π waterproof light probe (Walz, Germany) connected to a Li-Cor 189 quantum meter. In all cases a 12/12 h light/dark cycle and 21°C conditions were maintained.

[1]http://www.curveexpert.net/

## Pigment Extraction, Photosynthetic, and Respiratory Activity, PI-Curve

Rates of oxygen evolution were measured at 21°C in the light and in the dark using a fiber-optic oxygen meter (Pyroscience® FireSting $O_2$, Germany) with a diatom suspension (1.5 mL). The cells were illuminated at their growth photon flux density. Respiration was measured in the dark immediately after each measurement of photosynthesis. Gross photosynthesis was calculated as net photosynthesis plus respiration, assuming that respiratory activity ($R_d$) was the same in light and in darkness, respectively (Heydarizadeh et al., 2017). Because, $R_d$ is impacted by light photon flux density used during the gross photosynthesis measurement, $R_d$ was measured after the oxygen evolution measurement in the light. Calculated values were normalized to cell density or chlorophyll (Chl) *a* amount. Chl *a,* Chl c and total carotenoids were measured according to Heydarizadeh et al. (2017).

## Chlorophyll Fluorescence Yield Measurement

Chlorophyll fluorescence yield was monitored at the growth temperature using a fluorimeter FMS-1 (Hansatech®) using 2 mL of culture according to Roháček et al. (2014). To avoid $CO_2$ shortage during measurements, the cultures were provided with $NaHCO_3$ (final: 4 mM, 0.2 M/stock).

The analysis of the qN relaxation kinetics into its components qNi, qNf, and qNs was performed as explained in Roháček et al. (2014). The quality of the regression procedure was assessed using two parameters: (1) values of $qN_1 = qNf + qNi + qNs$ were compared to the experimental values of qN and (2) coefficient of determination of the fit ($R^2$) was taken as a measure of how well observed outcomes are replicated by the regression model (Steel and Torrie, 1960). In this work a regression was considered as good when $R^2 \geq 0.90$.

## Quantification of Intracellular Carbon and Nitrogen, Cellular Carbon, and Nitrogen Quotas, C and N Uptake Rate

$Q_N$ and $Q_C$ were determined for each growth phase using a C/N elemental analyzer (EAGER 300, Thermo Scientific). Samples were filtered through precombusted Whatman GF/C glass filters under gentle vacuum (50 mm Hg) and dried at 70°C for 48 h. The volume of solution filtered was adjusted to have either 0.1 or 0.3 $10^8$ cells per filter.

The C ($\rho_C$) and N uptake rates ($\rho_N$) were estimated according to Marchetti et al. (2012) using Equation 2 and Equation 3 when cultures were at equilibrium (i.e., at maximum growth rate and at stationary phase). During phase 1, $\rho$ was also estimated by $\mu * Q$, which is a default value for $\rho$. Indeed, since cultures were inoculated 3 days before sampling for $Q$ assessment, they were considered to be near equilibrium.

$$\rho_C(\text{pg cell}^{-1}\ \text{d}^{-1}) = \mu_{ddr} Q_C \quad (2)$$

$$\rho_N(\text{pg cell}^{-1}\ \text{d}^{-1}) = \mu_{ddr} Q_N \quad (3)$$

$$\text{Total amount of C immobilized (pg)} = Q_C N_{phase\_3} \quad (4)$$

$$\text{Total amount of N immobilized (pg)} = Q_N N_{phase\_3} \quad (5)$$

where $N_{phase\_3}$ represents the number of cells in phase 3.

## Determination of the Protein Content

To isolate total proteins, cell cultures were centrifuged (5000 × *g*, 5 min, 4°C), overlaid in 2 mM EDTA (ethylenediaminetetraacetic acid) and homogenized using Ultra Turrax® (IKA-Analysentechnik GmbH) for 10 min. After centrifugation of the mixture (13,000 × *g*, 5 min, 4°C), protein amount in the supernatant was measured according to Bradford (1976).

## Determination of the Lipid Content

Lipids were extracted from $10^8$ to $10^9$ cells following a modified Bligh and Dyer method (Bligh and Dyer, 1959). Briefly, freeze-dried cells were steeped in dichloromethane/methanol (2:1,v/v) for 2 h at room temperature. The extract was filtered, washed with distilled water and evaporated to dryness under a stream of nitrogen. The lipids were determined gravimetrically.

## Determination of Chrysolaminarin Content

Cellular β-1,3-glucan was extracted according to Granum and Myklestad (2002) with some modifications. Briefly, $10^7$ cells were harvested by filtration and each filter was transferred directly to a glass vial and stored at −20°C until analysis. The cellular β-1,3-glucans were extracted by $H_2SO_4$ (50 mM) at 60°C for 10 min using a water bath. The extract was centrifuged at maximum acceleration for 10 min (4°C). The resulting supernatant was collected and transferred into a new tube and dried at 60°C. Twenty five μL of 3% aqueous phenol and 2.5 mL concentrated $H_2SO_4$ were added to 2 mL of sample and the mixture was immediately vortexed. The tubes were allowed to stand for 30 min, and then cooled with running water. Absorbance at 485 nm was measured. The amount of chrysolaminarin was calculated using glucose (stock concentration: 50 μg $mL^{-1}$) as a standard.

## Primer Design

A total of 33 different enzymes involved in carbon metabolism pathways of the diatom *P. tricornutum* were selected and the corresponding genes (74) coding each enzyme (see **Figure 6** and **Supplemental Data 1**) were searched in genomic data published by Kroth et al. (2008).

## RNA Extraction and qRT-PCR

1.5 $10^8$ cells were collected by filtration at the 3 phases and at the 3 light intensities. Total RNA extraction, reverse transcription and real time PCR reactions were performed using the primers and the protocol described in Heydarizadeh et al. (2017). Out of the 12 housekeeping gene (HKG) candidates, the most stable (tbp, ubi, and rps) were selected to normalize the target genes (TG). The calculation of the relative expression (RE) was based on the comparative Ct method (Livak and Schmittgen, 2001): $RE = ((E_{TG})^{\Delta Ct TG})/(E_{HKG})^{\Delta Ct HKG})$ with $\Delta Ct = Ct_{Calibrator}$-

$Ct_{sample}$ (Pfaffl et al., 2004). Three biological replicates were used. Heatmap analyses were performed using Netwalker 1.0 (Komurov et al., 2012).

# RESULTS

## Effect of Light Intensity on the Growth of *Phaeodactylum tricornutum*

Regardless the growth irradiance intensity, the growth curve of *P. tricornutum* could be fitted using a logistic law. The curves presented typical phases, i.e., lag, exponential and plateau phases. In the rest of the manuscript, we will refer to these different phases as phase 1, phase 2, and phase 3, respectively (**Figure 1**). No significant difference ($p < 0.05$) between the growth curves under ML and HL was observed. Cell density under LL was significantly lower ($p < 0.05$) than under ML and HL and growth phases were delayed in LL. Accordingly, the specific maximum growth rate (μ) and generation time (G), were similar under ML and HL, whereas these values were lower under LL (**Table 1**).

**TABLE 1 |** Impact of the light intensity on culture growth rate and generation time of *Phaeodactylum tricornutum*.

| Irradiance (μmol photons PAR $m^{-2}$ $s^{-1}$) | 30 (LL) | 300 (ML) | 1000 (HL) |
|---|---|---|---|
| μ ($d^{-1}$) | 0.340 ± 0.003* | 0.873 ± 0.009 | 0.865 ± 0.010 |
| G (d) | 2.039 ± 0.048* | 0.797 ± 0.008 | 0.806 ± 0.009 |

*Growth rates (μ) and generation times (G) were calculated from the curves of **Figure 1** using the equation indicated in the "Materials and Methods" section. Under LL, the rate of cell division was circa 30% less than under ML and HL. Mean values ± SE (n = 3–5). Significant different data are indicated by an asterisk (Tukey Test, $p \leq 0.05$).*

## Pigment Content

Total pigment content was higher under LL compared to ML and HL regardless the growth phase. The total pigment content increased along with growth (**Figure 2**) due to the accumulation of Chl *a* and total carotenoids (**Supplemental Data 2**). However, the pigment content in phase 2 was impacted by the light intensity, i.e., it decreased when the photon flux density increased (**Figure 2**). The Chl a/Chl c ratio varied in opposite directions under LL and ML/HL: under LL, it increased from phases 1 to 2 and then decreased until phase 3 (**Supplemental Figure SD2.1**). At the end of phase 3 the ratio was similar for all conditions.

## Photosynthetic and Respiratory Activities

Regardless if the net photosynthesis ($A_{max}$) and respiratory activity ($R_d$) were expressed relatively to the cell number (**Figures 3A,B**) or to the Chl *a* content (**Figures 3C,D**), $A_{max}$ was always higher than $R_d$. When taken individually, $R_d$ and $A_{max}$ were relatively constant during growth but $R_d$ decreased in phase 3 suggesting a strong reduction of the metabolic activity.

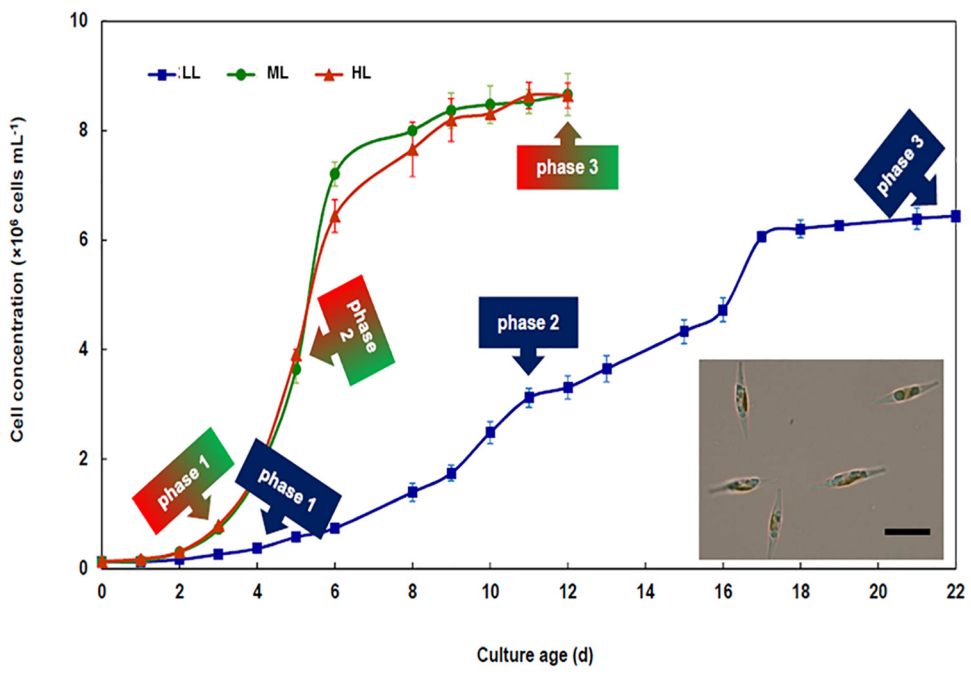


**FIGURE 1 |** Growth of *Phaeodactylum tricornutum* under different light intensities. Time course of cell density of cultures developing under 30 (LL), 300 (ML), and 1000 (HL) μmol photons PAR $m^{-2}$ $s^{-1}$. Each curve presents typical growth phases, i.e., lag (phase 1), exponential (phase 2), and plateau (phase 3). The sampling time in each phase is indicated using arrows. The insert presents a light microscopy picture of *Phaeodactylum tricornutum* grown under ML. The bar indicates 10 μm. Mean values obtained from three biological replicates and SD are presented.

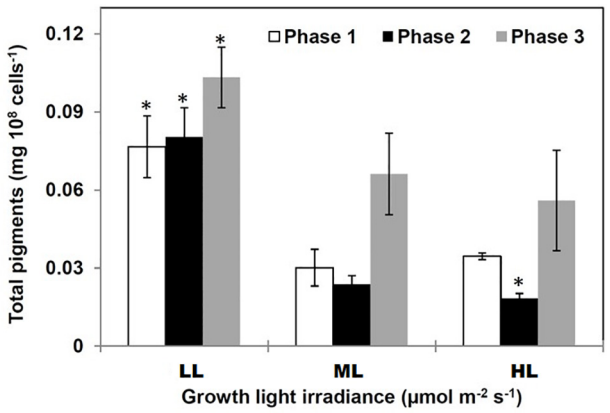


**FIGURE 2 |** Total pigments in *Phaeodactylum tricornutum* grown under different light intensities. Pigment accumulated in diatoms in two growing conditions: (1) under LL (regardless the growth phase) and in phase 3 (regardless the growth photon flux density). Data are mean values ± SE ($n$ = 3) and error bars represent SD. Means followed by asterisks are significantly different from the corresponding value in ML ($p < 0.05$, student's $t$-test).

## Photochemical and Nonphotochemical Quenching Analysis

Typical Chl *a* fluorescence recordings are presented in **Supplemental Figure SD3.1**. **Figure 4A** compares the variations of photochemical and nonphotochemical processes using characteristic parameters (photochemical: ΦP0, ΦII, qP, 1-qP; nonphotochemical: ($q_0$, qN)) during growth under the different light intensities. The meaning of the parameters and the equations used for calculations are presented in **Supplemental Table SD3.1**. The maximum quantum yield of photosystem II (PSII) photochemistry (ΦP0) in cells grown under different light conditions and different growth phases was around 0.6 (**Figure 4A**) suggesting that cells were healthy. This result contrasts with the effective quantum yield of photochemical energy conversion in PSII (ΦII), which progressively reduced from LL to HL. When compared to ML, the effective quantum yield of photochemical energy conversion in PSII was higher, about 60, 53, and 125% (Phases 1, 2, and 3, respectively) in cells grown under LL. No significant change of qP was observed during the different growth phases under either of the light intensities showing that diatoms were well adapted to the growth conditions. However, the qP values decreased as the light intensity increased. Under HL, qP values were approximately 50% of the values under LL (**Figure 4A**). The values of 1-qP, that quantifies the fraction of closed reaction centers, varied accordingly (**Figure 4A**). The absorption of an excess of photons triggers nonphotochemical quenching mechanisms of energy dissipation as heat (Roháček et al., 2008). The related parameters qN and q0 reflect the excess radiation converted to heat during the actinic radiation. These parameters increased with increasing photon flux density. Under LL, they were close to zero, indicating that under this lighting condition, there was no excess of absorbed energy.

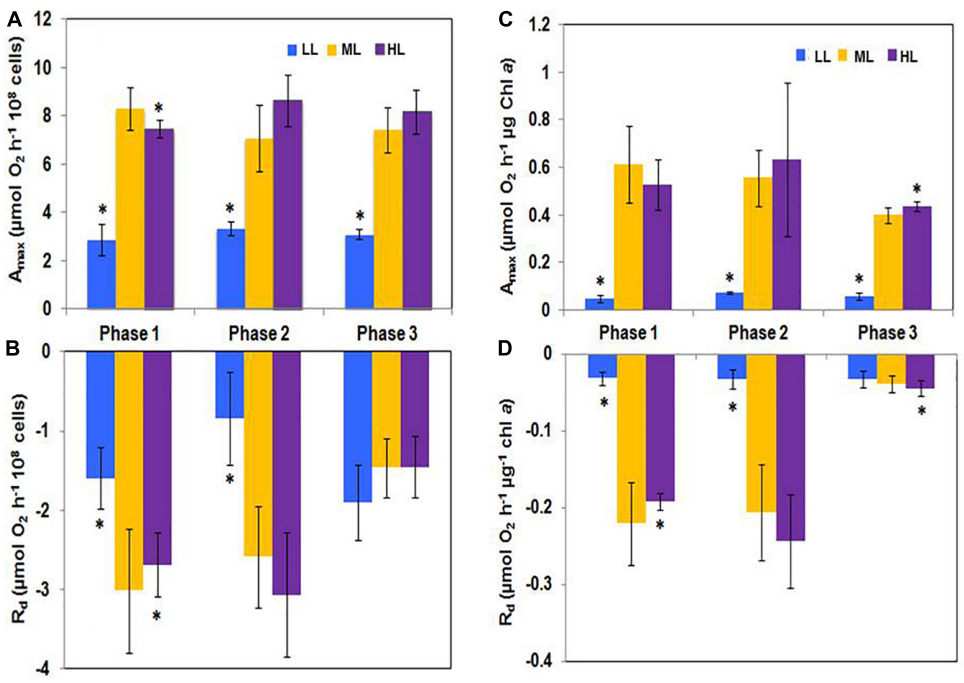


**FIGURE 3 | (A,C)** Net photosynthesis ($A_{max}$) and **(B,D)** respiration ($R_d$) activities in *Phaeodactylum tricornutum* grown under different light intensities. $A_{max}$ and $R_d$ were significantly higher under ML and HL than under LL. However, their values did not change along the growth at any of the grown photon flux densities. Under LL, $A_{max}$ was reduced while respiration was high, staying, however below. Values represent the mean ± SE ($n$ = 3) and error bars represent SD. Means followed by asterisks are significantly different from the corresponding value in ML ($p < 0.05$).

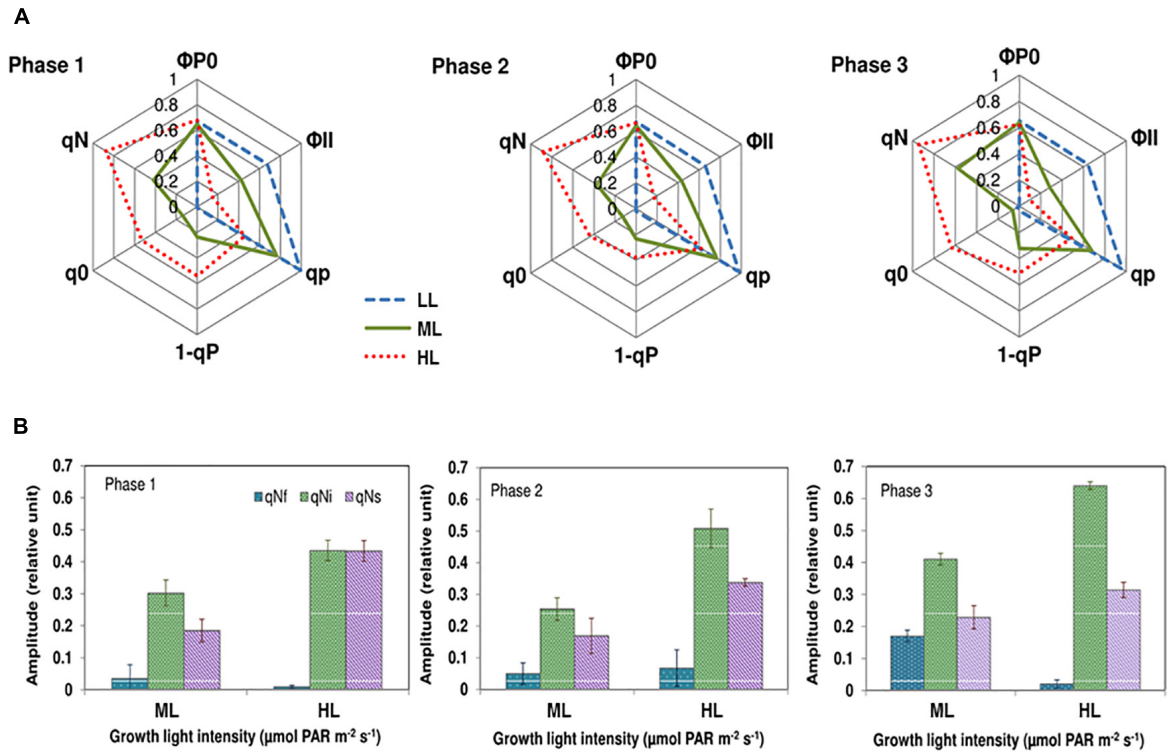


**FIGURE 4 |** Chlorophyll fluorescence kinetic parameters during the induction and the relaxation of the nonphotochemical quenching in *Phaeodactylum tricornutum* grown under different light intensities and during different growth phases. **(A)** The fluorescence kinetic parameters during the induction of the nonphotochemical quenching. The maximum quantum yield of PSII photochemistry (ΦP0) in cells grown under different light condition and different growth phases was constant (almost 0.6), suggesting that cells were healthy. This result contrasts with the effective quantum yield of photochemical energy conversion in PSII (ΦP0), which progressively reduced from LL to HL. The photochemical quenching (qP) that quantifies the actual fraction of PSII reaction centers staying open during the illumination. qP values decreased as the light intensity increased in an antiparallel manner with 1-qP, that quantifies the fraction of closed reaction centers. The nonphotochemical quenching parameters qN and q0 reflect the excess radiation converted to heat during the actinic radiation. Under LL, qN, and q0 are close to zero, indicating that under this lighting condition, there was no excess of absorbed energy. The intensity of these parameters was higher under ML and HL, suggesting that under these photon flux densities, part of the incoming energy needed to be dissipated as heat. **(B)** The components qNf, qNi, and qNs during the relaxation of the nonphotochemical quenching. Light-adapted cells relaxed qN in the dark (**Supplemental Data 3**). The mathematical analyses of the relaxation kinetic allowed the determination of three individual components that are denoted qNs, qNi, and qNf. The intensity of qNi and qNs were always the largest in cells grown under HL whereas the intensity of qNf was the largest under ML, except in phase 2 in which the values were not significantly different. The proportion of qNi increased from phases 1 to 3. qNs was the second mostly intense components. Its amplitude decreased from phases 1 to 3 under HL while it remained constant under ML.

To decipher the mechanisms contributing to the dissipation of the excess of energy activated under ML and HL, relaxation of the nonphotochemical quenching was recorded. When adapted to light conditions (Fs phase) cells were placed in the dark, qN gradually relaxed (**Supplemental Figure SD3.1**). In agreement to Roháček et al. (2014) three individual components were found: qNi relies on the dissipation of the proton gradient (ΔpH relaxation) and diatoxanthin epoxidation. qNf seems to be related to fast conformational changes occurring within the thylakoid membranes in the vicinity of the PSII complexes, whereas qNs could be related to photoinhibition and/or partial dissipation of the pH gradient (for a detailed explanation, see **Supplemental Data 3**). Regardless the growth phase and the growth light, the less intense component was qNf while the most intense component was qNi. The amplitude of qNf remains at the basic levels except in phase 3 under ML. The intensity of qNi and qNs were always higher in cells grown under HL than under ML whereas the intensity of qNf was always higher in cells grown under ML than under HL, except in phase 2 in which the values were not significantly different from each other. The proportion of qNi increased from phases 1 to 3 (**Figure 4B**). qNs was the second mostly intense component. Its amplitude slightly decreased from phases 1 to 3 under HL while it remained constant under ML (**Figure 4B**).

## N and C Fluxes to Lipids, Carbohydrates, and Proteins

Because primary metabolism and physiological activities mostly rely on the C and N availability and cell uptake, the cellular N and C quota ($Q_N$ and $Q_C$, respectively) were recorded. The time-courses of $Q_N$ and $Q_C$ were different according to the irradiance level: under LL, $Q_N$ and $Q_C$ decreased from phases 1 to 2 and increased from phases 2 to 3. Under ML, $Q_N$ and $Q_C$ decreased continuously whereas under HL, the decrease occurred only between phases 2 and 3 (**Figures 5A,B**). N and C uptake rates

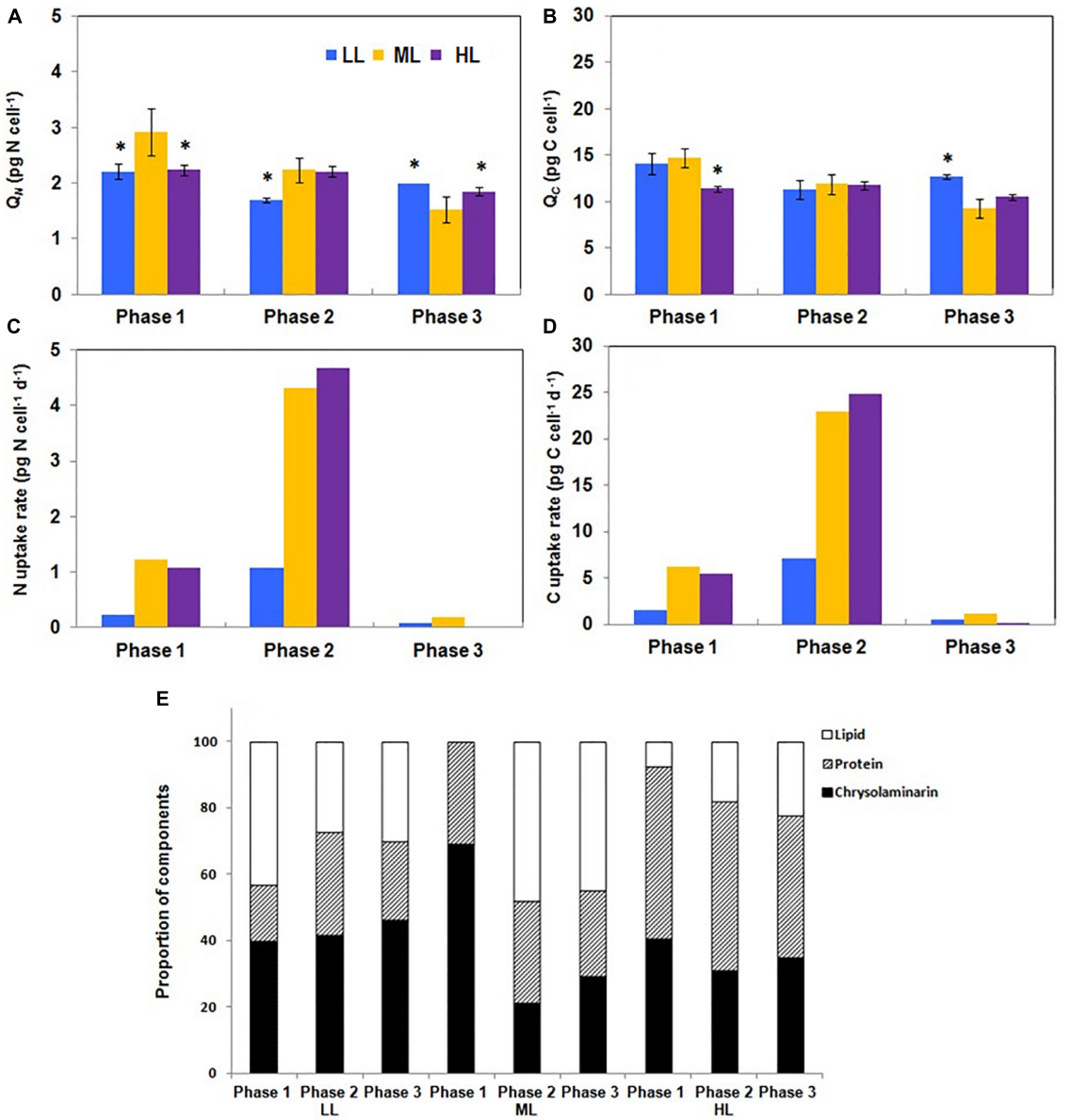


**FIGURE 5 |** Modifications of the carbon, nitrogen, chrysolaminarin, protein and lipid content of *Phaeodactylum tricornutum* during growth under different photon flux densities. **(A,B)** The carbon and nitrogen cellular quota are not constant along growth. Under LL, $Q_N$, and $Q_C$ decreased from phases 1 to 2 and increased from phases 2 to 3 whereas under ML, $Q_N$, and $Q_C$ decreased continuously. Under HL, the decrease occurred only between phases 2 and 3. **(C,D)** The carbon and nitrogen uptake are maximum in phase 2. The rate of C and N uptake were the most intense in phase 2 and very reduced in phases 1 and 3. **(E)** The celluar quota in proteins, lipids and chrysolaminarin is impacted by the growth photon flux density. The relative amount of LPC was greatly impacted by the photon flux density. Lipids were the most abundant in phase 1 under LL whereas under ML and HL, they were barely detectable **(E).** Under LL, the relative abundance of lipids decreased during the transition from phases 1 to 2 and then remained constant until phase 3. This contrasts with ML and HL for which lipid proportion increased until phase 2 (ML) or phase 3 (HL). Data are mean values ± SE ($n$ = 3) and error bars represent SD. Means followed by asterisks are significantly different from the corresponding value in ML ($P \leq 0.05$, student's $t$-test).

were the most intense in phase 2 and very reduced in phase 3 (**Figures 5C,D**). When expressed relatively to $Q_N$, $Q_C$ varied only significantly in phase 3 in function of the growth light intensity: it increased from LL to HL (data not shown). When normalized to the Chl amount, the $Q_C$/Chl *a* between phases 1 and 2 changed according to the growth light intensity: under LL, it slightly decreased, remained constant under ML and increased in HL. In phase 3, the values were similarly weak for each condition (data not shown).

The yield of C fixation ranged between 73 (LL and ML) and 78% (HL) whereas the yield of N fixation was around 10%, regardless of the light intensity (**Table 2**). The fixed N and C are used for the synthesis of cellular building blocks including lipids, proteins and chrysolaminarin (collectively "LPC"). To evaluate

**TABLE 2 |** Quantitative and relative amounts of C and N immobilized in the cells in phase 3.

| | LL | ML | HL |
|---|---|---|---|
| Total C amount (mg) | 197 | 197 | 199 |
| Relative amount of the initial C consumed (%) | 73 | 73 | 78 |
| Total N amount (mg) | 3.0 | 2.3 | 2.8 |
| Relative amount of the initial N consumed (%) | 10 | 8 | 9 |

*At the end of the studied period, approximately the same proportion of the initial carbon content has been consumed.*

if a shift in C and N orientation occurred, the total amount of LPC was measured in the culture media and in the cells. None of these compounds could be detected in the culture media (data not shown), showing that export of such material was low or under the detection limits. The relative amount of LPC was greatly impacted by light intensity. For instance, in phase 1 and under LL, lipids represent a bit more than 40% of the total cellular mass of LPC whereas under ML and HL, lipids were barely detectable at that stage of growth (**Figure 5E**). Under LL, the relative abundance of lipids decreased during the transition from phases 1 to 2 and then remained constant until phase 3. This contrasts with ML and HL for which the lipid proportion increased until phase 2 (ML) or phase 3 (HL) (**Figure 5E**).

The relative abundance of chrysolaminarin was the highest (70%) in phase 1 under ML. It dramatically decreased during the transition to phase 2 whereas under LL and HL it did not change by more than 8%. The relative amount of proteins was the highest (55%) under HL. Under this growth irradiance, it decreased only from phases 2 to 3 by *circa* 10% (**Figure 5E**).

## Changes in Selected mRNA Expression During Growth

To elucidate the reorganization of the metabolic circuits, the expression levels of 74 genes coding 33 enzymes involved in the central carbon metabolism were studied. A detailed description of the carbon metabolism is presented in **Figure 6**. A global view (heatmap) of the changes in the expression of the 74 genes of *P. tricornutum* based on growth phases under the three light intensities is shown in **Figure 7**. Out of the 74 genes, only 12 showed a particular profile regardless the light intensity (**Figure 7**): a particularly high up-regulation for PEPCK, FbaC5 and PPDK is observed while down-regulation occurred for PGP, GOX2, PYC2, GAPC1, PK2, CA7, TPI_2, ME1, and PDH1) (**Figure 7**). Under LL, genes encoding the $HCO_3^-$ transporters SLV4_1 and SLV4_3 involved in the biophysical CCM were down-regulated (up to −10 and −3-fold their expression in phase 1, respectively) while the two carbonic anhydrases (CA) (bCA4 and bCA5) were highly up-regulated in phase 3 (+12- and +3.5-fold the expression of these genes in phase 1). In the same conditions, the plastid rbcL and rbcS encoding two subunits of the RuBisCO from the Calvin cycle were down-regulated, (respectively, −11 and −3-fold the expression of phase 1 for phase 3). Most of the genes coding enzymes of the glycolysis in the three cell compartments in which glycolysis occurs were particularly down expressed. The genes encoding PGAM3 and GDCH (+3.5 and +4-fold respectively, in phase 2 compared to phase 1) were, however, up-regulated (**Figure 7**).

The pattern of mRNA expression during the growth of the culture for ML and HL was quite similar (**Figure 7**). An up-regulation of the genes encoding PYC1, Fba4, GDCT, GPI_1, GAPDH, and FBPC4 was highlighted (**Figure 7**) though not observed in LL. Genes particularly down-regulated along the growth in ML and HL (while not observed in LL) include genes encoding: (1) the single mitochondrial GAPC4 involved in glycolysis, reaching for ML (-29 and –47–fold, respectively, in phases 2 and 3 the expression of this gene in phase 1) and for HL (−27 and –61–fold, respectively); (2) FBP and PK4 both involved in cytosolic glycolysis (**Figure 6**).

## Light Intensity Influenced mRNA Expression

To determine how gene expression can be regulated under different light intensities, mRNA levels in each growth phase were compared and $\log_2$ fold change expressed relatively to ML (**Figure 8**). The strongest differences are found for LL and in particular in phases 1 and 3.

In phase 1, LL stimulated the expression of most of the genes studied and in particular (1) most of the genes encoding enzymes of the Calvin cycle and glycolysis and (2) mitochondrial genes encoding PYC1 and PEPCK from the biochemical CCM (+11 and +7-fold, respectively, their expression in ML). No sharp differences are observed for HL (**Figure 8**).

In phase 2, the strongest differences in LL and HL compared to ML were found in the biophysical CCM where mostly down-regulations were observed (**Figure 8**).

In phase 3, particular pathways are up-regulated: (1) the biophysical CCM: mostly genes encoding the two bCAs (bCA4 and bCA5) with +36 and +13-fold, respectively, in LL while mostly genes coding aCA and $HCO_3^-$ transporters (+4.5-fold in CA1) in HL (**Figure 8**); (2) the photorespiration pathway in LL: +8.5, +7, and +6-fold for, respectively, the mitochondrial GDCP, GOX2, and PGP (**Figure 7**) and (3) several genes encoding enzymes of the Calvin cycle (+8 and +5-fold for FbaC5 and TPI_1 respectively) or the chloroplast glycolysis (+60-fold for GAPC1). The genes encoding the plastid rbcS and rbcL were, however, strongly down-regulated in LL (−7.5 and −11-fold, respectively).

# DISCUSSION

Diatoms are among the most important contributors to the 100 gigatons of $CO_2$ yearly converted into biomaterials and organic compounds (Field et al., 1998). Both the capacity of carbon fixation and the fate of fixed carbon atoms are strongly impacted by environmental factors. Among them, carbon availability (Heydarizadeh et al., 2017) and light (Darko et al., 2014) occupy unique places because the former provides the atom units required for the production of other cellular molecules whereas the latter is a vehicle for environmental information and of energy for photosynthesis, that in turn, is used for the synthesis of carbon based molecules. Diatoms acclimate to changing light

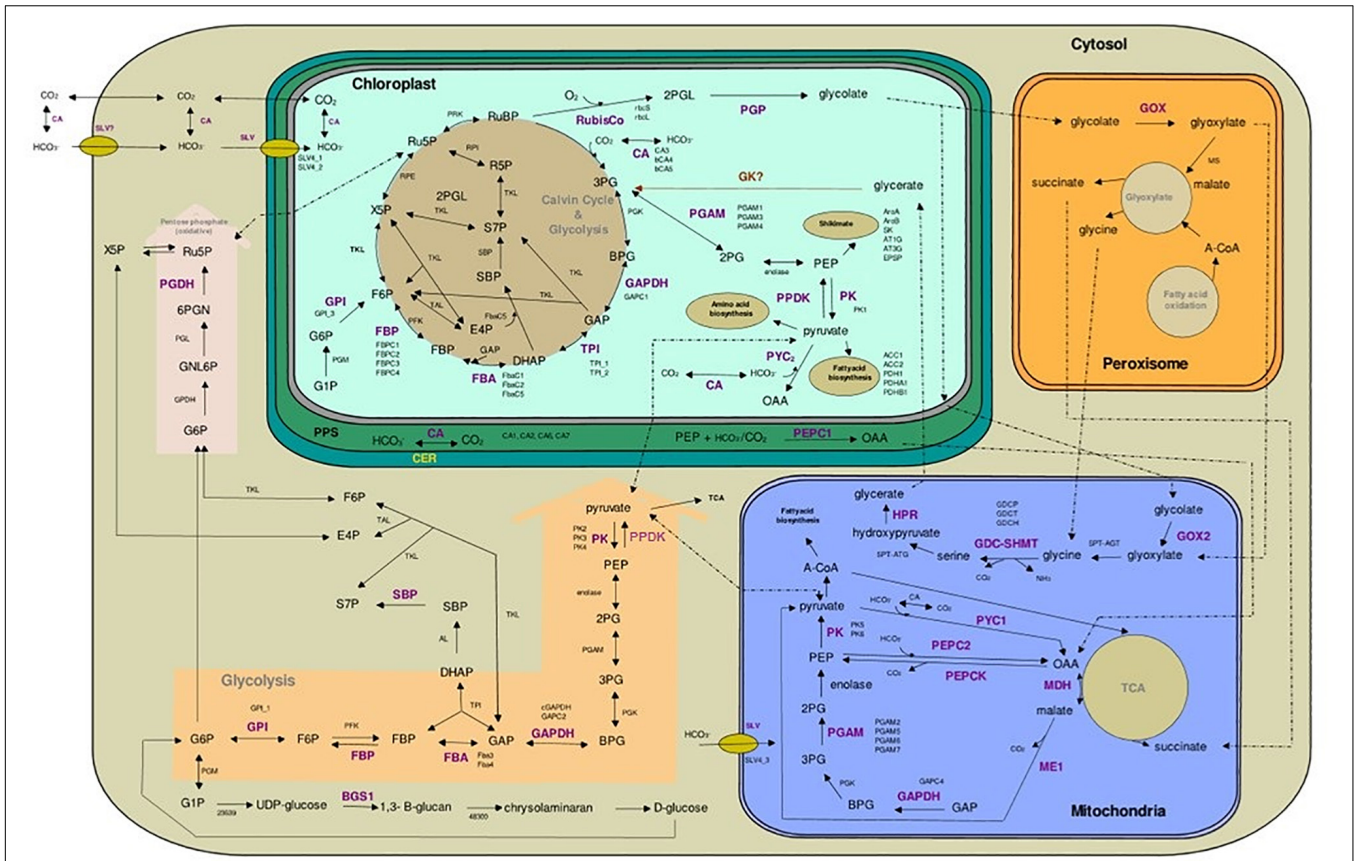


**FIGURE 6 |** Cellular pathways and processes of central carbon metabolism in *Phaeodactylum tricornutum*. All red depicted enzymes are the key enzymes and their related gene/isogenes are listed beside. RUBP, D-ribulose-1,5-bisphosphate; 3PG, 3-phospho-*D*-glycerate; BPG, 1,3-diphosphateglycerate; GAP, D-glyceraldehyde-3-phosphate; DHAP, dihydroxyacetone phosphate; FBAC, chloroplastic fructose-1,6-bisphosphate aldolase; FBP, fructose-1,6-bisphosphate; F6P, D-fructose-6-phosphate; X5P, D-xylulose-5-phosphate; Ru5P, D-ribulose-5-phosphate; SBP, D-sedoheptulose-1,7-bisphosphate; S7P, D-sedoheptulose-7-phosphate; R5P, D-ribose-5-phosphate; E4P, D-erythrose-4-phosphate; 2PGL, 2-phosphoglycolate; 2PG, 2-phosphoglycerate; PEP, phospho*enol*pyruvate; OAA, oxaloacetate; A-CoA, acetyl-CoA; G1P, D-glucose 1-phosphate; G6P, D-glucose-6-phosphate; GNL6P, D-glucono-δ-lactone-6-phosphate; 6PGN, 6-phospho-D-gluconate; PPS, periplasmic space; ER, endoplasmic reticulum (chloroplastic); ACC1, ACC2, Acetyl-CoA-carboxylase; PDH1, PDHA1, PDHB, pyruvate dehydrogenase E1; BGS1, glycosyl transferase.

intensities in a very efficient way (Wagner et al., 2006; Roháček et al., 2014). The regulation mechanisms involved in this process are still not completely elucidated (Nymark et al., 2009; Bailleul et al., 2010; Chauton et al., 2013). In this study, we have compared the impacts of the growth photon flux densities on the reorientation of the carbon metabolism of *P. tricornutum* grown under progressive $CO_2$ limitation with the aim to highlight how the partitioning of carbon among its potential sinks is impacted.

## The Photon Flux Density Impacts Growth and the Energetic Metabolism

The effects of environmental factors on cell development, physiology and regulation mechanisms depend on cell status (Jia et al., 2015). Therefore, a careful study on the effects of growth light intensity requires the comparison of cells from cultures at similar developmental stages. To fulfill this requirement, the actual growth rate was calculated and the samples were prepared when the actual growth rate was at either maximum or minimum. Under LL, the mitosis frequency was *circa* three times lower than under ML or HL, indicating that the low abundance of photons constituted a limiting factor for growth of *P. tricornutum*. Our values are lower than those reported for *P. tricornutum* grown under the same nominal irradiances (Geider et al., 1985) due to the use of different light sensors (planar (2π) in Geider et al. (1985) versus spherical (4π) in this study). Both studies, however, agree on the higher growth rate under ML. When compared to ML, the additional photons brought by HL did not promote growth rate but generated a stress as suggested by the increase of the different mechanisms of excess energy dissipation. Altogether, these results agreed with those already published on this topic (e.g., Xiang et al., 2015).

The time-course of Chl *a* and total carotenoids accumulations under ML and HL differed significantly from those of LL grown cells, affecting the Chl a/Chl c ratio, a proxy for the size of the light harvesting antenna complex (Lamote et al., 2003; Nguyen-Deroche et al., 2012). Under LL, the ratio increased from phases 1 to 2 and then decreased until phase 3 indicating progressive LHC

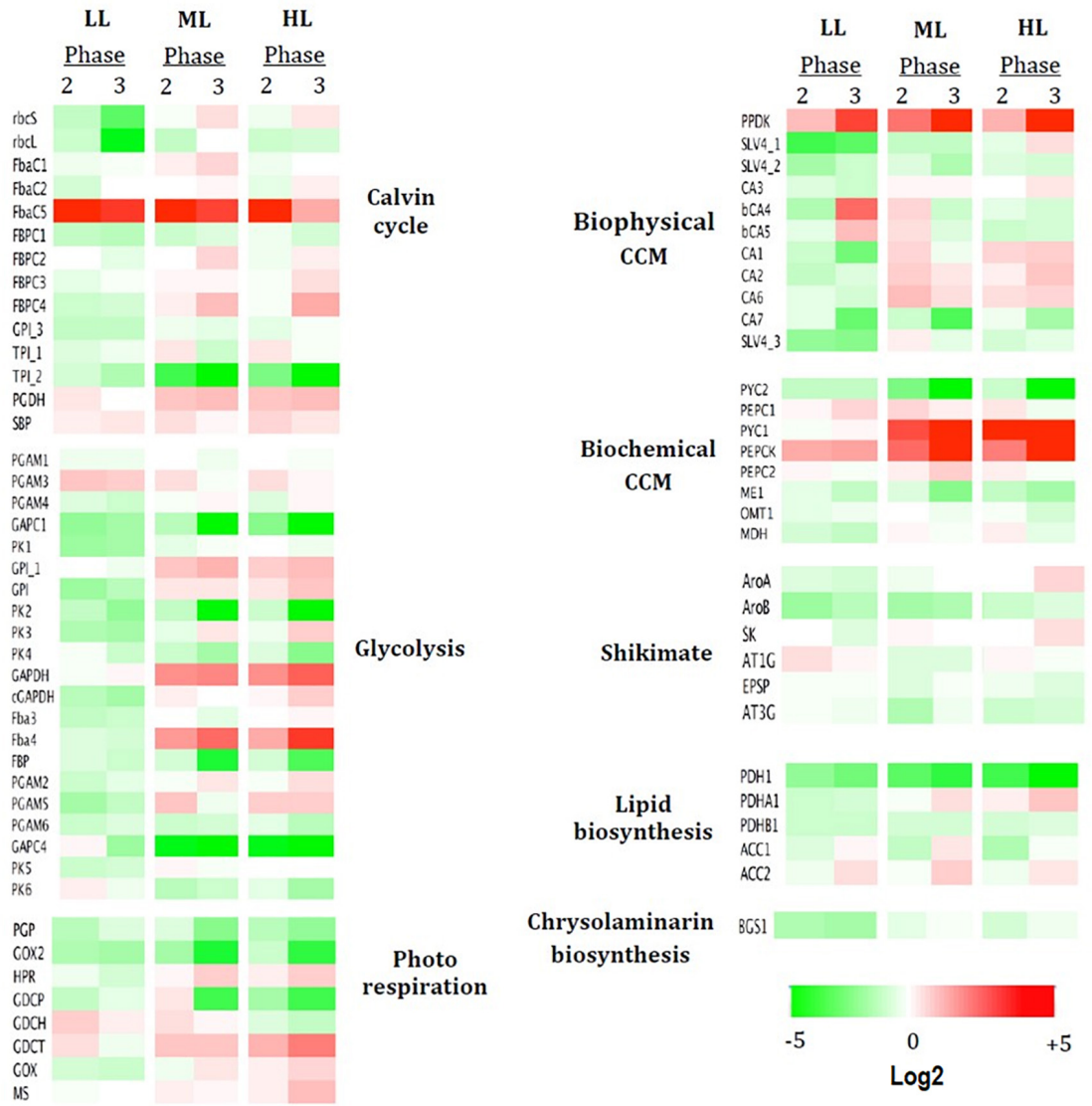


**FIGURE 7 |** mRNA profiles of genes either up- or down-regulated during three growth phases under three light conditions. Are presented the log2 expression pattern of 74 genes related to carbon metabolic pathways, with the greatest differences in expression (red: high, green: low). Columns represent growth photon flux densities under the different growth phase, phase 1 being taken as reference. Heatmap performed using Netwalker 1.0. Dysregulated heatmap showing the expression pattern of 74 genes related to carbon metabolic pathways, with the greatest differences in expression (red: high, green: low). Columns represent three growth phases under low light (LL) and high light (HL). Heatmap performed using Netwalker 1.0.

enlargement. At the end of phase 3, the antenna size was similar regardless the light intensity. In phase 3, under ML and HL, $R_d$, $A_{max}$ and rETR were reduced, suggesting a strong reduction of the metabolic activities. Under LL, $R_d$ increased relatively to $A_{max}$ suggesting the increase of the requirement of energy from nonphotosynthetic machinery.

## The Carbon Availability Along the Growth Indicates a Carbon Limitation

Among nutrient elements, C and N, above all else, are absolutely required for growth and the synthesis of metabolites. The variation of C- and N-uptake rates followed the rule observed by Marchetti et al. (2012) with *Isochrysis affinis galbana*, i.e., uptake variations follow those of growth rate. The C consumption was elevated along growth as over 70% had been consumed when the culture reached phase 3. Actually, it was estimated that only 4.5 μmol $NaHCO_3/10^6$ cells remained in phase 3. This level is far lower than that sufficient for optimal cell doubling (Riebesell et al., 1993). Altogether, this reasoning suggests that C deficiency was mostly responsible for the stationary phase. The fact that under ML and HL, the Chl *a* and total carotenoids amounts were the highest in phase 3 suggested that the cellular shading effect might also be partly responsible for the occurrence of the

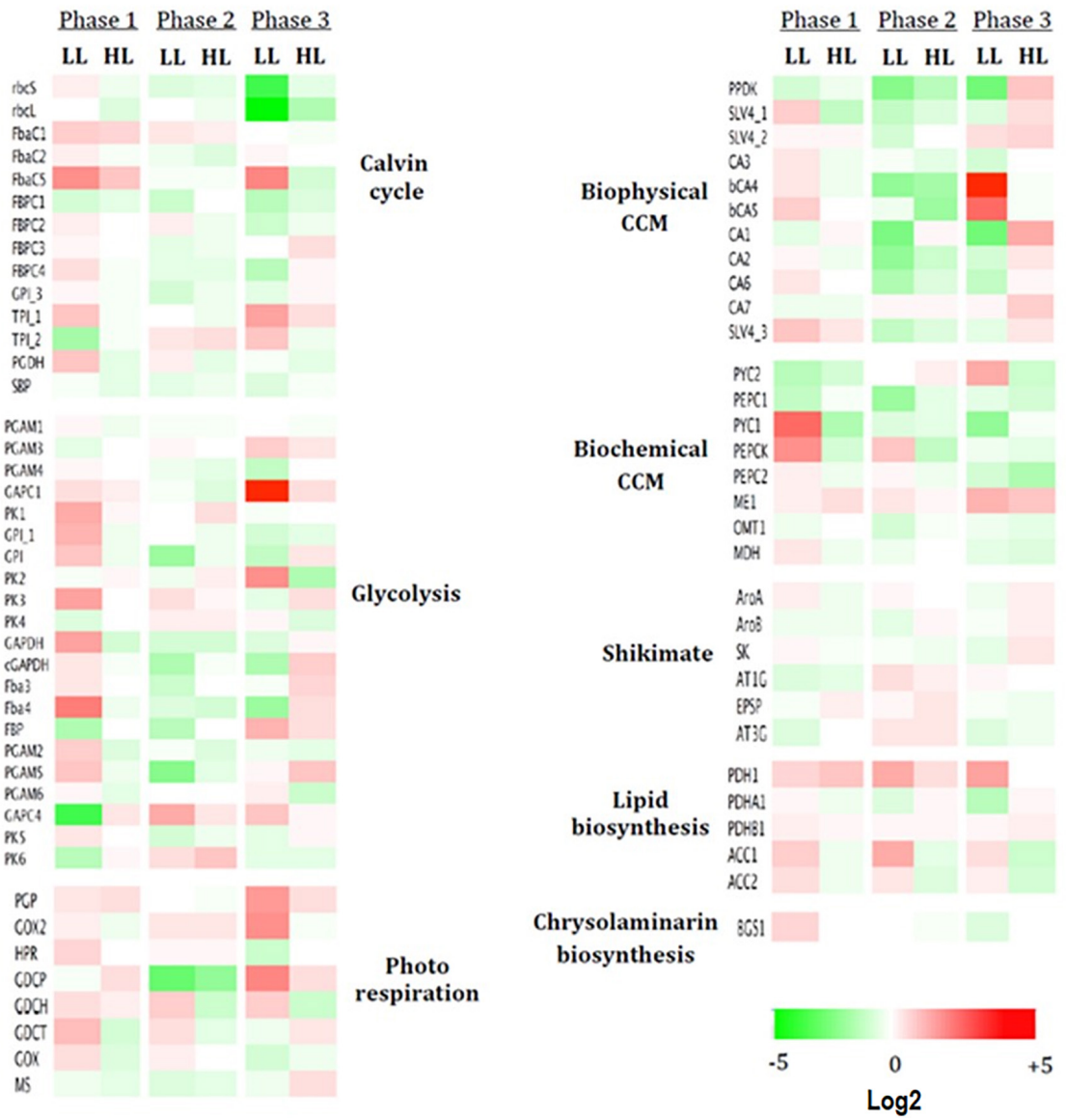


**FIGURE 8 |** Dysregulated heatmap of up- or down-regulated genes under different light intensities. Are presented the log2 expression pattern of 74 genes related to carbon metabolic pathways, with the greatest differences in expression (red: high, green: low). Columns represent three growth phases under low light (LL) and high light (HL). Heatmap performed using Netwalker 1.0.

stationary phase. Alternatively, this phenomenon could also be interpreted as a way to enhance the production of ATP and NADPH through the photochemical reactions of photosynthesis for carbon fixation by RuBisCO. This change was less intense under LL probably because the pigment cellular quota was already almost at its maximum. The slight increase in the qN values observed in phase 3 suggests that energy production and energy expenditure were somehow more unbalanced than during phase 2. This imbalance was deeper in HL and to a lesser extent in ML conditions because the rETR was strongly reduced, providing good conditions for ROS production and photoinhibition. The photosynthetically fixed C was mostly used to synthesize lipids, proteins and carbohydrates. It was reported that increasing the irradiance level triggered an increase of the *Qc* of the diatom *Thalassiosira pseudonana* (Taraldsvik and Myklestad, 2000; Shi et al., 2015). Our measurements did not confirm this conclusion. The discrepancy may result from progressive exhaustion of the carbon source. It is interesting to note that, in phase 2, the pH of the medium (8.7) is more alkaline than in phase 1 (8.2). In *Skeletonema costatum,* such an increase favors $CO_2$ uptake and the accumulation of amino acids (Taraldsvik and Myklestad, 2000). In our conditions, *P. tricornutum* accumulated relatively more proteins under HL.

As in cyanobacteria and green algae, diatoms possess CCMs for up-taking dissolved inorganic carbon from the surrounding environment. Two types of CCM have been reported to exist in

diatoms. One is a "biophysical CCM" in which $CO_2$ and $HCO_3^-$ are transported by CAs and bicarbonate transporters. The other CCM is called "biochemical CCM" and involves a prefixation of inorganic carbon into C4 compounds as in C4 land plants, and then a conversion into C3 compounds and $CO_2$ in proximity of RuBisCO favoring its carboxylation activity (Scarsini et al., 2019). Although the existence of a functional biochemical CCM was reported in *Conticribra weissflogii* (Grunow) Stachura-Suchoples & D.M. Williams) (formerly known as *Thalassiosira weissflogii*, there is no evidence for a functional evidence for a biochemical CCM in *P. tricornutum* (Haimovich-Dayan et al., 2013; Ewe et al., 2018).

The CA protein family is composed of proteins with different cellular sub-locations (e.g., chloroplast, PPS, cytosol) (Tachibana et al., 2011). Accordingly the up-regulation of genes coding proteins involved in the biophysical CCM was observed. Higher expression of "CCM genes" in phase 3 is consistent with the low $CO_2$ available at this growth phase. It is interesting that the different gene sets were induced according to the growth light intensity.

In *P. tricornutum*, Tachibana et al. (2011) showed that putative CA1, CA2, CA6 but not CA7 are transcriptionally active and expressed independently of light and $CO_2$ conditions, and thus appear to be synthesized constitutively. Similar results were found in our conditions. bCA4 and bCA5 were previously shown to be $CO_2$ responsive and changes in mRNAs content are consistent with those reported previously by several authors under different growth conditions (Harada and Matsuda, 2005; Harada et al., 2005; Tachibana et al., 2011). Only for LL, the two bCAs (bCA4/PtCA1 and bCA5/PtCA2 (Tachibana et al., 2011), were strongly up-regulated in phase 3. Higher expression of these genes under LL in phase 3 may compensate the lower efficiency of RuBisCO, consistent with the decrease of mRNA expression in phase 3 LL for rbcS and rbcL, thus providing more $CO_2$ around this enzyme. Also, down-regulation of the three $HCO_3^-$ transporters SLV (SLV4_1 SLV4_2 and SLV4_3) were observed in phase 3 under LL. Under LL, bCAs were mostly up-regulated whereas under HL, PPDK, SLVs and CAs were essentially over-expressed. Biochemical and biophysical CCM mechanisms together allow cells to increase inorganic carbon uptake and to keep high photosynthetic rates under low-$CO_2$ environmental conditions. This action is required because of the progressive carbon shortage of the culture. Under HL and ML, the genes coding for the transformation of pyruvate to PEP within the biochemical CCM are up-regulated, generating $CO_2$ that can be used for photosynthesis.

## Carbon Limitation Triggers the Reorientation of the Carbon Metabolism Toward Phospho*enol*pyruvate Formation

Regardless the photon flux density, the FbaC5 gene is highly up-regulated along the growth period and is accompanied by a significant down-regulation of TPI2 and GAPC1 both, involved in the reverse reaction that produce back trioses (Zgiby et al., 2000; Allen et al., 2011b). These changes may be interpreted as a lack of DHAP formation in the Calvin cycle. To feed the putative sink in DHAP, an import of this component from the cytosol using one of the triose phosphate translocators (TPT) can be postulated (for a review on transporters, see Marchand et al., 2018). The DHAP is probably transformed in Ru5P through the nonoxidative pentose-phosphate pathway or the Calvin-Benson cycle (**Figure 6**). The up-regulation of FBPC2 and FBPC4 genes under ML and HL, phase 3, suggests the use of the Calvin-Benson cycle for C5 regeneration along the growth period. The Ru5P can then serve as substrate for RuBisCO for binding $CO_2$. In case of $CO_2$ shortage (phase 3), Ru5P could be exported to the cytosol (Marchand et al., 2018) and metabolized through the oxidative pentose phosphate pathway after isomerization to D-xylulose-5-phosphaste (X5P) (**Figure 6**). The increase in the expression of the gene coding the cytosolic PGDH, the last enzyme of this pathway, agrees with this reasoning. Importantly, the reaction, from 6-phospho-D-gluconate (6PGN) to Ru5P catalyzed by PGDH, generates $CO_2$ in the periplasmic space (PPS). This autogenerated $CO_2$ can eventually be imported within the chloroplast and fixed by RuBisCO. Altogether, the data suggest that under $CO_2$ shortage, part of the carbon pool circulates between the different cell compartments, limiting lipid accumulation even more. To summarize, the fixed $CO_2$ is mostly used to form 3PG that is then transformed to 2PG. This conclusion is strengthened by the upregulation of genes coding for the enzyme catalyzing the transformation of 3PG to 2PG (PGAM) such as PGAM3 in phase 2 (>2-fold) under the three light intensities. 2PG is the substrate of enolase to form PEP, that, in turn, serves as a precursor of the Shikimate pathway or to produce pyruvate (**Figure 6**). The localization of PPDK, which converts pyruvate into PEP, is unclear. The sequence of the nonmaturated protein exhibits a plastid targeting presequence but the expression of PPDK::GFP fusion reveals a cytoplasmic localization (Ewe et al., 2018; **Figure 6**). Dual localization of proteins is an established possibility, including for PPDK in land plants (Parsley and Hibberd, 2006). According to Ewe et al. (2018), PEP and pyruvate generated in the cytoplasm could be reimported in the plastid by PEP and transporters, respectively. These transporteurs have still to be identified (Marchand et al., 2018). The gene coding the plastidic PPDK was among the highest up-regulated genes. Altogether, these results highlight that, regardless PPDK localization, the carbon flux is orientated toward PEP and pyruvate formation.

PEP can serve as acceptor for $CO_2/HCO_3^-$ fixation by PEPC in the $C_4$ route (**Figure 6**). The expression of PEPC1 (located in PPS) and PEPC2 (located in mitochondria) did not vary significantly as already observed in Valenzuela et al. (2012) in *P. tricornutum* under low $CO_2$ conditions. However, the mitochondrial PYC1 and PEPCK, the enzymes allowing the conversion of pyruvate into PEP (through the fixation of $HCO_3^-$ and the formation of OAA), were also among the highest upregulated genes in phase 3, especially in ML and HL. This result suggests that under ML and HL, the carbon allocation in the mitochondria is also oriented toward PEP. Under LL, a significant part of OAA enters the TCA cycle for respiration as is suggested by the higher the respiratory activity under this light condition. Pyruvate can also be produced by the mitochondrial ME1 from malate. ME1 supplies both carbon and reducing equivalents in

the form of NADPH for *de novo* fatty acid production (Kroth et al., 2008; Xue et al., 2015). Because no nitrogen depletion occurred in our conditions, it is unlikely that ME encoding genes stimulate lipid production (Yang et al., 2013; Xue et al., 2015). This would be consistent with the involvement of the mitochondrial pool of pyruvate in CCM to produce PEP that might be exported to other cell compartments, including plastids where it may serves as building blocks, e.g., aromatic amino acids and lipids. For aromatic amino acids, the expression of 6 genes coding enzymes involved in the Shikimate pathway were studied among which AroB and SK were slightly down-regulated in the three conditions, leading us to hypothesize that this is not the direction of carbon flux.

The activation of different pathways toward PEP (and pyruvate) synthesis highlighted at the mRNA level both in the plastid/cytoplasm and in the mitochondria is probably the consequence of a carbon limitation common in the different cultures along the growth period. Indeed, these two precursors constitute a hub from which the carbon is partitioned between the different biosynthetic pathways including protein and lipid biosynthesis. Also they are important intermediates in gluconeogenesis (the opposite direction of glycolysis) to produce energy (ATP), glucose and also storage (as chrysolaminarin) for the cell.

## The Carbon Partitioning Is Impacted by the Photon Flux Density

The PEP-pyruvate hub constitutes the starting point of different biosynthetic pathways including protein, lipid biosynthesis and aromatic compounds. Interestingly, under each light condition, the major compound was different in phase 1: under HL, proteins are proportionally higher whereas under ML and LL, chrysolaminarin and lipids, respectively, are proportionally higher. This is not unexpected because growth conditions under LL, phase 1, recall some conditions favoring lipid accumulation in diatoms: elevated amount of available C and reduced cell division rate (Nogueira et al., 2015). Under LL, the relative abundance of lipids decreased during the transition from phases 1 to 2 and then remained constant until phase 3 while the relative amount of chrysolaminarin increased. Indeed, mRNAs of the first enzyme of the chrysolaminarin synthesis, BGS1 (β-1,3-glucane glycosyltransferase) was found to be slightly overexpressed under LL compared to ML and HL and tend to decrease in phases 2 and 3. Under ML and HL, these conditions were only present transiently because division rate increased rapidly after the start of culturing. To sustain this growth, most of the C is incorporated into simple sugars that are used to generate ATP through respiration, which strongly increased during the phases 1–2 transition. The ATP produced could be imported in the chloroplast using NTT transporters (Ast et al., 2009) and used, for instance, in the Calvin cycle. Out of the three FbaC genes coding plastidial Fba (Allen et al., 2011a), only FbaC5, that represented *circa* 30% of the total "plastidial" FbaC mRNA (data not shown), was up-regulated in all three conditions. Indeed, in the land plant *Arabidopsis thaliana*, FBA is also one of the three Calvin-Benson cycle enzymes that was most sensitive to environmental perturbations and found to have an important rate-limiting role in regulating the carbon assimilation flux (Sun et al., 2003). Interestingly, no particular regulation of the genes coding the RuBisCO subunits was observed except under LL for which a reduction was observed along the growth period, confirming earlier reports (Kroth et al., 2008).

As a response to HL, lipids accumulated during phase the 2-to-phase 3 transition, as reported by Valenzuela et al. (2012), Mus et al. (2013), and Wu et al. (2015) but here, the accumulation was limited because of the progressive depletion in C. The origin of the lipid biosynthesis, i.e., PEP or pyruvate, is still under debate. Some authors have assumed that lipid biosynthesis branches from PEP (Kroth et al., 2008; Mus et al., 2013), while others noted that it goes through pyruvate (Radakovits et al., 2012; Yang et al., 2013; Ge et al., 2014; Schwender et al., 2014).

The pyruvate dehydrogenase complex (PDC) is an important enzyme of lipid metabolism. Three isoforms of pyruvate dehydrogenase, namely PDH1, PDHB1, and PDHA1, were found in the *P. tricornutum* genome (Chauton et al., 2013). PDH1 gene expression decreased in phases 2 and 3 while the expression of the PDHA1 increased. The PDHB1 level did not change significantly. Moreover, the mRNA expression of the two isoforms of acetyl-CoA carboxylase (ACC1 and ACC2), which catalyze the conversion of acetyl-CoA into malonyl-CoA for fatty acid production, indicated a singular pattern: a higher expression of both genes in LL and an up-regulation of ACC2 in phase 3, though not significantly under HL. It seems that a higher expression of these genes during phase 3 under LL speeds up the conversion of pyruvate to malonyl-CoA. This compound is a key cofactor of the fatty acid biosynthesis.

## The Involvement of the Photorespiration Pathway Is Not Enhanced, Even Under HL

It is well recognized that $O_2$ and $CO_2$ are in competition for the RuBisCO active site. When the gas partial pressure surrounding RuBisCO is in favor of $O_2$, RuBP enters the photorespiration pathway of which the first step consists in the oxidation of RuBP to 2PGL by RuBisCO (**Figure 6**; Sage and Stata, 2015). Therefore, in the case of C limitation, it could be expected that photorespiration will be strongly activated. Besides its role in diverting carbon atoms, photorespiration plays a critical role in nitrogen metabolism in diatoms and a role in excess energy dissipation under stress conditions (Kroth et al., 2008). This is unlikely in our conditions because qN measurements suggest that the capacity to dissipate the excess of absorbed light energy was too low to be saturated. The gene coding PGP, the enzyme catalyzing the formation of glycolate from 2PGL was down-regulated in LL, ML, and HL in phases 2 and 3 compared to phase 1. These changes were accompanied by the down-regulation of the expression of two other photorespiratory genes coding the mitochondrial GOX2 and GDCP. The former role was probably more easily filled as the N in the medium remained high whereas the latter is unlikely as the capacity to dissipate the excess of energy through the nonphotochemical quenching was far from

saturation. Altogether, our results highlight that photorespiration is not particularly enhanced, even under HL.

## CONCLUSION

To conclude, our results show that the impact of light intensity on cell development, physiology and gene regulation of *P. tricornutum* depends on growth phase, i.e., the cell's physiological state. Generally, diatom cells adapted to different light conditions in efficient ways to keep cell growth, processes and regulation. In all light conditions C-deficiency was mostly responsible for the occurrence of the plateau phase in these cultures, whereas no deficiency of N was observed in the cultures. A common point in all growth photon flux densities was the modification of gene transcription that would allow the synthesis of PEP and, in some cases in the reverse direction, to pyruvate. Our results confirm the recent finding of the existence of a pyruvate hub in microalgae (Smith et al., 2012; Heydarizadeh et al., 2017) and also show that reorientation of carbon metabolism might occur according to combination of environmental factors. Altogether, the data set presented in this manuscript shows that even in conditions of carbon deprivation, diatoms orient their metabolism toward the production of lipids.

## AUTHOR CONTRIBUTIONS

PH, JM, and BS conceived the idea of the manuscript. PH, BV, BH, EL, GW-C, AC-M, GB, JM, and BS performed the experiments and wrote the related parts of the manuscript. PH, JM, and BS wrote the introduction, the discussion and the conclusions as well as prepared the figures.

## ACKNOWLEDGMENTS

PH thanks the Isfahan University of Technology for a sabbatical program. AC-M and GW-C thanks Vony Rabesaotra, University of Nantes, for her technical assistance. PH thanks the doctoral school "Végétal Environnement Nutrition Alimentation Mer," the "Collège doctoral" of Le Mans University, the Region "Pays de la Loire" for their financial supports. PH, JM, and BS thanks the Ministery of Foreign Affairs of the French Republic for financial support through the programme Partenariat Hubert Curien Gundishapur. This study is part of the Ph.D. of P. Heyadrizadeh (Heydarizadeh, P. 2015. Regulation of secondary compounds synthesis by photosynthetic organisms under stress. Ph.D. Thesis, Le Mans University, France). The authors thank Prof. Kalina Manoylov (Georgia College and State University, United States) and Prof. Richard Gordon (Gulf Specimen Marine Lab & Aquarium and Wayne State University) for their critical reading of the text.

## SUPPLEMENTARY MATERIAL

The Supplementary Material for this article can be found online at: https://www.frontiersin.org/articles/10.3389/fpls.2019.00471/full#supplementary-material

## REFERENCES

Allen, A. E., Dupont, C. L., Obornik, M., Horak, A., Nunes-Nesi, A., McCrow, J. P., et al. (2011a). Evolution and metabolic significance of the urea cycle in photosynthetic diatoms. *Nature* 473, 203–207. doi: 10.1038/nature10074

Allen, A. E., Moustafa, A., Montsant, A., Eckert, A., Kroth, P. G., and Bowler, C. (2011b). Evolution and functional diversification of fructose bisphosphate aldolase genes in photosynthetic marine diatoms. *Mol. Biol. Evol.* 29, 367–379. doi: 10.1093/molbev/msr223

Ast, M., Gruber, A., Schmitz-Esser, S., Neuhaus, H. E., Kroth, P. G., Horn, M., et al. (2009). Diatom plastids depend on nucleotide import from the cytosol. *Proc. Natl. Acad. Sci. U.S.A.* 106, 3621–3626. doi: 10.1073/pnas.0808862106

Bailleul, B., Rogato, A., Martino, A., Coesel, S., Cardol, P., Bowler, C., et al. (2010). An atypical member of the light-harvesting complex stress related protein family modulated diatom response to light. *Proc. Natl. Acad. Sci. U.S.A.* 107, 18214–18219. doi: 10.1073/pnas.1007703107

Barofsky, A., Simonelli, P., Vidoudez, V., Troedsson, C., Nejstgaard, J. C., Jakobsen, H. H., et al. (2010). Growth phase of the diatom *Skeletonema marinoi* influences the metabolic profile of the cells and the selective feeding of the copepod *Calanus* spp. *J. Plankt. Res.* 32, 263–272. doi: 10.1093/plankt/fbp121

Barofsky, A., Vidoudez, C., and Pohnert, G. (2009). Metabolic profiling reveals growth stage variability in diatom exudates. *Limnol. Oceanogr. Methods* 7, 382–390. doi: 10.4319/lom.2009.7.382

Beauger, A., Wetzel, C. E., Voldoirea, O., and Ector, L. (2019). *Pseudostaurosira bardii* (Fragilariaceae, Bacillariophyta), a new species from a saline hydrothermal spring of the Massif Central (France). *Bot. Lett.* 166, 1–11.

Bligh, E. G., and Dyer, W. J. (1959). A rapid method of total lipid extraction and purification. *Can. J. Biochem. Physiol.* 37, 911–917. doi: 10.1139/y59-099

Bork, P., Bowler, C., de Vargas, C., Gorsky, G., Karsenti, E., and Wincker, P. (2015). Tara oceans studies plankton at planetary scale. *Science* 348:873. doi: 10.1126/science.aac5605

Bowler, C., Allen, A. E., Badger, J. H., Grimwood, J., Jabbari, K., Kuo, A., et al. (2008). The *Phaeodactylum* genome reveals the evolutionary history of diatom genomes. *Nature* 456, 239–244. doi: 10.1038/nature07410

Bradford, M. M. (1976). A rapid and sensitive method for the quantitation of microgram quantities of protein utilizing the principle of protein-dye binding. *Anal. Biochem.* 72, 248–254. doi: 10.1016/0003-2697(76)90527-3

Carvalho, A. P., Silva, S. O., Baptista, J. M., and Malcata, F. X. (2011). Light requirements in microalgal photobioreactors: an overview of biophotonic aspects. *Appl. Microbiol. Biotechnol.* 89, 1275–1288. doi: 10.1007/s00253-010-3047-8

Chauton, M. S., Winge, P., Brembu, T., Vadstein, O., and Bones, A. M. (2013). Gene regulation of carbon fixation, storage, and utilization in the diatom *Phaeodactylum tricornutum* acclimated to light/dark cycles. *Plant Physiol.* 161, 1034–1048. doi: 10.1104/pp.112.206177

Darko, E., Heydarizadeh, P., Schoefs, B., and Sabzalian, M. R. (2014). Photosynthesis under artificial light: the shift in primary and secondary metabolites. *Philos. Trans. R. Soc. London B* 369:20130243. doi: 10.1098/rstb.2013.0243

Depauw, F. A., Rogato, A., Alcalá, M. R., and Falciatore, A. (2012). Exploring the molecular basis of responses to light in marine diatoms. *J. Exp. Bot.* 63, 1575–1591. doi: 10.1093/jxb/ers005

Dron, A., Rabouille, S., Claquin, P., Le Roy, B., Talec, A., and Sciandra, A. (2012). Light-dark (12:12) cycle of carbon and nitrogen metabolism in *Crocosphaera watsonii* WH8501: relation to the cell cycle. *Environ. Microbiol.* 14, 967–981. doi: 10.1111/j.1462-2920.2011.02675.x

Ewe, D., Tachibana, M., Kikutani, S., Gruber, A., Bartulos, C. R., Konert, G., et al. (2018). The intracellular distribution of inorganic carbon fixing enzymes

does not support the presence of a C4 pathway in the diatom *Phaeodactylum tricornutum*. *Photosynth. Res.* 137, 263–280. doi: 10.1007/s11120-018-0500-5

Field, C. B., Behrenfeld, M. J., Randerson, J. T., and Falkowski, P. G. (1998). Primary production of the biosphere: integrating terrestrial and oceanic components. *Science* 281, 237–240. doi: 10.1126/science.281.5374.237

Ge, F., Huang, W., Chen, Z., Zhang, C., Xiong, Q., Bowler, C., et al. (2014). Methylcrotonyl-CoA carboxylase regulates triacylglycerol accumulation in the model diatom *Phaeodactylum tricornutum*. *Plant Cell* 26, 1681–1697. doi: 10.1105/tpc.114.124982

Geider, R. J., Osborne, B. A., and Raven, J. A. (1985). Light dependence of growth and photosynthesis in *Phaeodactylum tricornutum* (Bacillariophyceae). *J. Phycol.* 29, 609–619. doi: 10.1111/j.0022-3646.1985.00609.x

Goldman, J. C. (1980). "Physiological aspects in algal mass cultures," in *Algae Biomass*, eds G. Shelef and C. J. Soeder (Amsterdam: Elsevier), 343–359.

Granum, E., and Myklestad, S. M. (2002). A simple combined method for determination of β-1,3-glucan and cell wall polysaccharides in diatoms. *Hydrobiologia* 477, 155–161. doi: 10.1023/A:1021077407766

Gruber, A., and Kroth, P. G. (2017). Intracellular metabolic pathway distribution in diatoms and tools for genome-enabled experimental diatom research. *Philos. Trans. R. Soc. B Biol. Sci.* 372:20160402. doi: 10.1098/rstb.2016.0402

Guillard, R. R., and Ryther, J. H. (1962). Studies of marine planktonic diatoms: I. *Cyclotella nana* and *Detonula confervacea* (Cleve). *Can. J. Microbiol.* 8, 229–239. doi: 10.1139/m62-029

Haimovich-Dayan, M., Garfinkel, N., Ewe, D., Marcus, Y., Gruber, A., Wagner, H., et al. (2013). The role of C4 metabolism in the marine diatom *Phaeodactylum tricornutum*. *New Phytol.* 197, 177–185. doi: 10.1111/j.1469-8137.2012.04375.x

Harada, H., and Matsuda, Y. (2005). Identification and characterization of a new carbonic anhydrase in the marine diatom *Phaeodactylum tricornutum*. *Can. J. Bot.* 83, 909–916. doi: 10.1139/b05-078

Harada, H., Nakatsuma, D., Ishida, M., and Matsuda, Y. (2005). Regulation of the expression of intracellular β-carbonic anhydrase in response to CO2 and light in the marine diatom *Phaeodactylum tricornutum*. *Plant Physiol.* 139, 1041–1050. doi: 10.1104/pp.105.065185

Heydarizadeh, P., Boureba, W., Zahedi, M., Huang, B., Moreau, B., Lukomska, E., et al. (2017). Response of CO2-starved diatom *Phaeodactylum tricornutum* to light intensity transition. *Philos. Trans. R. Soc. B* 372:20160396. doi: 10.1098/rstb.2016.0396

Heydarizadeh, P., Marchand, J., Chenais, B., Sabzalian, M. R., Zahedi, M., Moreau, B., et al. (2014). Functional investigations in diatoms need more than transcriptomic approach. *Diatom Res.* 29, 75–89. doi: 10.1080/0269249X.2014.883727

Jia, J., Han, D., Gerken, H. G., Li, Y., Sommerfeld, M., Hu, Q., et al. (2015). Molecular mechanisms for photosynthetic carbon partitioning into storage neutral lipids in *Nannochloropsis oceanica* under nitrogen-depletion conditions. *Algal Res.* 7, 66–77. doi: 10.1016/j.algal.2014.11.005

Komurov, K., Dursun, S., Erdin, S., and Ram, P. T. (2012). NetWalker: a contextual network analysis tool for functional genomics. *BMC Genomics* 13:282. doi: 10.1186/1471-2164-13-282

Kroth, P. G., Bones, A. M., Daboussi, F., Ferrante, M. I., Jaubert, M., Kolot, M., et al. (2018). Genome editing in diatoms: achievements and goals. *Plant Cell Rep.* 37, 1401–1408. doi: 10.1007/s00299-018-2334-1

Kroth, P. G., Chiovitti, A., Gruber, A., Martin-Jézéquel, V., Mock, T., Schnitzler Parker, M., et al. (2008). A model of carbohydrate metabolism in the diatom *Phaeodactylum tricornutum* deduced from comparative whole genome analysis. *PLoS One* 3:e1426. doi: 10.1371/journal.pone.0001426

Kroth, P. G., Wilhelm, C., and Kottke, T. (2017). An update on aureochromes: phylogeny – mechanism – function. *J. Plant Physiol.* 217(Suppl. C), 20–26. doi: 10.1016/j.jplph.2017.06.010

Lamote, M., Darko, E., Schoefs, B., and Lemoine, Y. (2003). Assembly of the photosynthetic apparatus in embryos from *Fucus serratus* L. *Photosynth. Res.* 77, 45–52. doi: 10.1023/A:1024999024157

Livak, K. J., and Schmittgen, T. D. (2001). Analysis of relative gene expression data using real time quantitative PCR and the 2-Ct method. *Methods* 25, 402–408. doi: 10.1006/meth.2001.1262

Marchand, J., Heydarizadeh, P., Schoefs, B., and Spetea, C. (2018). Ion and metabolite transport in the chloroplast of algae: lessons from land plants. *Cell. Mol. Life Sci.* 75, 2153–2176. doi: 10.1007/s00018-018-2793-0

Marchetti, J., Bougaran, G., Le Dean, L., Mégrier, C., Lukomska, E., Kaas, R., et al. (2012). Optimizing conditions for the continuous culture of *Isochrysis affinis galbana* relevant to commercial hatcheries. *Aquaculture* 32, 106–113. doi: 10.1016/j.aquaculture.2011.11.020

Mus, F., Toussaint, J.-P., Cooksey, K. E., Fields, M. W., Gerlach, R., Peyton, B. M., et al. (2013). Physiological and molecular analysis of carbon source supplementation and pH stress-induced lipid accumulation in the marine diatom *Phaeodactylum tricornutum*. *Appl. Microbiol. Biotechnol.* 97, 3625–3642. doi: 10.1007/s00253-013-4747-7

Nguyen-Deroche, T. N., Caruso, A., Le, T. T., Viet Bui, T., Schoefs, B., Tremblin, G., et al. (2012). Zinc affects differently growth, photosynthesis, antioxidant enzyme activities and phytochelatin synthase expression of four marine diatoms. *ScienceWorldJournal* 2012:982957. doi: 10.1100/2012/982957

Nogueira, D. P. K., Silva, A. F., Araújo, O. Q., and Chaloub, R. M. (2015). Impact of temperature and light intensity on triacylglycerol accumulation in marine microalgae. *Biomass Bioenergy* 72, 280–287. doi: 10.1016/j.biombioe.2014.10.017

Nymark, M., Valle, K. C., Brembu, T., Hancke, K., Winge, P., Andresen, K., et al. (2009). An integrated analysis of molecular acclimation to high light in the marine diatom *Phaeodactylum tricornutum*. *PLoS One* 4:e7743. doi: 10.1371/journal.pone.0007743

Parsley, K., and Hibberd, J. M. (2006). The *Arabidopsis* PPDK gene is transcribed from two promoters to produce differentially expressed transcripts responsible for cytosolic and plastidic proteins. *Plant Mol. Biol.* 62, 339–349. doi: 10.1007/s11103-006-9023-0

Parupudi, P., Kethineni, C., Dhamole, P. B., Vemula, S., Allu, P. R., Botlagunta, M., et al. (2016). CO2 fixation and lipid production by microalgal species. *Korean J. Chem. Eng.* 33, 587–593. doi: 10.1007/s11814-015-0152-5

Pfaffl, M. W., Tichopad, A., Prgomet, C., and Neuvians, T. P. (2004). Determination of stable housekeeping genes, differentially regulated target genes and sample integrity: bestkeeper-excel-based tool using pairwise correlations. *Biotechnol. Lett.* 26, 509–515. doi: 10.1023/B:BILE.0000019559.84305.47

Radakovits, R., Jinkerson, R. E., Fuerstenberg, S. I., Tae, H., Settlage, R. E., Boore, J. L., et al. (2012). Draft genome sequence and genetic transformation of the oleaginous alga *Nannochloropsis gaditana*. *Nat. Commun.* 3:686. doi: 10.1038/ncomms1688

Riebesell, U., Wolf-Gladrow, D. A., and Smetacek, V. (1993). Carbon dioxide limitation of marine phytoplankton growth rates. *Nature* 361, 249–251. doi: 10.1038/361249a0

Roháçek, K., Bertrand, M., Moreau, B., Jacquette, J., Caplat, C., Morant-Manceau, A., et al. (2014). Relaxation of the non-photochemical chlorophyll fluorescence quenching in diatoms: kinetics, components and mechanisms. *Philos. Trans. R. Soc. B* 369:20130241. doi: 10.1098/rstb.2013.0241

Roháček, K., Soukupova, J., and Bartak, M. (2008). "Chlorophyll fluorescence: a wonderful tool to study plant physiology and plant stress," in *Plant Cell Organelles – Selected Topics*, ed. B. Schoefs (Trivandrum: Research Signpost), 251–284.

Sage, R. F., and Stata, M. (2015). Photosynthetic diversity meets biodiversity: the C4 plant example. *J. Plant Physiol.* 172, 104–119. doi: 10.1016/j.jplph.2014.07.024

Sayanova, O., Mimouni, V., Ulmann, L., Morant-Manceau, A., Pasquet, V., Schoefs, B., et al. (2017). Modulation of lipid biosynthesis by stress in diatoms. *Philos. Trans. R. Soc. B* 372:1728. doi: 10.1098/rstb.2016.0407

Scarsini, M., Marchand, J., Manoylov, K., and Schoefs, B. (2019). "Photosynthesis in diatoms," in *Diatoms: Fundamentals & Applications*, eds J. Seckbach and R. Gordon (Beverly, MA: Wiley-Scrivener).

Schoefs, B., Hu, H., and Kroth, P. G. (2017). The peculiar carbon metabolism in diatoms. *Philos. Trans. R. Soc. B* 372:20160405. doi: 10.1098/rstb.2016.0405

Schwender, J., König, C., Klapperstück, M., Heinzel, N., Munz, E., Hebbelmann, I., et al. (2014). Transcript abundance on its own cannot be used to infer fluxes in central metabolism. *Front. Plant Sci.* 5:668. doi: 10.3389/fpls.2014.00668

Shi, D., Li, W., Hopkinson, B., Hong, H., Li, D., Kao, S.-J., et al. (2015). Ultrastructure effects of light, nitrogen source, and carbon dioxide on energy metabolism in the diatom *Thalassiosira pseudonana*. *Limnol. Oceanogr.* 50, 1805–1822. doi: 10.1002/lno.10134

Smith, S. R., Abbriano, R. M., and Hildebrand, M. (2012). Comparative analysis of diatom genomes reveals substantial differences in the organization of carbon partitioning pathways. *Algal Res.* 1, 2–16. doi: 10.1016/j.algal.2012.04.003

Steel, R. G., and Torrie, J. H. (1960). *Principles and Procedures of Statistics. Principles and Procedures of Statistics*. New York, NY: McGraw-Hill Companies.

Sun, N., Ma, L. G., Pan, D. Y., Zhao, H. Y., and Deng, X. W. (2003). Evaluation of light regulatory potential of Calvin cycle steps based on large-scale gene expression profiling data. *Plant Mol. Biol.* 53, 467–478. doi: 10.1023/B:PLAN.0000019071.12878.9e

Tachibana, M., Allen, A., Kikutani, S., Endo, Y., Bowler, C., and Matsuda, Y. (2011). Localization of putative carbonic anhydrases in two marine diatoms, *Phaeodactylum tricornutum* and *Thalassiosira pseudonana*. *Photosynth. Res.* 109, 205–211. doi: 10.1007/s11120-011-9634-4

Taraldsvik, M., and Myklestad, S. M. (2000). The effect of pH on growth rate, biochemical composition and extracellular carbohydrate production of the marine diatom *Skeletonema costatum*. *Eur. J. Phycol.* 35, 189–194. doi: 10.1080/09670260010001735781

Thiriet-Rupert, S., Carrier, G., Chénais, B., Trottier, C., Bougaran, G., Cadoret, J.-P., et al. (2016). Transcription factors in microalgae: genome-wide prediction and comparative analysis. *BMC Genomics* 17:282. doi: 10.1186/s12864-016-2610-9

Valenzuela, J., Mazurie, A., Carlson, R. P., Gerlach, R., Cooksey, K. E., Peyton, B. M., et al. (2012). Potential role of multiple carbon fixation pathways during lipid accumulation in *Phaeodactylum tricornutum*. *Biotechnol. Biofuels* 5:40. doi: 10.1186/1754-6834-5-40

Vidoudez, C., and Pohnert, G. (2008). Growth phase specific release of polyunsaturated aldehydes by the diatom *Skeletonema marinoi*. *J. Plankt. Res.* 30, 1305–1313. doi: 10.1093/plankt/fbn085

Vinayak, V., Manoylov, K. M., Gateau, H., Blanckaert, V., Herault, J., Pencreac'h, G., et al. (2015). Diatom milking: a review and new approaches. *Marine Drugs* 13, 2629–2665. doi: 10.3390/md13052629

Wagner, H., Jakob, T., and Wilhelm, C. (2006). Balancing the energy flow from captured light to biomass under fluctuating light conditions. *New Phytol.* 169, 95–108. doi: 10.1111/j.1469-8137.2005.01550.x

Wu, S. C., Huang, A. Y., Zhang, B. Y., Huan, L., Zhao, P. P., Lin, A. P., et al. (2015). Enzyme activity highlights the importance of the oxidative pentose phosphate pathway in lipid accumulation and growth of *Phaeodactylum tricornutum* under CO2 concentration. *Biotechnol. Biofuels* 8:78. doi: 10.1186/s13068-015-0262-7

Xiang, T., Nelson, W., Rodriguez, J., Tolleter, D., and Grossman, A. R. (2015). *Symbiodinium* transcriptome and global responses of cells to immediate changes in light intensity when grown under autotrophic or mixotrophic conditions. *Plant J.* 82, 67–80. doi: 10.1111/tpj.12789

Xue, J., Niu, Y. F., Huang, T., Yang, W. D., Liu, J. S., and Li, H. Y. (2015). Genetic improvement of the microalga *Phaeodactylum tricornutum* for boosting neutral lipid accumulation. *Metab. Eng.* 27, 1–9. doi: 10.1016/j.ymben.2014.10.002

Yang, Z.-K., Niu, Y. F., Ma, Y. H., Xue, J., Zhang, M. H., Yang, W. D., et al. (2013). Molecular and cellular mechanisms of neutral lipid accumulation in diatom following nitrogen deprivation. *Biotechnol. Biofuels* 6:67. doi: 10.1186/1754-6834-6-67

Zgiby, S. M., Thomson, G. J., Qamar, S., and Berry, A. (2000). Exploring substrate binding and discrimination in fructose 1,6-bisphosphate and tagatose 1,6-bisphosphate aldolases. *Eur. J. Biochem.* 267, 1858–1868. doi: 10.1046/j.1432-1327.2000.01191.x

Zulu, N. N., Zienkiewicz, K., Vollheyde, K., and Feussner, I. (2018). Current trends to comprehend lipid metabolism in diatoms. *Prog. Lipid Res.* 70, 1–16. doi: 10.1016/j.plipres.2018.03.001

**Conflict of Interest Statement:** The authors declare that the research was conducted in the absence of any commercial or financial relationships that could be construed as a potential conflict of interest.

frontiers in Plant Science

ORIGINAL RESEARCH
published: 24 May 2019
doi: 10.3389/fpls.2019.00688

# Thermal Benefits From White Variegation of *Silybum marianum* Leaves

*Oren Shelef[1]*, Liron Summerfield[2], Simcha Lev-Yadun[3], Santiago Villamarin-Cortez[4], Roy Sadeh[5], Ittai Herrmann[5] and Shimon Rachmilevitch[2]*

*[1] Department of Natural Resources, Institute of Plant Sciences, Agricultural Research Organization, Rishon LeZion, Israel, [2] French Associates Institute for Agriculture and Biotechnology of Drylands, The Jacob Blaustein Institutes for Desert Research, Ben-Gurion University of the Negev, Beersheba, Israel, [3] Department of Biology and Environment, Faculty of Natural Sciences, University of Haifa–Oranim, Tivon, Israel, [4] Biology Department, University of Nevada, Reno, Reno, NV, United States, [5] The Robert H. Smith Institute of Plant Sciences and Genetics in Agriculture, The Robert H. Smith Faculty of Agriculture, Food and Environment, The Hebrew University of Jerusalem, Rehovot, Israel*

Leaves of the spiny winter annual *Silybum marianum* express white patches (variegation) that can cover significant surface areas, the outcome of air spaces formed between the epidermis and the green chlorenchyma. We asked: (1) what characterizes the white patches in *S. marianum* and what differs them from green patches? (2) Do white patches differ from green patches in photosynthetic efficiency under lower temperatures? We predicted that the air spaces in white patches have physiological benefits, elevating photosynthetic rates under low temperatures. To test our hypotheses we used both a variegated wild type and entirely green mutants. We grew the plants under moderate temperatures (20°C/10°C d/n) and compared them to plants grown under lower temperatures (15°C/5°C d/n). The developed plants were exposed to different temperatures for 1 h and their photosynthetic activity was measured. In addition, we compared in green vs. white patches, the reflectance spectra, patch structure, chlorophyll and dehydrin content, stomatal structure, plant growth, and leaf temperature. White patches were not significantly different from green patches in their biochemistry and photosynthesis. However, under lower temperatures, variegated wild-type leaves were significantly warmer than all-green mutants – possible explanations for that are discussed These findings support our hypothesis, that white variegation of *S. marianum* leaves has a physiological role, elevating leaf temperature during cold winter days.

**Keywords: patch, *Silybum marianum*, leaf color, thermoregulation, IRGA, plant physiology**

OPEN ACCESS

***Edited by:***
*Éva Hideg,*
*University of Pécs, Hungary*

***Reviewed by:***
*Knut Asbjørn Solhaug,*
*Norwegian University of Life Sciences, Norway*
*Georgios Liakopoulos,*
*Agricultural University of Athens, Greece*

****Correspondence:***
*Oren Shelef*
*shelef@volcani.agri.gov.il*

***Specialty section:***
*This article was submitted to Plant Abiotic Stress, a section of the journal Frontiers in Plant Science*

***Received:*** *15 December 2018*
***Accepted:*** *07 May 2019*
***Published:*** *24 May 2019*

***Citation:***
*Shelef O, Summerfield L, Lev-Yadun S, Villamarin-Cortez S, Sadeh R, Herrmann I and Rachmilevitch S (2019) Thermal Benefits From White Variegation of Silybum marianum Leaves. Front. Plant Sci. 10:688. doi: 10.3389/fpls.2019.00688*

## INTRODUCTION

Most live leaves in land plants contain chlorophyll and therefore appear to the human eye as green. Evolution drives plants to produce considerable amounts of green tissues in order to pursue sufficient photosynthesis. This selection pressure is especially pronounced in annuals, which are active during a limited and often very short season. However, in many vascular plants a prominent portion of the leaves is not green. Leaves of the Mediterranean spiny winter annual rosette plant

*Silybum marianum* (Asteraceae) express white patches (variegation) that can cover significant areas of its leaves. We asked, is there a potential physiological advantage of that white variegation. Plant scientists suggested several non-exclusive explanations to non-green plant coloration patterns (Jiang et al., 2004). These possible mechanisms can be sorted to three different groups: (1) Chlorophyll deficiency (Aluru et al., 2001; Sheue et al., 2012); (2) defense from enemies including by aposematic coloration, undermining the camouflage of herbivorous insects, mimicry of dead or infested plants, masquerade and camouflage (Lev-Yadun et al., 2004; Lev-Yadun, 2016, 2017; Niu et al., 2018); (3) white patterns as secondary byproducts of advantageous physiological structures such as adaptations for improved water or gas transport (Fooshee and Henny, 1990), or an unknown role (Tsukaya et al., 2004); (4) white patterns provide other physiological adaptations including mitigation of UV radiation (Roelfsema et al., 2006) and thermoregulation. White variegation in *S. marianum* as defense from herbivores by various methods was studied by Lev-Yadun (2003; 2009; 2016) suggested that white variegation in dozens of species with spiny leaves are related to protection against herbivores via visual aposematism, showing a positive correlation between white patchiness and spine number and size. White variegation presumably also mimic pest tunnels (e.g., Smith, 1986; Lev-Yadun, 2016), and signal both invertebrate and mammalian herbivores to avoid eating the already infested leaves (e.g., Soltau et al., 2009). Delayed greening is also related to anti-herbivory defense in tropical ecosystems (Kursar and Coley, 1992). Another interesting hypothesis is related to physiological explanations. This hypothesis suggests that bundle sheath extensions (BSEs) have a role in water transport between the mesophyll and the vascular tissue through the epidermis (McClendon, 1992; Buckley et al., 2011). Accumulating evidence suggest that BSEs play a role in mitigating high radiation in accordance with photosynthetic activity and leaf structure, and as a function of nutrition and water status (Barbosa et al., 2018). Unlike leaf variegation, BSEs are apparent only with transmitted light. Nevertheless – this is an example of a structural leaf feature that provides physiological plasticity to the plant. Xiao et al. (2016) have extensively studied the role of anatomical features in light absorptance. If variegation is structural, it may explain a possible physiological role.

A common type of variance in coloration is defined as variegation, and is a result of either pigment-expression-related heterogeneity, or differences in leaf structure (Sheue et al., 2012). Variegation in tropical leaves has been hypothesized to create a cellular lens structure, as an adaptation for poor light conditions. Two different types of structural variegation are known (Tsukaya et al., 2004) – the "air-space" is a variation in palisade-cell development, in which the palisade cells exhibit rounded shape with air spaces that produce pale grayish-green appearance, as can be found in *Begonia* spp. The second type, i.e., "epidermis" type of variegation, was described in several species, e.g., *Oxalis mariana*, where epidermal attachment to the underlying cell layers varies across a leaf, and sub-epidermal air spaces appear as white or whitish due to their stronger light reflectance (Hara, 1957). Konoplyova et al. (2008) showed that epidermal variegation does not result in loss of photosynthetic capacity. According to this concept variegation is an adaptive morphology leading to non-uniform photosynthesis (Terashima, 1992). Nevertheless, Brodersen and Vogelmann (2007) showed that lens shaped epidermal cells were not advantageous in capturing of indirect (diffuse) light, suggesting that other traits, such as leaf thickness, are more important. In *S. marianum*, the white leaf variegation is the outcome of the formation of sub-epidermal air spaces (Lev-Yadun, 2017).

Several researchers linked thermal advantage to the micro-environment formed by white patches (Hüner et al., 2012). They hypothesized that under cold conditions, bright patches form a microenvironment that alleviate the impact of temperatures to allow better conditions for photosynthesis. Avoidance of freezing and of low temperatures in plants is a widely reported phenomenon (Weiser, 1970; Pearce, 2001; Sakai and Larcher, 2012), but despite the recognition that anatomical structures such as leaf hardness contribute to this adaptation, the role of plant coloration as effecting warming was not studied extensively except for the translucent bracts of several *Rheum* species growing in very high elevations in the Himalaya (Omori and Ohba, 1996; Omori et al., 2000; Tsukaya, 2002; Song et al., 2013). Plants are exposed to various temperatures seasonally or diurnally, hence thermoregulation of these changes has a potentially enormous effect on physiological plant activity in general and specifically on cell photostasis (Hüner et al., 2012) and on photosynthetic rate (Berry and Bjorkman, 1980). Structural modifications in higher plants were reported in alpine and nival regions as an adaptation to low temperatures and to a short vegetation period (Lütz and Engel, 2007).

We hypothesized that by alleviating leaf temperatures, white patches in *S. marianum* leaves provide a microenvironment that promotes photosynthesis rate under the low morning temperatures prevailing in the mildly low winter temperatures that characterize the growth season of this Mediterranean annual. A well-known parallel adaptation under these conditions is diaheliotropism - sun-tracking by leaf movement (Koller, 2000). We are not aware of any study that tested this hypothesis in *S. marianum* or in other annuals with similar white patches (i.e., *Notobasis syriaca*). Our main questions were: (1) what is the nature of white patches in *S. marianum*? What differentiate them from green patches? Specifically we studied the physiological performance of white vs. green patches. (2) Do white patches specifically exhibit more efficient photosynthesis under lower temperatures? We predicted that chlorophyll content of white and green patches is not significantly different and that the morphological difference between the two color appearances allows white patches to provide improved microenvironment. We predicted that this microenvironment effect alleviates low-temperature stress and provides thermic advantage under low temperatures with sufficient photosynthetic active radiation. To test this hypothesis we compared green and white patches of *S. marianum*. We studied morphological traits (stomata abundance and cuticle shape), optic attributes (transmittance, reflectance, and absorptance) biochemistry (chlorophyll, total carotene, and dehydrin content) and physiological performance (photosynthetic activity in different conditions of temperature

and light). We also compared the wild type *S. marianum* expressing the white patches to mutants with green leaves.

# MATERIALS AND METHODS

## Plant Collection and Growth

*Silybum marianum* (L.) Gaertn. (Asteraceae) is a spiny rosette winter annual native to the Mediterranean basin, where it is widespread as a common ruderal weed. Historical records report that the seeds of milk thistle (*S. marianum*) were long used to treat liver related deficiencies (Křen and Walterova, 2005), and recent literature suggested that it does have a real medicinal impact (Karkanis et al., 2011), as well as a nutritional value (Vaknin et al., 2008). The branched canopy is 40–300 cm high, (Montemurro et al., 2007). The basal leaves are alternate, large and glabrous with spiny margins. Leaves of well-developed plants are commonly 50–60 cm long and 20–30 cm wide, and have typical white veins (Gresta et al., 2007), although leaves of very large rosettes may be more than 90 cm long (Lev-Yadun, 2003). Its main growth period is in the early winter, when day temperatures are usually relatively low (5–15°C) and water is available (**Supplementary Material S1**). The seeds are 5–8 mm long, formed at the center of a spiny inflorescence head about 5 cm in diameter, and typically pink in color, although white inflorescence heads are common in various populations (Keasar et al., 2016). Seeds for the plants grown for our study were collected from a wild population in Israel. For comparative studies, we used a wild occurring mutant that appears to have all green leaves, with no white variegation at all. 13 populations of such non-variegated mutants were found in various localities in Israel (Lev-Yadun, 2017). All-green mutant plants growing in a mixed population containing both all-green mutants and variegated wild type were marked by flags at the growing season. Seeds were collected from those marked all-green mutant plants growing in the wild at Nes Ziyyona (about 10 km south of Tel-Aviv) (e.g., Lev-Yadun, 2017).

## Experimental Design

In order to study the properties and function of white patches and to compare them to green patches under different temperature conditions, we used the following experimental setup. We compared three different types of *S. marianum* leaf patches: (1) an entirely green leaf in mutant plants; (2) white patches in wild type variegated leaves; (3) green patches in wild type variegated leaves. We sowed seeds in a greenhouse, one type per 10 liter pot, to establish plants for 3 weeks. The plants were grown in a potting soil. The two plant type seedlings (wild-type and all-green mutant) were then transferred and grown for 15 days in two controlled growth chambers (Percival, Perry, IA). The schedule light regime was 11.5/12.5 d/n with daily intensity of 600 PPFD, and with relative humidity (RH) kept on 70%. Plants were grown individually in 4 liter pots. For statistical power, 15 individuals per variety where used as replicates in each growth chamber with the following temperature levels. Normal temperature simulated an average Mediterranean winter conditions (20°C/10°C d/n); cold temperature (15°C/5°C d/n). All measurements were done on these six patches and temperature types: three patch types (all-green mutant, both green and white patches in wild-type plants), two temperature growth conditions (normal/cold). All experiments took place at December 2012–February 2013.

## Hyperspectral Data Collection With Integrating Sphere

To explore the leaf radiation balance, a FieldSpec PRO (Analytical Spectral Devices, Inc., [ASD], Longmont, CO, United States) was used with an Integrating Sphere I-800-12 (LI-COR Biosciences; Lincoln, NE, United States) as fore optics. This system allows reflectance and transmittance data collection that are used to calculate the leaf absorptance (Gitelson and Merzlyak, 1997; Herrmann et al., 2017). Measurements were acquired from 15 plants including 8 all-green mutants and 7 wild types with a total of 17 samples (few mixed patches were obtained from the same plant). Hyperspectral was obtained from four different patch types: (1) green patches on all-green mutants (eight samples); (2) white patches on wild type leaves (three samples); (3) green mixed where mixed patches spots on wild type, dominated by the green color (three samples); and (4) white mixed where mixed patches spots on wild type plants, dominated by white color (three samples). The mixed type dominancy was estimated by pictures obtained during data collection (% white patch). The spectral range presented (400–1,700 nm) can be divided to three main regions, based on their main influence on the spectral data: visible (VIS; 400–700 nm) mainly affected by pigments content, near infra-red (NIR; 700–1,300 nm) influenced mostly by the leaf internal structure, and shortwave infrared (SWIR; 1,300–1,700 nm) mainly influenced by water absorptance (Curran, 1989; Herrmann et al., 2010). The reflectance and transmittance were measured and the absorptance was calculated. The spectral data was averaged per patch type and measuring method.

## Patch Structure

Five variegated wild type leaves and five leaves of all-green mutant plants were sampled. In the variegated wild type leaves, the samples included half of a white sector and half of a green sector. The samples were immediately fixed in a mixture of 3:1 ethanol and glacial acetic acid overnight at room temperature. After fixation, samples were washed in water three times for 15 min each, dehydrated overnight in a series of ethanol solutions (25, 50, 75, 96, and 100%), and embedded in paraffin. Serial cross sections, 5–10 μm thick, were prepared with a rotary microtome (American Optical model 820, Spencer), from the sampled leaf segments, stained with Safranin and fast green, and mounted with Permount (Thermo Fisher Scientific, Cat. No. SP15-100). Slides were examined under bright field with a Leitz Dialux 20 microscope equipped with a Nikon F3 camera, at magnifications of X16 to X400.

## Stomata Structure

Stomata structure was estimated from epidermal impressions following Falik et al. (2011, 2012) and Sachs et al. (1993).

The abaxial and adaxial surfaces of mature leaves were copied using a fresh mixture of vinyl polysiloxane dental impression material (Elite HD +, Badia Polesine, Rovigo, Italy). The resulting hardened imprints were further copied with clear nail polish, which resulted in transparent preparations suitable for microscopic examination. For statistical repetitions, we used five imprints, from five different plants. Measurements of stomata size and density were carried out using AxioVision software (Carl Zeiss MicroImaging, Thornwood, NY, United States) on digital images of the nail-polish preparations.

## Phytochemical Content (Chlorophyll, Total Carotene and Dehydrin)

Chlorophyll-*a*, chlorophyll-*b* and carotenes were extracted in acetone (80%) and estimated from mature leaves, following the standard method of Arnon (1949). These pigments have a pivoting role in utilizing sun radiation. Hence, to study differences between patches, we wanted to estimate the biochemical characteristics of each patch type. Total carotene was quantified according to the formulas of Lichtenthaler and Wellburn (1985). Dehydrins (DHNs) are an important group of proteins, providing drought stress tolerance (Close and Bray, 1993; Yu et al., 2018) among other functions to the plant. Dehydrin was extracted following methods described by Nylander et al. (2001). The dehydrin content was evaluated by western blot analysis. Proteins were extracted in 50 mM Tris–HCl, 250 mM sucrose, 5 mM EDTA, 10 mM 2-mercaptoethanol pH 7.2, containing protease inhibitors. Antibodies against LTI29, ERD14, LTI30, and RAB18 were used as described by Nylander et al. (2001). We compared all treatments and patches – eight samples per patch (wild type green patch, wild type white patch, green mutant), in the two growth chambers – normal (20°C/10°C d/n) and cold temperatures (15°C/5°C d/n).

## Leaf Temperature

Measuring leaf temperature is challenging (Vermeulen et al., 2012) and measuring direct temperature differences between intra-leaf patches was beyond our capabilities. Hence, we used an IR camera (T-335, FLIR), at 8 am, to estimate the whole leaf temperature by proximate sensing. Image analysis has been done by FLIR Tools software package. We compared mutant green leaves to wild type variegated leaves as we could not distinguish white and green patches on variegated leaves. We took thermal images of five plants per growth temperature (normal/cold) and plant type (green/white), a total of 20 plants. Photos were taken at 8:00 to resemble natural conditions that expose plants to cold temperatures and low radiation. We assumed that if differences between green and white patches are distinguishable, they are likely to be apparent at this time of the day. Each image was divided to 4–7 rectangle sections, an average, minimum, and maximum temperatures were calculated per section according to pixel coloration, a reflection of the IR radiation. Each section served as a repetition, summarized to approximately 25 repetitions per combination of leaf type (green/varigated) and growth temperature (normal/cold).

## Photosynthetic Activity and Plant Growth

Plants were harvested at February 13th 2013 after 90 days of growth. Shoot dry weight (DW) served as a measure of plant development. Shoots were harvested and dried (65°C, 48 h) before measurement with analytical scale (Entris® Analytical Balance, Sartorius Corp., Goettingen, Germany). Five shoots per plant type and growth chamber were measured. To examine photosynthetic response of white and green patches to thermal conditions – we measured photosynthesis rate in three different temperature conditions. Five individuals per plant type (wild type or green mutant) and growth chamber temperature (normal/cold) were measured in three temperature conditions. The plants were measured in three different rooms to provide the partitioning of air temperatures, finely dictated by infra-red gas analyzer (IRGA) (LI-COR 6400, LI-COR Biosciences, Lincoln, NE, United States). Leaf gas exchange parameters were measured using an (IRGA) coupled with a 2 $cm^2$ leaf fluorescence chamber (Li-6400−40 leaf chamber fluorometer; Li-Cor., Inc.) This setup allowed an estimation of the non-photochemical quenching parameter (NPQ). NPQ is a good estimator of the heat dissipation, or the light energy that was not used by the plant for photosynthesis (Murchie and Lawson, 2013) To provide 20°C we used a growth chamber; 15°C was measured in the lab; to measure photosynthesis efficiency in 5°C we used a cold room. *Photosynthetic efficiency* is a measure of the maximal PSII efficiency, expressed by the ratio Fv/Fm (Papageorgiou and Govindjee, 2004). Fm is the maximum fluorescence re-emitted from the measured leaf; Fv is expressed as Fm-Fo, where Fo denotes fluorescence yield in the absence of actinic light (Maxwell and Johnson, 2000). Fv/Fm indicates the efficiency of PSII photochemistry during conversion of excitation energy to chemical energy in the photochemical electron transport chain. In healthy plants, this efficiency is about 80% or 0.8 Fv/Fm; values of Fv/Fm that are lower than ∼0.8 are considered as injurious levels, given that plants are measured at the same conditions (Bjorkman and Demmig, 1987; Johnson et al., 1993). Photochemical efficiency was always measured at the same time of the day for all plants (8:00–10:00 am). We measured darkened leaves with a MINI-PAM (Walz GmbH, Effeltrich, Germany). Leaves were dark-adapted for 20 min to ensure full oxidation of the electron transport chain and disengagement of the qE thermal energy-dependent quenching. We measured four combinations of patches and growth temperature (white and green patches in regular and cold growth temperatures). We used at least four patches for each patch combination as repetitions. We measured net photosynthetic rate by an IRGA, following light accumulation curve procedure as described by Carriquí et al. (2018). Net photosynthesis was measured in $CO_2$ concentrations leveled to 400 μmol $mol^{-1}$ (approximating ambient concentration, ∼378 μmol $mol^{-1}$) and under three levels of photosynthetic active radiation (PAR = 100, 500, 1,500 μmol photons $m^{-2}$ $s^{-1}$). The sequence of light curve performed was PAR = 100, 500, 1,500, 100, 1,500, 100 with

3 min intervals. The initial goal of this sequence was to trace light reaction after gradual increase of light intensity, a recovery, and a sharp increase of light intensity. Finally, for simplification, we considered only the first three sequential repetitions of PAR levels (100, 500, and 1,500 μE $m^{-2}$ $s^{-1}$ performed in this order).

# RESULTS

## Morphology and Phytochemistry of White and Green Patches

Our results suggest that variegation in *S. marianum* is created by an intercellular space above the chlorenchyma rather than by pigments (**Supplementary Material S2**). We found that stomata length in white and green patches did not differ across growth temperature and leaf aspect. Interestingly, compared to green patches – white patches seem to have higher density of stomata at the abaxial side, and lower density on the adaxial side, although we noticed differences with significance of $p = 0.06$ only in the case of plants growing under cold temperatures (**Table 1**). Biochemistry of the green and white patches did not show any clear and significant differences: total carotene, chlorophyll-*a* and chlorophyll-*b* did not differ significantly (**Figure 1**). Dehydrin content did not show any significant difference between patches or growth temperatures, and hence is not presented here.

## Optical Attributes of White, Green, and Mixed Patches

The measurements obtained by the integrated sphere provided information on the leaf reflectance (**Figure 2A**), transmittance (**Figure 2B**) and absorptance (**Figure 2C**). The averaged reflectance of the white patches was with the highest intensity for all the spectral range. The white dominated mixed patches intensity was intermediate and the green and green dominated mixed patches had the lowest intensity. Therefore, less VIS radiation is available for the chlorophyll in the white patches. The measured transmittance showed very similar intensities in the VIS region for all patches types. Thus, the absorptance of VIS radiation in the white patches is smaller than the other patches (**Figure 2C**). The radiation absorptance in the NIR had no visible differences between all four patches as a result of the opposite reflectance and transmittance trends in that spectral region. In the SWIR spectral region the white patches reflected more than other patches, transmitted less than others and absorbed less than other (**Figure 2**).

## Thermal Traits of White and Green Patches

**Figure 3** presents the thermal difference between wild type and all-green mutant leaves of *S. marianum*. Plants grown in mildly cold temperatures (15°C/5°C d/n) showed that wild type leaves were ∼7% warmer (9.5 ± 0.15°C average ± se) than all-green mutant leaves (8.9 ± se 0.17°C average ± se). Overall higher temperatures (13.8°C) were measured on leaves growing in the normal temperatures (20°C/10°C d/n). However, our measurements did not detect significant difference between patch types of plants grown in normal temperatures (**Figure 3A**). **Figure 3B** demonstrates the apparent difference between the two leaf types in two temperature regimes, in images taken by IR camera.

## Photosynthetic Activity and Efficiency of White and Green Patches

All-green mutants appeared to grow 28% heavier shoots than wild type plants (38.9 ± 2.7 g/30.2 ± 2.6 g average ± se). However, these results are not significant statistically. In colder temperatures, plants appear to grow less, but again, the differences between the wild-type and the green mutant are not significant (**Figure 4A**). We found a similar result for the NPQ – no significant differences between the patch types. Interestingly, the green patches appear to have higher NPQ in all conditions, meaning white patches may be more efficient, or dissipating less light for heat. However, the differences were not significant and are not presented in figures. The photosynthetic efficiency dropped as *S. marianum* plants were exposed temporarily to colder temperatures (**Figure 4B**), with the least photosynthesis rate at exposure to 5°C. Looking to compare white and green patches – our measurements did not find any significant advantage to one patch over the other, in plants grown at normal temperatures (**Figure 4B**). Similar insignificant differences between the two patches were found in plants grown in colder temperatures (not presented). The maximal PSII efficiency (Fv/Fm) was significantly lower in white patches that grew in normal temperature conditions (**Figure 4C**). However, the values of all four patches and growth temperatures were high and therefore there is no biological means for these minor differences: all plants presented values of considerable high levels of photosynthetic activity. Efficiency of 80% is considered as the threshold for healthy unstressed plants (Fv/Fm > 0.8).

# DISCUSSION

We studied white and green patches in *S. marianum*, aiming at figuring out if there are any distinguishable physiological differences between them. We tested the hypothesis that white patches provide a physiological advantage to the leaf, as they can alleviate temperatures during cold winter days, allowing improved thermal conditions for more efficient photosynthesis. In accordance to our predictions, we did not find significant differences in some phytochemical features of the two patch types. We found that the white colored patch is a result of a structural difference (sub-epidermal air spaces), and that the stomata dispersion did not differ significantly between green vs. white patches ($p > 0.05$). Under low temperature conditions, we measured higher temperatures on wild-type plants, in comparison to all-green mutant plants. We did not find any significant difference in the photosynthetic activity and NPQ of the two patches, suggesting that white patches are not hindering photochemical efficiency.

**TABLE 1 |** Stomata density and length of *Silybum marianum* white and green patches.

| Abaxial side (Down) | | | | | |
|---|---|---|---|---|---|
| **Growth temperature (°C)** | **Patch** | **Stomatal density (#mm$^{-2}$ ± se)** | **Results of statistic test** | **Stomatal length (mm ± se)** | **Results of statistic test** |
| **15** | Green | 136.5 ± 12.8 | $t = 0.85$, $p = 0.41$ | 0.038 ± 0.001 | $t = 0.43$, $p = 0.68$ |
| | White | 154 ± 16.1 | | 0.0372 ± 0.001 | |
| **20** | Green | 120.2 ± 11.1 | $t = 0.53$, $p = 0.61$ | 0.042 ± 0.002 | $t = 1.46$, $p = 0.17$ |
| | White | 140.3 ± 36.0 | | 0.0376 ± 0.002 | |
| **Adaxial side (UP)** | | | | | |
| **Growth temperature (°C)** | **Patch** | **Stomatal density (#mm$^{-2}$ ± se)** | **Results of statistic test** | **Stomatal length (mm ± se)** | **Results of statistic test** |
| **15** | Green | 106.2 ± 4.6 | $t = 2.15$, $p = 0.06$ | 0.04 ± 0.002 | $H = 9$, $p = 0.51$ |
| | White | 87.4 ± 7.4 | | 0.0376 ± 0.002 | |
| **20** | Green | 104.4 ± 9.9 | $t = 0.76$, $p = 0.46$ | 0.04 ± 0.001 | $t = 11$, $p = 0.91$ |
| | White | 88.1 ± 18.9 | | 0.0404 ± 0.003 | |

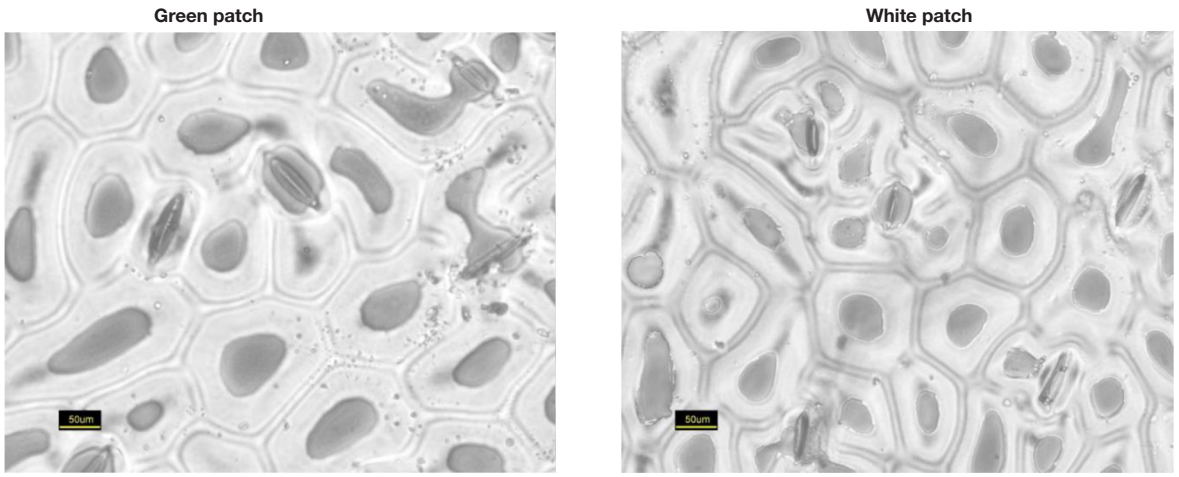


*Microscope images are randomly chosen from each patch and do not represent a typical character of the stomata in the different patches. Taken from transparent imprints, the gray colors of the images have no biological meaning. Pair-wise t-test results are given, or Mann-Whitney U in case that data was not distributed normally (n = 5).*

## White and Green Patches Are Distinguished Anatomically and Morphologically and Not Biochemically

Our study confirmed that the white variegation in *S. marianum* is structural: sub-epidermal air spaces, is the mechanism creating the patches of white coloration (**Supplementary Material S2**). The optical features that we measured are in accordance to this finding (**Figure 2**). In the VIS spectral range, white patches exhibited the lowest absorptance rates, due to high reflectance, meaning that the morphological coloration is correlated with lower absorptance rates. These findings suggest that pigment functioning is reduced in the white patches as the pigment levels are similar to those in the green patches, but in the white patches, the miniature air spaces are masking the chlorophyll. Regarding water content, affecting the SWIR spectral range, although in the water-affected region, the relatively high reflectance might be partly increased by the air spaces (Karnieli et al., 2013), which is a leaf structure property. The absorptance in the SWIR region is the lowest for the white patches as they might have higher water content than green patches. Since there is no information about the actual water content, the above mentioned difference can only be assumed. Sheue et al. (2012) explained how the epidermal tissue, when loosely connected to the mesophyll, is creating tiny air spaces that appear as light areas in *Begonia*. According to Sheue et al. (2012) the air spaces are photosynthetically active. Our results support the findings and interpretation of Sheue et al. (2012). Nevertheless, we noticed some slight differences in stomata density (**Table 1**), where white patches seem to have in average more stomata at the abaxial side as compared to the adaxial side. These differences were not significant statistically ($p > 0.05$). Having more stomata on the leaf's lower surface (hypostomy) is common (Fahn, 1990), mainly in fast growing plants, such as annuals (Muir, 2015). If this hypostomy is pronounced more prominently in white patches, it may induce different functioning of the photosynthesis dynamics in the two patch types. The stomatal ratio between abaxial and adaxial sides has a role in transpiration and therefore affecting the heat balance of the leaves (Lee, 2018). To show the impacts of distinguished stomatal ratio in white versus green patches, it requires firmer results, and statistics that are more robust.

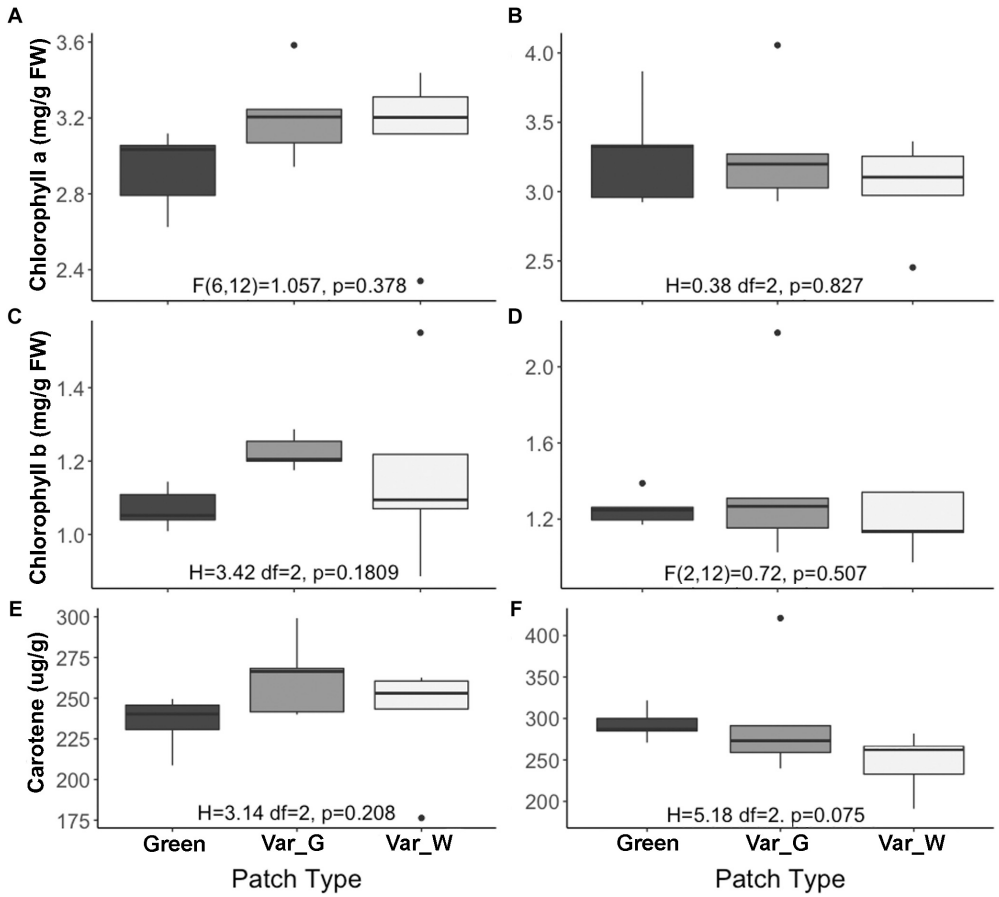


**FIGURE 1 |** Biochemical content of *Silybum marianum* white and green patches. The *X* axis shows three categories of patch types: Green, patch of a green mutant; Var-G, green patch on a variegated leaf; Var-W, white patch on a variegated leaf. The left figures **(A,C,E)** describe measurements of plants grown under normal conditions (20°/10°C d/n). The right figures **(B,D,F)** describe measurements of plants grown under cold conditions (15°/5°C d/n). **(A,B)** Chlorophyll-*a* content; **(C,D)** Chlorophyll-*b* content; **(E,F)** Total carotene content (mg/g). Results of one-way ANOVA test are given per figure. Boxplots represent median. The lower and upper hinges correspond to the 25 and 75th percentiles. Dots represent outliers.

Muir (2015) suggested that stomata ratio is also related to defense against pathogens – more stomata on the adaxial (upper) side means more efficient photosynthesis, but this trend is constrained by a higher risk of pathogen intrusion. We did not look at stomata resistance that can provide the plant with the flexibility to respond to a variety of stresses (Lu, 1989). Nevertheless, a variety of stomata spacing, ratio and resistance, may hypothetically enable the leaf a greater flexibility of response arsenal to different environmental conditions. Hence, if we can show that such a difference between stomata density in the two patch type exists, it may suggest that white variegation is related to a higher level of physiological flexibility. At this point, this is only hypothetical explaining variable, as it is uncertain if stomatal resistance would show any differences between the patch types.

## White Patches Can Provide Thermal Advantages

We found that in plants grown in a cold temperature regime (15°C/5°C d/n), the wild type leaves were significantly warmer than those of all-green mutants (**Figure 3**). The major factors affecting the energy budget of a leaf are energy gain or loss by absorptance/emission of long and short-wave radiation, energy gain or loss by convection and energy loss by transpiration. The temperature of the leaf relative to the air temperature will vary depending on external parameters including light intensity, temperature, wind and relative humidity. Hypothetically, factors that may cause slightly higher temperatures in the white patches are: (1) absorptance. However, lower absorptance of visible light, as appeared in the white patches is likely to result in less heat gain by radiation. Hence, absorptance is not the leading factor to warmer white patches; (2) active stomata structure – more stomata means more efficient photosynthesis, that may affect the heat balance. However, our results did not confirm significant differences in stomata structure. (3) Sub-epidermal air spaces alleviate the temperatures locally. This effect may be the result of reduced heat convection, or another mechanism. In other words, the results support the hypothesis that white variegation in *S. marianum* are able to increase leaf temperatures presumably functioning as miniature greenhouses. The patchy nature of

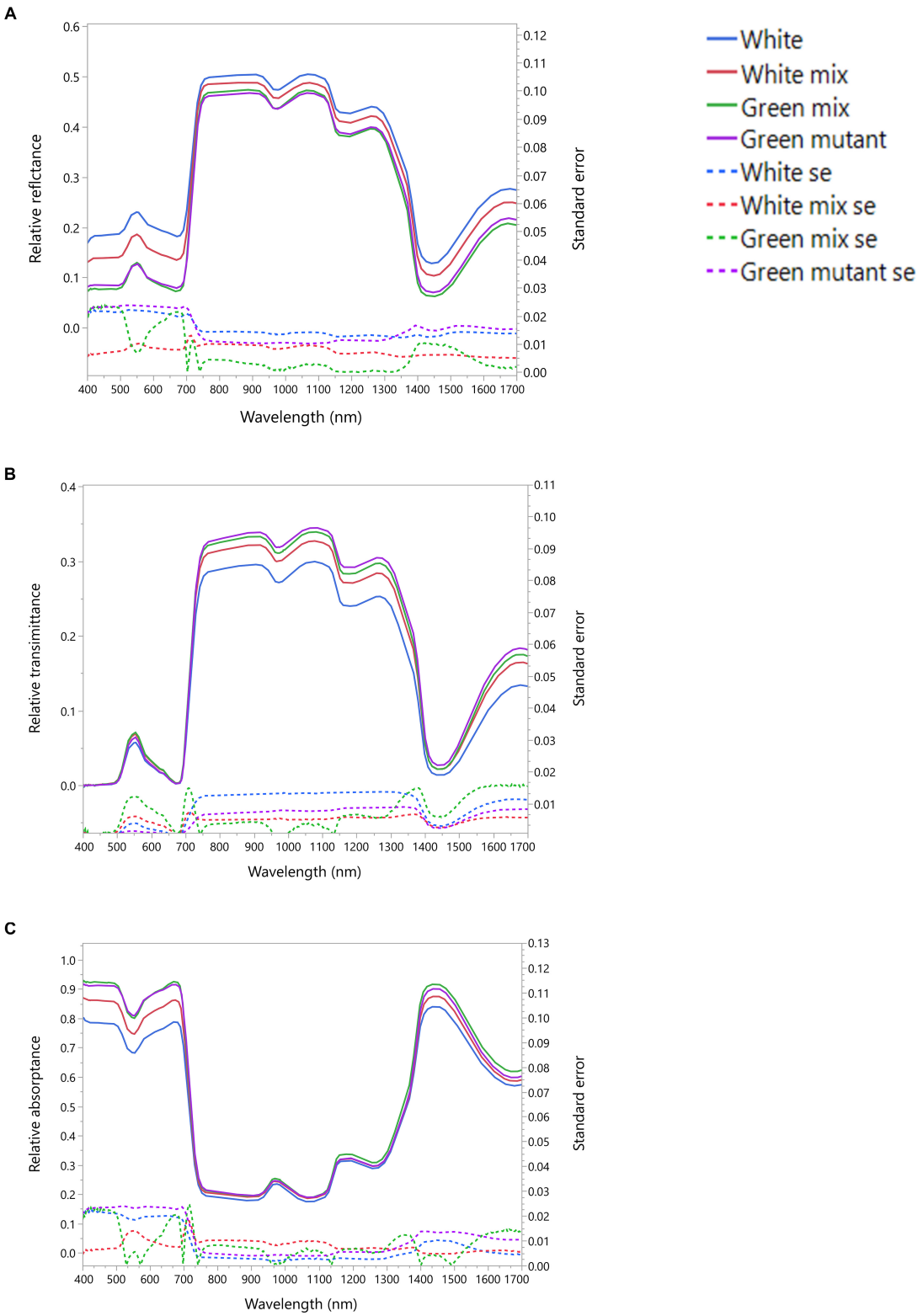


**FIGURE 2 |** Averaged spectral signatures of *S. marianum*. The spectral signature was measured in four different patch types, along a gradient of white to green variegation. White – is an entirely white patch on a variegated wild type leaf. Green mutant – is an entirely green patch, on a green leaf mutant. White mix and Green mix – are the intermediate patches on a wild type variegated leaf, where the white mix is a patch dominated by white variegation, and the green mix is dominantly green. **(A)** Leaf averaged reflectance and standard error; **(B)** leaf averaged transmittance and standard error; **(C)** leaf averaged absorptance and standard error. Dotted lines represent standard error (se).

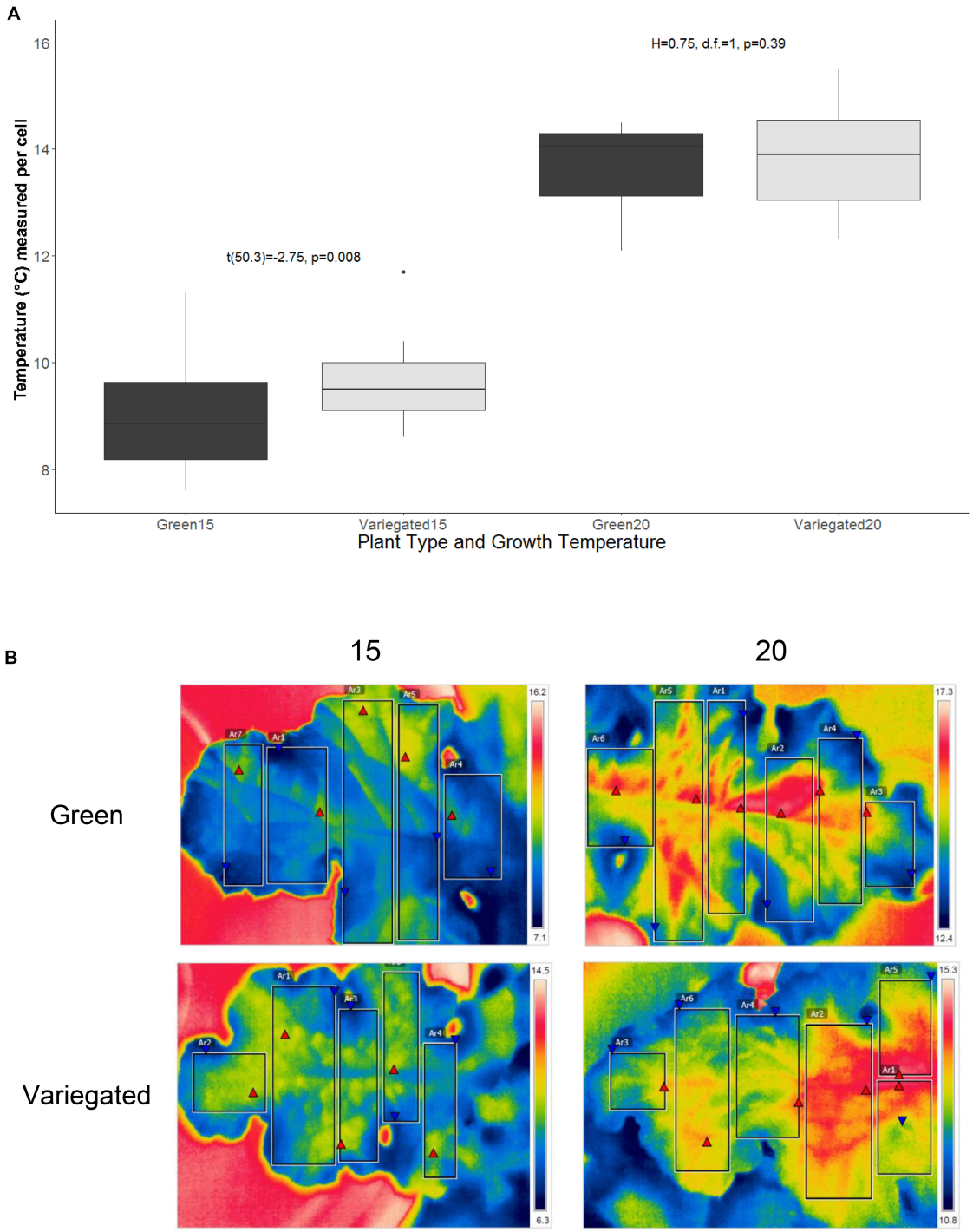


**FIGURE 3 |** Thermal traits of *Silybum marianum*'s white and green patches. The temperature of five adult leaves per plant type and growth temperature was measured by an IR camera at 8 am. Variegated leaves are the wild-type, green leaves are of the all-green mutants without any white patches. Growth temperature relate to the conditions maintained within the growth chambers. 20 represents the normal conditions (20°/10°C d/n) whereas 15 denotes cold temperatures (15°/5°C d/n). **(A)** Average pixel temperature of variegated and green leaves was calculated from 4 to 6 rectangular areas in the leaf image. Results of *t*-test are given within the figure. Boxplots represent median. The lower and upper hinges correspond to the 25 and 75th percentiles. Dots represent outliers; **(B)** Four typical IR images that served as the data to analyze thermal traits. Each leaf was divided to 4–6 rectangular areas, from which various values are presented and calculated. These include min (red triangular) and max (blue triangular) temperatures, and average pixel temperature, with color-temperature scale on the right side of the image.

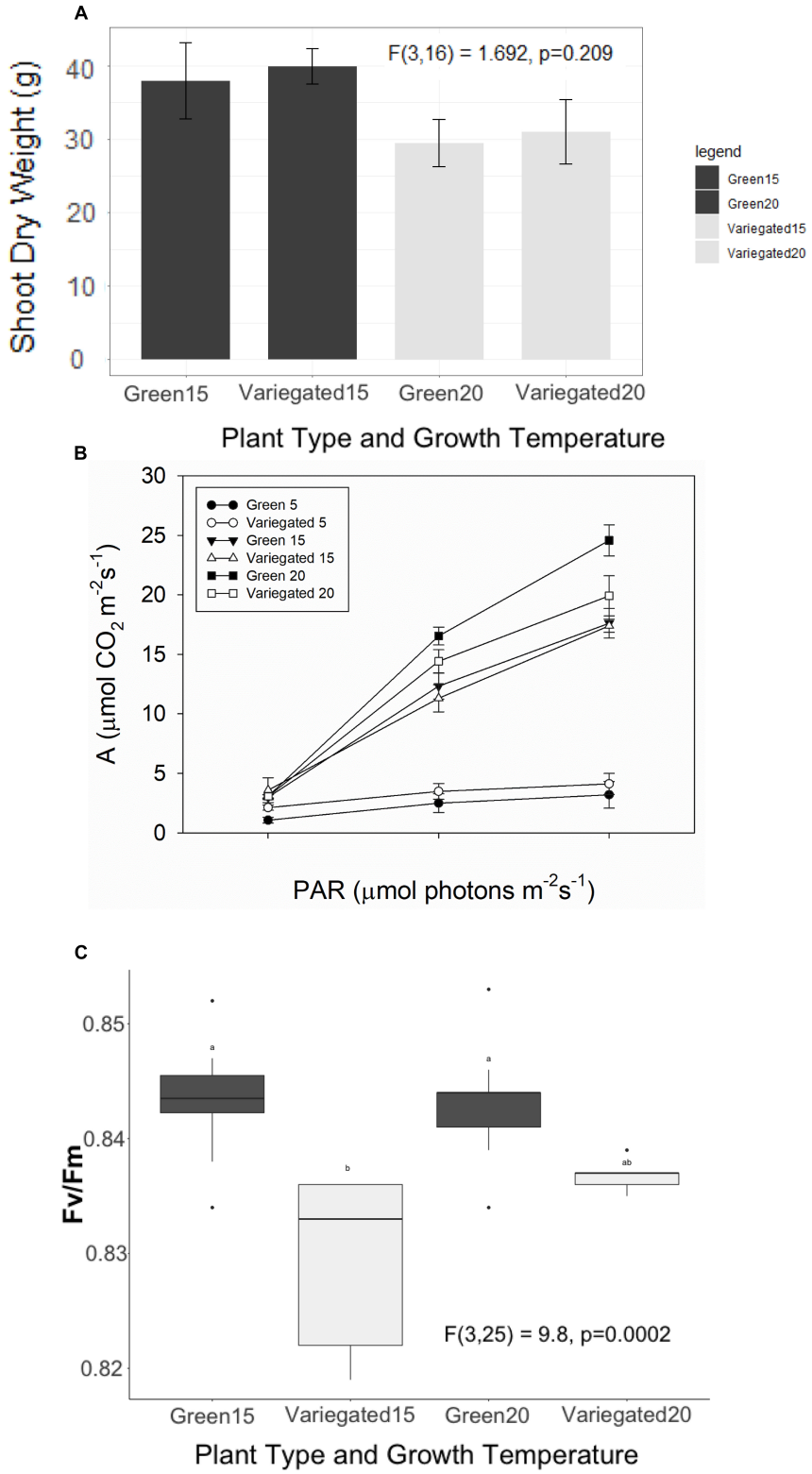


**FIGURE 4 |** Photosynthetic efficiency of *Silybum marianum* white and green patches. Variegated denotes wild type patched leaves, Green represents an all-green mutant. **(A)** Plant growth. The values represent the total shoot dry biomass, as harvested at the end of the experiment; **(B)** Photosynthetic efficiency as measured by Infra-Red Gas Analyzer (LICOR-6400) for plants grown at normal winter temperatures (20°/10°C d/n). Light curves were measured at ambient $CO_2$ level (380 ppm) following a short time acclimation (1 h) to 5°, 15°, or 20°C; **(C)** Maximal PSII efficiency (Fv/Fm) measured by WALTZ miniPAM after a dark period. Boxplots represent median. The lower and upper hinges correspond to the 25 and 75th percentiles. Dots represent outliers. Different letters denote significant differences.

leaf variegation in *S. marianum* can provide the plant with near optimal thermal micro-conditions in a variety of climatic conditions that are typical to the Mediterranean winter. Leaf thermoregulation is a key factor in carbon economics, among other parts of leaf optimization to maximize carbon gain in different and dynamic environments (Michaletz et al., 2016), and probably concerning other metabolic functions. In addition, the structure and distribution of leaf veins play a key role in mitigation of frost stress (Stevenson, 2015; Lim et al., 2017) or improved transport in the phloem channels. Hypothetically, regulating the temperature in the veins by sufficient structure can reduce the exposure to freezing point by shortening the time of exposure, and the range of temperatures. This hypothesis has to be studied in more details to get further support.

### Photosynthetic Activity in White Patches Is as Efficient as in Green Patches

Our results did not support the hypothesis that white patches alleviate photosynthetic rate by creating warmer spots under cold air temperature conditions. However, the results do suggest that photosynthesis in white patches is not inferior to green patches: in spite of the apparent screening of chlorophyll in white patches, the photosynthetic efficiency and activity are the same as in green patches, in all tested conditions (**Figure 4**). The shoot dry weight of the all-green mutant seems to be marginally heavier (**Figure 4A**), though insignificantly. Apparently, all-green mutants are growing more efficiently in controlled temperatures. Nevertheless – they do not prevail in natural conditions, being a rare phenotype in a dominant population of white variegated wild type (Lev-Yadun, 2017). The dominance of the white variegated phenotype shows that the advantage of white patches is overtaking the potential disadvantages of partly masking the direct green tissue. In other words, even though visible light absorptance rates in the white patches are reduced – the same chlorophyll content is more effective under higher temperature conditions in a warmer microenvironment. Our results suggest that the thermoregulation flexibility of the white patches may be the mechanism behind the dominancy of white patches in *S. marianum* and maybe in other species. If indeed as suggested, the white patches also serve as visual defense from herbivory (Lev-Yadun, 2003, 2016) – the gain from variegation is even larger.

## CONCLUSION

This study showed that white variegation on *S. marianum* leaves, the outcome of sub-epidermal air spaces, may provide the leaf with thermal advantages during cold winter days. These findings can give an additional explanation to patterns of colors in variegated plant leaves, revealing a physiological mechanism in the evolution of non-green coloration of leaves, and of its physiological function in leaves.

## AUTHOR CONTRIBUTIONS

OS lead the experiments and wrote the process. LS was in charge of plant growth and conducting all experiments. SL-Y provided seeds of WT and green mutants and initiated ideas. RS and IH analyzed the hyperspectral data. SV-C assisted with data analysis and presentation. SR coordinated the study. All authors contributed to writing the manuscript.

## ACKNOWLEDGMENTS

We would like to express our gratitude to Alexander Goldberg for executing the data collection by Integrating Sphere, in collaboration with The Remote Sensing Laboratory, Jacob Blaustein Institutes for Desert Research, Ben-Gurion University of the Negev. We thank to Amir Eppel for his contribution in executing experiments, and to Amnon Cochavi for his part in reviewing the text.

## SUPPLEMENTARY MATERIAL

The Supplementary Material for this article can be found online at: https://www.frontiersin.org/articles/10.3389/fpls.2019.00688/full#supplementary-material

## REFERENCES

Aluru, M. R., Bae, H., Wu, D., and Rodermel, S. R. (2001). The *Arabidopsis immutans* mutation affects plastid differentiation and the morphogenesis of white and green sectors in variegated plants. *Plant Physiol.* 127, 67–77. doi: 10.1104/pp.127.1.67

Arnon, D. I. (1949). Copper enzymes in isolated chloroplasts. polyphenol oxidase in *Beta vulgaris*. *Plant Physiol.* 24:1. doi: 10.1104/pp.24.1.1

Barbosa, M. A. M., Chitwood, D. H., Azevedo, A. A., Araújo, W. L., Ribeiro, D. M., Peres, L. E., et al. (2018). Bundle sheath extensions affect leaf structural and physiological plasticity in response to irradiance. *Plant Cell Environ.* 42, 1575–1589. doi: 10.1111/pce.13495

Berry, J., and Bjorkman, O. (1980). Photosynthetic response and adaptation to temperature in higher plants. *Ann. Rev. Plant Physiol.* 31, 491–543. doi: 10.1146/annurev.pp.31.060180.002423

Bjorkman O., and Demmig B. (1987). Photon yield of O-2 evolution and chlorophyll fluorescence characteristics at 77-K among vascular plants of diverse origins. *Planta* 170, 489–504. doi: 10.1007/bf00402983

Brodersen, C. R., and Vogelmann, T. C. (2007). Do epidermal lens cells facilitate the absorptance of diffuse light? *Am. J. Bot.* 94, 1061–1066. doi: 10.3732/ajb.94.7.1061

Buckley, T. N., Sack, L., and Gilbert, M. E. (2011). The role of bundle sheath extensions and life form in stomatal responses to leaf water status. *Plant Physiol.* 156, 962–973. doi: 10.1104/pp.111.175638

Carriquí, M., Douthe, C., Molins, A., and Flexas, J. (2018). Leaf anatomy does not explain apparent short-term responses of mesophyll conductance to light and CO2 in tobacco. *Physiol. Plant.* 165, 604–618. doi: 10.1111/ppl.12755

Close, T. J., and Bray, E. A. (1993). Plant responses to cellular dehydration during environmental stress. in *Proceedings of the Riverside Symposium in Plant Physiology 1993*, eds T. J. Close, and E. A. Bray (Riverside: American Society of Plant Physiologists).

Curran, P. J. (1989). Remote sensing of foliar chemistry. *Remote Sens. Environ.* 30, 271–278. doi: 10.1016/0034-4257(89)90069-2

Fahn, A. (1990). *Plant Anatomy*, 4th ed. (Oxford: Pergamon Press).

Falik, O., Mordoch, Y., Ben-Natan, D., Vanunu, M., Goldstein, O., and Novoplansky, A. (2012). Plant responsiveness to root–root communication of stress cues. *Ann. Bot.* 110, 271–280. doi: 10.1093/aob/mcs045

Falik, O., Mordoch, Y., Quansah, L., Fait, A., and Novoplansky, A. (2011). Rumor has it: relay communication of stress cues in plants. *PLoS One* 6:e23625. doi: 10.1371/journal.pone.0023625

Fooshee, W. C., and Henny, R. J. (1990). Chlorophyll levels and anatomy of variegated and nonvariegated areas of *Aglaonema nitidum* leaves. *Proc. Fla. State Hortic. Soc.* 103, 170–172.

Gitelson, A. A., and Merzlyak, M. N. (1997). Remote estimation of chlorophyll content in higher plant leaves. *Int. J. Remote Sens.* 18, 2691–2697. doi: 10.1080/014311697217558

Gresta, F., Avola, G., and Guarnaccia, P. (2007). Agronomic characterization of some spontaneous genotypes of milk thistle (*Silybum marianum* L. *Gaertn.*) in mediterranean environment. *J. Herbs Spices Med. Plants* 12, 51–60. doi: 10.1300/j044v12n04_05

Hara, N. (1957). Study of the variegated leaves with special reference to those caused by air spaces. *Jpn. J. Bot.* 16, 86–101.

Herrmann, I., Berenstein, M., Paz-Kagan, T., Sade, A., and Karnieli, A. (2017). Spectral assessment of two-spotted spider mite damage levels in the leaves of greenhouse-grown pepper and bean. *Biosyst. Eng.* 157, 72–85. doi: 10.1016/j.biosystemseng.2017.02.008

Herrmann, I., Karnieli, A., Bonfil, D J., Cohen, Y., and Alchanatis, V. (2010). SWIR-based spectral indices for assessing nitrogen content in potato fields. *Int. J. Remote Sens.* 31, 5127–5143. doi: 10.1080/01431160903283892

Hüner, N. P., Bode, R., Dahal, K., Busch, F. A., Possmayer, M., Szyszka, B., et al. (2012). Shedding some light on cold acclimation, cold adaptation, and phenotypic plasticity 1. *Botany* 91, 127–136. doi: 10.1139/cjb-2012-0174

Jiang, W., Zhuang, M., Han, H., Dai, M., and Hua, G. (2004). Progress on color emerging mechanism and photosynthetic characteristics of colored-leaf plants. *Acta Hortic. Sin.* 32, 352–358. doi: 10.1139/cjb-2012-0174

Johnson, G. N., Young, A. J., Scholes, J. D., and Horton, P. (1993). The dissipation of excess excitation-energy in British plant-species. *Plant Cell Environ.* 16, 673–679. doi: 10.1111/j.1365-3040.1993.tb00485.x

Karkanis, A., Bilalis, D., and Efthimiadou, A. (2011). Cultivation of milk thistle (*Silybum marianum* L. Gaertn.), a medicinal weed. *Industr. Crops Prod.* 34, 825–830. doi: 10.1016/j.indcrop.2011.03.027

Karnieli, A., Bayarjargal, Y., Bayasgalan, M., Mandakh, B., Dugarjav, C., Burgheimer, J., et al. (2013). Do vegetation indices provide a reliable indication of vegetation degradation? A case study in the mongolian pastures. *Int. J. Remote Sens.* 34, 6243–6262. doi: 10.1080/01431161.2013.793865

Keasar, T., Gerchman, Y., and Lev-Yadun, S. (2016). A seven-year study of flower-color polymorphism in a mediterranean annual. *Basic Appl. Ecol.* 17, 741–750. doi: 10.1016/j.baae.2016.10.003

Koller, D. (2000). Plants in search of sunlight. *Adv. Bot. Res.* 33, 35–131. doi: 10.1016/s0065-2296(00)33041-5

Konoplyova, A., Petropoulou, Y., Yiotis, C., Psaras, G. K., and Manetas, Y. (2008). The fine structure and photosynthetic cost of structural leaf variegation. *Flora* 203, 653–662. doi: 10.1016/j.flora.2007.10.007

Křen, V., and Walterova, D. (2005). Silybin and silymarin-new effects and applications. *Biomed. Papers* 149, 29–41. doi: 10.5507/bp.2005.002

Kursar, T. A., and Coley, P. D. (1992). Delayed greening in tropical leaves: an antiherbivore defense? *Biotropica* 24, 256–262. doi: 10.1002/ece3.4859

Lee, X. (ed.). (2018). "Energy Balance, Evaporation, and Surface Temperature," in *Fundamentals of Boundary-Layer Meteorology*. (Cham: Springer), 191–213. doi: 10.1007/978-3-319-60853-2_10

Lev-Yadun, S. (2003). Why do some thorny plants resemble green zebras? *J. Theor. Biol.* 224, 483–489. doi: 10.1016/s0022-5193(03)00196-6

Lev-Yadun, S. (2009). Müllerian and Batesian mimicry rings of white-variegated aposematic spiny and thorny plants: a hypothesis. *Isr. J. Plant Sci.* 57, 107–116. doi: 10.1560/ijps.57.1-2.107

Lev-Yadun, S. (2016). *Defensive (Anti-Herbivory) Coloration in Land Plants. Anti-Herbivory Plant Coloration and Morphology*. Zug: Springer.

Lev-Yadun, S. (2017). Local loss of the zebra-like coloration supports the aposematic and other visual defense hypotheses in *Silybum marianum*. *Isr. J. Plant Sci.* 64, 170–178.

Lev-Yadun, S., Dafni, A., Flaishman, M. A., Inbar, M., Izhaki, I., Katzir, G., et al. (2004). Plant coloration undermines herbivorous insect camouflage. *BioEssays* 26, 1126–1130. doi: 10.1002/bies.20112

Lichtenthaler, H. K., and Wellburn, A. R. (1985). Determination of total carotenoids and chlorophylls A and B of leaf in different solvents. *Biol. Soc. Trans.* 11, 591–592. doi: 10.1042/bst0110591

Lim, F. K., Pollock, L. J., and Vesk, P. A. (2017). The role of plant functional traits in shrub distribution around alpine frost hollows. *J. Veg. Sci.* 28, 585–594. doi: 10.1111/jvs.12517

Lu, Z. M. (1989). Ratio of stomatal resistance on two sides of wheat leaves as affected by soil water content. *Agric. For. Meteorol.* 49, 1–7. doi: 10.1016/0168-1923(89)90057-9

Lütz, C., and Engel, L. (2007). Changes in chloroplast ultrastructure in some high-alpine plants: adaptation to metabolic demands and climate? *Protoplasma* 231, 183–192. doi: 10.1007/s00709-007-0249-8

Maxwell, K., and Johnson, G. N. (2000). Chlorophyll fluorescence — a practical guide. *J. Exp. Bot.* 51, 659–668. doi: 10.1093/jexbot/51.345.659

McClendon, J. H. (1992). Photographic survey of the occurrence of bundle-sheath extensions in deciduous dicots. *Plant Physiol.* 99, 1677–1679. doi: 10.1104/pp.99.4.1677

Michaletz, S. T., Weiser, M. D., McDowell, N. G., Zhou, J., Kaspari, M., Helliker, B. R., et al. (2016). The energetic and carbon economic origins of leaf thermoregulation. *Nat. Plants* 2:16129. doi: 10.1038/nplants.2016.129

Montemurro, P., Fracchiolla, M., and Lonigro, A. (2007). Effects of some environmental factors on seed germination and spreading potentials of *Silybum marianum* Gaertner. *Ital. J. Agron.* 2, 315–320.

Muir, C. D. (2015). Making pore choices: repeated regime shifts in stomatal ratio. *Proc. R. Soc. B* 282:20151498. doi: 10.1098/rspb.2015.1498

Murchie, E. H., and Lawson, T. (2013). Chlorophyll fluorescence analysis: a guide to good practice and understanding some new applications. *J. Exp. Bot.* 64, 3983–3998. doi: 10.1093/jxb/ert208

Niu, Y., Sun, H., and Stevens, M. (2018). Plant camouflage: ecology, evolution, and implications. *Trends Ecol. Evol.* 33, 608–618. doi: 10.1016/j.tree.2018.05.010

Nylander, M., Svensson, J., Palva, E. T., and Welin, B. V. (2001). Stress-induced accumulation and tissue-specific localization of dehydrins in Arabidopsis thaliana. *Plant Mol. Biol.* 45, 263–279.

Omori, Y., and Ohba, H. (1996). Pollen development of *Rheum nobile* Hook.f. & Thomson (Polygonaceae), with reference to its sterility induced by bract removal. *Botan. J. Linnean Soc.* 122, 269–278. doi: 10.1111/j.1095-8339.1996.tb02076.x

Omori, Y., Takayama, H., and Ohba, H. (2000). Selective light transmittance of translucent bracts in the Himalayan giant glasshouse plant *Rheum nobile* Hook.f. & Thomson (Polygonaceae). *Bot. J. Linnean Soc.* 132, 19–27. doi: 10.1006/bojl.1999.0280

Papageorgiou, G. C., and Govindjee. (2004). *Chlorophyll a Fluorescence: a Signature of Photosynthesis (Advances in Photosynthesis and Respiration)*. Dordrecht: Springer.

Pearce, R. S. (2001). Plant freezing and damage. *Ann. Bot.* 87, 417–424. doi: 10.1006/anbo.2000.1352

Roelfsema, M., Konrad, K. R., Marten, H., Psaras, G. K., Hartung, W., and Hedrich, R. (2006). Guard cells in albino leaf patches do not respond to photosynthetically active radiation, but are sensitive to blue light, CO2 and abscisic acid. *Plant Cell Environ.* 29, 1595–1605. doi: 10.1111/j.1365-3040.2006.01536.x

Sachs, T., Novoplansky, N., and Kagan, M. L. (1993). Variable development and cellular patterning in the epidermis of *Ruscus hypoglossum*. *Ann. Bot.* 71, 237–243. doi: 10.1006/anbo.1993.1030

Sakai, A., and Larcher, W. (2012). *Frost Survival of Plants: Responses and Adaptation to Freezing Stress*, Vol. 62. Cham: Springer.

Sheue, C. R., Pao, S. H., Chien, L. F., Chesson, P., and Peng, C. I. (2012). Natural foliar variegation without costs? the case of *Begonia*. *Ann. Bot.* 109, 1065–1074. doi: 10.1093/aob/mcs025

Smith, A. P. (1986). Ecology of leaf color polymorphism in a tropical forest species: habitat segregation and herbivory. *Oecologia* 69, 283–287. doi: 10.1007/bf00377635

Soltau, U., Dötterl, S., and Liede-Schumann, S. (2009). Leaf variegation in *Caladium steudneriifolium* (Araceae): a case of mimicry? *Evol. Ecol.* 23, 503–512. doi: 10.1007/s10682-008-9248-2

Song, B., Zhang, Z.-Q., Stöcklin, J., Yang, Y., Niu, Y., Chen, J.-G., et al. (2013). Multifunctional bracts enhance plant fitness during flowering and seed development in *Rheum nobile* (Polygonaceae), a giant herb endemic to the high Himalayas. *Oecologia* 172, 359–370. doi: 10.1007/s00442-012-2518-2

Stevenson, G. (2015). *Plant Functional Traits Associated With Frost Susceptibility*. Doctoral dissertation, Lincoln University, Lincoln.

Terashima, I. (1992). Anatomy of non-uniform leaf photosynthesis. *Photosynth. Res.* 31, 195–212. doi: 10.1007/BF00035537

Tsukaya, H. (2002). Optical and anatomical characteristics of bracts from the Chinese "glasshouse" plant, *Rheum alexandrae* Batalin (Polygonaceae), in Yunnan, China. *J. Plant Res.* 115, 59–63. doi: 10.1007/s102650200009

Tsukaya, H., Okada, H., and Mohamed, M. (2004). A novel feature of structural variegation in leaves of the tropical plant *Schismatoglottis calyptrata*. *J. Plant Res.* 117, 477–480. doi: 10.1007/s10265-004-0179-x

Vaknin, Y., Hadas, R., Schafferman, D., Murkhovsky, L., and Bashan, N. (2008). The potential of milk thistle (*Silybum marianum* L.), an Israeli native, as a source of edible sprouts rich in antioxidants. *Int. J. Food Sci. Nutr.* 59, 339–346. doi: 10.1080/09637480701554095

Vermeulen, K., Aerts, J. M., Dekock, J., Bleyaert, P., Berckmans, D., and Steppe, K. (2012). Automated leaf temperature monitoring of glasshouse tomato plants by using a leaf energy balance model. *Comput. Electron. Agric.* 87, 19–31. doi: 10.1016/j.compag.2012.05.003

Weiser, C. J. (1970). Cold resistance and injury in woody plants. *Science* 169, 1269–1278. doi: 10.1126/science.169.3952.1269

Xiao, Y., Tholen, D., and Zhu, X. G. (2016). The influence of leaf anatomy on the internal light environment and photosynthetic electron transport rate: exploration with a new leaf ray tracing model. *J. Exp. Bot.* 67, 6021–6035. doi: 10.1093/jxb/erw359

Yu, Z., Wang, X., and Zhang, L. (2018). Structural and functional dynamics of dehydrins: a plant protector protein under abiotic stress. *Int. J. Mol. Sci.* 19:3420. doi: 10.3390/ijms19113420

**Conflict of Interest Statement:** The authors declare that the research was conducted in the absence of any commercial or financial relationships that could be construed as a potential conflict of interest.

frontiers in Plant Science

ORIGINAL RESEARCH
published: 19 June 2019
doi: 10.3389/fpls.2019.00767

# Leaf Orientation as Part of the Leaf Developmental Program in the Semi-Deciduous Shrub, *Cistus albidus* L.: Diurnal, Positional, and Photoprotective Effects During Winter

*Marina Pérez-Llorca[1,2], Andrea Casadesús[1], Maren Müller[1] and Sergi Munné-Bosch[1,2]**

[1]*Department of Evolutionary Biology, Ecology and Environmental Sciences, Faculty of Biology, University of Barcelona, Barcelona, Spain,* [2]*Department of Evolutionary Biology, Ecology and Environmental Sciences, Faculty of Biology, Institut de Recerca de la Biodiversitat, University of Barcelona, Barcelona, Spain*

OPEN ACCESS

**Edited by:**
*Éva Hideg,*
*University of Pécs, Hungary*

**Reviewed by:**
*Raquel Esteban,*
*University of the Basque Country, Spain*
*Mauro Guida Santos,*
*Federal University of Pernambuco, Brazil*

***Correspondence:**
*Sergi Munné-Bosch*
*smunne@ub.edu*

**Specialty section:**
*This article was submitted to Plant Abiotic Stress, a section of the journal Frontiers in Plant Science*

**Received:** *15 March 2019*
**Accepted:** *27 May 2019*
**Published:** *19 June 2019*

**Citation:**
*Pérez-Llorca M, Casadesús A, Müller M and Munné-Bosch S (2019) Leaf Orientation as Part of the Leaf Developmental Program in the Semi-Deciduous Shrub, Cistus albidus L.: Diurnal, Positional, and Photoprotective Effects During Winter. Front. Plant Sci. 10:767. doi: 10.3389/fpls.2019.00767*

Mediterranean ecosystems harbor a very important part of Earth's biodiversity, and they are a conservation priority due to the effects of global change. Here, we examined the performance of the semi-deciduous shrub *Cistus albidus* under Mediterranean conditions during winter, including changes in leaf angle governed by diurnal, seasonal, and positional effects and their relationship with winter photoinhibition and photoprotection. We found marked diurnal variations in leaf angle during the day in autumn, which disappeared as the photoperiod shortened during winter due to a progressive decrease in the predawn leaf angle from November to January. During this period, auxin contents decreased, while those of melatonin increased, and the $F_v/F_m$ ratio, chlorophyll, and tocopherol contents kept unaltered, thus indicating the absence of photoinhibitory damage. A marked decrease in the leaf angle toward the shoot apex occurred during winter, which was associated with slightly higher $F_v/F_m$ ratios. An analysis of the inter-individual variability and sun orientation effects on leaf movements in a population growing in the Montserrat mountains revealed a very marked variability of 46.8% in the leaf angle, while $F_v/F_m$ ratio showed a variation of 7.5% only. West orientation, which was associated with reduced leaf temperatures, but with no differences in the photosynthetic photon flux density, led to enhanced tocopherol contents, while leaf angle, $F_v/F_m$ ratio, chlorophyll, auxin, and melatonin contents kept unaltered. It is concluded that (1) *C. albidus* has very effective and fine-regulated photoprotection mechanisms, including an adequate orientation of decussate leaves as part of the developmental program, (2) leaf angle is modulated on a diurnal and seasonal basis, thus contributing to prevent photoinhibition as a first line of defense, and (3) enhanced tocopherol contents help withstand combined high light with low temperature stress in *C. albidus* growing at high elevation.

**Keywords: abiotic stress, *Cistus albidus* L., leaf orientation, leaf positional effects, low temperature stress, melatonin, photoinhibition, photoprotection**

## INTRODUCTION

The Mediterranean basin is one of the most unique biomes that harbors an important portion of Earth's plant biodiversity. Mediterranean ecosystems have been described as especially delicate upon the predicted extreme climatic events due to climate change (Peñuelas et al., 2017), and given that there is already a constant loss of biodiversity (Butchart et al., 2010), Mediterranean plant species are a conservation priority (Bellard et al., 2014). Light has been classically considered as one of the main stressors in Mediterranean-type ecosystems for plants (Joffre et al., 1999; Karavatas and Manetas, 1999), particularly excess of light, which together with drought (typically occurring during summer) or low temperatures (during winter) can cause considerable damage to the photosynthetic apparatus (Martínez-Ferri et al., 2004; Fernández-Marín et al., 2017).

Mediterranean plants have evolved different photoprotection mechanisms to avoid this excess of light, building a first line of defense. There are structural adaptations to avoid excess of light absorption such as tomentosus leaves that reflect light (Ehleringer and Björkman, 1978), chloroplast movements during the day (Haupt and Scheuerlein, 1990), changes in leaf orientation (Ehleringer and Comstock, 1987), paraheliotropism (Lambers et al., 2008), and a phyllotaxis with an opposite disposition of leaves (Brites and Valladares, 2005). In the case of leaf paraheliotropism, for instance, not all plants species exhibit it but it has developed in multiple lineages, including the well-known common bean (*Phaseolus vulgaris* L.), where this movement is triggered by an endogenous circadian oscillator and light-induced signals that lead to turgor-dependent changes in the pulvinus, which is located at the juncture of the leaf base and the petiole (Mayer et al., 1985). In several Mediterranean plants, such as the white-leaved rockrose (*Cistus albidus* L.), reduced leaf angles occur as part of the developmental program with opposite and decussate leaves (without petioles) increasing their leaf angle as they develop at the shoot apex and progressively occupy more distal positions (De Bolòs, 1993).

Once light has gone through the structural photoprotection mechanisms, it is absorbed by leaves and penetrates the chloroplasts, plants activate a second line of defense to counteract excess solar radiation. The first and one of the most flexible mechanisms to counteract the excess excitation energy and, consequently, photo-oxidative stress in chloroplasts is the xantophyll cycle (Demmig-Adams and Adams, 2006). However, if the excited triple chlorophyll ($^3$Chl*) derived from excited chlorophyll a ($^1$Chl*) is not quenched by the non-photochemical quenching (NPQ) in the photosystem II, this can lead to the production of singlet oxygen ($^1O_2$) and ultimately to the oxidation of lipids and other molecules in the chloroplast. At the same time, $O_2$ can also be over-reduced by the electrons originated in the photosystem I to superoxide radicals ($O_2^-$) and then form hydrogen peroxide ($H_2O_2$) and finally hydroxyl radical ($OH^-$), which is highly reactive (Asada, 2006). The joint effects of these ROS can cause photoinhibition, and if this is sustained, plants will experience photo-oxidative damage (Takahashi and Badger, 2011). This can be prevented by the concerted action of a myriad of antioxidant compounds. Among them, lipophilic compounds, such as tocopherols (vitamin E), have been shown to play a major role in photoprotection (Havaux et al., 2005) acting as a sentinel for stress sensing and signaling (Munné-Bosch, 2019). On the other hand, melatonin, a tryptophan-derived compound (sharing part of the biosynthesis pathway with the phytohormone indole-3-acetic acid, Pérez-Llorca et al., 2019) has been postulated as a putative antioxidant and photoprotective compound in plants (Ding et al., 2017). However, it is still not fully elucidated whether or not melatonin always acts directly as an antioxidant or indirectly through its modulatory effects on gene expression (Arnao and Hernández-Ruiz, 2019).

The aim of this study was to get new insights into the performance of the semi-deciduous shrub, *C. albidus* during high light stress and suboptimal (low) temperatures during the Mediterranean winter, with a particular emphasis on the causes and consequences of changes in leaf orientation as part of the developmental program. We hypothesized that leaf movements may be governed on a diurnal and seasonal basis and that they may significantly influence the extent of photoinhibition and photoprotective demand of leaves during winter. To test this hypothesis, we measured (1) leaf angles during predawn and midday from November to January, (2) leaf positional effects on leaf angles during winter (January), and (3) the inter-individual variability and sun orientation influence on leaf angles and the $F_v/F_m$ ratio in a natural population growing at 1,100 m.a.s.l., which was exposed to a combination of high light and low temperatures. Furthermore, we studied the endogenous variations in melatonin in relation to a biosynthesis-related phytohormone (auxin) and a well-known chloroplastic antioxidant (α-tocopherol) to get new insights into the possible protective effects of this compound against environmental stress in plants.

## MATERIALS AND METHODS

### Experimental Design and Sampling

Three independent, complementary experiments were performed using white-leaved rockrose (*Cistus albidus* L.). The first experiment was focused on the study of diurnal variations in leaf angle from autumn to winter, including measurements at predawn (1 h before sunrise) and midday (at maximum diurnal photosynthetic photon flux density; PPFD). The samplings were performed on November 6 and December 4, 2017 (autumn), and January 16, 2018 (winter) in a population growing in the experimental garden of the Faculty of Biology at the University of Barcelona (41.384 N, 2.119E, 59 m.a.s.l.). All measurements from this study were made using leaves situated on the second whorl of the plant (second leaf position) from the top of shoots. The second experiment was focused on the study of leaf positional effects on leaf angle during winter. Leaves situated on the first, second, third, fourth, and fifth whorl (designated here, arbitrarily, as positions 1–5 and corresponding to two different leaf

dispositions on the stem) from the top of shoots of the same plants as those used for the first experiment were selected for measurements during January 16, 2018 at midday (at maximum diurnal PPFD). The third experiment focused on sun orientation and inter-individual driven variability in the leaf angle of a natural population in the Natural Park of the Montserrat mountains, Spain (41.586 N–1.830 E, 1100 m.a.s.l.) during March 22, 2018. A stressful cold and sunny day was selected for measurements, with maximum and minimum air temperatures during the day of 14.7°C and −0.2°C, respectively (mean relative humidity was 30% and maximum diurnal PPFD 1570 μmol $m^{-2}$ $s^{-1}$, while no precipitation during the day was recorded). Sixty individuals of the same population, but with different sun orientations, were sampled; 30 were East oriented and 30 were West oriented (with an average leaf temperature of 11°C and 19°C, respectively, with no difference in the average relative humidity and maximum diurnal PPFD). All measurements for this study were made using leaves situated on the second whorl (position 2) from the top of shoots in all individuals. Details of soil characteristics of both sites (experimental garden from the University of Barcelona and the Montserrat mountains) can be found in Müller et al. (2013).

For the three experiments, all samplings at each time point were performed using two leaves of the same whorl per shrub from same-aged individuals that were randomly selected at the beginning of the study. Aside from leaf angle, which was described with the zenith and the azimuth angles of the surface normal to a small flat plate (Itakura and Hosoi, 2018), leaf biomass, leaf mass per area ratio, leaf hydration, chlorophyll contents, $F_v/F_m$ ratio, indole-3-acetic acid (IAA), melatonin, and α-tocopherol contents were measured as described below. For all biochemical analyses, samples were immediately snap frozen in liquid nitrogen and stored at −80°C until subsequent processing in the laboratory.

## Environmental Conditions, Photoinhibition, and Other Physiological Markers

PPFD, leaf temperature, and the $F_v/F_m$ ratio (after 1 h of darkness), the latter used as an indicator of photoinhibition (Bolhar-Nordenkampf et al., 1991), were measured with a Mini-PAM II (Photosynthesis Yield Analyzer, Walz, Germany) *in situ*. Leaves were immediately weighed to estimate leaf biomass and leaf area was measured using a flatbed scanner (model Officejet Pro 8610, HP, California, USA). Then, dry mass was estimated by weighing the sample after oven drying it at 65°C to constant weight. Leaf hydration (H) was calculated as (fresh mass-dry mass)/dry mass, and leaf mass per area (LMA) was calculated as dry mass/area.

## Biochemical Analyses

The chlorophyll a + b content of leaves was determined spectrophotometrically in methanol extracts using the equations described by Lichtenthaler (1983). Melatonin and auxin contents were determined by ultrahigh-performance liquid chromatography coupled to tandem mass spectrometry (UHPLC-MS/MS), and α-tocopherol was determined by high-performance liquid chromatography (HPLC). In short, 50 mg per sample was extracted with 250 μl of cold methanol using ultrasonication and vortexing (Branson 2510 ultrasonic cleaner, Bransonic, Danbury, CT, USA) for 30 min. Deuterium-labeled indole-3-acetic and melatonin were then added, and after centrifugation at 12,000 rpm for 10 min at 4°C, the pellet was re-extracted using the same procedure. Supernatants were pooled and filtered through a 0.22-μm PTFE filter (Waters, Milford, MA, USA) before UHPLC-MS/MS and HPLC analyses. Indole-3-acetic and melatonin contents were analyzed by using UHPLC-ESI-MS/MS as described in Müller and Munné-Bosch (2011). Quantification was made considering recovery rates for each sample by using deuterium-labeled internal standards. α-Tocopherol contents were determined by using a normal-phase HPLC system coupled to a fluorescent detector as described in Cela et al. (2011). α-Tocopherol was identified by co-elution with an authentic standard (Sigma-Aldrich, Steinheim, Germany) and quantified using a calibration curve.

## Statistical Analysis

To assess the combined effects of month ("November," "December," "January") and daytime ("Predawn," "Midday") on leaf angle, leaf biomass, leaf mass per area, hydration, chlorophyll a + b, $F_v/F_m$ ratio, IAA, melatonin, and α-tocopherol, we used a linear mixed model (LMM). Different combinations of "Month," "Daytime," and their interaction were tested as fixed terms using Akaike information criterion (AIC), i.e., the model that best fitted the data should have the lowest AIC value. "Plant" was included in all models as a random term to account for repeated measures (Zuur et al., 2009). Models were fitted with maximum likelihood (ML) for model comparison. Final models were fitted using restricted maximum likelihood (REML). Additionally, when "Daytime" had a significant effect, an LMM with "Daytime" as an explanatory variable was used to test for significant differences within each month. To assess significant differences within leaf position on the response variables above mentioned, we used a LMM where "Leaf position" was fitted as the fixed term and "Plant" as a random term. To assess the effect of sun orientation in the Montserrat natural-growing population, a linear regression was used with "Orientation" as explanatory variable. In all models, the $p$ of the main fixed effects were estimated using conditional $F$-tests (generally, ANOVA type II or ANOVA type III when an interaction term was included), and when main effects were significant, multiple comparisons between "Month" and "Daytime," or "Leaf position" levels, were tested with the Tukey HSD post hoc test. All models were validated by visually checking the distribution of residuals for normality and homoscedasticity (Zuur et al., 2009). Before analyses, leaf angle, chlorophyll a + b, IAA, and melatonin were $\log_{10}$-transformed; leaf mass per area and α-tocopherol were square root-transformed; and $F_v/F_m$ ratio was logit-transformed. Finally, to explore possible relationships between all response variables, we used the Spearman's rank correlation test. All analyses were performed using the computing environment R (R Core Team 2019).

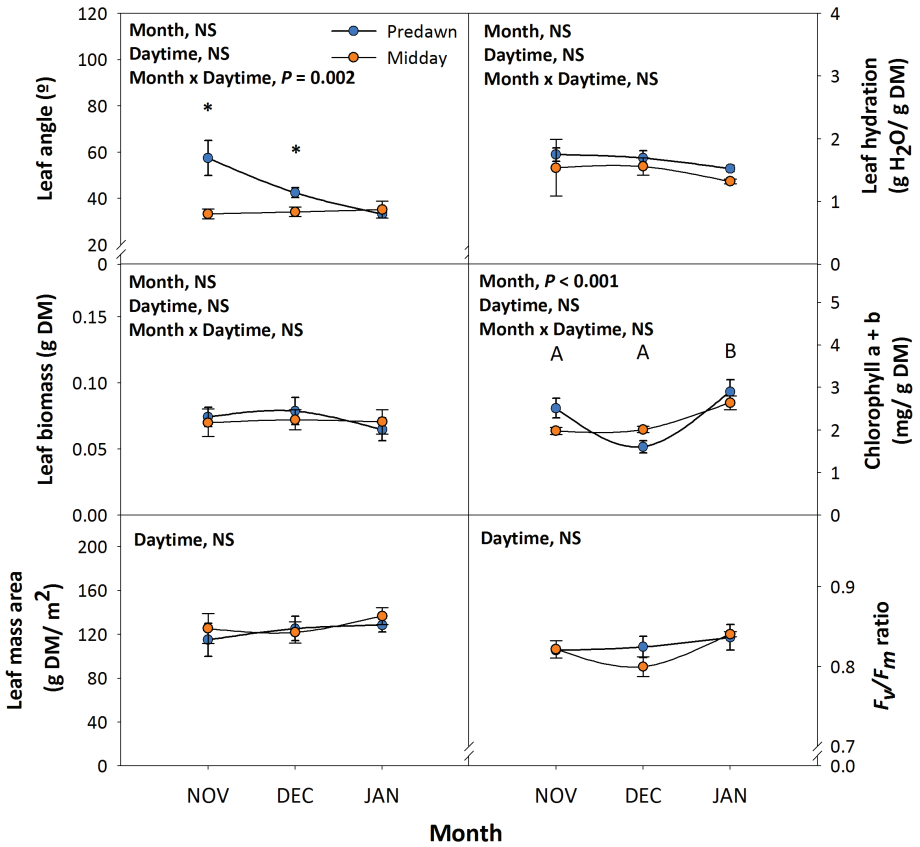


**FIGURE 1 |** Diurnal and seasonal changes in leaf orientation in the Mediterranean shrub, *C. albidus*. A comparison of leaf angle, biomass, mass per area ratio, hydration, chlorophyll contents, and the $F_v/F_m$ ratio between predawn and midday from autumn (November) to winter (January) in plants growing at the experimental garden of the University of Barcelona is shown. Data correspond to leaf position 2 from the apex (see photograph in **Figure 3** for details) and represent the mean ± SE of $n = 6$ individuals. After model selection, significant differences in "Month" and "Daytime" were tested by conditional Fisher tests ($p \leq 0.05$). Different capital letters indicate significant differences in Tukey's HSD multiple comparison test ($p \leq 0.05$) with all data. Asterisks indicate significant differences in Tukey's HSD multiple comparison test in "Daytime" within "Month". NS, not significant; DM, dry matter.

**TABLE 1 |** Environmental conditions during the sampling days both in the Experimental garden at the Faculty of Biology of the University of Barcelona and in the Natural Park of the Montserrat mountains.

| | Min $T^e$ (°C) | Max $T^e$ (°C) | Mean $T^e$ (°C) | Mean RH (%) | Mean PPFD (μmol/m² s⁻¹) | Max PPFD (μmol/m² s⁻¹) |
|---|---|---|---|---|---|---|
| Experimental garden | | | | | | |
| 6th November | 10.0 | 17.8 | 13.2 ± 0.34 | 33.56 ± 2.05 | 671 ± 79.45 | 989 |
| 4th December | 3.9 | 15.2 | 9.2 ± 0.45 | 41 ± 1.37 | 459 ± 84.80 | 892 |
| 16th January | 7.9 | 18.0 | 12.8 ± 0.46 | 58.2 ± 0.67 | 330 ± 85.25 | 936 |
| Montserrat mountains | | | | | | |
| 22nd March | –0.2 | 14.7 | 4.18 ± 0.93 | 51.09 ± 3.53 | 510 ± 68.35 | 2531 |

*Min $T^e$, minimum temperature; Max $T^e$, maximum temperature; Mean $T^e$, mean temperature; Mean RH, mean relative humidity, Mean PPFD, mean daily photosynthetic photon flux density; Max PPFD, maximum photosynthetic photon flux density. Climate data were obtained from a public database (Servei meteorològic de Catalunya).*

# RESULTS

## Leaf Angle Is Modulated on a Diurnal and Seasonal Basis in *C. albidus*

Leaf angle measurements at predawn and midday during 6th November, 4th December, and 16th January revealed significant diurnal variations in leaf orientation. Leaves had a reduced angle during the day in autumn (November and December) but not in winter (January), when maximum orientation parallel to sun's rays was attained already at predawn (**Figure 1**). It is interesting to note that despite diurnal variations in leaf orientation in autumn, maximum orientation parallel to the sunbeam was always attained at midday, with leaf angles around 35°, irrespective of the day of measurements (**Figure 1**). Diurnal PPFD during

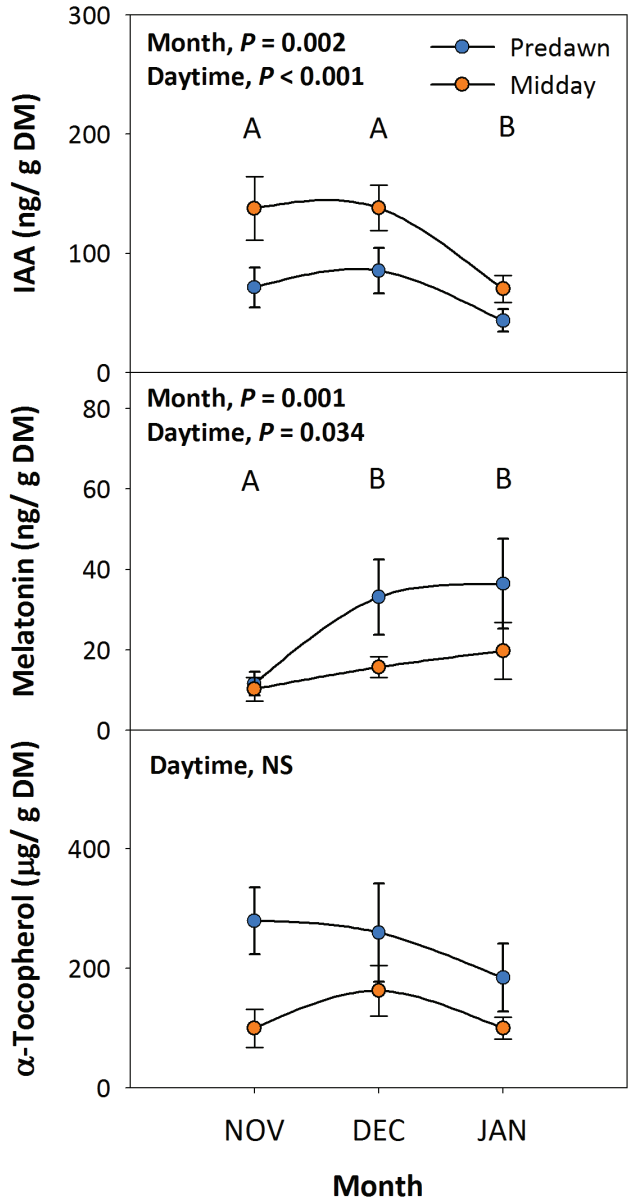


**FIGURE 2 |** Diurnal and seasonal changes in endogenous melatonin contents in the Mediterranean shrub, *C. albidus*. A comparison between melatonin contents relative to those of the biosynthesis-related phytohormone auxin and the well-known chloroplastic antioxidant α-tocopherol between predawn and midday from autumn (November) to winter (January) in plants growing at the experimental garden of the University of Barcelona is shown. Data correspond to leaf position 2 from the apex (see photograph in **Figure 3** for details) and represent the mean ± SE of $n = 6$ individuals. After model selection, significant differences in "Month" and "Daytime" were tested by conditional Fisher tests ($p \leq 0.05$). Different capital letters indicate significant differences in Tukey's HSD multiple comparison test ($p \leq 0.05$) with all data. Asterisks indicate significant differences in Tukey's HSD multiple comparison test in "Daytime" within "Month". NS, not significant; DM, dry matter.

this period changed from non-detectable values at predawn to values ranging between 892 and 989 µmol $m^{-2}$ $s^{-1}$ at midday, while the photoperiod was shortened from 10.3 h on 6th November to 9.5 h on 16th January. Leaf biomass, leaf mass per area ratio, and leaf hydration kept unaltered throughout the study (**Figure 1**). Despite chlorophyll contents decreased slightly on 4th December at predawn, which might be associated with temperatures reaching minimum values of 3.9°C (**Table 1**), the $F_v/F_m$ ratio, an indicator of photoinhibition, kept unaltered throughout the study (**Figure 1**).

To investigate the possible protective effects of melatonin against environmental stress in plants, we studied the endogenous variations in melatonin in relation to its biosynthesis-related phytohormone auxin (indole-3-acetic acid, IAA) and a well-known chloroplastic antioxidant (α-tocopherol). Endogenous auxin contents decreased as the season progressed from autumn to winter, and values at midday were higher than those at predawn, whereas melatonin contents increased slightly during the same period with higher values at predawn than at midday (**Figure 2**). While melatonin contents were on the same order of magnitude than those of auxin, they were, however, four orders of magnitude smaller than those of α-tocopherol, the levels of which kept unaltered throughout the study (**Figure 2**).

## Positional Effects on Leaf Orientation in *C. albidus*

Leaf angle measurements at midday during 16th January revealed a marked positional effect on leaf orientation, with opposite, decussate leaves progressively showing an increased leaf angle from top to bottom of the shoot (**Figure 3**). Leaf biomass and leaf mass per area ratio kept unaltered with leaf position, while leaf hydration slightly increased by a 20% from leaf position 1 to 5 (**Figure 3**). Despite chlorophyll contents kept unaltered with leaf position, the $F_v/F_m$ ratio decreased slightly with leaf opening. It is noteworthy, however, that this ratio kept always above 0.80 in all studied leaf positions (**Figure 3**).

Positional effects on the endogenous variations in melatonin in relation to auxin and α-tocopherol revealed that, although endogenous auxin contents were different between even and odd whorls, neither auxin nor melatonin contents were altered by increased leaf angle from top to bottom (**Figure 4**). In contrast, the contents of α-tocopherol increased concomitantly with less steep leaf angles from top to bottom (**Figure 4**).

## Influence of Sun Orientation and Inter-Individual Variability on Leaf Angle in *C. albidus*

Leaf angle measurements at midday during 22nd March in a natural population of *C. albidus* growing in the Montserrat mountains at 1,100 m.a.s.l. revealed a strong variability – quantified as percentage deviation (standard deviation/population mean) × 100 – on leaf orientation. Leaf at position 2 from top of the shoot from 60 individuals showed angles ranging from 10 to 80° (**Figure 5**). The variation in the leaf angle of both West-oriented and East-oriented individuals was much higher than that of leaf biomass, leaf mass per area ratio, leaf hydration, chlorophyll contents, and the $F_v/F_m$ ratio (**Figure 5**). Indeed, variability in leaf angle was 46.8%, while that of the $F_v/F_m$ ratio was 7.5% only. West orientation, which was associated with markedly reduced leaf temperatures and slightly lower leaf water contents compared to the East – but

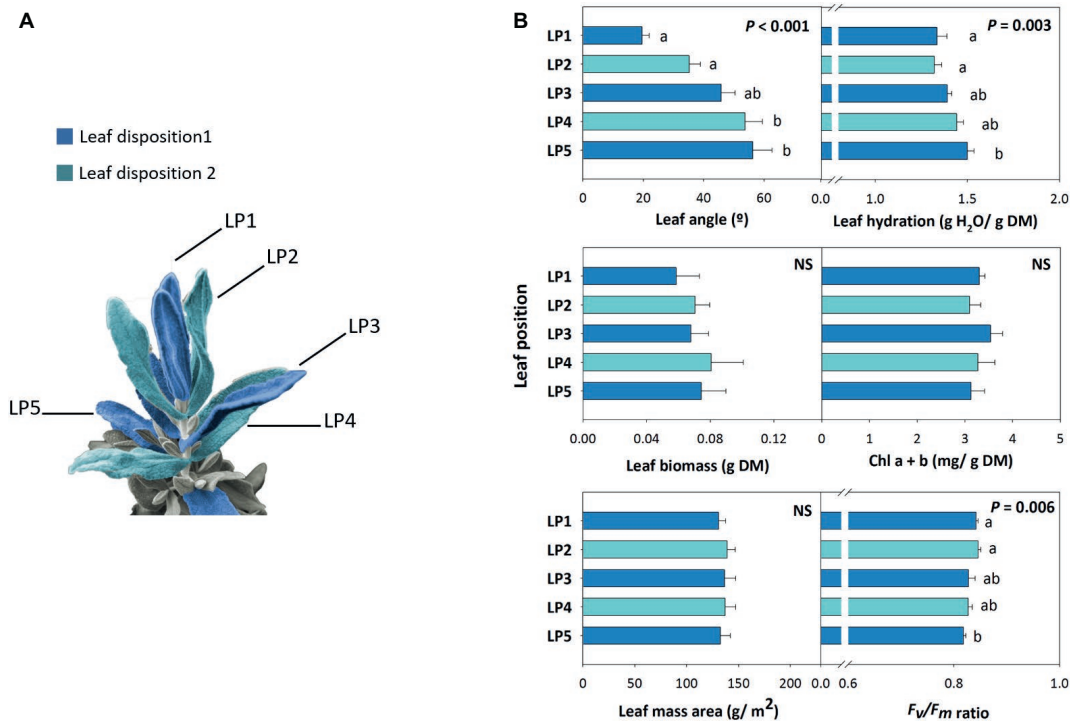


**FIGURE 3 |** Positional effects in leaf orientation in the Mediterranean shrub, *C. albidus*. **(A)** Schematic representation of the disposition on the shoot (Leaf disposition 1 and 2 shown in dark blue and light blue, respectively) of the five leaf positions (LP1…LP5). **(B)** A comparison between leaf positions on leaf angle, biomass, mass per area ratio, hydration, chlorophyll contents, and the $F_v/F_m$ ratio in plants growing at the experimental garden of the University of Barcelona in January at midday is shown. Data represent the mean ± SE of $n = 6$ individuals. Significant differences in "Leaf position" were tested by conditional Fisher tests ($p \leq 0.05$), and different letters indicate significant differences in Tukey's HSD multiple comparison test ($p \leq 0.05$). NS, not significant; DM, dry matter.

with no differences in the PPFD (**Figure 5**, see also materials and methods for details) –, led to enhanced tocopherol contents, while leaf angle, $F_v/F_m$ ratios, chlorophyll, IAA, and melatonin contents kept unaltered (**Figures 5, 6**).

## DISCUSSION

Several semi-deciduous shrubs that represent an important hotspot of the Mediterranean flora, such as the white-leaved rockrose (*Cistus albidus* L.), show changes in leaf angle as part of their developmental program with opposite and decussate leaves without petioles increasing their leaf angle as they develop from top to bottom of the shoot apex. An enhanced leaf angle in more distal positions from the uppermost side of the shoot progressively leads to a leaf orientation more perpendicular to the sun's rays, which results in an increased exposure to high light. Therefore, the youngest leaves, which develop later in time, are the ones with smaller leaf angles and, therefore, enhanced photoprotection due to reduced light incidence. There are several studies in *Cistus* spp. that report that higher leaf inclinations (i.e., steeper leaf angles) prevent photoinhibition and confer a higher stress tolerance during summer drought (*C. incanus*, Grattani and Bombelli, 2000; *C. monspeliensis*, Werner et al., 1999, 2001; *C. ladanifer*, Brites and Valladares, 2005; *C. salviifolius* and *C. monspeliensis*, Puglielli et al., 2017). However, the implications of these leaf movements to prevent winter photoinhibition have not been considered in detail thus far, with the exception of the study performed by Oliveira and Peñuelas (2002), which showed reduced cold-induced photoinhibition in leaves with smaller leaf angles and therefore less sun-exposed leaves in *C. albidus*. Here, we show that changes in leaf angle are governed by leaf position, as part of the leaf developmental program of shoots, and by environmental conditions both diurnally and seasonally, all providing a first line of defense to prevent photoinhibition in this plant species. At the same time, we also show that, in nature, the variability in leaf angles is so high that other mechanisms operating at the chloroplast level, such as an enhanced vitamin E biosynthesis, are required for counteracting the potential harmful effects of combined high light with low temperatures in populations growing at high elevation.

Leaf orientation was not only influenced by the intrinsic shoot developmental program in *C. albidus,* but it also changed on a diurnal and seasonal basis, both factors interacting between them. As it occurs with paraheliotropism in some legumes (Mayer et al., 1985; Raeini-Sarjaz, 2011), the leaf angle seemed to be governed to some extent, at least, by circadian rhythms in *C. albidus* since leaves had a steeper angle at midday compared to predawn, particularly in autumn. However, the absence of a petiole and

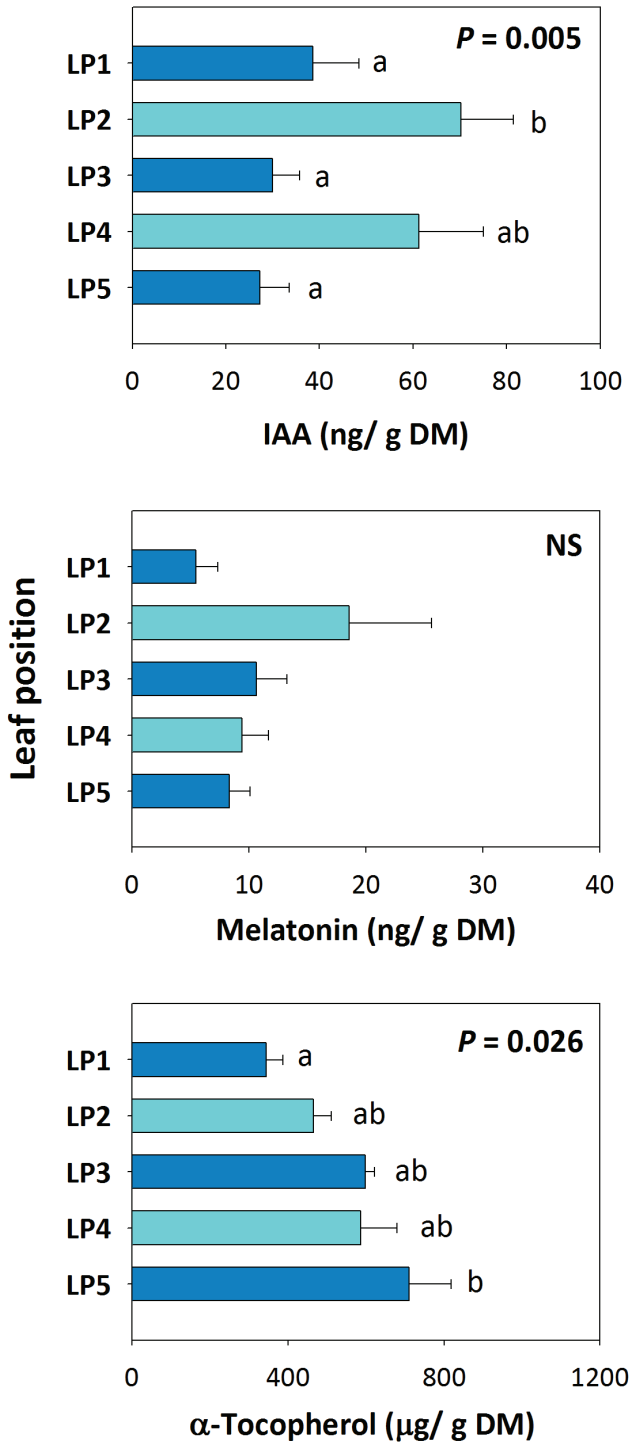


**FIGURE 4 |** Positional effects in endogenous melatonin contents in the Mediterranean shrub, *C. albidus*. A comparison between melatonin contents relative to those of the biosynthesis-related phytohormone auxin and the well-known chloroplastic antioxidant α-tocopherol in plants growing at the experimental garden of the University of Barcelona during January at midday is shown. Data represent the mean ± SE of $n = 6$ individuals. Significant differences in "Leaf position" were tested by conditional Fisher tests ($p \leq 0.05$), and different letters indicate significant differences in Tukey's HSD multiple comparison test ($p \leq 0.05$). NS, not significant; DM, dry matter.

most probably of a pulvinus in *C. albidus* leaves suggests that this movement is not as "active" as in some legumes such as common bean (Lambers et al., 2008), but the result of a more "passive" process associated with the plant developmental program. However, the fact that leaves move on a diurnal basis indicates that this leaf movement responds to light and can, therefore, be considered a type of paraheliotropism, as recently suggested by Puglielli et al. (2017) and *sensu* Häder and Lebert (2001).

Enhanced tocopherol contents were observed in the West-oriented individuals compared to the East-oriented ones, which might help withstand combined high light with low temperature stress in *C. albidus* growing at high elevation. Mean leaf temperature during samplings in the West orientation was 11°C, in contrast to the 19°C in East orientation, while the PPFD did not differ between both orientations. Reduced leaf temperature in the West led to a slightly reduced leaf hydration, which may be associated with dehydration caused by chilling (Hussain et al., 2018). In turn, low temperatures have been shown to increase α-tocopherol contents in other plant species as a mean to counteract ROS production and allow stabilization of membranes (Munné-Bosch, 2005; El Kayal et al., 2006). Indeed, tocopherols may not only protect the photosynthetic apparatus during plant exposure to extreme temperatures but also influence retrograde signaling, thus acting in stress sensing and signaling (Fang et al., 2019; Munné-Bosch, 2019). Interestingly, the $F_v/F_m$ ratio did not differ between the West and East orientation, thus suggesting that enhanced tocopherol contents in the West orientation served as a photoprotective strategy, as it has been previously shown in model plant species (Havaux et al., 2005). By contrast, melatonin contents did not increase in response to low temperature stress in the West-oriented individuals, despite exogenous applications of this compound have been shown to protect the photosynthetic apparatus from excess light stress, either caused by drought (Fleta-Soriano et al., 2017) or low temperatures (Ding et al., 2017). Inter-individual variability in melatonin contents was very high, as it occurred with leaf angles, which might mask a possible protective effect of these two mechanisms in populations growing under natural conditions. Indeed, the endogenous contents of melatonin found (in the order of ng/g dry matter, even lower than those found for indole-3-acetic acid) in *C. albidus* leaves suggest a modulatory role of this compound in plants, rather than a direct function as an antioxidant, which is in agreement with previous studies (Fleta-Soriano et al., 2017, see also Arnao and Hernández-Ruiz, 2019).

Correlation analyses revealed interesting relationships between various parameters in the natural population, both when the analysis included all data and the East and West individuals separately (**Figure 7**). In the natural population from the Montserrat mountains, leaf angle did not correlate with any of the other studied parameters but the $F_v/F_m$ ratio correlated very significantly, strongly, and positively with leaf hydration ($\rho = 0.68$, $p < 0.001$), which might indicate a prevalent occurrence of increased photoinhibition in the more water-stressed leaves. Small reductions in leaf hydration, which may be caused by chilling stress in the West-oriented individuals, could explain this result. This correlation was confirmed when all data were pooled together, although the relationship was

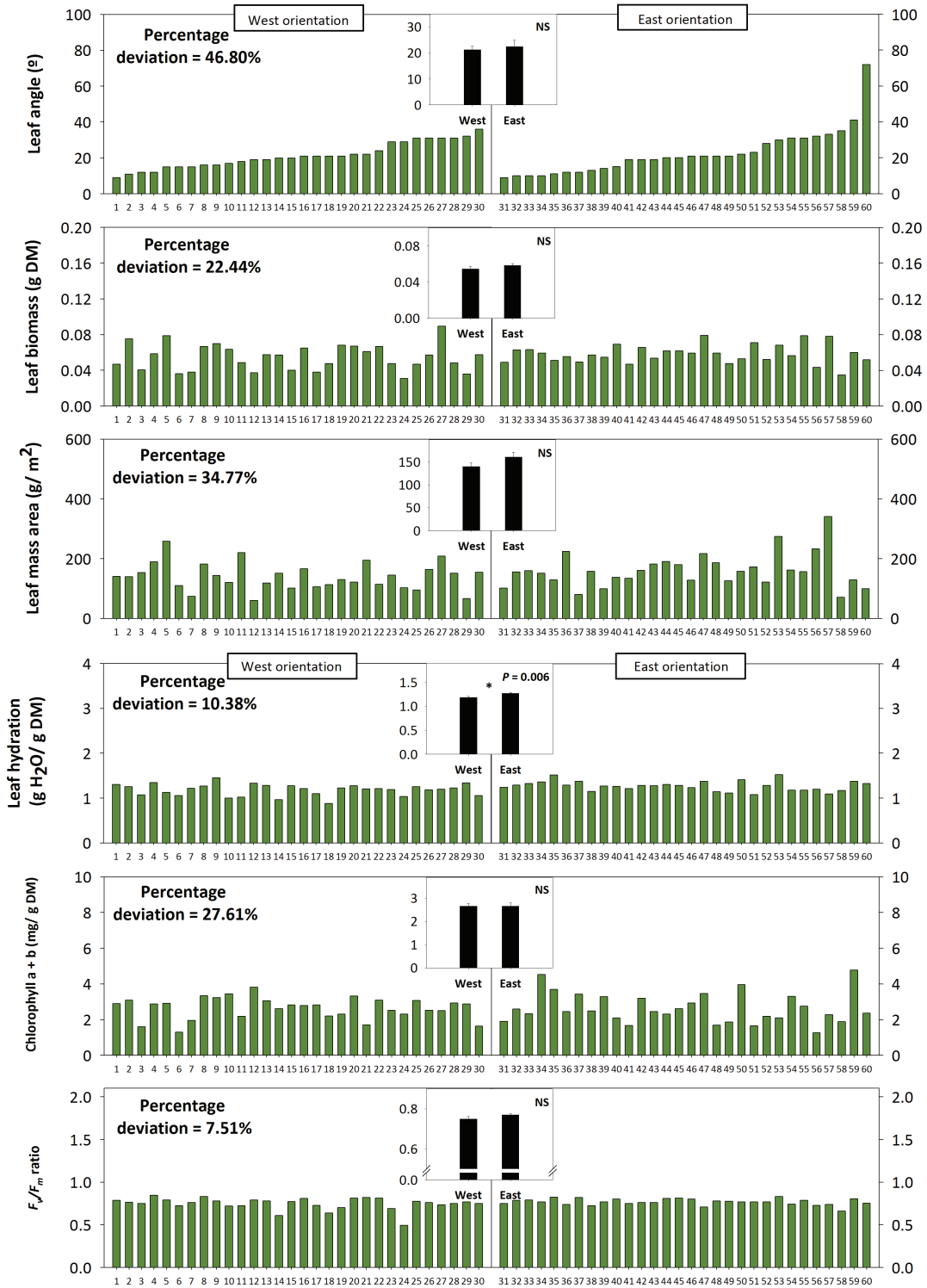


**FIGURE 5 |** Effects of sun orientation and inter-individual variability on leaf orientation in the Mediterranean shrub, *C. albidus*. A comparison between leaf angle, biomass, mass per area ratio, hydration, chlorophyll contents, and the $F_v/F_m$ ratio in a *C. albidus* population growing at 1,100 m.a.s.l. in the Natural Park of the Montserrat Mountains with different sun orientation (East orientation, $n = 30$ individuals; West orientation, $n = 30$ individuals) during winter (22nd March 2018) is shown. Data correspond to leaf position 2 from the apex (see photograph in **Figure 3** for details) for all studied individuals. The number of the individual (ordered from lower to higher leaf angle) is indicated in the x-axis. Percent deviation for every variable is given as (SD/Population mean) × 100, where SD corresponds to standard deviation. The mean ± SE for each sun orientation is shown in the graphs located in the inlets. Significant differences between groups were tested by a one-way analysis of variance (ANOVA, $p \leq 0.05$) and indicated with an asterisk. NS, not significant.

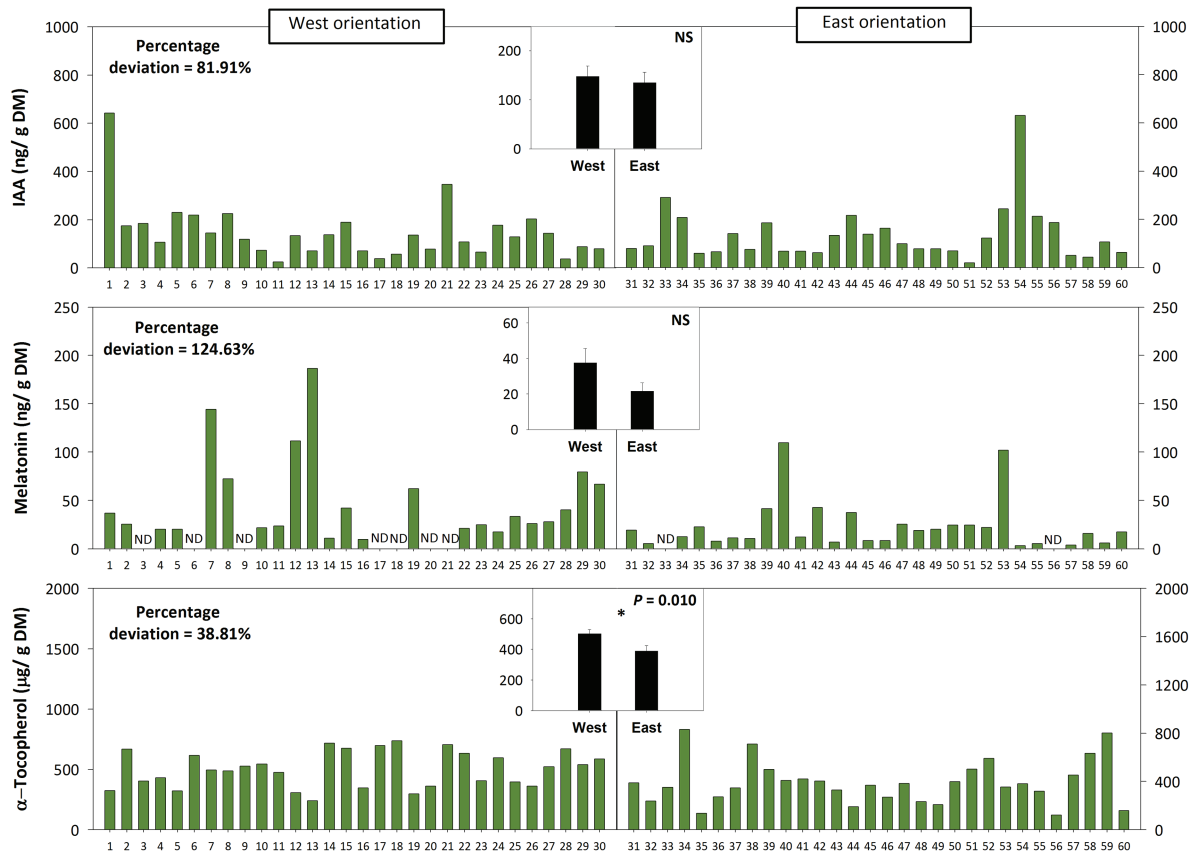


**FIGURE 6 |** Effects of sun orientation and inter-individual variability on endogenous melatonin contents in the Mediterranean shrub, *C. albidus*. A comparison of melatonin contents relative to those of the biosynthesis-related phytohormone auxin and the well-known chloroplastic antioxidant α-tocopherol in a *C. albidus* population growing at 1,100 m.a.s.l. in the Natural Park of the Montserrat Mountains with different sun orientation (East orientation, $n = 30$ individuals, West orientation, $n = 30$ individuals) during winter (22nd March 2018) is shown. Data correspond to leaf position 2 from the apex (see photograph in **Figure 3** for details) for all studied individuals. The number of the individual (ordered from lower to higher leaf angle) is indicated in the x-axis. Percent deviation for every variable is given as (SD/population mean) × 100, where SD corresponds to standard deviation. The mean ± SE for each sun orientation is shown in the graphs located in the inlets. Significant differences between groups were tested by a one-way analysis of variance (ANOVA, $p \leq 0.05$) and indicated with an asterisk. NS, not significant; DM, dry matter.

more moderate ($\rho = 0.56$, $p < 0.001$). Furthermore, a moderate, but very significant, positive correlation was found between leaf hydration and total chlorophylls ($\rho = 0.51$, $p < 0.001$) pooling all data together that were consistent in both West and East-oriented individuals ($\rho = 0.53$, $p < 0.001$; $\rho = 0.63$, $p < 0.001$, respectively). Simultaneously, the relationship between $F_v/F_m$ ratio and α-tocopherol was also significant, although not too strong, in both orientations but this time being negative ($\rho = -0.32$, $p < 0.05$; $\rho = -0.46$, $p < 0.05$, respectively). In this manner, given that leaf hydration was slightly lower and tocopherol contents were higher in the West-oriented individuals than in the East-oriented ones, α-tocopherol might be acting as an important photoprotection compound under abiotic stress conditions. Therefore, these results suggest that *C. albidus* plants activate two photoprotection mechanisms. First, reductions in leaf angle, which might serve as a first line of defense from winter photoinhibition in leaves, particularly occurring in the uppermost position of shoots; and second, increased accumulation of α-tocopherol, which might serve as a stress sensing and signaling mechanism to counteract combined high light and low temperature stress during winter. The increased accumulation of α-tocopherol appears to be particularly relevant when photoprotection by leaf orientation is minimal and leaves consequently require more sophisticated biochemical, photoprotection mechanisms. In this study, higher levels of α-tocopherol are observed under more stressful conditions (e.g., West-oriented individuals exposed to a combination of abiotic stresses) and when leaves occupy positions more distal to the top of the shoot, due to the developmental program, and they orient more perpendicular to sun's rays.

It is concluded that *C. albidus* has very effective and fine-regulated photoprotection mechanisms, including (1) an adequate orientation of decussate leaves as part of the developmental program, in which the leaf angle is additionally modulated on a diurnal and seasonal basis, therefore contributing to prevent photoinhibition as a first line of defense and (2) enhanced tocopherol contents that may help withstand

ALL DATA

| | Leaf angle | $F_v/F_m$ ratio | Leaf biomass | Leaf mass area | Leaf hydration | Chlorophylls | IAA | Melatonin | α-Tocopherol | PPFD |
|---|---|---|---|---|---|---|---|---|---|---|
| Leaf angle | - | - | - | - | - | - | - | - | - | - |
| $F_v/F_m$ ratio | -0.20 | - | - | - | - | - | - | - | - | - |
| Leaf biomass | -0.01 | 0.33* | - | - | - | - | - | - | - | - |
| Leaf mass area | 0.02 | 0.09 | 0.56*** | - | - | - | - | - | - | - |
| Leaf hydration | -0.23 | 0.56*** | 0.12 | -0.04 | - | - | - | - | - | - |
| Chlorophylls | -0.14 | 0.30* | 0.21 | -0.17 | 0.51*** | - | - | - | - | - |
| IAA | -0.16 | 0.30* | 0.10 | 0.13 | 0.14 | 0.06 | - | - | - | - |
| Melatonin | 0.02 | 0.10 | 0.01 | -0.15 | 0.24 | 0.16 | -0.03 | - | - | - |
| α-Tocopherol | 0.10 | -0.32* | -0.10 | -0.21 | -0.29* | 0.04 | -0.08 | -0.05 | - | - |
| PPFD | 0.06 | 0.24 | 0.26* | 0.07 | 0.18 | 0.04 | -0.05 | -0.02 | -0.08 | - |
| Temperature | -0.16 | 0.20 | 0.08 | 0.16 | 0.37** | -0.02 | -0.19 | -0.04 | -0.30* | 0.24 |

WEST-ORIENTED

| | Leaf angle | $F_v/F_m$ ratio | Leaf biomass | Leaf mass area | Leaf hydration | Chlorophylls | IAA | Melatonin | α-Tocopherol | PPFD |
|---|---|---|---|---|---|---|---|---|---|---|
| Leaf angle | - | - | - | - | - | - | - | - | - | - |
| $F_v/F_m$ ratio | -0.18 | - | - | - | - | - | - | - | - | - |
| Leaf biomass | -0.03 | 0.37* | - | - | - | - | - | - | - | - |
| Leaf mass area | -0.03 | 0.13 | 0.59*** | - | - | - | - | - | - | - |
| Leaf hydration | -0.04 | 0.68*** | 0.09 | -0.23 | - | - | - | - | - | - |
| Chlorophylls | -0.15 | 0.51** | 0.30 | -0.17 | 0.53*** | - | - | - | - | - |
| IAA | -0.31 | 0.28 | 0.08 | 0.20 | 0.07 | 0.01 | - | - | - | - |
| Melatonin | -0.09 | 0.14 | -0.08 | -0.24 | 0.35* | 0.24 | -0.01 | - | - | - |
| α-Tocopherol | 0.02 | -0.21 | -0.14 | -0.20 | -0.24 | -0.02 | -0.17 | -0.17 | - | - |
| PPFD | 0.13 | 0.35* | 0.35* | 0.06 | 0.18 | 0.23 | 0.03 | -0.10 | 0.04 | - |
| Temperature | 0.26 | 0.11 | -0.01 | 0.02 | 0.03 | -0.04 | -0.23 | -0.13 | -0.10 | 0.27 |

EAST-ORIENTED

| | Leaf angle | $F_v/F_m$ ratio | Leaf biomass | Leaf mass area | Leaf hydration | Chlorophylls | IAA | Melatonin | α-Tocopherol | PPFD |
|---|---|---|---|---|---|---|---|---|---|---|
| Leaf angle | - | - | - | - | - | - | - | - | - | - |
| $F_v/F_m$ ratio | 0.09 | - | - | - | - | - | - | - | - | - |
| Leaf biomass | 0.21 | 0.15 | - | - | - | - | - | - | - | - |
| Leaf mass area | 0.32 | -0.06 | 0.61** | - | - | - | - | - | - | - |
| Leaf hydration | -0.13 | 0.33 | 0.11 | 0.20 | - | - | - | - | - | - |
| Chlorophylls | -0.27 | 0.04 | 0.01 | -0.11 | 0.63** | - | - | - | - | - |
| IAA | -0.03 | 0.37 | 0.14 | 0.01 | 0.34 | 0.19 | - | - | - | - |
| Melatonin | 0.43* | 0.07 | 0.25 | 0.02 | 0.12 | -0.03 | -0.16 | - | - | - |
| α-Tocopherol | 0.04 | -0.46* | 0.09 | -0.19 | -0.17 | 0.03 | -0.09 | 0.23 | - | - |
| PPFD | 0.10 | -0.11 | -0.16 | 0.00 | 0.14 | -0.24 | -0.18 | 0.20 | -0.12 | - |
| Temperature | -0.12 | -0.02 | -0.03 | 0.24 | 0.28 | 0.31 | -0.01 | 0.04 | 0.02 | -0.08 |

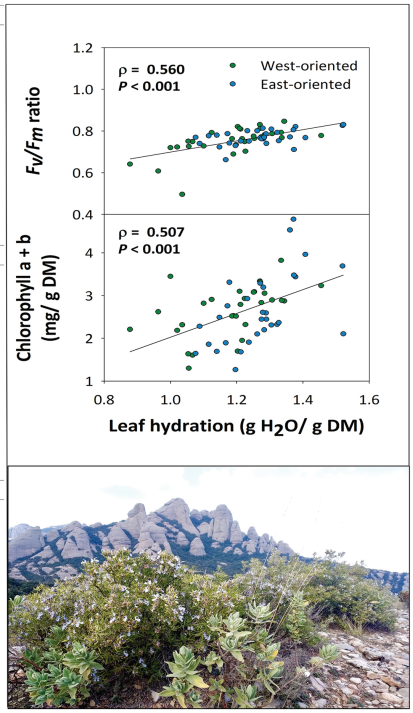


**FIGURE 7 |** Relationship between all measured parameters in *C. albidus* from a natural population in the Natural Park of the Montserrat Mountains. Tables show the results of the Spearman's rank correlation analyses (including the correlation coefficient, $\rho$, and $p$ indicated with asterisks) for all data pooled together, for West-oriented individuals only and for East-oriented individuals only. All correlations were considered statistically significant at $p \leq 0.05$, with one, two, and three asterisks indicating $p$ below 0.05, 0.01, and 0.001, respectively. Correlations with a correlation coefficient, $\rho \geq 0.50$, are shown in red, green, and blue for all data pooled together, West-oriented individuals, and East-oriented individuals, respectively. The plots in the right side of the figure show a graphical representation of the most biologically significant correlations. IAA, indole-3-acetic acid; PPFD, photosynthetic photon flux density.

combined high light and low temperature stress in *C. albidus* growing under Mediterranean field conditions.

## DATA AVAILABILITY

All datasets generated for this study are included in the manuscript and/or the supplementary files.

## AUTHOR CONTRIBUTIONS

MP-L and SM-B conceived and designed the experiment. MP-L, AC, and MM performed the experiments. MP-L analyzed the data. SM-B wrote the manuscript with the help of MP-L. All authors revised and approved the final manuscript.

## FUNDING

This research was supported by the Spanish Government through BFU2015-64001/FEDER and Generalitat de Catalunya through the ICREA Academia prize given to SM-B.

## ACKNOWLEDGMENTS

We are very grateful to Serveis Científico-tècnics (University of Barcelona) for their help with the biochemical analyses.

## REFERENCES

Arnao, M. B., and Hernández-Ruiz, J. (2019). Melatonin: a new plant hormone and/or a plant master regulator? *Trends Plant Sci.* 24, 38–48. doi: 10.1016/j.tplants.2018.10.010

Asada, K. (2006). Production and scavenging of reactive oxygen species in chloroplasts and their functions. *Plant Physiol.* 141, 391–396. doi: 10.1104/pp.106.082040

Bellard, C., Leclerc, C., Leroy, B., Bakkenes, M., Veloz, S., Thuiller, W., et al. (2014). Vulnerability of biodiversity hotspots to global change. *Glob. Ecol. Biogeogr.* 23, 1376–1386. doi: 10.1111/geb.12228

Bolhar-Nordenkampf, H. R., Hofer, M., and Leclmer, E. G. (1991). Analysis of light-induced reduction of the photochemical capacity in field-grown plants. Evidence for photoinhibition? *Photosynthesis Res.* 27, 31–39. doi: 10.1007/BF00029974

Brites, D., and Valladares, F. (2005). Implications of opposite phyllotaxis for light interception efficiency of Mediterranean woody plants. *Trees* 19, 671–679. doi: 10.1007/s00468-005-0431-6

Butchart, S. H. M., Walpole, M., Collen, B., van Strien, A., Scharlemann, J. P. W., Almond, R. E. A., et al. (2010). Global biodiversity: indicators of recent declines. *Science* 328, 1164–1168. doi: 10.1126/science.1187512

Cela, J., Chang, C., and Munné-Bosch, S. (2011). Accumulation of γ- rather than α-tocopherol alters ethylene signaling gene expression in the vte4 mutant of *Arabidopsis thaliana*. *Plant Cell Physiol.* 52, 1389–1400. doi: 10.1093/pcp/pcr085

De Bolòs, O. (1993). *Flora manual dels països catalans,* 2nd edn. (Barcelona: Pòrtic).

Demmig-Adams, B., and Adams, W. W. (2006). Photoprotection in an ecological context: the remarkable complexity of thermal energy dissipation. *New Phytol.* 172, 11–21. doi: 10.1111/j.1469-8137.2006.01835.x

Ding, F., Wang, M., Liu, B., and Zhang, S. (2017). Exogenous melatonin mitigates photoinhibition by accelerating non-photochemical quenching in tomato seedlings exposed to moderate light during chilling. *Front. Plant Sci.* 8:244. doi: 10.3389/fpls.2017.00244

Ehleringer, J. R., and Björkman, O. (1978). Pubescence and leaf spectral characteristics in a desert shrub, *Encelia farinosa*. *Oecologia* 36, 151–162. doi: 10.1007/BF00349805

Ehleringer, J. R., and Comstock, J. (1987). "Leaf absorptance and leaf angle: mechanisms for stress avoidance" in *Plant response to stress - functional analysis in Mediterranean ecosystems*. eds. J. D. Tenhunen, F. M. Catarino, O. L. Lange, and W. C. Oechel (Berlin: Springer), 55–76.

El Kayal, W., Keller, G., Debayles, C., Kumar, R., Weier, D., Teulières, C., et al. (2006). Regulation of tocopherol biosynthesis through transcriptional control of tocopherol cyclase during cold hardening in *Eucalyptus gunnii*. *Physiol. Plant.* 126, 212–223. doi: 10.1111/j.1399-3054.2006.00614.x

Fang, X., Zhao, G., Zhang, S., Li, Y., Gu, H., Li, Y., et al. (2019). Chloroplast-to-nucleus signaling regulates microRNA biogenesis in *Arabidopsis*. *Dev. Cell* 48, 371–382. doi: 10.1016/j.devcel.2018.11.046

Fernández-Marín, B., Hernández, A., Garcia-Plazaola, J. I., Esteban, R., Míguez, F., Artetxe, U., et al. (2017). Photoprotective strategies of Mediterranean plants in relation to morphological traits and natural environmental pressure: a meta-analytical approach. *Front. Plant Sci.* 8:1051. doi: 10.3389/fpls.2017.01051

Fleta-Soriano, E., Díaz, L., Bonet, E., and Munné-Bosch, S. (2017). Melatonin may exert a protective role against drought stress in maize. *J. Agron. Crop Sci.* 203, 286–294. doi: 10.1111/jac.12201

Grattani, L., and Bombelli, A. (2000). Correlation between leaf age and other leaf traits in three Mediterranean maquis shrub species: *Quercus ilex*, *Phillyrea latifolia* and *Cistus incanus*. *Environ. Exp. Bot.* 43, 141–153. doi: 10.1016/S0098-8472(99)00052-0

Häder, D.-P., and Lebert, M. (2001). *Photomovement*. (Amsterdam, The Netherlands: Elsevier).

Haupt, W., and Scheuerlein, R. (1990). Chloroplast movement. *Plant Cell Environ.* 13, 595–614. doi: 10.1111/j.1365-3040.1990.tb01078.x

Havaux, M., Eymery, F., Porfirova, S., Rey, P., and Dörmann, P. (2005). Vitamin E protects against photoinhibition and photooxidative stress in *Arabidopsis thaliana*. *Plant Cell* 17, 3451–3469. doi: 10.1105/tpc.105.037036

Hussain, H. A., Hussain, S., Khaliq, A., Ashraf, U., Anjum, S. A., Men, S., et al. (2018). Chilling and drought stresses in crop plants: implications, cross talk, and potential management opportunities. *Front. Plant Sci.* 9:393. doi: 10.3389/fpls.2018.00393

Itakura, K., and Hosoi, F. (2018). Automatic leaf segmentation for estimating leaf area and leaf inclination angle in 3D plant images. *Sensors* 18:3576. doi: 10.3390/s18103576

Joffre, R., Rambal, S., and Damesin, C. (1999). "Functional attributes in Mediterranean-type ecosystems" in *Handbook of functional plant ecology*. eds. F. I. Pugnaire, and F. Valladares (New York: Marcel Dekker), 347–380.

Karavatas, S., and Manetas, Y. (1999). Seasonal patterns of photosystem 2 photochemical efficiency in evergreen sclerophylls and drought semi-deciduous shrubs under Mediterranean field conditions. *Photosynthetica* 3, 41–49.

Lambers, H., Chapin, F. S., and Pons, T. L. (2008). *Plant physiological ecology*. 2nd edn. (New York: Springer).

Lichtenthaler, H. K., and Wellburn, A. R. (1983). Determination of total carotenoids and chlorophylls a and b of leaf extracts in different solvents. *Biochem. Soc. Trans.* 11, 591–592. doi: 10.1042/bst0110591

Martínez-Ferri, E., Manrique, E., Valladares, F., and Balaguer, L. (2004). Winter photoinhibition in the field involves different processes in four co-occurring Mediterranean tree species. *Tree Physiol.* 24, 981–990. doi: 10.1093/treephys/24.9.981

Mayer, E.-W., Flach, D., Raju, M. V. S., Starrach, N., and Wiech, E. (1985). Mechanics of circadian pulvini movements in *Phaseolus coccineus* L. *Planta* 163, 381–390. doi: 10.1007/BF00395147

Müller, M., and Munné-Bosch, S. (2011). Rapid and sensitive hormonal profiling of complex plant samples by liquid chromatography coupled to electrospray ionization tandem mass spectrometry. *Plant Methods* 7:37. doi: 10.1186/1746-4811-7-37

Müller, M., Siles, L., Cela, J., and Munné-Bosch, S. (2013). Perennially young: seed production and quality in controlled and natural populations of *Cistus albidus* reveal compensatory mechanisms that prevent senescence in terms of seed yield and viability. *J. Exp. Bot.* 65, 287–297. doi: 10.1093/jxb/ert372

Munné-Bosch, S. (2005). The role of α-tocopherol in plant stress tolerance. *J. Plant Physiol.* 162, 743–748. doi: 10.1016/j.jplph.2005.04.022

Munné-Bosch, S. (2019). Vitamin E function in stress sensing and signaling in plants. *Dev. Cell* 48, 290–292. doi: 10.1016/j.devcel.2019.01.023

Oliveira, G., and Peñuelas, J. (2002). Comparative protective strategies of *Cistus albidus* and *Quercus ilex* facing photoinhibitory winter conditions. *Environ. Exp. Bot.* 47, 281–289. doi: 10.1016/S0098-8472(02)00003-5

Peñuelas, J., Sardans, J., Filella, I., Estiarte, M., Llusià, J., Ogaya, R., et al. (2017). Impacts of global change on Mediterranean forests and their services. *Forests* 8, 972–980. doi: 10.3390/f8120463

Pérez-Llorca, M., Muñoz, P., Müller, M., and Munné-Bosch, S. (2019). Biosynthesis, metabolism and function of auxin, salicylic acid and melatonin in climacteric and non-climacteric fruits. *Front. Plant Sci.* 10:136. doi: 10.3389/fpls.2019.00136

Puglielli, G., Redondo-Gómez, S., Gratani, L., and Mateos-Naranjo, E. (2017). Highlighting the differential role of leaf paraheliotropism in two Mediterranean *Cistus* species under drought stress and well-watered conditions. *J. Plant Physiol.* 213, 199–208. doi: 10.1016/j.jplph.2017.02.015

Raeini-Sarjaz, M. (2011). Circadian rhythm leaf movement of *Phaseolus vulgaris* and the role of calcium ions. *Plant Signal. Behav.* 6, 962–967. doi: 10.4161/psb.6.7.15483

R Core Team, (2019). R: a language and environment for statistical computing. R Foundation for Statistical Computing. Vienna, Austria. https://www.R-project.org/

Takahashi, S., and Badger, M. R. (2011). Photoprotection in plants: a new light on photosystem II damage. *Trends Plant Sci.* 16, 53–60. doi: 10.1016/j.tplants.2010.10.001

Werner, C., Correia, O., and Beyschlag, W. (1999). Two different strategies of Mediterranean macchia plants to avoid photoinhibitory damage by excessive radiation levels during summer drought. *Acta Oecol.* 20, 15–23. doi: 10.1016/S1146-609X(99)80011-3

Werner, C., Ryel, R. J., Correia, O., and Beyschlag, W. (2001). Structural and functional variability within the canopy and its relevance for carbon gain and stress avoidance. *Acta Oecol.* 22, 129–138. doi: 10.1016/S1146-609X(01)01106-7

Zuur, A. F., Ieno, E. N., and Elphick, C. S. (2009). A protocol for data exploration to avoid common statistical problems. *Methods Ecol. Evol.* 1, 3–14. doi: 10.1111/j.2041-210x.2009.00001.x

**Conflict of Interest Statement:** The authors declare that the research was conducted in the absence of any commercial or financial relationships that could be construed as a potential conflict of interest.

frontiers in Plant Science

ORIGINAL RESEARCH
published: 12 July 2019
doi: 10.3389/fpls.2019.00916

# Photoinhibition of Photosystem I Provides Oxidative Protection During Imbalanced Photosynthetic Electron Transport in *Arabidopsis thaliana*

*Yugo Lima-Melo[1,2], Vicente T. C. B. Alencar[1], Ana K. M. Lobo[1], Rachel H. V. Sousa[1], Mikko Tikkanen[2], Eva-Mari Aro[2], Joaquim A. G. Silveira[1]* and Peter J. Gollan[2]**

[1] Department of Biochemistry and Molecular Biology, Federal University of Ceará, Fortaleza, Brazil, [2] Molecular Plant Biology, Department of Biochemistry, University of Turku, Turku, Finland

OPEN ACCESS

**Edited by:**
*Éva Hideg,*
*University of Pécs, Hungary*

**Reviewed by:**
*Jean-David Rochaix,*
*Université de Genève, Switzerland*
*Alexander G. Ivanov,*
*Bulgarian Academy of Sciences, Bulgaria*

***Correspondence:**
*Joaquim A. G. Silveira*
*silveira@ufc.br*
*Peter J. Gollan*
*petgol@utu.fi;*
*peter.gollan@utu.fi*

**Specialty section:**
*This article was submitted to Plant Abiotic Stress, a section of the journal Frontiers in Plant Science*

**Received:** *08 March 2019*
**Accepted:** *28 June 2019*
**Published:** *12 July 2019*

**Citation:**
*Lima-Melo Y, Alencar VTCB, Lobo AKM, Sousa RHV, Tikkanen M, Aro E-M, Silveira JAG and Gollan PJ (2019) Photoinhibition of Photosystem I Provides Oxidative Protection During Imbalanced Photosynthetic Electron Transport in Arabidopsis thaliana. Front. Plant Sci. 10:916. doi: 10.3389/fpls.2019.00916*

Photosynthesis involves the conversion of sunlight energy into stored chemical energy, which is achieved through electron transport along a series of redox reactions. Excess photosynthetic electron transport might be dangerous due to the risk of molecular oxygen reduction, generating reactive oxygen species (ROS) over-accumulation. Avoiding excess ROS production requires the rate of electron transport to be coordinated with the capacity of electron acceptors in the chloroplast stroma. Imbalance between the donor and acceptor sides of photosystem I (PSI) can lead to inactivation, which is called PSI photoinhibition. We used a light-inducible PSI photoinhibition system in *Arabidopsis thaliana* to resolve the time dynamics of inhibition and to investigate its impact on ROS production and turnover. The oxidation state of the PSI reaction center and rates of $CO_2$ fixation both indicated strong and rapid PSI photoinhibition upon donor side/acceptor side imbalance, while the rate of inhibition eased during prolonged imbalance. PSI photoinhibition was not associated with any major changes in ROS accumulation or antioxidant activity; however, a lower level of lipid oxidation correlated with lower abundance of chloroplast lipoxygenase in PSI-inhibited leaves. The results of this study suggest that rapid activation of PSI photoinhibition under severe photosynthetic imbalance protects the chloroplast from over-reduction and excess ROS formation.

**Keywords: photosystem I, photosynthesis, ROS, $CO_2$ fixation, photoinhibition, P700, redox**

## INTRODUCTION

Light is vital for photosynthesis, but when supplied in excess it can damage the photosynthetic apparatus and cause photo-oxidative stress. This condition occurs during states of photosynthetic imbalance, when the electron pressure in the photosynthetic electron transport chain exceeds the capacity of reducing power consumption by sink pathways, which is usually associated with stressful environmental conditions. As a result, transient or sustained production of reactive oxygen species (ROS) can occur. Excessive accumulation of ROS can impair metabolic homeostasis through oxidative damage to cells because of their high reactivity with lipids, proteins, and nucleic acids (McCord, 2000; Apel and Hirt, 2004; Munns, 2005; Sharma et al., 2012). On the other hand,

ROS play an important role in signaling pathways essential for acclimation to environmental conditions (for recent reviews, see Mittler, 2017; Czarnocka and Karpiński, 2018; Mullineaux et al., 2018). ROS can induce signaling responses directly, or indirectly by driving redox changes that modulate signaling networks (de Souza et al., 2017; Exposito-Rodriguez et al., 2017; Noctor et al., 2018; Souza et al., 2018). In addition, oxidation by-products, including oxidized lipids and pigments, transduce signals (Mueller et al., 2008; Mosblech et al., 2009; López et al., 2011; Ramel et al., 2012; Satoh et al., 2014). Because ROS are harmful at high concentrations, but at the same time are important for signaling and plant acclimation, the precise control of ROS concentrations is critical for metabolic homeostasis. Accordingly, plants control photosynthetic ROS production by regulating light-harvesting and electron transport (reviewed in Tikkanen and Aro, 2014), in particular through protonation of the thylakoid lumen that requires the proton gradient regulation 5 (PGR5) protein (Munekage et al., 2002; Suorsa et al., 2012). In the chloroplast stroma, ROS concentrations are regulated by antioxidant systems involving numerous redox enzymes, including the superoxide dismutases (SOD), which catalyze the dismutation of superoxide radical ($O_2^{\bullet -}$) to hydrogen peroxide ($H_2O_2$), that in turn can be subsequently reduced to water by ascorbate peroxidases (APX) and other peroxidases through the Foyer–Halliwell–Asada cycle, using ascorbate (ASC), glutathione (GSH) and thioredoxins as electron donors (Asada, 1999; Foyer and Shigeoka, 2011).

A central consequence of photo-oxidative stress is inactivation of the photosystems, a phenomenon known as "photoinhibition" (reviewed in Aro et al., 1993; Gururani et al., 2015). Photoinhibition decreases photosynthetic capacity and can therefore be deleterious to plant growth and yield (Takahashi and Murata, 2008; Kato et al., 2012; Simkin et al., 2017). Photosystem I (PSI) is particularly resistant to photoinhibition under oxidative stress conditions, due to the high efficacy of protective mechanisms that regulate the flow of electrons to the PSI donor side, including non-photochemical quenching (NPQ), lumen pH-dependent regulation of cytochrome *b6f* activity, and even PSII photoinhibition (reviewed in Tikkanen and Aro, 2014). Electron consumption at the PSI acceptor side through the Calvin-Benson cycle, photorespiration, cyclic and pseudo-cyclic electron flow are also protective factors that prevent PSI over-reduction (Yamori, 2016; Li et al., 2018).

Despite this, PSI photoinhibition occurs under specific conditions of excessive electron pressure from PSI electron donors on the lumenal side, or/and insufficient capacity of electron acceptors at the stromal side. Under these stress conditions, reduction of $O_2$ produces $O_2^{\bullet -}$ that can inactivate PSI iron-sulfur (FeS) clusters and cause PSI inhibition (Sonoike and Terashima, 1994; Sonoike, 1995; Takagi et al., 2016; Tiwari et al., 2016). In contrast to PSII, the recovery of inhibited PSI has been shown to occur very slowly, over several days (Barth et al., 2001; Kudoh and Sonoike, 2002; Huang et al., 2010; Lima-Melo et al., 2019). PSI photoinhibition in wild type plants has been observed under low irradiance at chilling temperatures, due to down-regulation of stromal electron sinks (Inoue et al., 1986; Terashima et al., 1994; Tjus et al., 1998; Zhang and Scheller, 2004) as well as under fluctuating light (Kono et al., 2014). On the other hand, resistance against PSI photoinhibition can be induced by acclimation to low temperature and high light conditions (Ivanov et al., 1998, 2012). Severe PSI photoinhibition can occur when pH-dependent control of electron transport is inactivated, such as in plants lacking the PGR5 protein (Munekage et al., 2002; Nandha et al., 2007; Suorsa et al., 2012; Tiwari et al., 2016). High light treatment of the *pgr5* mutant of *Arabidopsis thaliana* has provided an inducible model for PSI inhibition that has been used to study the mechanisms of PSI damage and the impacts of PSI photoinhibition on photosynthesis and metabolism of plants (Tiwari et al., 2016; Gollan et al., 2017; Lima-Melo et al., 2019). Exposure of *pgr5* to sudden increases in light intensity causes PSI FeS cluster damage (Tiwari et al., 2016) and degradation of PSI subunit proteins (Suorsa et al., 2012; Lima-Melo et al., 2019).

Although several studies have shown that PSI photoinhibition is triggered by ROS (Sonoike and Terashima, 1994; Sonoike, 1995; Sejima et al., 2014; Takagi et al., 2016), the correlation between PSI photoinhibition and ROS metabolism is not clear. In the current study, we investigated the dynamics of PSI photoinhibition in *pgr5* mutants under high light stress, and the relationship between PSI photoinhibition and ROS accumulation associated with occurrence of oxidative stress at the whole leaf level. Our data suggest that PSI photoinhibition is a mechanism to prevent excessive ROS production in order to minimize oxidative stress, at the expense of carbon assimilation and normal growth.

# MATERIALS AND METHODS

## Plants, Growth and Treatment Conditions

The *proton gradient regulation 5* (*pgr5*) mutant plants of *A. thaliana* L. Heynh. ecotype Columbia, which are in the *glabrous 1* genetic background (Munekage et al., 2002), were used alongside wild-type (WT) *glabrous 1* plants in all experiments. Plants were grown for 6 weeks in a growth chamber at 23°C, relative humidity 60%, 8/16 h of light/dark photoperiod under constant white light of 125 μmol photons $m^{-2}$ $s^{-1}$ (GL). For high light (HL) treatments, plants were shifted from GL to 1,000 μmol photons $m^{-2}$ $s^{-1}$ for 1 h, while control groups were kept under GL. Experiments were repeated at least twice and at least three independent replicates were used in every experiment.

## Photochemical and Gas Exchange Measurements

Photosystem II and photosystem I photochemistry were measured simultaneously using a Dual-PAM-100 system (Walz, Germany) based on chlorophyll *a* fluorescence (Schreiber et al., 1995) and P700 absorbance (Klughammer and Schreiber, 1998). Detached leaves were analyzed after 30 min of dark acclimation. Gas exchange measurements (net $CO_2$ assimilation, *A*; transpiration, *E*; stomatal conductance, $g_S$; and internal $CO_2$ concentration, *C*i) were performed in detached leaves after 15 min dark acclimation, using a LI-6400XT Portable Infrared Gas Analyzer (IRGA) equipped with an LED source (LI-COR Biosciences, United States). The environmental conditions inside

the IRGA chamber were: 400 ppm $CO_2$, 1.0 ± 0.2 kPa VPD and 25°C. For the net $CO_2$ assimilation ($A$) time-course assay, $A$ was recorded every 15 s during changes of light intensity between GL and HL with the following protocol: 15 min of dark, 30 min of GL, 60 min of HL, 60 min of GL, 30 min of HL. For rapid light curves, a PPFD gradient of five increasing steps (0, 50, 125, 500, and 1,000 μmol photons $m^{-2}$ $s^{-1}$) was used. Gas exchange data were logged after IRGA parameters reached steady-state values after the start of each light intensity (usually around 120 s). The water use efficiency (WUE) and the maximum carboxylation efficiency were calculated as $A/E$ and $A/Ci$, respectively.

## Leaf Membrane Damage and $H_2O_2$ Content

Leaf membrane damage (MD) was estimated through the electrolyte leakage method (Blum and Ebercon, 1981). Detached leaves (5 plants, 2 leaves from each plant) were placed in tubes containing deionized water and incubated in a shaking water bath at 25°C for 24 h. After measuring electric conductivity (L1), the solution was heated at 95°C for 1 h and then cooled to 25°C, after which the second electric conductivity (L2) was measured. Membrane damage was calculated as MD = (L1/L2) × 100. The $H_2O_2$ content was quantified using the Amplex Red Hydrogen Peroxide/Peroxidase Assay Kit (Life Technologies, Carlsbad, CA, United States) according to the manufacturer protocols. Fresh leaves were ground to a fine powder in liquid $N_2$ followed by the addition of potassium phosphate buffer (final concentration of 100 mM; pH 7.5). The absorbance at 560 nm was measured to quantify the $H_2O_2$ concentration (Zhou et al., 1997) and results were expressed as μmol $H_2O_2$ $g^{-1}$ fresh weight (FW).

## Histochemical Detection of Superoxide and Hydrogen Peroxide

Nitroblue tetrazolium (NBT) and diaminobenzidine (DAB) staining were performed for *in situ* detection of superoxide ($O_2^{\bullet-}$) and hydrogen peroxide ($H_2O_2$) accumulation, respectively, in leaves, as previously described (Ogawa et al., 1997; Thordal-Christensen et al., 1997). High light-treated leaves were detached and submerged in tubes containing DAB solution [4.67 mM DAB; 1% isopropanol (v/v) and 0.1% Triton (v/v)] or NBT solution [0.1% NBT (m/v) and 10 mM $NaN_3$ in 10 mM potassium phosphate buffer, pH 7.8], both protected from light, and incubated for 24 h. For NBT staining, leaves were moved to petri dishes containing water and treated with light (approximately 20 μmol $m^{-2}$ $s^{-1}$) for 30 min prior to the end of the 24 h incubation. DAB- and NBT-stained leaves were then incubated in a bleaching solution [TCA 0.15% (m/v) diluted in ethanol:chloroform (4:1 v/v)] for 48 h. Stained leaves were then submerged in 80% ethanol and heated (70°C) in a water bath for 15 min, followed by several washes with 80% ethanol until complete removal of pigments. Leaves were then dried and photographed.

## Lipid Peroxidation (TBARS Content and Autoluminescence Imaging)

Lipid peroxidation was estimated according to the formation of thiobarbituric acid-reactive substances (TBARS; Heath and Packer, 1968). Fresh leaves were ground to a fine powder in liquid $N_2$ followed by the addition of TCA [final concentration of 5% (w/v)]. After centrifugation at 12,000 × $g$ for 15 min, 500 μl of the supernatants were immediately diluted in 2 ml of a solution containing 0.5% (w/v) of thiobarbituric acid (TBA) and 20% (w/v) of TCA and heated at 95°C in a water bath for 1 h. After cooling to 25°C, the solutions were centrifuged at 10,000 × $g$ for 5 min and supernatants were collected for absorbance readings at 532 and 660 nm using a spectrophotometer. The absorption values at 660 nm obtained from blank samples without leaf tissue were subtracted. The concentration of TBARS was calculated using the absorption coefficient of the thiobarbituric acid-malondialdehyde complex (TBA-MDA), which is 155 $mM^{-1}$ $cm^{-1}$, and the results were expressed as nmol TBA-MDA $g^{-1}$ FW. Lipid peroxidation was also assessed by the autoluminescence of leaves and rosettes according to the method described in Birtic et al. (2011). Detached leaves or rosettes treated with GL (control), HL or physical wounding with forceps were incubated in darkness for 2 h before the luminescence signal was collected over 20 min on an electrically cooled charged-couple device (CCD) camera, using an IVIS Lumina II system (Caliper Life Sciences, United States).

## Protein Extraction and Enzymatic Activity Assays

Fresh leaves were ground to a fine powder in liquid $N_2$ followed by the addition of potassium phosphate buffer (final concentration of 100 mM; pH 7.0) containing EDTA (final concentration of 1 mM). The homogenate was centrifuged at 15,000 × $g$ at 4°C for 15 min, and the resulting supernatant was used for determination of all enzymatic activities. Total soluble protein content was measured according to Bradford (1976), and all the activities were expressed on the basis of protein. All enzymatic activities were determined spectrophotometrically. Superoxide dismutase (SOD; EC 1.15.1.1) activity was determined based on inhibition of nitro blue tetrazolium chloride (NBT) photoreduction (Giannopolitis and Reis, 1977). The reaction mixture contained 75 μM NBT, 20 μM riboflavin, and 100 μl of the protein extract, all diluted in 50 mM potassium phosphate buffer (pH 6.0) containing 1 mM EDTA in a final volume of 2 ml, which was incubated under illumination (30 μmol photons $m^{-2}$ $s^{-1}$) at 25°C for 5 min. The absorbance was measured at 540 nm. One SOD activity unit (U) was defined as the amount of enzyme required to inhibit 50% of the NBT photoreduction, expressed as U $mg^{-1}$ protein $min^{-1}$. Catalase (CAT; EC 1.11.1.6) activity was based on the reduction of $H_2O_2$ (Beers and Sizer, 1952; Havir and McHale, 1987). The reaction mixture contained 20 mM $H_2O_2$, and 25 μl of the protein extract, all diluted in 50 mM potassium phosphate buffer (pH 7.0) in a final volume of 1.5 ml. The reaction was started by adding the protein extract and the decrease in absorbance at 240 nm at 30°C was monitored for 300 s. CAT activity

was calculated using the molar extinction coefficient of $H_2O_2$ (40 $mM^{-1}$ $cm^{-1}$) and expressed as μmol $H_2O_2$ $mg^{-1}$ protein $min^{-1}$. APX (EC 1.11.1.11) activity was measured based on the oxidation of ascorbate (ASC) (Nakano and Asada, 1981) in a reaction mixture containing 0.45 mM ASC, 3 mM $H_2O_2$, and 50 μl of the protein extract, all diluted in 100 mM potassium phosphate buffer (pH 7.0) containing 1 mM EDTA in a final volume of 1.5 ml. The reaction was started by adding the $H_2O_2$ solution and the decrease in absorbance at 290 nm at 25°C was monitored for 300 s. APX activity was expressed as μmol ASC $mg^{-1}$ protein $min^{-1}$. Monodehydroascorbate reductase (MDHAR; EC 1.6.5.4) activity was assayed based on the generation of monodehydroascorbate (MDHA) free radicals by ascorbate oxidase (AO; 1.10.3.3) and following oxidation of NADH (Hossain et al., 1984) in a reaction mixture containing 0.1 mM NADH, 2.5 ASC, 0.84 units/ml AO, and 75 μl of the protein extract. The reaction mixture was adjusted to 725 μl with 50 mM Tris-HCl buffer (pH 7.6). The reaction was started by adding the AO solution and the decrease in absorbance at 340 nm at 25°C was monitored for 300 s. MDHAR activity was calculated using the extinction coefficient of NADH (6.2 $mM^{-1}$ $cm^{-1}$) and expressed as nmol NADH $mg^{-1}$ protein $min^{-1}$. Dehydroascorbate reductase (DHAR; EC 1.8.5.1) activity was assayed based on the oxidation of GSH (Nakano and Asada, 1981) in a reaction mixture containing 2.5 mM GSH, 0.2 mM dehydroascorbate (DHA), and 50 μl of the protein extract, all diluted in 50 mM potassium phosphate (pH 7.0) in a final volume of 1.5 ml. The reaction was started by adding the DHA solution and the increase in absorbance at 265 nm at 25°C was monitored for 300 s. DHAR activity was expressed as nmol NADH $mg^{-1}$ protein $min^{-1}$.

## Gene Expression Analysis

Plants were treated with GL and HL, after which leaves were detached and frozen in liquid $N_2$. Leaf samples contained four leaves from individual plants. Frozen leaves were ground to a powder in liquid $N_2$ and total RNA was purified using TRIsure (Bioline, United States), according to the protocol supplied, with an additional final purification in 2.5 M LiCl overnight at −20°C. RNAseq libraries were constructed, and libraries were sequenced in 50 bp single-end reads using Illumina Hiseq 2500 technology (BGI Tech Solutions, Hong Kong). Reads were aligned to the reference genome (*A. thaliana* TAIR 10) using Strand NGS 2.7 software (Agilent, United States). Aligned reads were normalized and quantified using the DESeq R package. Gene expression fold changes were calculated using a two-way ANOVA test on triplicate samples ($n$ = 3) with Benjamini–Hochberg $p$-value correction to determine the false discovery rate (FDR) for each gene.

## Western Blotting

Leaf tissue was ground to a powder in liquid nitrogen and then incubated in 20 mM Tris buffer (pH 7.8) containing 2% SDS for 20 min at 37°C, followed by 5 min centrifugation at 15,000 × $g$. The supernatant containing total leaf protein was used for Western blotting. 10 μg of total protein were separated on SDS-PAGE gels containing 12% acrylamide, transferred to polyvinylidene difluoride (PVDF) membranes and blotted with polyclonal antibodies against LOX-C antiserum (AS07 258; Agrisera).

# RESULTS

## High Light Rapidly Induces PSI Photoinhibition in *pgr5* Mutants

Photosynthetic parameters were monitored in leaves of wild-type (WT) and *pgr5* mutant plants that were grown under 125 μmol photons $m^{-2}$ $s^{-1}$ (growth light; GL) and then exposed to 1,000 μmol photons $m^{-2}$ $s^{-1}$ (high light; HL). Chlorophyll *a* fluorescence and P700 absorbance were measured during 5 h HL treatments. The PSI photoinhibition levels were estimated through the evaluation of the maximum oxidation of P700 at the PSI reaction center ($P_m$). Before the HL treatment, the average $P_m$ value of WT leaves (1.2) was almost 30% higher than that of *pgr5* leaves (0.85; see 0 h in **Figure 1A**). The $P_m$ value of WT leaves remained virtually unchanged through the 5 h HL treatment, whereas the same parameter in *pgr5* decreased to 60% of the pre-treatment level after only 15 min under HL, with further decreases to 45 and 35% after 30 min and 1 h HL, respectively. $P_m$ in HL-treated *pgr5* reached a steady-state value of around 0.15 (20% of pre-treatment $P_m$) after 3 h of HL treatment.

PSII photoinhibition was evaluated by monitoring the decrease of the maximum chlorophyll *a* fluorescence ($F_m$) during the same time-course experiment. The $F_m$ values before the onset of the HL treatment were almost identical in WT and *pgr5* (**Figure 1B**). After 15 min, $F_m$ values decreased to 0.75 and 0.65 in WT and *pgr5*, respectively, and then showed a steady decline over the course of the 5 h HL treatment in both genotypes. In contrast, the HL-induced decline in the calculated $F_v/F_m$ (maximum quantum efficiency of PSII) parameter was substantially greater in the *pgr5* mutant (**Figure 1C**), which corresponded to significantly higher levels of minimum chlorophyll *a* fluorescence ($F_o$) after 30 min HL exposure, when compared to WT (**Figure 1D**).

## Time-Resolved Diminution of $CO_2$ Assimilation During PSI Photoinhibition

In order to investigate the consequences of progressive HL-induced photoinhibition of PSI on net $CO_2$ assimilation rate ($A$) and respiration in WT and *pgr5* mutant plants, these processes were evaluated during cycles of GL and HL exposure (**Figure 2**). In both genotypes, similar rates of $CO_2$ assimilation and day-time respiration (measured by $CO_2$ evolution in the dark) were observed in GL-treated plants (**Figure 2A**). During the first minutes of the transition from GL to HL, $A$ increased at a rate of approximately 1.6–1.7 μmol $CO_2$ $m^{-2}$ $s^{-1}$ *per* min in both WT and *pgr5* plants (**Figure 2B**). After approximately 10 min in HL, WT $A$ decreased until the end of the first hour of HL treatment at a rate of approximately 0.03 μmol $CO_2$ $m^{-2}$ $s^{-1}$ *per* min, while $A$ decline in *pgr5* during the HL treatment was far more rapid than in the WT, especially during the early phase of HL exposure (0.11 μmol $CO_2$ $m^{-2}$ $s^{-1}$ *per* min) compared to

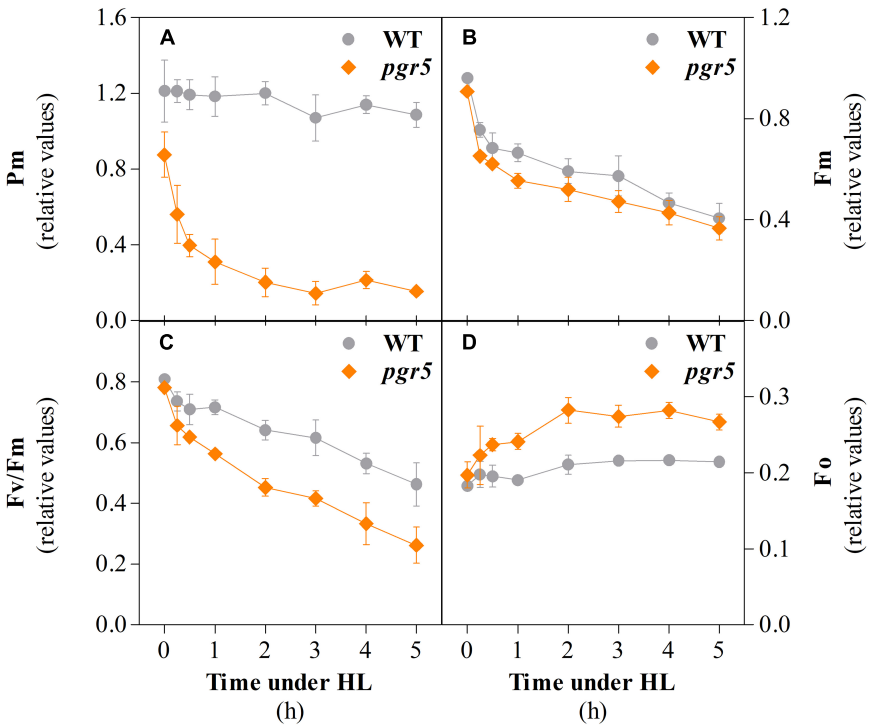


**FIGURE 1 |** Parameters associated with PSI and PSII integrity in wild type (WT) and *pgr5* mutants during treatment with high light (HL). Maximum oxidizable P700 ($P_m$, **A**); maximum chlorophyll *a* fluorescence ($F_m$, **B**); maximum efficiency of PSII ($F_v/F_m$, **C**); minimum chlorophyll *a* fluorescence ($F_o$, **D**) measured in detached leaves of WT and *pgr5* plants grown under a photosynthetic photon flux density of 125 μmol $m^{-2}$ $s^{-1}$ and treated with 1,000 μmol $m^{-2}$ $s^{-1}$ for 5 h. Error bars show standard deviation among replicates ($n$ = 4). Significant differences between genotypes are indicated by non-overlapping error bars (Student's $t$-test, $p < 0.05$).

the latter phase (0.05 μmol $CO_2$ $m^{-2}$ $s^{-1}$ *per* min) of treatment (**Figure 2C**). At the end of the 1 h HL treatment, *A* was 40% lower in *pgr5* mutants than in WT (**Figures 2A,C**). Under a second phase of GL following the HL treatment, *A* in WT leaves was slightly lower than the level observed in the first GL phase prior to the HL treatment, while the rate in HL-treated *pgr5* mutants was approximately 0 μmol $CO_2$ $m^{-2}$ $s^{-1}$ (**Figure 2A**). A second HL treatment after 1 h GL induced another rapid increase in $CO_2$ fixation for both genotypes, and in each case the maximum initial rates under the second treatment were approximately equivalent to the rates observed before the end of the previous HL treatment (7.5 μmol $CO_2$ $m^{-2}$ $s^{-1}$ in WT and 5 μmol $CO_2$ $m^{-2}$ $s^{-1}$ in *pgr5*), corresponding to approximately 35% lower $CO_2$ fixation in *pgr5* than in WT during the second HL treatment (**Figure 2A**). Notably, the rate of increase in *A* during the second HL treatment was slower in both WT and *pgr5* (0.13 and 0.16 μmol $CO_2$ $m^{-2}$ $s^{-1}$ *per* min, respectively; **Figure 2D**) in comparison to the rates of increase during the first HL treatment (1.74 and 1.58 μmol $CO_2$ $m^{-2}$ $s^{-1}$ *per* min, respectively; **Figure 2B**). The rate of decline in *A* during the second HL treatment was similar between WT and *pgr5* (**Figure 2E**), and smaller than that observed during the first HL treatment (**Figure 2C**).

Analyses of gas exchange in WT and *pgr5* plants pre-treated with GL or HL for 1 h were conducted using light-response curves to investigate the effects of PSI photoinhibition under different irradiances. $CO_2$ assimilation rates over increasing light intensities were similar in both WT and *pgr5* plants treated with GL and were substantially decreased in both genotypes after 1 h HL treatment (**Figure 3A**). Significantly lower *A* values were observed in HL-treated *pgr5* compared to HL-treated WT, especially in the region of the curve measured under irradiances below 200 μmol photons $m^{-2}$ $s^{-1}$ (**Figure 3A**). Higher internal $CO_2$ concentration ($C_i$) was recorded in HL-treated *pgr5* at the lowest irradiances of the light curve when compared to all other plants, while there were no significant differences in *Ci* at high irradiances (**Figure 3B**). Stomatal conductance ($g_s$) values were higher in GL-treated *pgr5* when compared to GL-treated WT, and were substantially lower in both genotypes after the HL treatment, compared to GL-treated plants (**Figure 3C**). No differences in $g_s$ values between the genotypes were observed after the HL treatment. The changes in transpiration rate (*E*) over the light curve were similar to that observed for $g_s$ (**Figure 3D**). The trends observed in the maximum carboxylation efficiency ($A/C_i$)-PPFD curve were similar to those in the *A*-PPFD curve (**Figures 3A,E**, respectively), although the difference between the HL-treated *pgr5* and the other groups was more evident, as a consequence of the higher $C_i$ values under low irradiances (**Figure 3B**). Water use efficiency (WUE) was strikingly lower in the HL-treated *pgr5* mutants when measured under low irradiances, compared to the other treatments (**Figure 3F**), reflecting the very low *A* measured in those leaves (**Figure 3A**).

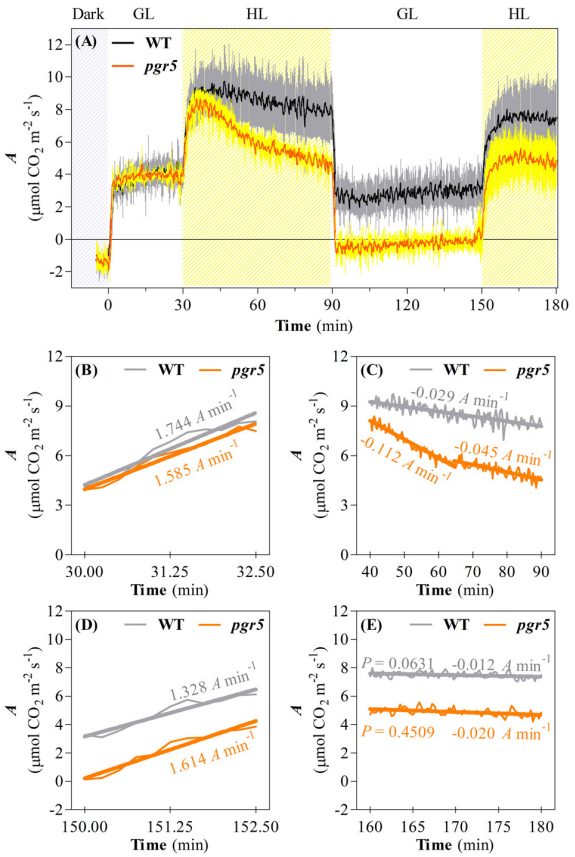


**FIGURE 2 |** Changes in net $CO_2$ assimilation during a time-course PSI photoinhibition. **(A)** $CO_2$ assimilation (*A*) in leaves of WT and *pgr5* mutants during changes of light intensity between growth light (GL; 125 μmol $m^{-2}$ $s^{-1}$) and high light (HL; 1,000 μmol $m^{-2}$ $s^{-1}$). Hatched gray and hatched yellow sections indicate dark and HL treatments, respectively. Error margins are shown in gray (WT) and yellow (*pgr5*) and indicate standard deviation among replicates ($n = 6$). Significant differences between treatments and genotypes are indicated by non-overlapping error bars (Student's *t*-test, $p < 0.05$). Linear regression lines of changes in *A* drawn in key steps of the time-course like the onset of the first HL treatment **(B)**, during the first HL treatment **(C)**, the onset of the second HL treatment **(D)**, and during the second HL treatment **(E)**. *P*-values were calculated to estimate if the slopes are significantly different from zero. All *P*-values were lower than 0.0001, except where shown in **(E)**.

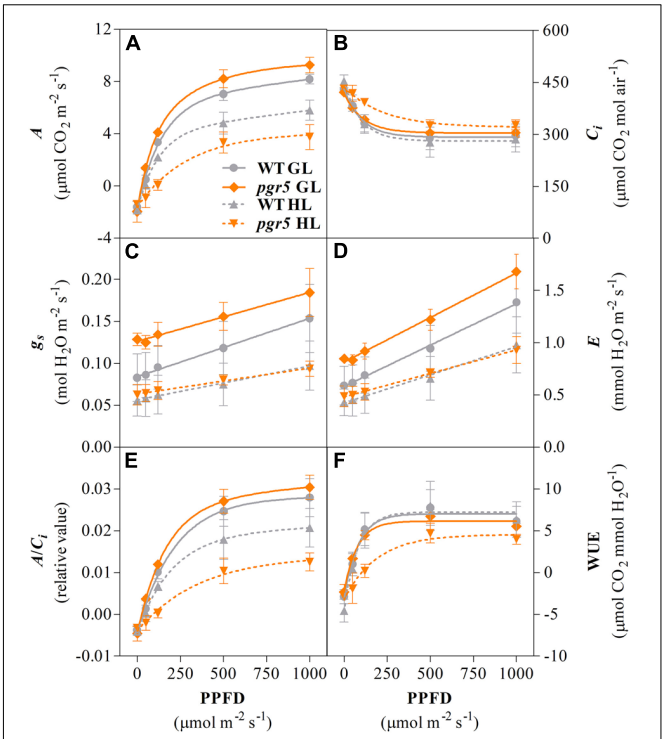


**FIGURE 3 |** Gas exchange response to increasing light intensity. Net $CO_2$ assimilation rate (*A*, **A**); internal $CO_2$ concentration ($C_i$, **B**); stomatal conductance rate ($g_s$, **C**); transpiration rate (*E*, **D**); maximum carboxylation efficiency ($A/C_i$, **E**); water use efficiency (WUE, **F**) measured in leaves of WT and *pgr5* plants previously treated with growth light (GL; 125 μmol $m^{-2}$ $s^{-1}$) or high light (HL; 1,000 μmol $m^{-2}$ $s^{-1}$) for 1 h. Error bars show standard deviation among replicates ($n = 4$). Significant differences between treatments and genotypes are indicated by non-overlapping error bars (Student's *t*-test, $p < 0.05$).

## ROS Accumulation, and Activities and Expression of Antioxidant Systems After PSI Photoinhibition

To explore the relationship between PSI photoinhibition and accumulation of ROS, several markers of oxidative stress were evaluated in HL-treated leaves of WT and *pgr5* mutants. Membrane damage, estimated through electrolyte leakage, increased significantly after 1 h of HL treatment in both genotypes, compared to the GL controls; however, no difference was detected between WT and *pgr5* mutants in either condition (**Figure 4A**). Spectrophotometric measurements of $H_2O_2$ concentrations in leaf tissue showed no difference between GL and 1 h HL treatments or between genotypes (**Figure 4B**). Qualitative *in situ* assessments of $H_2O_2$ and superoxide ($O_2^{\bullet-}$) accumulation in HL-treated leaves by 3,3′-diaminobenzidine (DAB) and nitro-blue tetrazolium (NBT) staining, respectively, also showed no obvious differences between WT and *pgr5* in terms of accumulation of these ROS (**Figures 4C,D**).

Activities of SOD, CAT, APX, MDHAR, and DHAR were measured in leaves to assess any effects of PSI photoinhibition on ROS scavenging capacity. Overall, the results showed slightly higher enzyme activities in *pgr5*, in comparison to WT, in both light conditions (**Figure 5**). Total leaf CAT activity was significantly higher in *pgr5* than in WT under GL (**Figure 5B**), while total DHAR activity showed a significant increase in HL-treated *pgr5*, compared to GL-treated *pgr5*, which was not evident in WT (**Figure 5E**). Changes in the expression of genes involved in the Foyer–Halliwell–Asada cycle were assessed in WT and *pgr5* plants prior to HL treatment, as well as after 15 min and 1 h HL exposure. Most genes were upregulated by HL treatment in both WT and *pgr5* plants, with only minor differential expression between genotypes in most cases. Despite the similar trend of HL-induced expression in both genotypes, APX2, DHAR1 and the SOD enzymes CDS1, CDS2, and FSD2, were down-regulated in *pgr5* under HL relative to WT levels (**Figure 6**). Conversely,

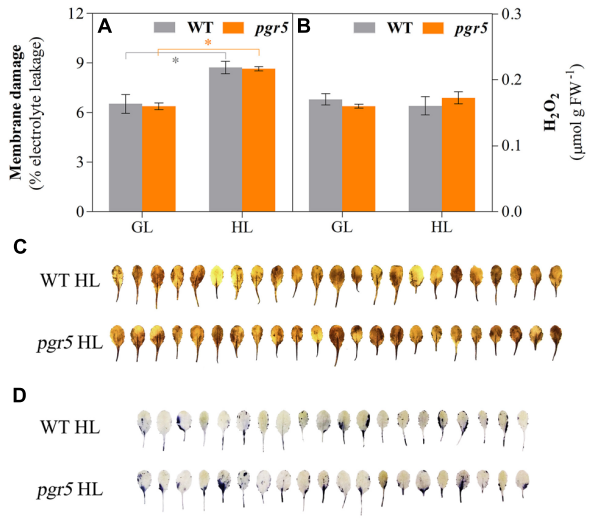


**FIGURE 4 |** Indicators of oxidative stress in WT and *pgr5* mutants under growth light or after high light treatment. Membrane damage **(A)** and $H_2O_2$ content **(B)** in leaves of WT and *pgr5* mutants treated with growth light (GL; 125 μmol $m^{-2}$ $s^{-1}$) or high light (HL; 1,000 μmol $m^{-2}$ $s^{-1}$) for 1 h. Error bars show standard error among replicates ($n$ = 4). Significant differences between treatments and genotypes are indicated by asterisks (Student's $t$-test, $p < 0.05$). 3,3-diaminobenzidine (DAB, **C**) and nitro-blue tetrazolium (NBT, **D**) staining to assess the accumulation of $H_2O_2$ and superoxide accumulation, respectively, in detached leaves of HL-treated WT and *pgr5* plants.

APX1, CAT2 and FSD1 were upregulated in HL-treated *pgr5* compared to the WT.

Assessment of thiobarbituric acid-reactive substances (TBARS) content provides an indication of lipid peroxidation. TBARS detected in GL-treated *pgr5* did not differ significantly from GL-treated WT, while after 1 h HL treatment TBARS content in *pgr5* was markedly lower than GL and WT levels (**Figure 7A**). Autoluminescence imaging showed that levels of lipid oxidation in leaves and rosettes increased in WT after 1 h HL treatment, in comparison to GL-treated plants, but a corresponding increase was not detected in HL-treated *pgr5* (**Figures 7B,C**). In contrast, strong autoluminescence signals were detected in both genotypes after mechanical wounding of leaves (**Figure 7B**). Western blots showed increases in the abundance of chloroplast lipoxygenase (LOX2) in both WT and *pgr5* after 1 h HL treatment. However, substantially lower LOX2 abundance was detected in both GL- and HL-treated *pgr5* leaves, in comparison to WT controls (**Figure 7D**), corroborating the results of TBARS tests (**Figure 7A**).

## DISCUSSION

Oxidative stress in plants is closely linked to photosynthetic activity, as the transfer of photosynthetic excitation or electrons to oxygen can lead to the overproduction of ROS (for a recent review, see Mullineaux et al., 2018). Excess ROS production resulting from disturbed photosynthetic redox homeostasis is the cause of photodamage to both PSII and PSI, although the mechanisms of damage and repair differ considerably between the two photosystems and distinct intersystem regulation is evident. For example, it has become well established that PSII damage can serve as a photoprotective mechanism by preventing over-reduction and inactivation of downstream factors, especially PSI (Tikkanen et al., 2014; Huang et al., 2016). The current work suggests that rapid PSI photoinhibition under severe photosynthetic imbalance can also prevent excessive ROS production and oxidative damage.

PSI photoinhibition under disturbed redox homeostasis is associated with insufficient stromal acceptor capacity and increased utilization of $O_2$ as an alternative electron acceptor, leading to formation of $O_2^{\bullet-}$ that can inactivate PSI iron-sulfur (FeS) clusters (reviewed in Sonoike, 2011). Protection from PSI photoinhibition is especially dependent on functional pH-dependent regulation of electron flow to PSI during increased irradiance (Suorsa et al., 2012; Kono et al., 2014; Tiwari et al., 2016; Gollan et al., 2017; Lima-Melo et al., 2019; Yamamoto and Shikanai, 2019). In the current work, a large decrease in $P_m$ within the first minutes of exposure of *pgr5* mutants to HL shows that PSI photoinhibition occurs rapidly upon the onset of imbalance between the PSI donor and acceptor sides. This rapid inhibition suggests that the normal levels of antioxidant activity measured in *pgr5* (**Figure 5**) were not sufficient to mitigate ROS-induced PSI damage within the initial stages of imbalance. These results support other findings that showed that chloroplast antioxidant

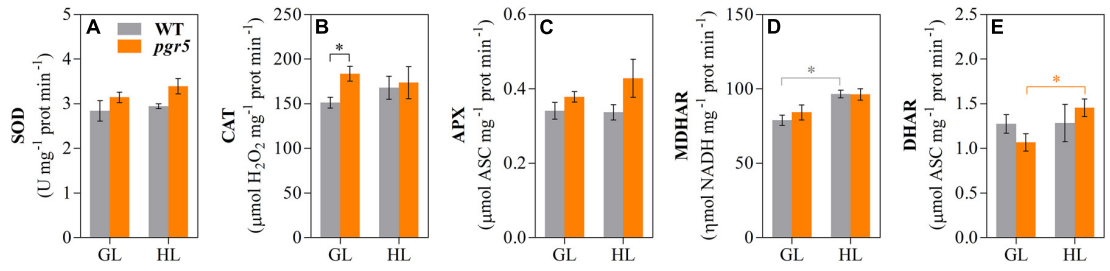


**FIGURE 5 |** Activities of Foyer–Halliwell–Asada cycle enzymes. Activities of superoxide dismutase (SOD, **A**); catalase (CAT, **B**); ascorbate peroxidase (APX, **C**); monodehydroascorbate reductase (MDHAR, **D**) and dehydroascorbate reductase (DHAR, **E**) were measured in total leaf extracts of WT and *pgr5* mutants treated with growth light (GL; 125 μmol $m^{-2}$ $s^{-1}$) or high light (HL; 1,000 μmol $m^{-2}$ $s^{-1}$) for 1 h. Activities are normalized to protein content. Error bars show standard error among replicates ($n$ = 4). Significant differences between treatments and genotypes are indicated by asterisks (Student's $t$-test, $p < 0.05$).

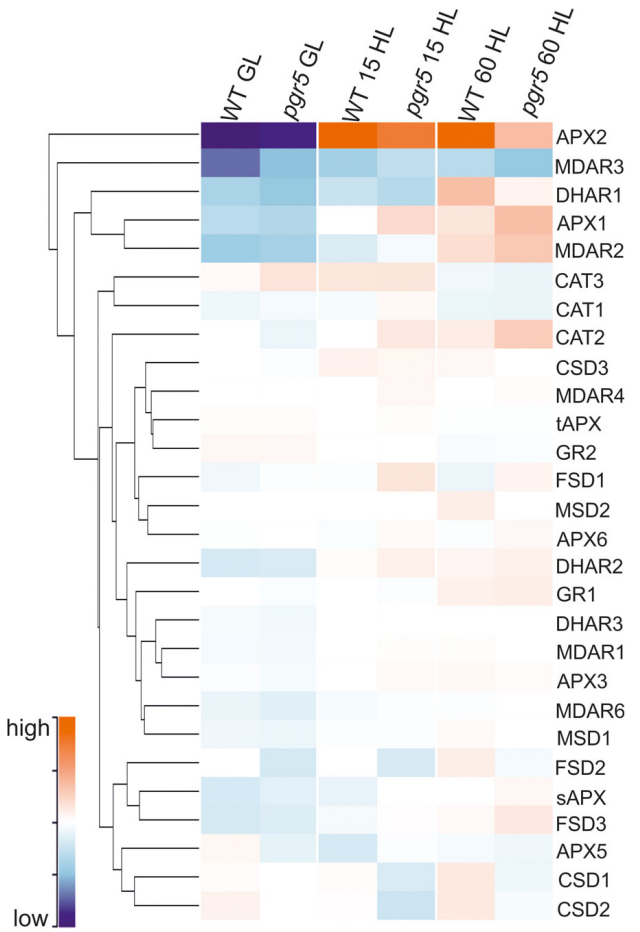


**FIGURE 6 |** Clustered heatmap showing normalized abundance of transcripts encoding enzymes in the Foyer–Halliwell–Asada cycle. Samples show gene expression in WT and *pgr5* mutant plants under growth light (GL; 125 μmol $m^{-2}$ $s^{-1}$) and after 15 and 60 min in high light (HL; 1,000 μmol $m^{-2}$ $s^{-1}$). Color intensities indicate transcript abundance, according to the key. APX, ascorbate peroxidase; MDAR, monodehydroascorbate reductase; DHAR, dehydroascorbate reductase; CAT, catalase; CSD, Cu/Zn-superoxide dismutase; tAPX, thylakoidal ascorbate peroxidase; GR, glutathione reductase; FSD, Fe-superoxide dismutase; MSD, Mn-superoxide dismutase; sAPX, stromal ascorbate peroxidase.

scavengers cannot prevent PSI photoinhibition under conditions of donor/acceptor side imbalance (Sejima et al., 2014; Zivcak et al., 2015a,b; Takagi et al., 2016).

A slower rate of $P_m$ decline in *pgr5* after 30 min in HL, and the eventual stabilization of $P_m$ after 2 h (**Figure 1**), indicated progressive decrease in ROS-induced PSI inactivation induced by decreasing intensity of stromal over-reduction. Again, this could not be attributed to any improvement in stromal ROS scavenging in *pgr5* (**Figure 5**) and was also not associated with decreased abundance of ROS after 1 h HL (**Figure 4**). Instead, a slower rate of PSI inhibition was likely directly related to alleviation of electron pressure on stromal acceptors caused by inactivation of PSI electron transport (described in **Figure 8**). This observation highlights the protective nature of PSI photoinhibition against over-production of ROS in the chloroplast stroma, which has been previously suggested (Tikkanen and Aro, 2014). Furthermore, in the absence of adequate pH-dependent photosynthetic control, as in the *pgr5* mutant, the extent of PSI inhibition appears to correlate to the level of imbalance between PSI donor and acceptor sides, which was high during the initial stages of HL and diminished as PSI inhibition progressed. In this way, PSI photoinhibition can be seen to support PSI donor side regulation in preventing oversupply of reductants to the stromal acceptor side. The idea that PSI photoinhibition is sensitive to the extent of photosynthetic imbalance was also evident in the changes in $CO_2$ assimilation in *pgr5* during the HL treatments. A rapid rate of decline during the first 15 min of HL (**Figure 2**) corresponded with rapid PSI photoinhibition (**Figure 1A**), while slower decline during the latter part of the HL treatment correlated with a slower decrease in $P_m$ during this phase of treatment. During the second HL treatment, rapid $A$ decline was not observed in *pgr5* (**Figure 2**, 150–180 min), presumably because PSI inhibition from the previous HL exposure had effectively "pre-set" PSI activity to suit the capacity of stromal acceptors at 1,000 μmol photons $m^{-2}$ $s^{-1}$.

Although PSI inhibition can protect against over-production of stromal ROS during conditions of insufficient stromal acceptor capacity, PSI damage is a major impediment to carbon metabolism under normal growth conditions (Gollan et al., 2017; Lima-Melo et al., 2019). In the current study, this was especially

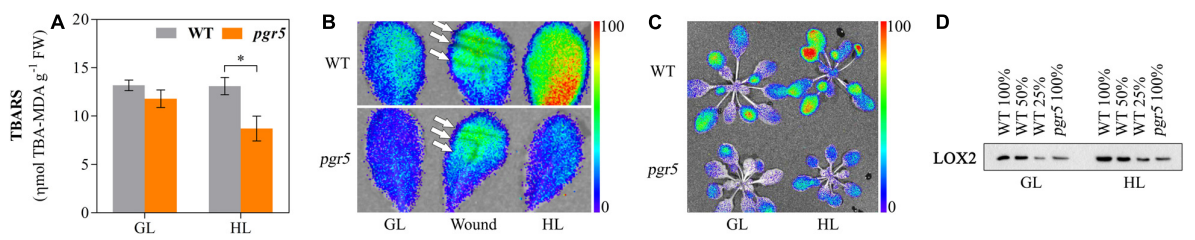


**FIGURE 7 |** Lipid oxidation in *pgr5* mutants after high light treatment. Content of thiobarbituric acid-reactive substances (TBARS; **A**), autoluminescence imaging **(B,C)**, and Western blotting detection of chloroplast lipoxygenase (LOX2) abundance **(D)** in WT and *pgr5* mutants treated with growth light (GL; 125 μmol $m^{-2}$ $s^{-1}$) and high light (HL; 1,000 μmol $m^{-2}$ $s^{-1}$) for 1 h. Luminescence intensities **(B,C)** correspond to color scales as shown. Luminescence images overlay photographs of the same leaf/rosette samples. Wounding of leaves is indicated by white arrows in **(B)**. Error bars show standard error among replicates ($n$ = 4). Significant differences between treatments and genotypes are indicated by asterisks (Student's $t$-test, $p < 0.05$).

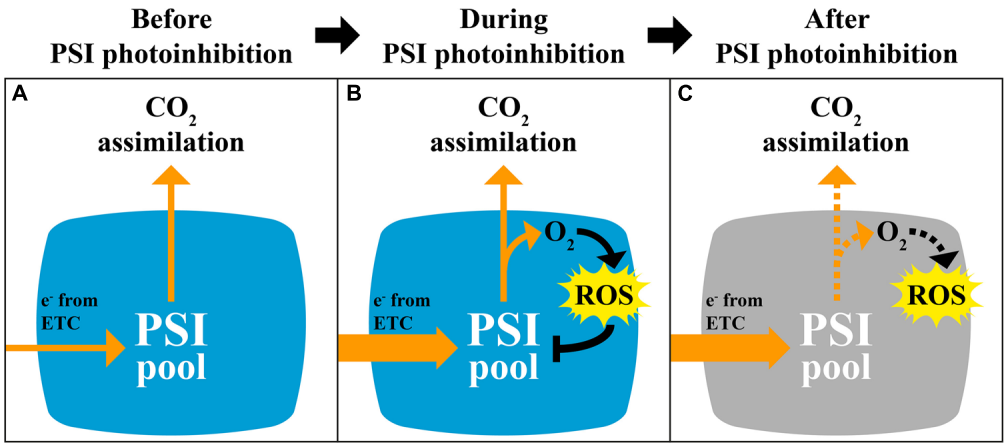


**FIGURE 8 |** Hypothetical scheme describing the mechanism and impact of PSI photoinhibition on $CO_2$ fixation and ROS production. **(A)** Under constant conditions, electron pressure at the donor and acceptor sides of PSI is balanced due to partially oxidized state of P700 and stromal electron carriers. Excess ROS production is minimal. **(B)** During the first minutes of electron imbalance between PSI donor and acceptor sides, such as during exposure of *pgr5* mutants to high light, or during low light and cold temperature (Sonoike and Terashima, 1994) or fluctuating light (Kono et al., 2014), limited stromal electron acceptor capacity leads to increased reduction of molecular oxygen. Increased ROS production leads to inactivation of PSI, presumably through oxidation of FeS clusters. **(C)** Partial inactivation of the PSI pool leads to decreased electron flow to the stroma, which limits the capacity for $CO_2$ fixation, especially under low light, and presumably decreases excess ROS production to protect downstream electron acceptors.

clear in the diminished $CO_2$ fixation in HL-treated *pgr5* plants under subsequent GL (**Figures 2**, **3A**). This phenomenon was not due to decreased availability of $CO_2$ in *pgr5* leaves, as internal $CO_2$ concentration ($C_i$) in *pgr5* plants was equivalent to WT levels, and higher in HL-treated *pgr5* plants. Instead, the light-dependent effect on *A* in PSI-inhibited plants reflects PSI quantum efficiency, where the highly reduced state of P700 under low light is exacerbated by PSI damage, while more $P700^+$ is formed under HL due to more active PSI electron transport, in combination with high light-activated electron transport regulation (Baker et al., 2007; Lima-Melo et al., 2019). Despite the positive effects of HL, $CO_2$ assimilation rates in PSI-inhibited plants remained lower than WT controls during the second HL treatment (**Figure 2**). Considering these results, we expect that the generation of $O_2^{\bullet-}$ during a subsequent HL treatment would also have been diminished in plants with inhibited PSI, although this was not specifically tested. Slightly higher stomatal conductance ($g_s$) in *pgr5* mutants compared to WT under GL correlated with higher transpiration rates (*E*) in the mutant under GL, while lower water use efficiency (WUE) in HL-treated *pgr5* reflected low levels of $CO_2$ fixation (**Figure 3**). Abnormal gas exchange in *pgr5* leaves may be related to the influence of plastoquinone (PQ) reduction state on stomatal opening and regulation of WUE in response to light (Busch, 2014; Głowacka et al., 2018), given that over-reduction of the PQ pool has been demonstrated in *pgr5* mutants, especially after HL-treatment (Nandha et al., 2007; Munekage et al., 2008; Suorsa et al., 2012; Kono et al., 2014; Gollan et al., 2017; Lima-Melo et al., 2019).

Decreased production $O_2^{\bullet-}$ and $H_2O_2$, generated from $O_2$ reduction and $O_2^{\bullet-}$ dismutation, respectively, was previously observed in *pgr5* mutant seedlings exposed to fluctuating light stress (Suorsa et al., 2012). In addition, $H_2O_2$-related gene expression was negatively affected in HL-stressed *pgr5* plants (Gollan et al., 2017). These results were attributed to increased antioxidant capacity in *pgr5* (Suorsa et al., 2012) and/or decreased $O_2$ reduction by inactivated PSI (Gollan et al., 2017). However, results of the current study demonstrated that ROS accumulation and oxidative stress after severe PSI photoinhibition was not substantially different from HL-stressed leaves with functional PSI, despite oxidative damage that was seen to occur in both genotypes by increases in electrolyte leakage after HL treatment (**Figure 4A**). Our results showing no apparent over-accumulation of $H_2O_2$ or $O_2^{\bullet-}$ in HL-treated *pgr5* leaves, compared to WT, may differ from previous results because we measured ROS levels after completion of HL treatments, rather than assaying accumulation of ROS during stress treatments (Suorsa et al., 2012). It is likely that foliar $O_2^{\bullet-}$ and $H_2O_2$ contents did increase during the first minutes under HL in both WT and *pgr5* plants, but were returned to basal levels during the 1 h treatment, as has been previously demonstrated (Galvez-Valdivieso et al., 2009; König et al., 2018). Efficient $H_2O_2$ scavenging during HL relies on the activity of the Foyer–Halliwell–Asada cycle for redox turnover of ascorbate and GSH (reviewed in Foyer and Shigeoka, 2011), which appeared to function normally in HL-treated *pgr5* plants according to similar transcript levels and activities of enzymes of the cycle (**Figures 5**, **6**). An exception was DHAR, which showed increased total activity in HL-treated *pgr5* leaves, despite the expression of the mitochondrial DHAR1 isoform being significantly down-regulated in this condition. DHAR converts DHA to ascorbate using electrons from the reduced form of GSH, suggesting a higher accumulation of DHA in *pgr5* during HL stress. Similarly, expression of APX2 was significantly down-regulated in *pgr5* after HL treatment, as previously reported (Gollan et al., 2017). Induction of Arabidopsis APX2 expression is dependent on the occurrence of photosynthetic electron transport (Karpiński et al., 1997, 1999; Chang et al., 2004; Galvez-Valdivieso et al., 2009),

which is lower in the case of severe PSI photoinhibition. Interestingly, the total activity of catalase (CAT) in *pgr5* leaves was higher under non-stress conditions than in WT leaves, correlating with increased expression of peroxisomal CAT3 in these conditions.

PSI photoinhibition in *pgr5* plants appeared to have a substantial negative effect on lipid oxidation, as measured by quantification of TBARS content and autoluminescence of leaves and rosettes. We previously detected no difference in lipid oxidation between WT and *pgr5* plants that were treated with severe high light stress that also caused chlorophyll bleaching in affected leaves of both genotypes (Gollan et al., 2017). In the current study, exposure to 1,000 μmol photons $m^{-2}$ $s^{-1}$ for 1 h did not bleach leaves, and this treatment revealed substantially lower levels of lipid oxidation in *pgr5* in comparison to WT. Lipid peroxides can be formed in the chloroplast either non-enzymatically, through the reaction between singlet oxygen ($^1O_2$) and unsaturated lipids (reviewed in Laloi and Havaux, 2015), or enzymatically through the activity of lipoxygenase (LOX) enzymes (reviewed in Wasternack and Hause, 2013). Non-enzymatic lipid peroxidation is associated with $^1O_2$ formation in PSII, especially under conditions of PSII over-reduction (Triantaphylidès et al., 2008). PSI photoinhibition is known to increase excitation pressure on PSII (Suorsa et al., 2012; Kono et al., 2014; Lima-Melo et al., 2019), suggesting that higher non-enzymatic lipid oxidation may be expected in HL-treated *pgr5*. On the contrary, decreases in HL-induced lipid oxidation observed in *pgr5* likely relate to the low abundance of chloroplast-localized lipoxygenase LOX2, which was evident in both GL- and HL-treated plants (**Figure 7C**). Down-regulation of LOX2 suggests disrupted chloroplast signaling in *pgr5*, which is in line with our previous detection of decreased oxylipin signaling in PSI-photoinhibited *pgr5* (Gollan et al., 2017). Indeed, LOX gene expression is induced by oxylipins (Porta et al., 2008; Sarde et al., 2018), while lipid peroxidation is an early step in enzymatic oxylipin synthesis (Wasternack and Hause, 2013), making it difficult to distinguish the cause of low lipid oxidation from the effect in this case. Equivalent luminescence signals were detected in both WT and *pgr5* after physical wounding of leaves (**Figure 7B**), indicating that wound-responsive lipid oxidation pathways were operational in *pgr5* plants.

## CONCLUSION

This study shows that PSI photoinhibition is rapidly induced under conditions of imbalanced reduction pressure between PSI donor and acceptor sides, and that PSI photoinhibition is not associated with increases in HL-induced ROS accumulation at the whole leaf level. It should be noted that the donor/acceptor side imbalance in *pgr5* under HL is more severe than that induced by natural conditions like low temperatures or fluctuating light (Terashima et al., 1994; Kono et al., 2014; Lima-Melo et al., 2019). Therefore the extent, and probably the mechanism, of PSI photoinhibition in the *pgr5* system can be considered overly severe. Nonetheless, the current results can improve our understanding of PSI inhibition induced by natural stresses, while also underscoring the importance of PGR5-dependent protection of PSI. We present the notion that PSI inactivation prevents ROS over-production and oxidative stress in the chloroplast stroma and in the wider cell. This resembles the protective effect of PSII photodamage that prevents over-reduction of downstream components (Tikkanen et al., 2014; Huang et al., 2016), except that damaged PSII is replenished far more efficiently than damaged PSI (Aro et al., 1993; Scheller and Haldrup, 2005). In light of its slow recovery, PSI protection is often considered to be the main target of photosynthetic regulation mechanisms (Tikkanen et al., 2012; Larosa et al., 2018); however, the current work suggests that PSI is also expendable in the effort to mitigate stromal over-reduction. Considering our recent findings that a partially inhibited PSI pool can support normal $CO_2$ metabolism (Lima-Melo et al., 2019), inactivation of PSI may be more affordable than commonly thought.

## DATA AVAILABILITY

The raw data supporting the conclusions of this manuscript will be made available by the authors, without undue reservation, to any qualified researcher.

## AUTHOR CONTRIBUTIONS

YL-M, E-MA, and PG devised the work. YL-M, VA, AL, RS, and PG conducted the experiments. YL-M, MT, E-MA, JS, and PG analyzed the data. YL-M, E-MA, JS, and PG wrote the manuscript.

## FUNDING

The authors acknowledge financial support from: CAPES (project BEX10758/14-3, YL-M); CIMO (project TM-16-10130, E-MA); CNPq (Proc. 154471/2018-6, AL; INCT Plant Stress Biotech, Proc. 465480/2014-4, JS); FCT-Portugal/FUNCAP-Brazil (FUNCAP – FCT AAC No. 02/SAICT/2017, JS); and Academy of Finland (projects 26080341, PG; and 307335 and 303757, E-MA).

## REFERENCES

Apel, K., and Hirt, H. (2004). Reactive oxygen species: metabolism, oxidative stress, and signal transduction. *Annu. Rev. Plant Biol.* 55, 373–399. doi: 10.1146/annurev.arplant.55.031903.141701

Aro, E. M., Virgin, I., and Andersson, B. (1993). Photoinhibition of photosystem II. Inactivation, protein damage and turnover. *Biochim. Biophys. Acta* 1143, 113–134. doi: 10.1016/0005-2728(93)90134-2

Asada, K. (1999). The water-water cycle in chloroplasts: scavenging of active oxygens and dissipation of excess photons. *Annu. Rev. Plant Physiol. Plant Mol. Biol.* 50, 601–639. doi: 10.1146/annurev.arplant.50.1.601

Baker, N. R., Harbinson, J., and Kramer, D. M. (2007). Determining the limitations and regulation of photosynthetic energy transduction in leaves. *Plant Cell Environ.* 30, 1107–1125. doi: 10.1111/j.1365-3040.2007.01680.x

Barth, C., Krause, G. H., and Winter, K. (2001). Responses of photosystem I compared with photosystem II to high-light stress in tropical shade and sun leaves. *Plant Cell Environ.* 24, 163–176. doi: 10.1046/j.1365-3040.2001.00673.x

Beers, R. F., and Sizer, I. W. (1952). A spectrophotometric method for measuring the breakdown of hydrogen peroxide by catalase. *J. Biol. Chem.* 195, 133–140.

Birtic, S., Ksas, B., Genty, B., Mueller, M. J., Triantaphylidès, C., and Havaux, M. (2011). Using spontaneous photon emission to image lipid oxidation patterns in plant tissues. *Plant J.* 67, 1103–1115. doi: 10.1111/j.1365-313X.2011.04646.x

Blum, A., and Ebercon, A. (1981). Cell membrane stability as a measure of drought and heat tolerance in wheat. *Crop Sci.* 21, 43–47.

Bradford, M. M. (1976). A rapid and sensitive method for the quantification of microgram quantities of protein utilizing the principle of protein-dye binding. *Anal. Biochem.* 72, 248–254. doi: 10.1016/0003-2697(76)90527-3

Busch, F. A. (2014). Opinion: the red-light response of stomatal movement is sensed by the redox state of the photosynthetic electron transport chain. *Photosynth. Res.* 119, 131–140. doi: 10.1007/s11120-013-9805-6

Chang, C. C.-C., Ball, L., Fryer, M. J., Baker, N. R., Karpiński, S., and Mullineaux, P. M. (2004). Induction of ASCORBATE PEROXIDASE 2 expression in wounded Arabidopsis leaves does not involve known wound-signalling pathways but is associated with changes in photosynthesis. *Plant J.* 38, 499–511. doi: 10.1111/j.1365-313x.2004.02066.x

Czarnocka, W., and Karpiński, S. (2018). Friend or foe? Reactive oxygen species production, scavenging and signaling in plant response to environmental stresses. *Free Radic. Biol. Med.* 122, 4–20. doi: 10.1016/j.freeradbiomed.2018.01.011

de Souza, A., Wang, J.-Z., and Dehesh, K. (2017). Retrograde signals: integrators of interorganellar communication and orchestrators of plant development. *Annu. Rev. Plant Biol.* 68, 85–108. doi: 10.1146/annurev-arplant-042916-041007

Exposito-Rodriguez, M., Laissue, P. P., Yvon-Durocher, G., Smirnoff, N., and Mullineaux, P. M. (2017). Photosynthesis-dependent H2O2 transfer from chloroplasts to nuclei provides a high-light signalling mechanism. *Nat. Commun.* 8:49. doi: 10.1038/s41467-017-00074-w

Foyer, C. H., and Shigeoka, S. (2011). Understanding oxidative stress and antioxidant functions to enhance photosynthesis. *Plant Physiol.* 155, 93–100. doi: 10.1104/pp.110.166181

Galvez-Valdivieso, G., Fryer, M. J., Lawson, T., Slattery, K., Truman, W., Smirnoff, N., et al. (2009). The high light response in Arabidopsis involves ABA signaling between vascular and bundle sheath cells. *Plant Cell* 21, 2143–2162. doi: 10.1105/tpc.108.061507

Giannopolitis, C. N., and Reis, S. K. (1977). Superoxide dismutases. I. Occurrence in higher plants. *Plant Physiol.* 59, 309–314. doi: 10.1104/pp.59.2.309

Głowacka, K., Kromdijk, J., Kucera, K., Xie, J., Cavanagh, A. P., Leonelli, L., et al. (2018). Photosystem II subunit S overexpression increases the efficiency of water use in a field-grown crop. *Nat. Commun.* 9:868. doi: 10.1038/s41467-018-03231-x

Gollan, P. J., Lima-Melo, Y., Tiwari, A., and Tikkanen, M. (2017). Interaction between photosynthetic electron transport and chloroplast sinks triggers protection and signalling important for plant productivity. *Philos. Trans. R. Soc. B. Biol. Sci.* 372:20160390. doi: 10.1098/rstb.2016.0390

Gururani, M. A., Venkatesh, J., and Tran, L.-S. P. (2015). Regulation of photosynthesis during abiotic stress-induced photoinhibition. *Mol. Plant* 8, 1304–1320. doi: 10.1016/j.molp.2015.05.005

Havir, E. A., and McHale, N. A. (1987). Biochemical and developmental characterization of multiple forms of catalase in tobacco leaves. *Plant Physiol.* 84, 450–455. doi: 10.1104/pp.84.2.450

Heath, R. L., and Packer, L. (1968). Photoperoxidation in isolated chloroplasts. I. Kinects and stoichiometry of fatty acid peroxidation. *Arch. Biochem. Biophys.* 125, 189–198. doi: 10.1016/0003-9861(68)90654-1

Hossain, M. A., Nakano, Y., and Asada, K. (1984). Monodehydroascorbate reductase in spinach chloroplasts and its participation in regeneration of ascorbate for scavenging hydrogen peroxide. *Plant Cell Physiol.* 25, 385–395.

Huang, W., Yang, Y.-J., Hu, H., and Zhang, S.-B. (2016). Moderate photoinhibition of photosystem II protects photosystem I from photodamage at chilling stress in tobacco leaves. *Front. Plant Sci.* 7:182. doi: 10.3389/fpls.2016.00182

Huang, W., Zhang, S.-B., and Cao, K.-F. (2010). The different effects of chilling stress under moderate light intensity on photosystem II compared with photosystem I and subsequent recovery in tropical tree species. *Photosynth. Res.* 103, 175–182. doi: 10.1007/s11120-010-9539-7

Inoue, K., Sakurai, H., and Hiyama, T. (1986). Photoinactivation sites of photosystem I in isolated chloroplasts. *Plant Cell Physiol.* 27, 961–968.

Ivanov, A. G., Morgan, R. M., Gray, G. R., Velitchkova, M. Y., and Huner, N. P. A. (1998). Temperature/light dependent development of selective resistance to photoinhibition of photosystem I. *FEBS Lett.* 430, 288–292. doi: 10.1016/s0014-5793(98)00681-4

Ivanov, A. G., Rosso, D., Savitch, L. V., Stachula, P., Rosembert, M., Oquist, G., et al. (2012). Implications of alternative electron sinks in increased resistance of PSII and PSI photochemistry to high light stress in cold-acclimated *Arabidopsis thaliana*. *Photosynth. Res.* 113, 191–206. doi: 10.1007/s11120-012-9769-y

Karpiński, S., Escobar, C., Kaspinska, B., Creissen, G., and Mullineaux, P. M. (1997). Photosynthetic electron transport regulates the expression of cytosolic ascorbate peroxidase genes in Arabidopsis during excess light stress. *Plant Cell* 9, 627–640. doi: 10.1105/tpc.9.4.627

Karpiński, S., Reynolds, H., Karpinska, B., Wingsle, G., Creissen, G., and Mullineaux, P. (1999). Systemic signaling and acclimation in response to excess excitation energy in Arabidopsis. *Science* 284, 654–657. doi: 10.1126/science.284.5414.654

Kato, Y., Sun, X., Zhang, L., and Sakamoto, W. (2012). Cooperative D1 degradation in the photosystem II repair mediated by chloroplastic proteases in arabidopsis. *Plant Physiol.* 159, 1428–1439. doi: 10.1104/pp.112.199042

Klughammer, C., and Schreiber, U. (1998). "Measuring P700 absorbance changes in the near infrared spectral region with a dual wavelength pulse modulation system," in *Photosynth. Mech. Eff*, ed. G. Garab (Dordrecht: Springer), 4357–4360. doi: 10.1007/978-94-011-3953-3_1008

König, K., Vaseghi, M. J., Dreyer, A., and Dietz, K. J. (2018). The significance of glutathione and ascorbate in modulating the retrograde high light response in *Arabidopsis thaliana* leaves. *Physiol. Plant* 162, 262–273. doi: 10.1111/ppl.12644

Kono, M., Noguchi, K., and Terashima, I. (2014). Roles of the cyclic electron flow around PSI (CEF-PSI) and O2-dependent alternative pathways in regulation of the photosynthetic electron flow in short-term fluctuating light in *Arabidopsis thaliana*.pdf. *Plant Cell Physiol.* 55, 990–1004. doi: 10.1093/pcp/pcu033

Kudoh, H., and Sonoike, K. (2002). Irreversible damage to photosystem I by chilling in the light: cause of the degradation of chlorophyll after returning to normal growth temperature. *Planta* 215, 541–548. doi: 10.1007/s00425-002-0790-9

Laloi, C., and Havaux, M. (2015). Key players of singlet oxygen-induced cell death in plants. *Front. Plant Sci.* 6:39. doi: 10.3389/fpls.2015.00039

Larosa, V., Meneghesso, A., La Rocca, N., Steinbeck, J., Hippler, M., and Szabò, I. (2018). Mitochondria affects photosynthetic electron transport and photosensitivity in a green alga. *Plant Physiol.* 176, 2305–2314. doi: 10.1104/pp.17.01249

Li, L., Aro, E.-M., and Millar, A. H. (2018). Mechanisms of photodamage and protein turnover in photoinhibition. *Trends Plant Sci.* 23, 667–676. doi: 10.1016/j.tplants.2018.05.004

Lima-Melo, Y., Gollan, P. J., Tikkanen, M., Silveira, J. A. G., and Aro, E.-M. (2019). Consequences of photosystem-I damage and repair on photosynthesis and carbon use in *Arabidopsis thaliana*. *Plant J.* 97, 1061–1072. doi: 10.1111/tpj.14177

López, M. A., Vicente, J., Kulasekaran, S., Vellosillo, T., Martínez, M., Irigoyen, M. L., et al. (2011). Antagonistic role of 9-lipoxygenase-derived oxylipins and ethylene in the control of oxidative stress, lipid peroxidation and plant defence. *Plant J.* 67, 447–458. doi: 10.1111/j.1365-313X.2011.04608.x

McCord, J. M. (2000). The evolution of free radicals and oxidative stress. *Am. J. Med.* 108, 652–659.

Mittler, R. (2017). ROS are good. *Trends Plant Sci.* 22, 11–19. doi: 10.1016/j.tplants.2016.08.002

Mosblech, A., Feussner, I., and Heilmann, I. (2009). Oxylipins: structurally diverse metabolites from fatty acid oxidation. *Plant Physiol. Biochem.* 47, 511–517. doi: 10.1016/j.plaphy.2008.12.011

Mueller, S., Hilbert, B., Dueckershoff, K., Roitsch, T., Krischke, M., and Mueller, M. J. (2008). General detoxification and stress responses are mediated by oxidized lipids through TGA transcription factors in Arabidopsis. *Plant Cell* 20, 768–785. doi: 10.1105/tpc.107.054809

Mullineaux, P. M., Exposito-Rodriguez, M., Laissue, P. P., and Smirnoff, N. (2018). ROS-dependent signalling pathways in plants and algae exposed to high light: comparisons with other eukaryotes. *Free Radic. Biol. Med.* 122, 52–64. doi: 10.1016/j.freeradbiomed.2018.01.033

Munekage, Y., Hojo, M., Meurer, J., Endo, T., Tasaka, M., and Shikanai, T. (2002). PGR5 is involved in cyclic electron flow around photosystem I and is essential for photoprotection in Arabidopsis. *Cell* 110, 361–371. doi: 10.1016/s0092-8674(02)00867-x

Munekage, Y. N., Genty, B., and Peltier, G. (2008). Effect of PGR5 impairment on photosynthesis and growth in *Arabidopsis thaliana*. *Plant Cell Physiol.* 49, 1688–1698. doi: 10.1093/pcp/pcn140

Munns, R. (2005). Genes and salt tolerance: bringing them together. *New Phytol.* 167, 645–663. doi: 10.1111/j.1469-8137.2005.01487.x

Nakano, Y., and Asada, K. (1981). Hydrogen peroxide is scavenged by ascorbate-specific peroxidase in spinach chloroplasts. *Plant Cell Physiol.* 22, 867–880.

Nandha, B., Finazzi, G., Joliot, P., Hald, S., and Johnson, G. N. (2007). The role of PGR5 in the redox poising of photosynthetic electron transport. *Biochim. Biophys. Acta* 1767, 1252–1259. doi: 10.1016/j.bbabio.2007.07.007

Noctor, G., Reichheld, J. P., and Foyer, C. H. (2018). ROS-related redox regulation and signaling in plants. *Semin. Cell Dev. Biol.* 80, 3–12. doi: 10.1016/j.semcdb.2017.07.013

Ogawa, K., Kanematsu, S., and Asada, K. (1997). Generation of superoxide anion and localization of CuZn-superoxide dismutase in the vascular tissue of spinach hypocotyls: their association with lignification. *Plant Cell Physiol.* 38, 1118–1126. doi: 10.1093/oxfordjournals.pcp.a029096

Porta, H., Figueroa-Balderas, R. E., and Rocha-Sosa, M. (2008). Wounding and pathogen infection induce a chloroplast-targeted lipoxygenase in the common bean (*Phaseolus vulgaris* L.). *Planta* 227, 363–373. doi: 10.1007/s00425-007-0623-y

Ramel, F., Birtic, S., Ginies, C., Soubigou-Taconnat, L., Triantaphylidès, C., and Havaux, M. (2012). Carotenoid oxidation products are stress signals that mediate gene responses to singlet oxygen in plants. *Proc. Natl. Acad. Sci. U.S.A.* 109, 5535–5540. doi: 10.1073/pnas.1115982109

Sarde, S. J., Kumar, A., Remme, R. N., and Dicke, M. (2018). Genome-wide identification, classification and expression of lipoxygenase gene family in pepper. *Plant Mol. Biol.* 98, 375–387. doi: 10.1007/s11103-018-0785-y

Satoh, M., Tokaji, Y., Nagano, A. J., Hara-Nishimura, I., Hayashi, M., Nishimura, M., et al. (2014). Arabidopsis mutants affecting oxylipin signaling in photo-oxidative stress responses. *Plant Physiol. Biochem.* 81, 90–95. doi: 10.1016/j.plaphy.2013.11.023

Scheller, H. V., and Haldrup, A. (2005). Photoinhibition of photosystem I. *Planta* 221, 5–8.

Schreiber, U., Bilger, W., and Neubauer, C. (1995). "Chlorophyll fluorescence as a nonintrusive indicator for rapid assessment of in vivo photosynthesis," in *Ecophysiology of Photosynthesis*, 1st Edn, eds E.-D. Schulze and M. M. Caldwell (Berlin: Springer-Verlag), 49–70. doi: 10.1007/978-3-642-79354-7_3

Sejima, T., Takagi, D., Fukayama, H., Makino, A., and Miyake, C. (2014). Repetitive short-pulse light mainly inactivates photosystem I in sunflower leaves. *Plant Cell Physiol.* 55, 1184–1193. doi: 10.1093/pcp/pcu061

Sharma, P., Jha, A. B., Dubey, R. S., and Pessarakli, M. (2012). Reactive oxygen species, oxidative damage, and antioxidative defense mechanism in plants under stressful conditions. *J. Bot.* 2012, 1–26. doi: 10.1016/j.plaphy.2016.05.038

Simkin, A. J., McAusland, L., Lawson, T., and Raines, C. A. (2017). Over-expression of the RieskeFeS protein increases electron transport rates and biomass yield. *Plant Physiol.* 175, 134–145. doi: 10.1104/pp.17.00622

Sonoike, K. (1995). Selective photoinhibition of photosystem I in isolated thylakoid membranes from cucumber and spinach. *Plant Cell Physiol.* 36, 825–830. doi: 10.1093/oxfordjournals.pcp.a078827

Sonoike, K. (2011). Photoinhibition of photosystem I. *Physiol. Plant* 142, 56–64. doi: 10.1111/j.1399-3054.2010.01437.x

Sonoike, K., and Terashima, I. (1994). Mechanism of photosystem-I photoinhibition in leaves of *Cucumis sativus* L. *Planta* 194, 287–293. doi: 10.1007/bf01101690

Souza, P. V. L., Lima-Melo, Y., Carvalho, F. E., Reichheld, J.-P., Fernie, A. R., Silveira, J. A. G., et al. (2018). Function and compensatory mechanisms among the components of the chloroplastic redox network. *Crit. Rev. Plant Sci.* 38, 1–28. doi: 10.1080/07352689.2018.1528409

Suorsa, M., Järvi, S., Grieco, M., Nurmi, M., Pietrzykowska, M., Rantala, M., et al. (2012). PROTON GRADIENT REGULATION5 is essential for proper acclimation of Arabidopsis photosystem I to naturally and artificially fluctuating light conditions. *Plant Cell* 24, 2934–2948. doi: 10.1105/tpc.112.097162

Takagi, D., Takumi, S., Hashiguchi, M., Sejima, T., and Miyake, C. (2016). Superoxide and singlet oxygen produced within the thylakoid membranes both cause photosystem I photoinhibition. *Plant Physiol.* 171, 1626–1634. doi: 10.1104/pp.16.00246

Takahashi, S., and Murata, N. (2008). How do environmental stresses accelerate photoinhibition? *Trends Plant Sci.* 13, 178–182. doi: 10.1016/j.tplants.2008.01.005

Terashima, I., Funayama, S., and Sonoike, K. (1994). The site of photoinhibition in leaves of *Cucumis sativus* L. At low temperatures is photosystem I, not photosystem II. *Planta* 193, 300–306.

Thordal-Christensen, H., Zhang, Z., Wei, Y., and Collinge, D. B. (1997). Subcellular localization of H2O2 in plants. H2O2 accumulation in papillae and hypersensitive response during the barley-powdery mildew interaction. *Plant J.* 11, 1187–1194. doi: 10.1046/j.1365-313x.1997.11061187.x

Tikkanen, M., and Aro, E.-M. (2014). Integrative regulatory network of plant thylakoid energy transduction. *Trends Plant Sci.* 19, 10–17. doi: 10.1016/j.tplants.2013.09.003

Tikkanen, M., Grieco, M., Nurmi, M., Rantala, M., Suorsa, M., and Aro, E.-M. (2012). Regulation of the photosynthetic apparatus under fluctuating growth light. *Philos. Trans. R. Soc. B Biol. Sci.* 367, 3486–3493. doi: 10.1098/rstb.2012.0067

Tikkanen, M., Mekala, N. R., and Aro, E.-M. (2014). Photosystem II photoinhibition-repair cycle protects photosystem I from irreversible damage. *Biochim. Biophys. Acta* 1837, 210–215. doi: 10.1016/j.bbabio.2013.10.001

Tiwari, A., Mamedov, F., Grieco, M., Suorsa, M., Jajoo, A., Styring, S., et al. (2016). Photodamage of iron-sulphur clusters in photosystem I induces non-photochemical energy dissipation. *Nat. Plants* 2:16035. doi: 10.1038/nplants.2016.35

Tjus, S. E., Møller, B. L., and Scheller, H. V. (1998). Photosystem I is an early target of photoinhibition in barley illuminated at chilling temperatures. *Plant Physiol.* 116, 755–764. doi: 10.1104/pp.116.2.755

Triantaphylidès, C., Krischke, M., Hoeberichts, F. A., Ksas, B., Gresser, G., Havaux, M., et al. (2008). Singlet oxygen is the major reactive oxygen species involved in photooxidative damage to plants. *Plant Physiol.* 148, 960–968. doi: 10.1104/pp.108.125690

Wasternack, C., and Hause, B. (2013). Jasmonates: biosynthesis, perception, signal transduction and action in plant stress response, growth and development. An update to the 2007 review in Annals of Botany. *Ann. Bot.* 111, 1021–1058. doi: 10.1093/aob/mct067

Yamamoto, H., and Shikanai, T. (2019). PGR5-dependent cyclic electron flow protects photosystem I under fluctuating light at donor and acceptor sides. *Plant Physiol.* 179, 588–600. doi: 10.1104/pp.18.01343

Yamori, W. (2016). Photosynthetic response to fluctuating environments and photoprotective strategies under abiotic stress. *J. Plant Res.* 129, 379–395. doi: 10.1007/s10265-016-0816-1

Zhang, S., and Scheller, H. V. (2004). Photoinhibition of photosystem I at chilling temperature and subsequent recovery in *Arabidopsis thaliana*. *Plant Cell Physiol.* 45, 1595–1602. doi: 10.1093/pcp/pch180

Zhou, M., Diwu, Z., Panchuk-Voloshina, N., and Haugland, R. P. (1997). A stable nonfluorescent derivative of resorufin for the fluorometric determination of trace hydrogen peroxide: applications in detecting the activity of phagocyte

NADPH oxidase and other oxidases. *Anal. Biochem.* 253, 162–168. doi: 10.1006/abio.1997.2391

Zivcak, M., Brestic, M., Kunderlikova, K., Olsovska, K., and Allakhverdiev, S. I. (2015a). Effect of photosystem I inactivation on chlorophyll a fluorescence induction in wheat leaves: does activity of photosystem I play any role in OJIP rise? *J. Photochem. Photobiol. B Biol.* 152, 318–324. doi: 10.1016/j.jphotobiol.2015.08.024

Zivcak, M., Brestic, M., Kunderlikova, K., Sytar, O., and Allakhverdiev, S. I. (2015b). Repetitive light pulse-induced photoinhibition of photosystem I severely affects CO2 assimilation and photoprotection in wheat leaves. *Photosynth. Res.* 126, 449–463. doi: 10.1007/s11120-015-0121-1

**Conflict of Interest Statement:** The authors declare that the research was conducted in the absence of any commercial or financial relationships that could be construed as a potential conflict of interest.

frontiers in Plant Science

ORIGINAL RESEARCH
published: 14 August 2019
doi: 10.3389/fpls.2019.01026

# Distinct Morphological, Physiological, and Biochemical Responses to Light Quality in Barley Leaves and Roots

*Karel Klem[1]*, Albert Gargallo-Garriga[1,2], Wutthida Rattanapichai[3], Michal Oravec[1], Petr Holub[1], Barbora Veselá[1], Jordi Sardans[1,2,4], Josep Peñuelas[1,2,4] and Otmar Urban[1]*

[1] Global Change Research Institute, Czech Academy of Sciences, Brno, Czechia, [2] Centro de Investigación Ecológica y Aplicaciones Forestales (CREAF), Barcelona, Spain, [3] Department of Soil Science, Kasetsart University, Bangkok, Thailand, [4] Global Ecology Unit CREAF-CSIC-UAB, Barcelona, Spain

Light quality modulates plant growth, development, physiology, and metabolism through a series of photoreceptors perceiving light signal and related signaling pathways. Although the partial mechanisms of the responses to light quality are well understood, how plants orchestrate these impacts on the levels of above- and below-ground tissues and molecular, physiological, and morphological processes remains unclear. However, the re-allocation of plant resources can substantially adjust plant tolerance to stress conditions such as reduced water availability. In this study, we investigated in two spring barley genotypes the effect of ultraviolet-A (UV-A), blue, red, and far-red light on morphological, physiological, and metabolic responses in leaves and roots. The plants were grown in growth units where the root system develops on black filter paper, placed in growth chambers. While the growth of above-ground biomass and photosynthetic performance were enhanced mainly by the combined action of red, blue, far-red, and UV-A light, the root growth was stimulated particularly by supplementary far-red light to red light. Exposure of plants to the full light spectrum also stimulates the accumulation of numerous compounds related to stress tolerance such as proline, secondary metabolites with antioxidative functions or jasmonic acid. On the other hand, full light spectrum reduces the accumulation of abscisic acid, which is closely associated with stress responses. Addition of blue light induced accumulation of γ-aminobutyric acid (GABA), sorgolactone, or several secondary metabolites. Because these compounds play important roles as osmolytes, antioxidants, UV screening compounds, or growth regulators, the importance of light quality in stress tolerance is unequivocal.

**Keywords: light quality, photosynthesis, morphology, root system architecture, metabolomics**

OPEN ACCESS

***Edited by:***
*Tibor Janda,*
*Centre for Agricultural Research (MTA), Hungary*

***Reviewed by:***
*Péter Poór,*
*University of Szeged, Hungary*
*Muhammad Abass Ahanger,*
*Northwest A&F University, China*

****Correspondence:***
*Karel Klem*
*klem.k@czechglobe.cz*

***Specialty section:***
*This article was submitted to Plant Abiotic Stress, a section of the journal Frontiers in Plant Science*

***Received:*** *06 May 2019*
***Accepted:*** *23 July 2019*
***Published:*** *14 August 2019*

***Citation:***
*Klem K, Gargallo-Garriga A, Rattanapichai W, Oravec M, Holub P, Veselá B, Sardans J, Peñuelas J and Urban O (2019) Distinct Morphological, Physiological, and Biochemical Responses to Light Quality in Barley Leaves and Roots. Front. Plant Sci. 10:1026. doi: 10.3389/fpls.2019.01026*

## INTRODUCTION

Plants growing under natural conditions are exposed to light that varies in intensity, duration, and spectral quality due to changes in canopy filtering, cloud cover, and diurnal and seasonal variations. In addition, it can be challenging to determine the optimal light spectrum and intensity when cultivating plants under artificial conditions, such as in greenhouses or growth chambers (Ouzounis et al., 2015). Light-mediated photosynthesis is the predominant source of energy for plants, but

light also provides important sensory signals for plants because it can promote acclimation to different environmental conditions, modulate growth and development, alter physiological functions, and regulate biochemical pathways (Kami et al., 2010).

Research during recent decades has identified three major groups of sensory photoreceptors in plants (Chen et al., 2004): the phytochromes (PHYs), which absorb light strongly in the red (600 to 700 nm) and far-red (700 to 800 nm) regions (Casal et al., 1998); the cryptochromes (CRYs), phototropins (PHOTs), and Zeitlupe family proteins, which absorb light strongly in the blue (400 to 500 nm) and ultraviolet-A (UV-A; 315 to 400 nm) regions (Galvão and Fankhauser, 2015); and UVB-RESISTANCE locus 8 (UVR8), which absorbs light strongly in the UV-B (280 to 315 nm) region (Tilbrook et al., 2013). In contrast to the many photobiology studies on above-ground plant organs, very few studies have investigated the role of light spectral quality on roots (Gundel et al., 2014). However, there is evidence that the red:far-red (R:FR) ratio mediates plant–plant interactions, in that it allows a plant to detect neighboring plants, and promotes rapid root growth and escape from the main zone of competition (Ballaré, 2009). Light spectral quality is also an important signal that allows plants to acclimate to changing environmental conditions, particularly abiotic stressors (Catalá et al., 2011). Light-induced metabolic reprogramming can lead to accumulation of anti-stress compounds, such as osmolytes, antioxidants, and stress-responsive proteins (Obata and Fernie, 2012).

Plant growth largely depends on the availability of carbohydrates synthesized during photosynthesis, and this is limited by numerous environmental factors in addition to light, such as temperature, water availability, nutrient availability, and pathogens (Kangasjärvi et al., 2012). The sugar-mediated regulation of plant growth interacts with multiple phytohormones (Das et al., 2012) and the circadian clock (Lastdrager et al., 2014), and both are connected to light signaling (de Lucas and Prat, 2014). Thus, it is likely that crosstalk between sugar production and light signaling also regulates plant growth. Monochromatic red light stimulates the accumulation of glucose and fructose, while combined red and blue light significantly enhances the accumulation of sucrose and starch (Li et al., 2017). Such changes are mainly associated with activities of invertases and explain also the effects on photosynthetic performance and plant morphology. Sugar, and particularly sucrose allocation, plays a crucial role in long-distance communications between shoot and root and coupling of carbon and nitrogen metabolisms involving cytokinin, auxin, and small peptide signals (Wang and Ruan, 2016). Since the phosphorylated hexoses are required in different metabolic processes and plant development, hexose-phosphorylating enzymes (mainly hexokinase) are essential in sugar sensing and orchestration of photosynthetic carbon fixation and water and nutrient uptake (Granot et al., 2014). Light intensity and daytime have a major effect on sugar transport in the phloem, but it was significantly affected also by light quality at the medium photosynthetic rates (Lanoue et al., 2018). Sugar-mediated regulation of plant growth and photosynthesis can be thus attributed to the effects of both light intensity and quality.

Besides the effects of light on primary metabolism, its spectral quality also influences the biosynthesis of secondary metabolites (particularly carotenoids, phenolic compounds, and anthocyanins) that function as antioxidants or UV screening compounds (Bian et al., 2015). UV and blue light (perceived by UVR8 and CRYs) affect the biosynthesis of numerous secondary metabolites including phenolic acids (e.g., chlorogenic acid, *p*-coumaric acid, caffeic acid), flavonoids (e.g., kaempferol, quercetin, rutin, anthocyanin), and carotenoids (lutein, violaxanthin, zeaxanthin, neoxanthin, β-carotene; reviewed by Ouzounis et al., 2015). These compounds, in turn, enhance the photoprotective capacity of plants against high radiation stress (Klem et al., 2015). Although the transition between regulatory effect and stress response to light intensity and quality is gradual (Robson et al., 2015), particularly at high intensities of UV-B radiation, the stress responses involving DNA damage, lipid peroxidation, photoinhibition, and/or growth inhibition often occur in plants (Hideg et al., 2013).

Based on a review of the literature, Gundel et al. (2014) suggested that light spectral quality considerably affects root growth, morphology, and functional interactions with soil microorganisms. Light spectral quality can thus play an important ecological role by altering root–shoot interactions. For instance, Sadras et al. (1989) showed that the roots of crops grown at high density penetrate deeper soil layers than crops grown at low density because of differences in the above-ground R:FR ratio. Light spectral quality can therefore greatly impact the efficiency of the uptake of resources (water and nutrients) from the soil and affect the way the plants adjust to competition for soil resources. However, a meta-analysis by Poorter et al. (2012) found that the response of roots to the R:FR ratio depended on plant ontogeny (Green-Tracewicz et al., 2012), intensity of light (McLaren and Smith, 1978), proximity of other plants (Murphy and Dudley, 2009), and nutrient availability (Aphalo and Lehto, 2001). Gundel et al. (2014) proposed that the R:FR ratio affects root system architecture (RSA) by altering the levels of the plant hormone auxin. Auxin is a well-known regulator of root development (Blilou et al., 2005) and architecture (Péret et al., 2009) and can also induce directional root growth away from potential competitors.

The blue and UV light photoreceptors (CRYs, PHOTs, and UVR8) also alter signaling pathways connected to the phytohormone-mediated regulation of growth, development, physiological functions, and biochemical pathways, so it seems likely that they also affect RSA (Gelderen van et al., 2018a). Photoreceptors have important roles in plant resource management because they control the allocation of resources needed for growth and the transition of metabolism between growth and stress-coping states based on light availability. Thus, crop scientists have a renewed interest in photoreceptors because of their effect on root–shoot interactions and the possible implications of these responses to economically important crops.

Besides the direct effect of light intensity and quality on balancing plant growth and defense mechanisms, the circadian clock and redox rhythm serve also as an important regulatory mechanism. Such mechanisms involve especially biosynthesis of the major antioxidant (glutathione) and plant defense hormones

[jasmonic acid (JA) and salicylic acid], thus adjusting plant immunity (Karapetyan and Dong, 2018).

The main aim of this study was to test the hypothesis that light spectral quality changes the allocation of plant biomass between above-ground parts and roots, alters the RSA, affects interactions among neighboring plants, and impacts the ability of plants to cope with reduced availability of water or nutrients. The effect of spectral quality was tested on two barley varieties. Barke variety is considered as highly sensitive to oxidative stress, while the variety Bojos is commonly grown in Central European conditions without symptoms of oxidative stress damage. We also hypothesized that light spectral quality affects the accumulation and allocation of metabolites involved in stress tolerance, such as plant hormones, antioxidants, and osmolytes, and thereby modulates tolerances to different stressors.

# MATERIAL AND METHODS

## Plant Material and Experimental Design

Seeds of spring barley (*Hordeum vulgare*) varieties Barke (sensitive to oxidative stress; Klem et al., 2012) and Bojos (tolerant to oxidative stress) were provided by the barley gene bank of the Agricultural Research Institute Kroměříž Ltd., Czech Republic. Seeds were germinated on moistened germination paper for 48 h at 26°C in the dark. Germinating seeds were then transplanted into the growth unit, in which the roots grew on black filter paper that was between two black plastic sheets, and a micro-irrigation system recirculated a nutrient solution through the roots (**Figure S1**; for details, see Rattanapichai and Klem, 2016). The nutrient solution was Hoagland's No. 2 basal salt mixture (Sigma Aldrich Chemie, Steinheim, DE; concentration: 1.6 g $L^{-1}$, pH range: 4.5 to 5.2). The solution was replaced every 7 days throughout the 26-day experiments.

The growth units were placed in five large growth chambers (FS-SI-3400, PSI, Drásov, CZ), which allowed continuous regulation of light intensity in the red, blue, far-red, and UV-A spectral regions. Light-emitting diodes (LEDs) were the source for radiation in the red (R; maximum emission: 640 nm), blue (B; maximum emission: 450 nm), and far-red (FR; maximum emission: 740 nm) regions, and fluorescent lamps (LT 30W T8/010UV, Narva, DE) were the source for UV-A radiation (maximum emission: 370 nm). The following five light regimens were used: **R**, R light only; **R-B**, R and B lights at 1:1 ratio of photon flux density; **R-FR**, R and FR lights; **R-UVA**, R and UV-A lights; and **R-B-FR-UVA**, R and B radiation in a 1:1 ratio of photon flux density with additional FR and UV-A light. The intensity of photosynthetically active radiation (PAR, 400 to 700 nm) was the same for all treatments (130 μmol photons $m^{-2}$ $s^{-1}$). The intensity of UV-A was set to 4 W $m^{-2}$, and the intensity of FR light was adjusted to provide a 0.6 ratio of R:FR. Each light regimen and barley variety had four replicates (four separate growth units), which were randomized within each growth chamber. The growth units and plants were transferred between growth chambers while maintaining the same light regimen, and newly randomized every 7 days to avoid possible artifacts from individual growth chambers. All plants were grown under a 12/12 h day/night regimen, with a day/night temperature of 25/20°C and a day/night relative humidity of 60%/80%. Photon flux density in the range of 400–700 nm (PAR) was measured using light meter Li-250 (LI-COR Biosciences, Lincoln, NE, US) with quantum sensor Li-190 (LI-COR Biosciences). The emission spectra of LEDs and fluorescent lamps were measured using spectroradiometer AvaSpec-2048-USB2 (Avantes BV, Apeldoorn, NL), with grating and a measurement range of 200–1100 nm. R:FR ratio was calculated by integration photon flux density between 655–665 nm UV/VIS/NIR (R) and 725–735 nm (FR).

## Root and Shoot Morphology

Roots and shoots were scanned with a large area scanner (LA2400, Regent Instruments, Quebec, CA) at a resolution of 300 pixels per inch. Total (projected) leaf area (TLA) and leaf length were then measured using ImageJ software. For subsequent statistical analyses, TLA and length of the youngest completely developed leaf (4$^{th}$ leaf) were determined because these were most sensitive to light regimens.

The RSA parameters were evaluated using WinRHIZO software (Regent Instruments). The parameters measured were: total root length (TRL), total seminal root length (TSL), total lateral root length (TLL), total root surface area (TSA), and average branching angle (BA). Plant material was subsequently used for metabolomic analyses.

## Plant Physiology

All physiological measurements were conducted between 10:00 and 14:00 Central European Time (CET). Basic photosynthetic parameters were measured on the 4$^{th}$ leaf using a Li-6400 gas-exchange system (LI-COR Biosciences) at a $CO_2$ concentration of 400 μmol $CO_2$ $mol^{-1}$. During these measurements, leaf temperature (25°C) and humidity (60%) were kept constant in the growth chamber. Light-saturated rates of the following photosynthetic parameters were measured at a photosynthetic photon flux density of 1200 μmol photons $m^{-2}$ $s^{-1}$ after 3 to 5 min of acclimation: light-saturated $CO_2$ assimilation rate, $A_{max}$; light-saturated stomatal conductance, $G_{Smax}$; and light-saturated transpiration rate, Tr.

Chlorophyll *a* fluorescence (Chl-F) parameters were estimated on the light-adapted 4$^{th}$ leaves using a pulse amplitude modulated fluorometer (PAM 2500, H. Walz, Effeltrich, DE). Before these measurements, the leaves were acclimated to a photosynthetic photon flux density of 130 μmol photons $m^{-2}$ $s^{-1}$ for 3 min, and the same photon flux density of actinic light was used for the measurement. The Chl-F signal at the red band (near 690 nm) was measured using short flashes (10 ms pulses, intensity approximately 0.003 μmol photons $m^{-2}$ $s^{-1}$) that were 800 ms apart ($F_S$). Maximum Chl-F ($F_M'$) was recorded during 1 s application of a saturating light pulse (approx. 5,000 μmol photons $m^{-2}$ $s^{-1}$). Minimum Chl-F in the light-adapted state ($F_0'$) was estimated after a saturating pulse when the actinic light was off, and the FR light was on for 5 s. The actual quantum yield of photosystem (PS) II photochemistry [$\Phi_{PSII} = (F_M' - F_S)/F_M'$] and thermal energy dissipation [$D = 1 - (F_M' - F_0')/F_M'$] were calculated according to Demmig-Adams et al. (1996).

Chlorophyll and epidermal flavonols were estimated indirectly as chlorophyll and flavonol indices, based on light transmittance

and UV screening of Chl-F (Dualex Flav, Force A, Orsay, FR). Two measurements in the central part of the 4th leaf were performed.

## Metabolomic Analyses

The upper three leaves (2nd–4th leaf) and roots from each replicate were sampled between 11:00 and 14:00 (CET) and immediately frozen in liquid nitrogen for metabolomic analyses. The samples were homogenized using a mortar and pestle with liquid nitrogen and then extracted using methanol:chloroform:$H_2O$ solution (1:2:2). An aliquot of the upper (polar) phase was used to analyze metabolites using an UltiMate 3000 high-performance liquid chromatograph (HPLC) (Thermo Fisher Scientific, US/Dionex RSLC, Dionex, US) coupled with an LTQ Orbitrap XL high resolution mass spectrometer (HRMS) (Orbitrap, Thermo Fisher Scientific, Waltham, MA, US) that was equipped with a heated electrospray ionization source. All samples were analyzed in the positive and negative polarity of Orbitrap, operated in full-scan mode over a range of m/z 50 to 1,000 (positive mode) and 65 to 1,000 (negative mode).

A Hypersil Gold column (C18; 150 mm × 2.1 mm, 3 μm; Thermo Fisher Scientific, US) was used for chromatographic separation. The flow rate of the mobile phase was 0.3 ml $min^{-1}$, and the column temperature was 30°C. The mobile phase consisted of A) acetonitrile and B) water with 0.1% acetic acid. Both mobile phases (A and B) were filtered and degassed for 10 min in an ultrasonic bath before use. Gradient elution chromatography was performed starting with 10% A and 90% B for 5 min. From 5 to 20 min, the proportion of A increased steadily to 90% as B declined to 10%, and this condition was maintained for 5 min. Then, the system was equilibrated to the initial condition (10% A and 90% B) over 5 min. The absorbances at 254, 272, 274, and 331 nm were monitored. Acetonitrile hypergrade for liquid chromatography - mass spectrometry (LC-MS) LiChrosolvR was from Merck KgaA (Darmstadt, DE), acetic acid was from Sigma Aldrich Chemie, and the Purelab Classic (ELGA LabWater, High Wycombe, Bucks, UK) was used to generate high-purity water for preparation of the aqueous mobile phase.

First, all metabolites were identified using a standard library (>200 compounds) and confirmed by mass, retention time (RT), isotopic pattern, and ring double-bon+d parameters. Then, identifications were confirmed by comparing chromatogram peaks with the KEGG database (Kanehisa and Goto, 2000) using a built-in M/Z MINE utility with a 5 ppm threshold. The third approach of metabolite identification used the MASSBANK databases (Horai et al., 2010), with searches for each mass spectra (MS) and tandem mass spectra (MS/MS). We tentatively assigned metabolites to molecular ions and exact masses corresponding to metabolites in these databases. Data, including detailed interpretations of the MS/MS spectra that supported our tentative identifications of masses, are referred to as not positively identified throughout the manuscript. The raw data from the HPLC-HRMS system were processed and compared using the XCMS processing platform for peak detection and matching (Smith et al., 2006).

## Statistical and Bioinformatic Analyses

Morphological and physiological data were analyzed using a two-way fixed-effect analysis of variance (ANOVA) model using Statistica 12 software (StatSoft, Tulsa, US). Tukey's *post hoc* test ($p = 0.05$) was used to identify significant differences between the means.

The peak area corresponding to each metabolite was normalized based on the total peak area in the sample. Neutral masses obtained in positive and negative modes were evaluated to avoid duplicates (same RT and neutral mass in different modes) and to retain the greatest number and largest peaks. The differences of the metabolomes of each barley variety that received different light regimens were identified by a permutational analysis of variance (PERMANOVA) (Anderson et al., 2008) of the HPLC–HRMS data for each replication using Euclidean distances, in which light regimen and variety were the fixed factors, and there were 2000 permutations. We also used principal component analysis (PCA) to determine the relationships of light regimen, barley variety, and root and shot metabolites most responsible for these differences between different levels of experimental factors. The PCA was performed using R v2.12 Core functions.

# RESULTS

## Leaf Area and Length

The Barke variety generally had a greater TLA than the Bojos variety by 23%, but this difference was only significant for the R-UVA regimen (**Figure 1A**). The R-B, R-FR, and R-UVA regimens led to greater TLA than the R regimen (by 29%, 40%, and 13%, respectively), but these differences were not statistically significant for the R-B and R-UVA regimens. Relative to the R regimen, the R-B-UVA-FR regimen significantly increased TLA in both varieties (by 54%), but the R-FR regimen significantly increased the TLA only in the Bojos variety. Generally, the R-B-UVA-FR regimen led to the greatest TLA. The length of the 4th leaf was similar for the different light regimens, and there were no differences between varieties (**Figure 1B**). Relative to the R regimen, the R-FR and R-B-FR-UVA regimens led to significantly greater length of the 4th leaf in both varieties (by 25% and 30%, respectively). The length of the 4th leaf was also significantly greater under the R-B regimen than under the R regimen in the Bojos variety (by 26%).

## Root System Architecture

Similar to the TLA results, TSA, TRL, and lengths of the seminal and lateral roots (TSL and TLL) were greater in the Barke variety than the Bojos variety under most light regimens (by 42%, 32%, 41%, and 26%, respectively; **Figures 2A**, **B**, **C**, **D**); however, these varieties only had statistically significant differences in TSA, TRL, and TSL for the R-FR regimen. Relative to the R regimen, the R-FR regimen significantly increased TRL (by 217%), TSA (by 225%), TSL (by 206%), and TLL (by 222%) in both varieties, but this regimen significantly decreased the BA in the Barke variety (by 21%) (**Figure 2E**). Also, relative to the R regimen, the R-UVA and R-B-UVA-FR regimens substantially increased TRL (by 65% and 59%, respectively), TSA (by 135% and 81%, respectively), and TSL (by 157% and 104%, respectively) in the Barke variety, although the effects were statistically insignificant in the Bojos variety.

The TSA : TLA ratio was significantly greater under the R-FR (by 136%) and R-UVA (by 73%) regimens than the R regimen.

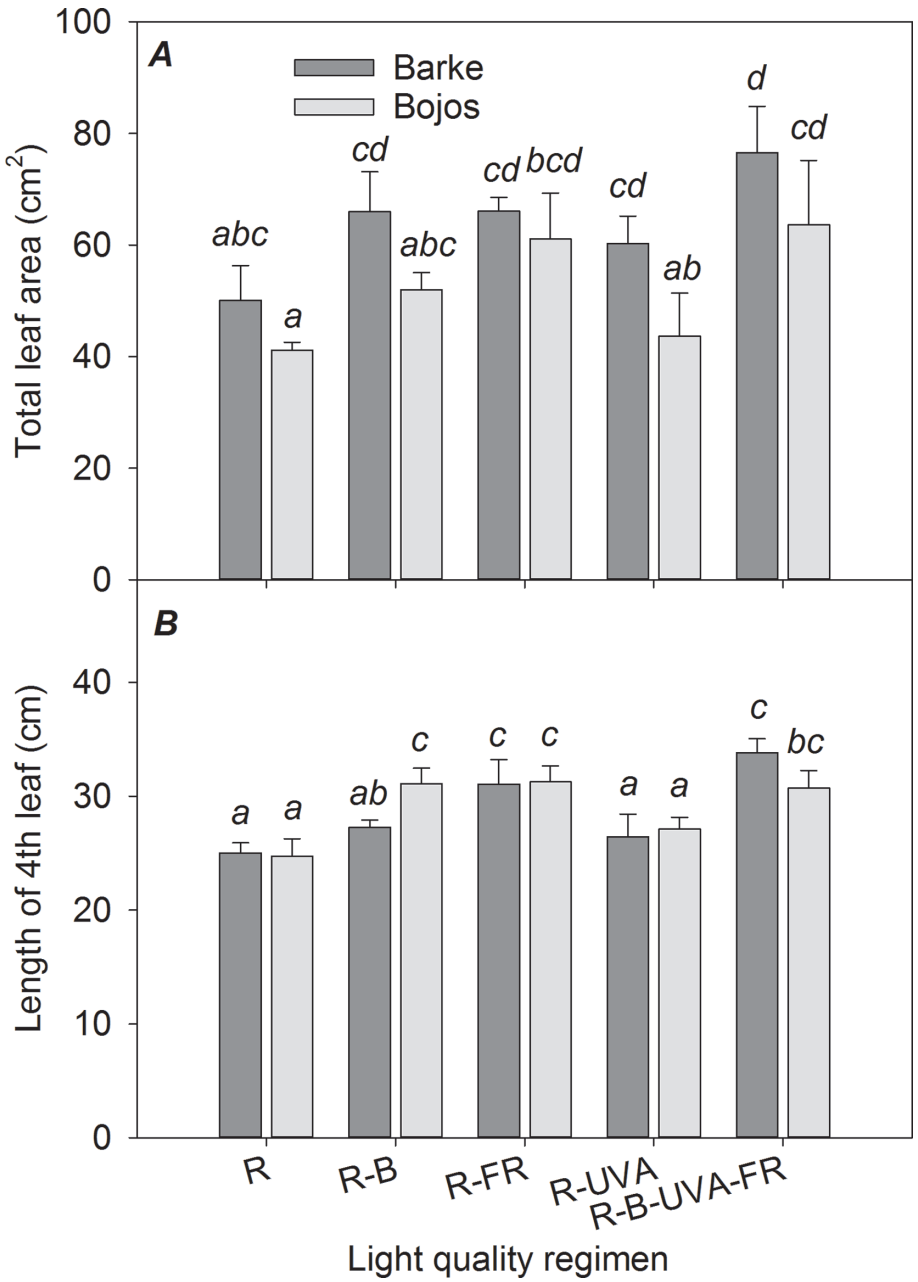


**FIGURE 1 |** Effect of 26 days exposure to different light regimens on total leaf area per plant **(A)** and length of the last completely developed (4th) leaf **(B)** of spring barley varieties Barke (dark grey) and Bojos (light grey). Here and in subsequent figures: R, only red radiation; R-B, red and blue radiation (1:1 ratio of photon flux density); R-FR, red and far-red radiation; R-UVA, R and UV-A radiation; R-B-FR-UVA, red and blue radiation (1:1 ratio of photon flux density) with far-red and UV-A radiation. All treatments used a photosynthetic photon flux density of 130 µmol $m^{-2}$ $s^{-1}$. Column height indicates mean, vertical bars indicate standard deviations ($n$ = 4), and different letters indicate significant differences ($p \leq 0.05$) based on Tukey's ANOVA post hoc test.

The effect of the R-FR regimen on this ratio was only significantly greater that of the R-UVA in the Barke variety (**Figure 2F**).

## Chlorophyll and Epidermal Flavonols

The chlorophyll index (**Figure 3A**) was greater under the R-B regimen than the R regimen in both varieties (by 35%). Furthermore, relative to the R regimen, the R-UVA regimen led to a greater chlorophyll index in the Barke variety (by 47%), and the R-B-UVA-FR regimen led to a greater chlorophyll index in the Bojos variety (by 28%). The light regimen had a stronger effect on the flavonol index (**Figure 3B**) in the Barke variety than the Bojos variety. Relative to the R regimen, the flavonol index was only greater in the Bojos variety under the R-B-UVA-FR regimen (by

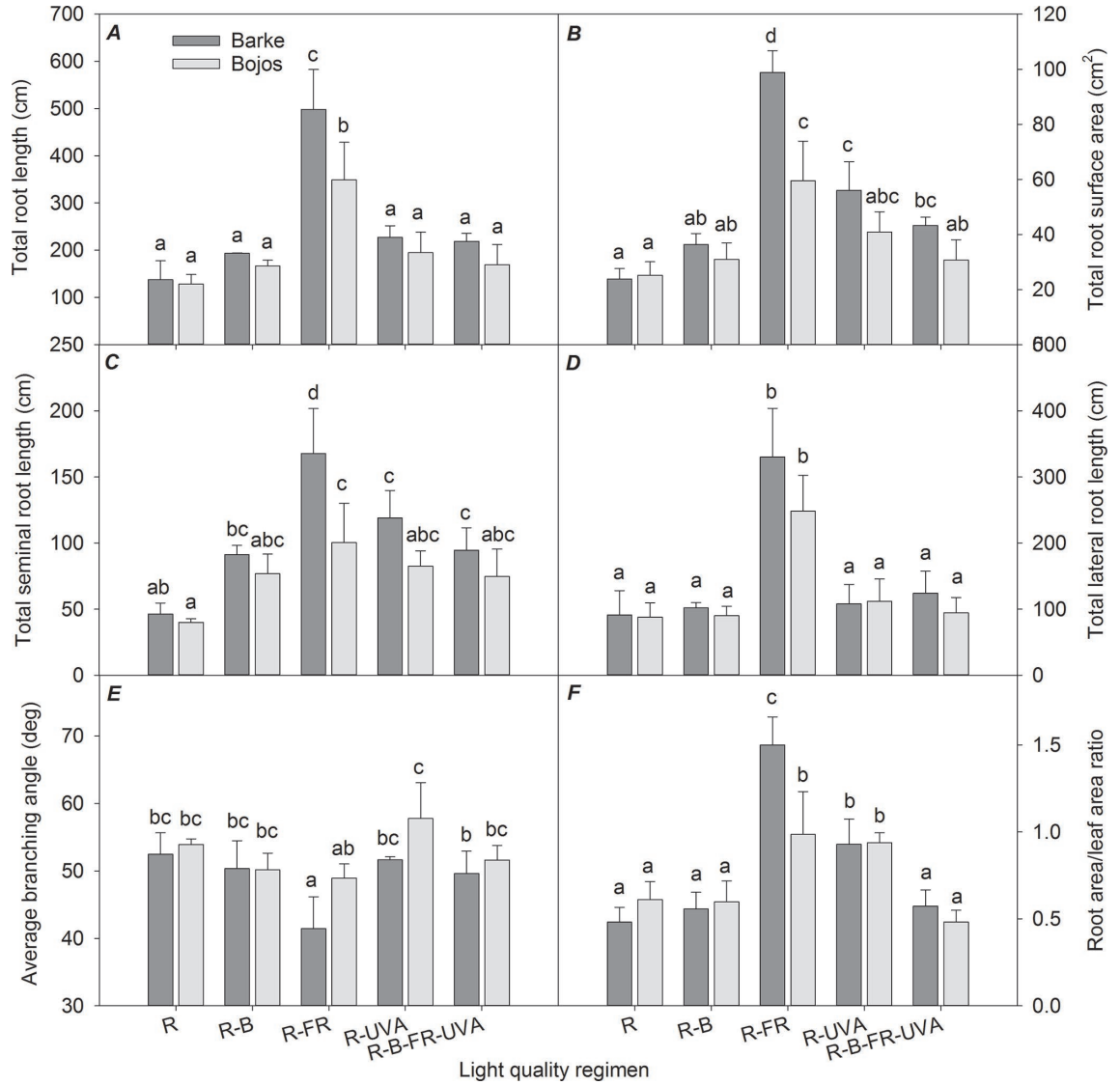


**FIGURE 2 |** Effect of 26 days exposure to different light regimens on total root length **(A)**, total root surface area **(B)**, total seminal root length **(C)**, total lateral root length **(D)**, average branching angle **(E)**, and ratio of total root area:total leaf area **(F)** of spring barley varieties Barke (dark grey) and Bojos (light grey). Additional details are in the **Figure 1** legend.

51%); the R-B-UVA-FR, R-UVA, and R-B regimens increased the flavonol indexes in the Barke variety (by 110%, 58%, and 44%, respectively). Relative to the R regimen, the R-B-UVA-FR regimen led to the greatest increase of the flavonol index.

## Photosynthetic Parameters

The actual quantum yield of PSII photochemistry ($F_{PSII}$) was significantly greater in the Barke variety under the R-UVA (by 94%), R-B (by 145%), and R-B-UVA-FR (by 231%) regimens relative to the R regimen (**Figure 4A**). The results were similar but less pronounced in the Bojos variety (by 39%, 44%, and 85%, respectively); the only significant increase in this variety was under the R-B-UVA-FR regimen. The effects of both light regimens on non-photochemical energy dissipation were generally small and statistically insignificant in both varieties (**Figure 4B**).

The light-saturated rates of $CO_2$ assimilation ($A_{max}$), transpiration ($Tr_{max}$), and stomatal conductance ($G_{Smax}$) were similar to the $F_{PSII}$ results (**Figures 5A**, **B**, **C**). In both varieties, these parameters were significantly increased under the R-B (by 151%, 65%, and 118%, respectively), R-UVA (by 106%, 52%, and 73%, respectively), and R-B-UVA-FR (by 157%, 68%, and 124%, respectively) regimens relative to the R regimen. In addition, the R-FR regimen significantly increased the $A_{max}$ and $G_{Smax}$ in the Barke variety (by 77% and 48%, respectively). Water use efficiency (ratio of $A_{max}$ and $Tr_{max}$) was significantly less under the R regimen than under the other four regimens (the regimens with

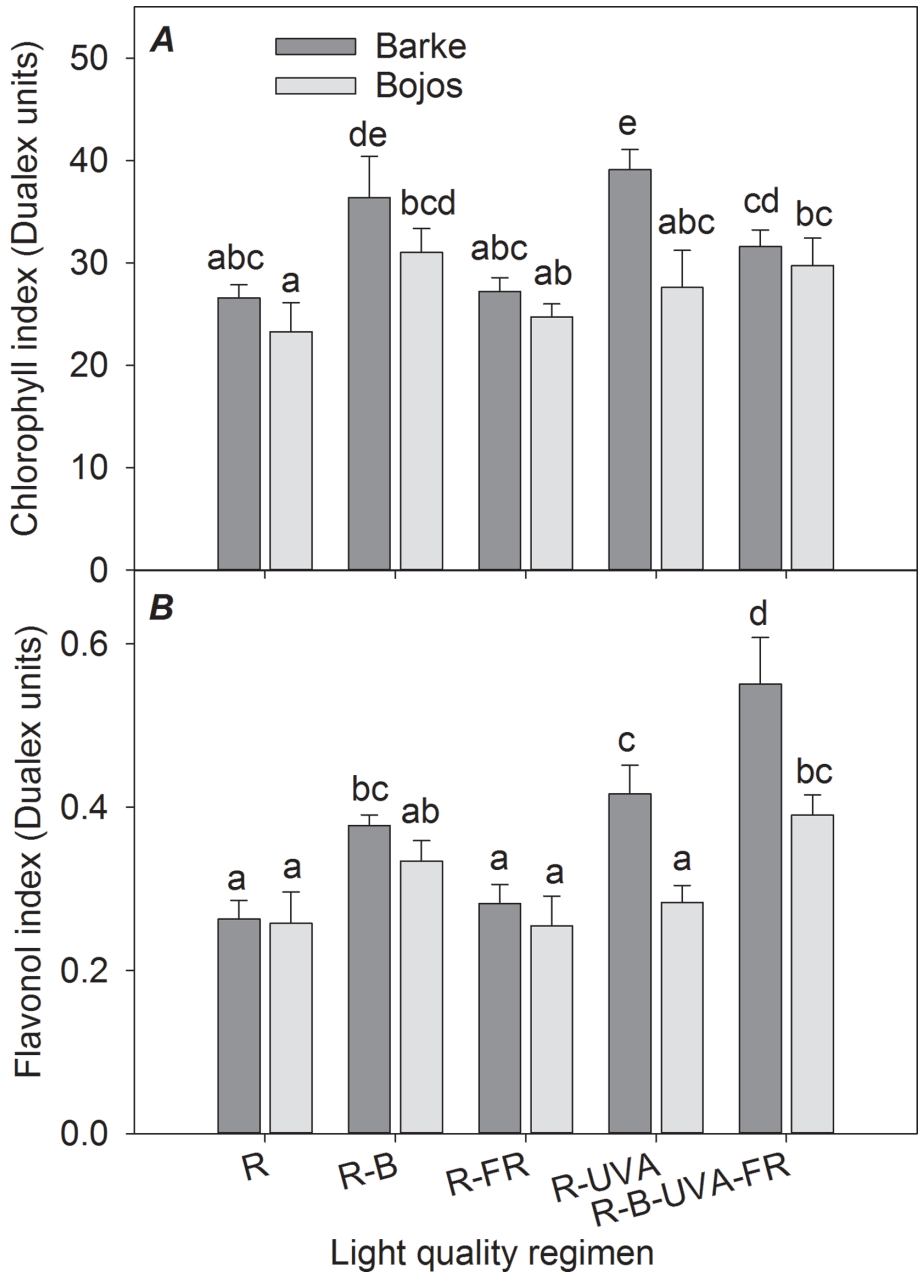


**FIGURE 3 |** Effect of 26 days exposure to different light regimens on chlorophyll index **(A)** and flavonol index **(B)** of spring barley varieties Barke (dark grey) and Bojos (light grey). Additional details are in the **Figure 1** legend.

the addition of B, FR, and UV-A increased water use efficiency by 28–51%; **Figure 5D**).

## Metabolite Profiling

Overall, we detected 1,785 metabolites and identified 73 of them. Among the identified metabolites, amino acids were the most abundant, followed by carbohydrates, organic acids, and secondary metabolites. When the entire metabolomic data set was analyzed jointly for leaves and roots using PERMANOVA, the plant organ (root *vs.* shoot) explained almost half of the variance (pseudo-F = 49.03, $p < 0.001$; **Table 1**). The light regimen explained less of the total variance, but its effect was also significant (pseudo-F = 3.26, $p < 0.001$). Barley variety had a significant but smaller effect on the metabolite profile (pseudo-F = 2.19, $p < 0.05$). Analysis of all interactions indicated that the only significant interaction was between light regimen and plant organ (pseudo-F = 2.57, $p < 0.05$).

A PCA analysis of metabolites in barley leaves also indicated a major effect of light regimen and small differences between

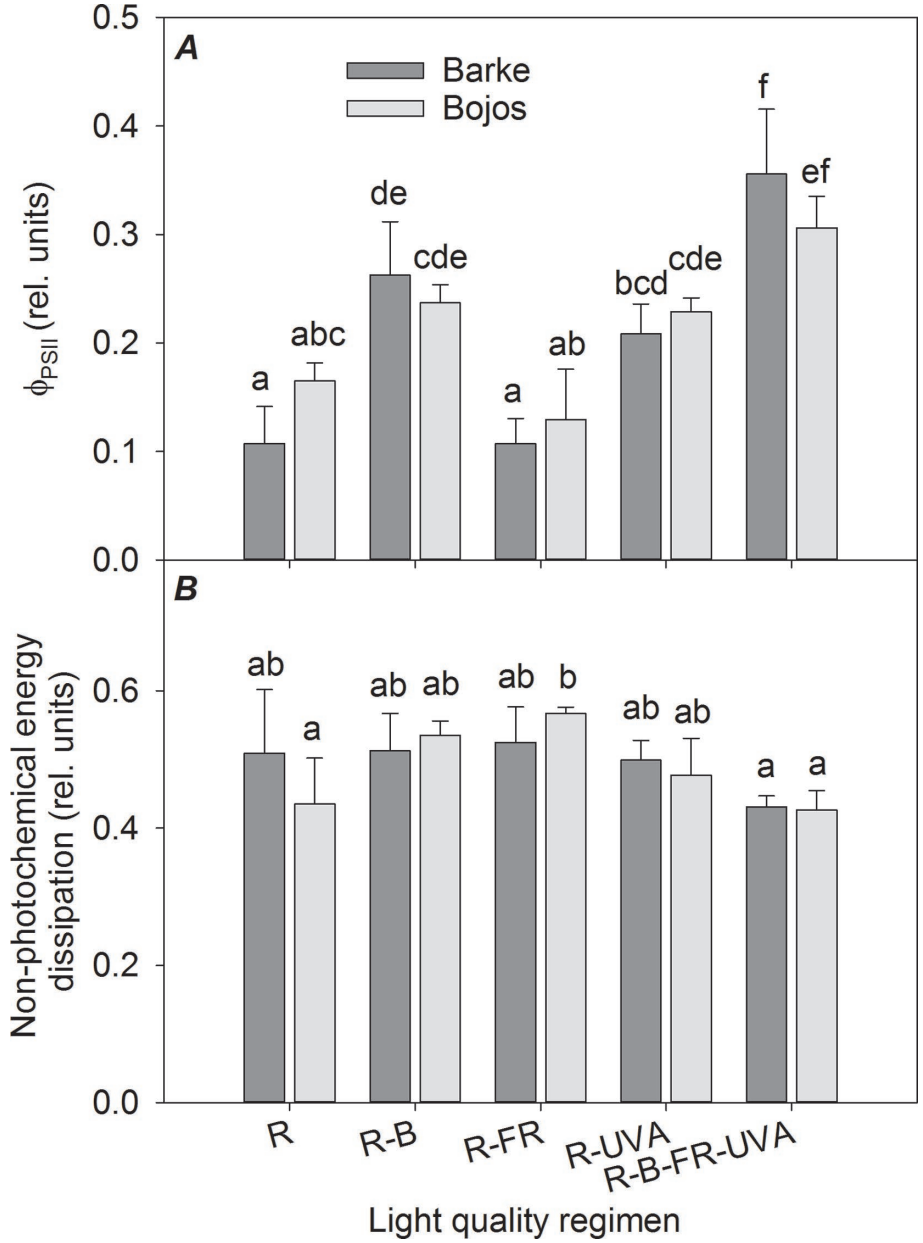


**FIGURE 4 |** Effect of 26 days exposure to different light regimens on actual quantum yield of PSII photochemistry ($\Phi_{PSII}$, **A**) and non-photochemical energy dissipation **(B)** of spring barley varieties Barke (dark grey) and Bojos (light grey). Additional details are in the **Figure 1** legend.

varieties (**Figure 6**). PC1 mainly separated the effect of the R-B-UVA-FR regimen from other regimens, and PC2 showed the dominant effect of the R-B regimen. The R-B-UVA-FR regimen was associated with an accumulation of D-xylose and D-fructose and some secondary metabolites (isovitexin or kaempferol). The R, R-FR, and R-UVA regimens led to the accumulation of glycine-betaine, abscisic acid (ABA), mannitol, and ferulic acid. On the other hand, the R-B regimen led to the accumulation of γ-aminobutyric acid (GABA), sorgolactone, and several secondary metabolites (homoorientin, myricetin, aucubin, and acacetin). Analysis of barley variety indicated greater accumulation of glucose, serine, proline, isoleucine, and phenylalanine in the Barke variety than the Bojos variety.

**Figure 7** shows selected metabolites in barley leaves that had large differences among the different light regimens. These results show that there were high levels of proline and *p*-coumaric acid under the R-B-UVA-FR (by 365% and 983% relative to the R regimen) and R-B regimens (by 123% and 445% relative to the R regimen); however, the R-B regimen only had a significant effect on *p*-coumaric acid (**Figures 7A**, **B**).

The Barke variety was generally more sensitive to the R-B-UVA-FR regimen than the Bojos variety, in terms of proline

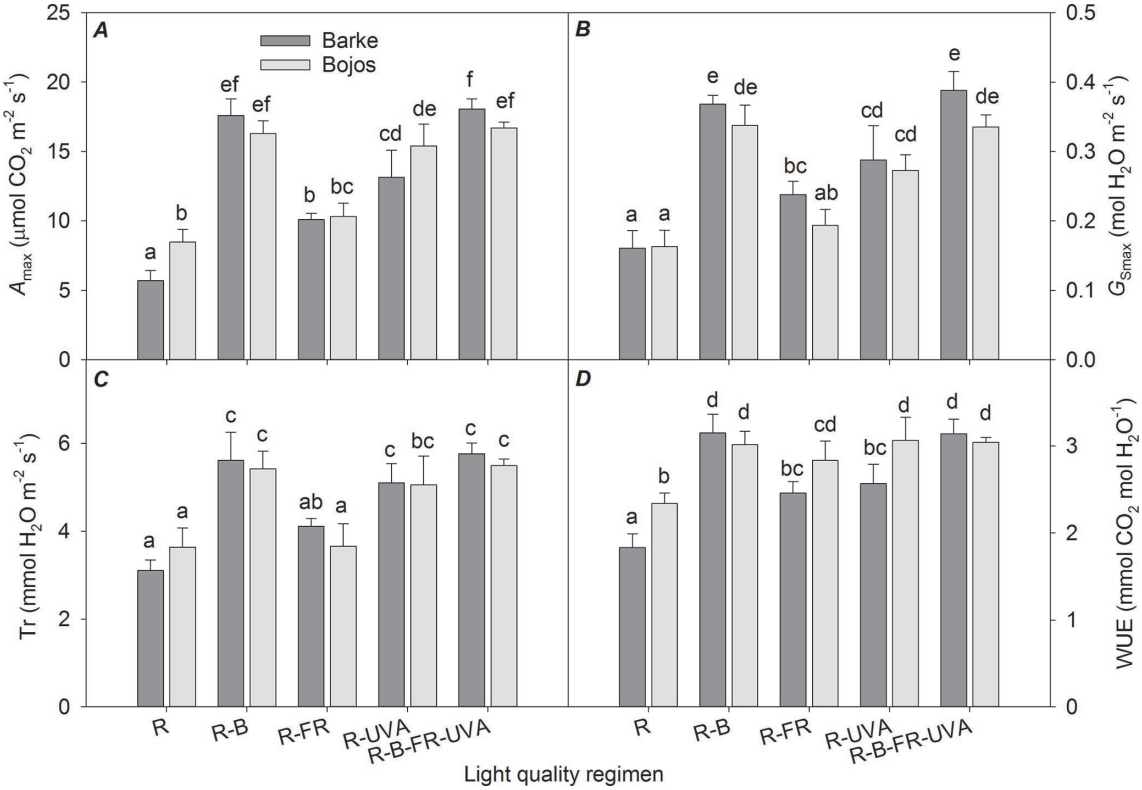


**FIGURE 5 |** Effect of 26 days exposure to different light regimens on light-saturated $CO_2$ assimilation rate ($A_{max}$, **A**), light-saturated stomatal conductance ($G_{Smax}$, **B**), transpiration rate (Tr, **C**), and water use efficiency (WUE, **D**) of spring barley varieties Barke (dark grey) and Bojos (light grey). Additional details are in the **Figure 1** legend.

**TABLE 1 |** PERMANOVA results for the entire metabolomic data set.

| | Df | SS | MS | Pseudo-F | $R^2$ | P(perm) | |
|---|---|---|---|---|---|---|---|
| Barley variety | 1 | 0.1818 | 0.1818 | 2.189 | 0.01551 | 0.05 | * |
| Light regimen (Light) | 4 | 1.085 | 0.2713 | 3.265 | 0.09256 | 0.001 | *** |
| Plant organ | 1 | 4.0714 | 4.0714 | 49.013 | 0.34734 | 0.001 | *** |
| Variety:Light | 4 | 0.2971 | 0.0743 | 0.894 | 0.02535 | 0.582 | |
| Variety:Organ | 1 | 0.1722 | 0.1722 | 2.073 | 0.01469 | 0.054 | . |
| Light:Organ | 4 | 0.8539 | 0.2135 | 2.57 | 0.07285 | 0.002 | ** |
| Variety:Light:Organ | 4 | 0.3254 | 0.0814 | 0.979 | 0.02776 | 0.484 | |
| Residuals | 57 | 4.7348 | 0.0831 | | 0.40394 | | |
| Total | 76 | 11.7217 | | | 1 | | |

**P(perm) 0.05>=0.01, **P(perm) 0.01>=0.001, ***P(perm) <=0.001.*

(by 516% in Barke and 211% in Bojos relative to the R regimen) and JA (by 741% in Barke and 346% in Bojos relative to the R regimen) accumulation (**Figures 7A**, **C**), but the Barke variety accumulated less ABA (by 19% relative to Bojos; **Figure 7D**). Analysis of sorgolactone indicated increased accumulation under the R-B regimen relative to the R regimen (by 2,818%), but the R-B-UVA-FR regimen only had a weak effect (by 103%; **Figure 7E**). On the contrary, relative to the R regimen, the R-B-UVA-FR regimen led to significant accumulation of the flavonoid isovitexin (by 847%; **Figure 7F**).

Analysis of roots indicated that they had substantially lower levels of metabolites than leaves. A PCA analysis indicated a small effect of barley variety on root metabolites (**Figure 8**). In particular, PC1 separated the effect of the R-B-UVA-FR regimen from the other regimens, and PC2 mainly separated the effects of the R-B and R-UVA regimens. The R-B-UVA-FR regimen was associated with greater levels of thymidine, D-sorbose, GABA, aucubin, and D-lyxose, but the addition of UV-A radiation increased the accumulation of L-malic acid, fructose, and acacetin in roots.

We also analyzed the changes in metabolite allocation between leaves and roots, expressed as leaf:root ratios (**Figure 9**). PC1 mainly separated the effects of the R-FR and R-B-UVA-FR regimens. In particular, these treatments

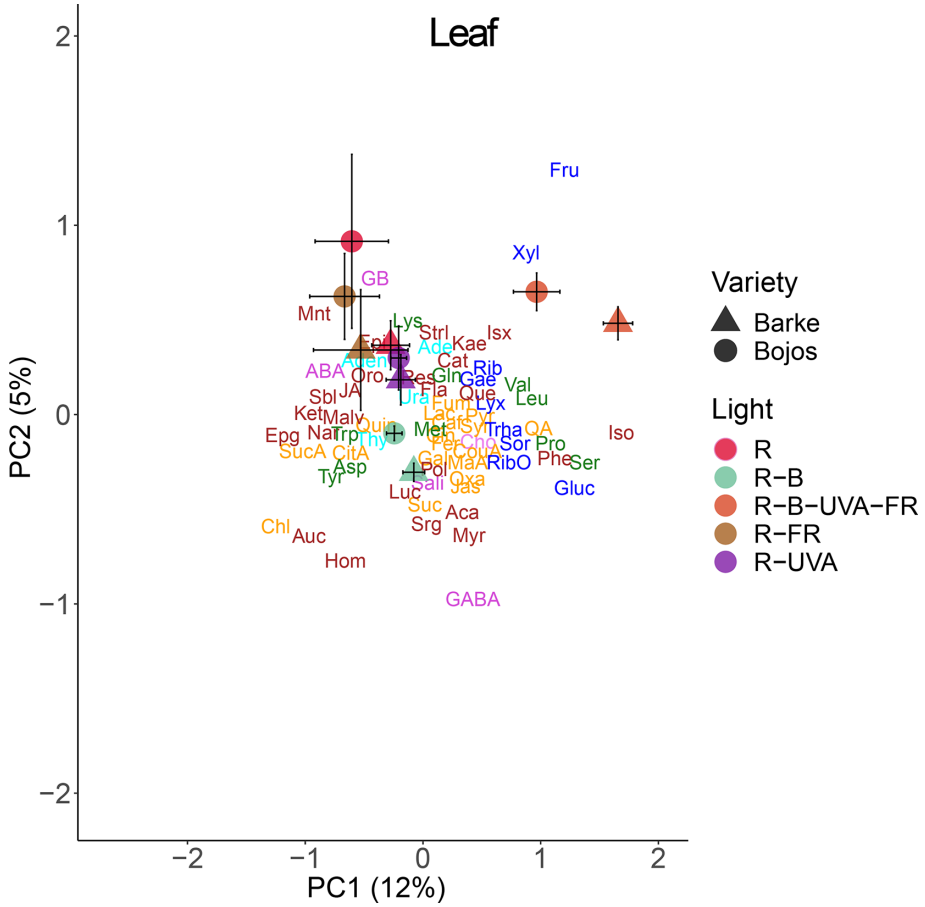


**FIGURE 6 |** Principal component analysis (PC1 *vs.* PC2) of leaf metabolite concentrations of two barley varieties grown for 26 days under different light regimens. Here and in **Figures 8** and **9**: values for each variety (circles, Bojos; triangles, Barke) and light regimen (red, R; R-B, cyan; R-B-UVA-FR, orange; R-FR, brown; R-UVA, purple) are presented as means and standard deviations (error bars). Loadings of PC1 and PC2 for individual metabolite concentrations are represented by abbreviations. The data from individual replicates ($n$ = 4) were used for the analysis. Biochemical families are represented by colors: dark blue, sugars; green, amino acids; yellow, compounds involved in the metabolism of amino acids and sugars; cyan, nucleotides; brown, phenolics; and violet, others. Abbreviations of metabolites: uracil (Ura), adenine (Ade), thymidine (Thy), adenosine (Aden), D-ribose (Rib), D-lyxose (Lyx), D-xylose (Xyl), D-fructose (Fru), 5-methylthio-D-ribose (RibO), D-sorbose (Sor), D-glucose (Gluc), D-galactose (Gae), D-(+)-trehalose dehydrate (Trha), lysine (Lys), glutamine (Gln), leucine (Leu), isoleucine (Iso), phenylalanine (Phe), methionine (Met), tryptophan (Trp), valine (Val), acid aspartic (Asp), tyrosine (Tyr), proline (Pro), serine (Ser), succinic acid (SucA), citrate acid (CitA), malic acid (Mal), lactic acid (Lac), quinic acid (Qui), pyruvate acid (Pyr), *p*-coumaric acid (CouA), jasmone (Jas), gallic acid (Gal), maleic acid (MaA), fumarate (Fum), trans-caffeic acid (Caf), aconitate (Suc), quinic acid (QA), trans-ferulic acid (Fer), syringic acid (Syr), oxaloglutarate (Oxa), jasmonic acid (JA), cinnamic acid (Cin), chlorogenic acid (Chl), γ-aminobutyric acid (GABA), glycine-betaine (GB), choline (Cho), sodium salicylate (Sali), (-)-abscisic acid (ABA), resveratrol (Res), acacetin (Aca), kaempferol (Kae), epicatechin (Epi), alpha-ketoglutaric acid (Ket), quercetin (Que), epigallocatechin (Epg), myricetin (Myr), aucubin (Auc), isovitexin (Isx), homoorientin (Hom), lucenin (Luc), malvidin (Malv), naringenin (Nar), flavan-3-ol (Fla), catechin (Cat), sorgolactone (Srg), (+)-orobanchol (Oro), (+)-strigol (Strl), polyols (Pol), mannitol (Mnt), sorbitol (Sbl).

were mainly associated with more allocation of fructose, myricetin, naringenin, mannitol, and glutathione to roots than leaves. PC2 mainly separated the effects of the R-B and R-UVA regimens, which were associated with more allocation of JA, kaempferol, *p*-coumaric acid, and D-lyxose to roots than leaves. On the other hand, the R regimen was associated with more allocation of glucose, sorbitol, and ABA to roots than leaves.

**Figure 10** shows the selected metabolites that had large differences in roots and root/leaf ratios among the different light regimens. Although the glucose content had large variance in roots and leaves, the R-FR regimen (Barke variety) and the R-UVA regimen (Bojos variety) altered the leaf:root ratios (**Figure 10A**). Relative to the R regimen, leaf fructose level was significantly greater under the R-B-UVA-FR regimen (by 1,371%) but lower under the R-B and R-FR (by 86% and 87%, respectively), and this led to significant effects on the leaf:root ratio (**Figure 10B**). The light regimen also had a significant effect on the leaf:root ratio for mannitol, with a particularly high ratio under the R-FR regimen and a decreased ratio under the R-UVA regimen (**Figure 10C**). Similarly, root naringenin was only present at very low levels under the R-FR and R-B-UVA-FR regimens (**Figure 10D**).

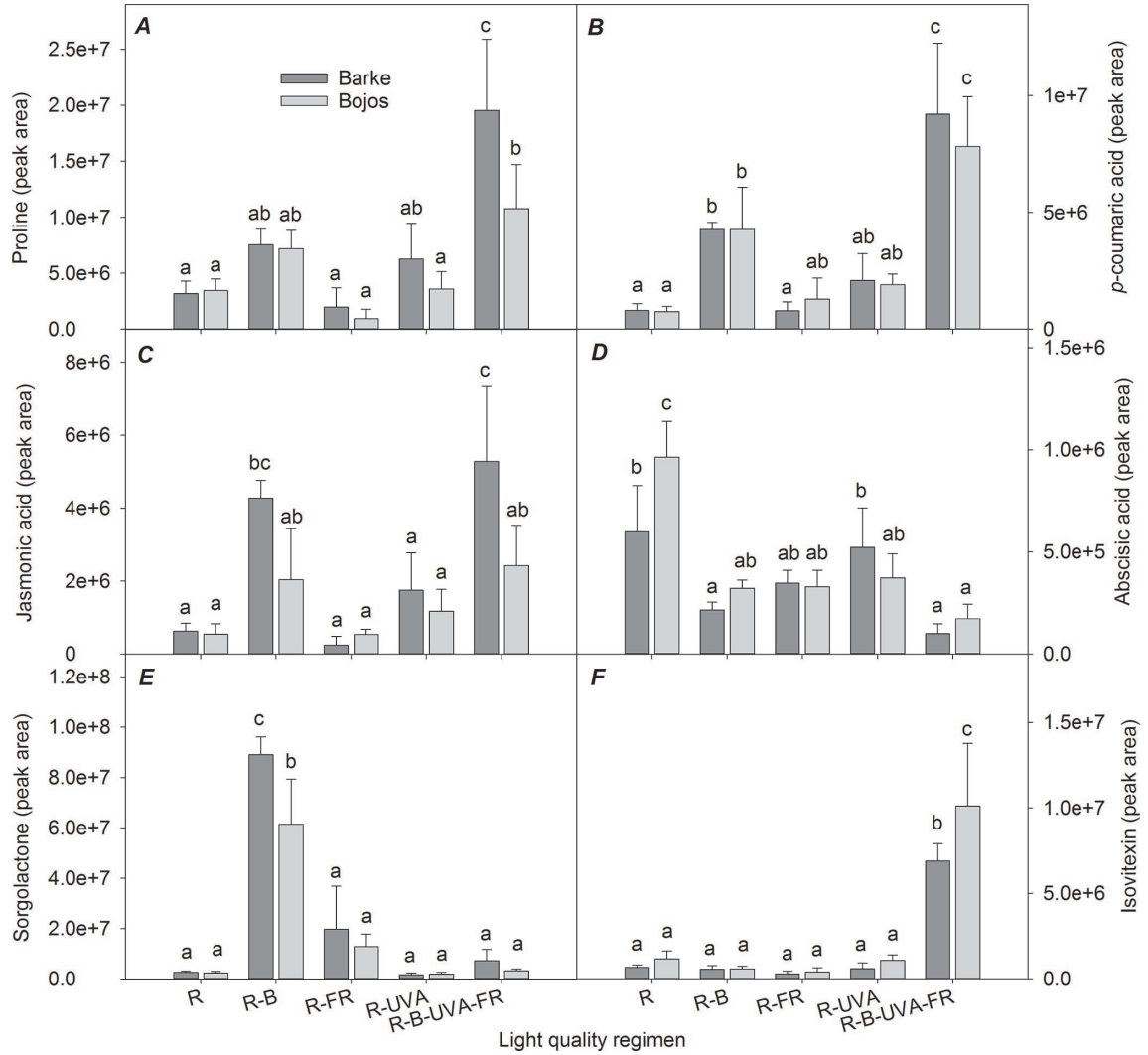


**FIGURE 7 |** Effects of 26 days exposure to different light regimens on the levels of a representative amino acid (proline, **A**), plant hormones or compounds with regulatory effects (jasmonic acid, **C**; abscisic acid, **D**; sorgolactone, **E**), and phenolic compounds (*p*-coumaric acid, **B**; isovitexin, **F**) in leaves of spring barley varieties Barke (dark grey) and Bojos (light grey). Additional details are in the **Figure 1** legend.

# DISCUSSION

## Responses to Far-Red Light

Phytochromes in a plant shoot sense changes in the R:FR ratio and signal that neighboring plants are competing for light. This signal allows competing plants rapid elongation of leaves and stems and upward reorientation of leaves (Franklin, 2008). In monocotyledonous plants, a low R:FR ratio also stimulates apical dominance and reduces tiller formation (Kebrom and Brutnell, 2007). In accordance with these results, we found that the two varieties of barley studied here had significant increases of leaf length and TLA under the R-FR regimen relative to the R regimen.

Less is known about the effect of the R:FR ratio on root development. However, there is evidence that a low R:FR ratio leads to a reduced root-to-shoot biomass ratio in soybean (Kasperbauer, 1987), reduced lateral root density in *Arabidopsis thaliana* (Gelderen van et al., 2018b), and reduced root hair density in *Arabidopsis thaliana* (de Simone et al., 2000). However, these findings differ from our results for barley, which showed that a low R:FR ratio stimulated most RSA traits, although it reduced root BA. Lee et al. (2015) showed that the response of root biomass to the R:FR ratio is non-linear and that decreasing the R:FR ratio beyond a certain level stimulated the growth of root biomass and increased the root-to-shoot ratio. An interactive effect of circadian clock and R:FR ratio on root and shoot growth mediated by phytochrome-interacting factor 4 (PIF4) and PIF5 transcription factors also has to be taken into account. While the PIF4 and PIF5 expression peaks in the morning hours of long days, the maximum expression occurs in the night when the photoperiods are short (Farré, 2012).

Light-induced regulation of plant growth, physiology, and metabolism involves multiple hormonal pathways such as

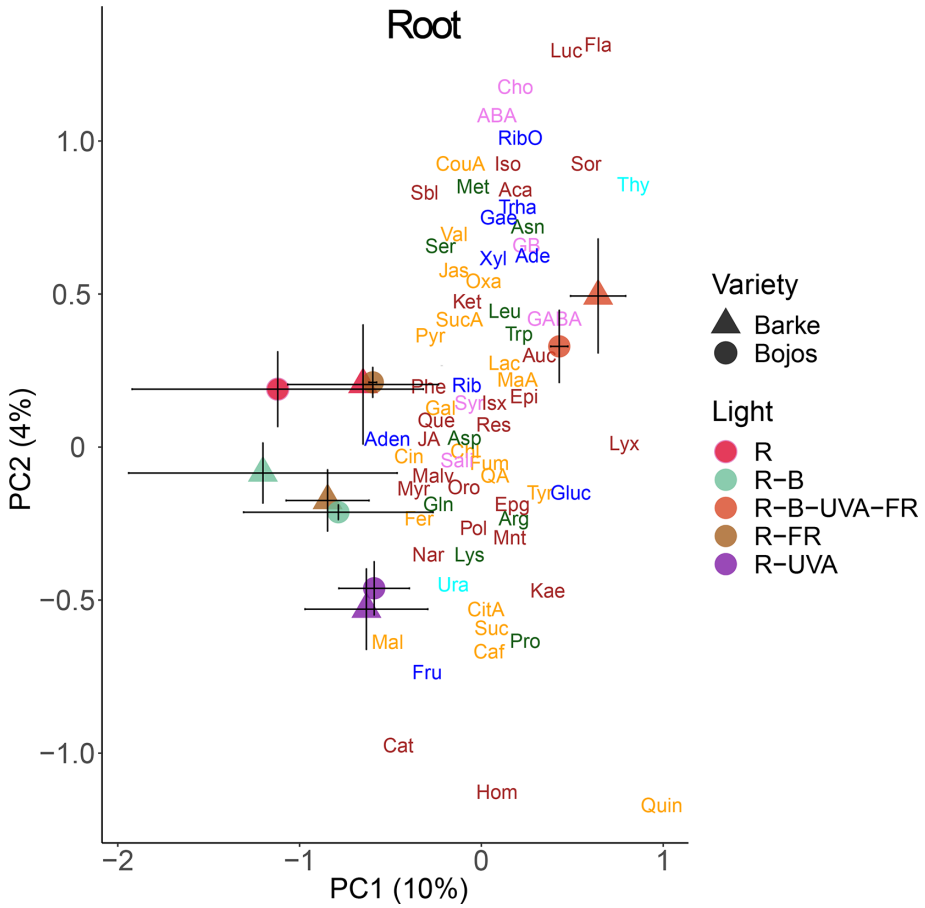


**FIGURE 8 |** Principal component analysis (PC1 *vs.* PC2) of root metabolite concentrations of two barley varieties grown for 26 days under different light regimens. Additional details are in the **Figure 6** legend.

gibberellins, ABA, auxins, ethylene, and cytokinins; however, the molecular links between these pathways and light signaling are not yet completely understood (Lau and Deng, 2010). A low R:FR ratio stimulates the accumulation of at least three plant hormones: gibberellins (de Lucas et al., 2008), auxin (Procko et al., 2014), and ethylene (Kurepin et al., 2010). A low R:FR ratio also desensitizes plants to defense-associated plant hormones, such as JA and salicylic acid. Auxin is the dominant physiological regulator when plants are growing in an environment with a low R:FR ratio (Yang and Li, 2017), and its polar transport affects root growth and development (Saini et al., 2013). The complex nature of auxin shoot-to-root transport and its interactions with other plant hormones may lead to a wide range of shoot and root responses (Lavenus et al., 2013), as observed under the different light regimens used in this study. Moreover, a recent study showed that JA, whose abundance was affected by the R:FR ratio, links the molecular mechanisms responsible for plant growth and immunity (Campos et al., 2016). This suggests that the R:FR ratio determines the allocation of plant resources to growth or defense. However, our results showed that FR light had only a small effect on JA biosynthesis in leaves, in contrast to B light.

Previous research indicated that JA (Suzuki et al., 2011) and photosynthetic products (Kircher and Schopfer, 2012) might link the detection of the R:FR ratio by the shoot with morphogenesis in the root. In accordance with other research (Park and Runkle, 2017), we found that the presence of FR stimulated photosynthesis. Nevertheless, our metabolomic analyses indicated an increased content of glucose in roots and reduced content in leaves in the presence of FR. A high glucose content can affect root length, a number of lateral roots, and root growth direction because of the strong interactions of glucose with auxin (Mishra et al., 2009). On the contrary, we found that fructose and mannitol levels were reduced in roots under the R-FR regimen, which indicates that different sugars have different effects on root growth. Although the function of fructose as sugar regulator is less explored, its interactions with signaling pathways of ABA and ethylene suggest an inhibitory role in root growth (Cho and Yoo, 2011). In contrast, sucrose promotes cell division in root meristems, modifies the expression of numerous genes related to P deficiency, and thus leads to altered root growth and morphology (Horacio and Martinez-Noel, 2013). On the other hand, mannitol and other sugar alcohols play a role in reactive oxygen species (ROS) scavenging rather than in plant growth regulation (Bolouri-Moghaddam et al., 2010).

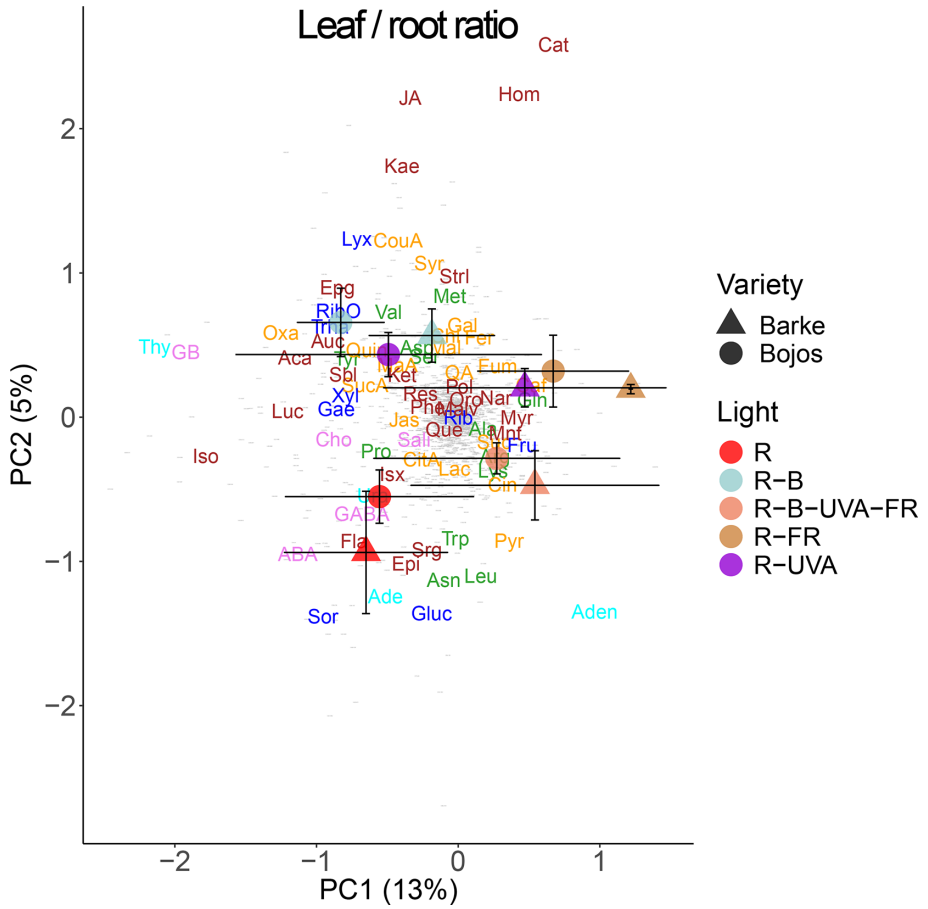


**FIGURE 9 |** Principal component analysis (PC1 *vs.* PC2) of root-to-leaf ratios of metabolite concentrations of two barley varieties grown for 26 days under different light regimens. Additional details are in the **Figure 6** legend.

## Responses to Blue Light

Blue light is an essential environmental signal that also controls plant cell elongation (Huché-Thélier et al., 2016). Blue light represses gibberellin synthesis and auxin synthesis and affects several genes involved in growth repression (Folta et al., 2003). Although the "shade avoidance syndrome" is most often associated with a reduced R:FR ratio, some studies have shown that a reduced level of blue light had a similar effect and suggested that a PHY-B–independent hormonal cascade can also lead to the shade avoidance syndrome (Keller et al., 2011). The blue light–induced shade avoidance syndrome is predominantly mediated by CRY1 and brassinosteroid hormones. Previous studies showed that a high blue-to-red light ratio increased biomass in wheat (Goins et al., 1997) but decreased biomass in lettuce (Kang et al., 2016) and rice (Ohashi-Kaneko et al., 2006). Folta and Childers (2008) reported that responses to blue light are organ-specific and depend on the total photon flux density and blue-to-red light ratio. In our study, the R regimen and the R-B regimen had similar effects, in that the R-B regimen only significantly increased leaf length in the Bojos variety. The blue light also had no significant effect on RSA parameters in either variety of barley.

Many studies demonstrated that supplementary blue light increased photosynthetic performance (Hogewoning et al., 2010; Wang et al., 2016), chlorophyll (Chl) content, and the Chl *a*/*b* ratio (Hogewoning et al., 2010; Kopsell and Sams, 2013). Similarly, we found that the addition of blue light (R-B regimen) significantly increased most of the photosynthetic parameters in our two barley varieties. An increased $CO_2$ assimilation rate under blue light is particularly associated with increased stomatal conductance (Boccalandro et al., 2012) being mediated by phototropins PHOT1 and PHOT2 (Kinoshita et al., 2001). However, high photosynthetic carbon uptake may lead, under the conditions of limited C sink, to the accumulation of soluble sugars and consequently to stomata closure. Such feedback regulation is mediated by hexokinase within the guard cells of stomatal pores (Granot and Kelly, 2019). If there is sufficient sink for sugars in roots, these (mainly sucrose) are rapidly transported by phloem and stimulate root growth, the process mediated by auxin and cytokinin (Wang and Ruan, 2016). Re-allocation of sugars between roots and shoots is tightly coupled with plant N metabolism. N uptake controls the availability of sugars because carbon skeletons are

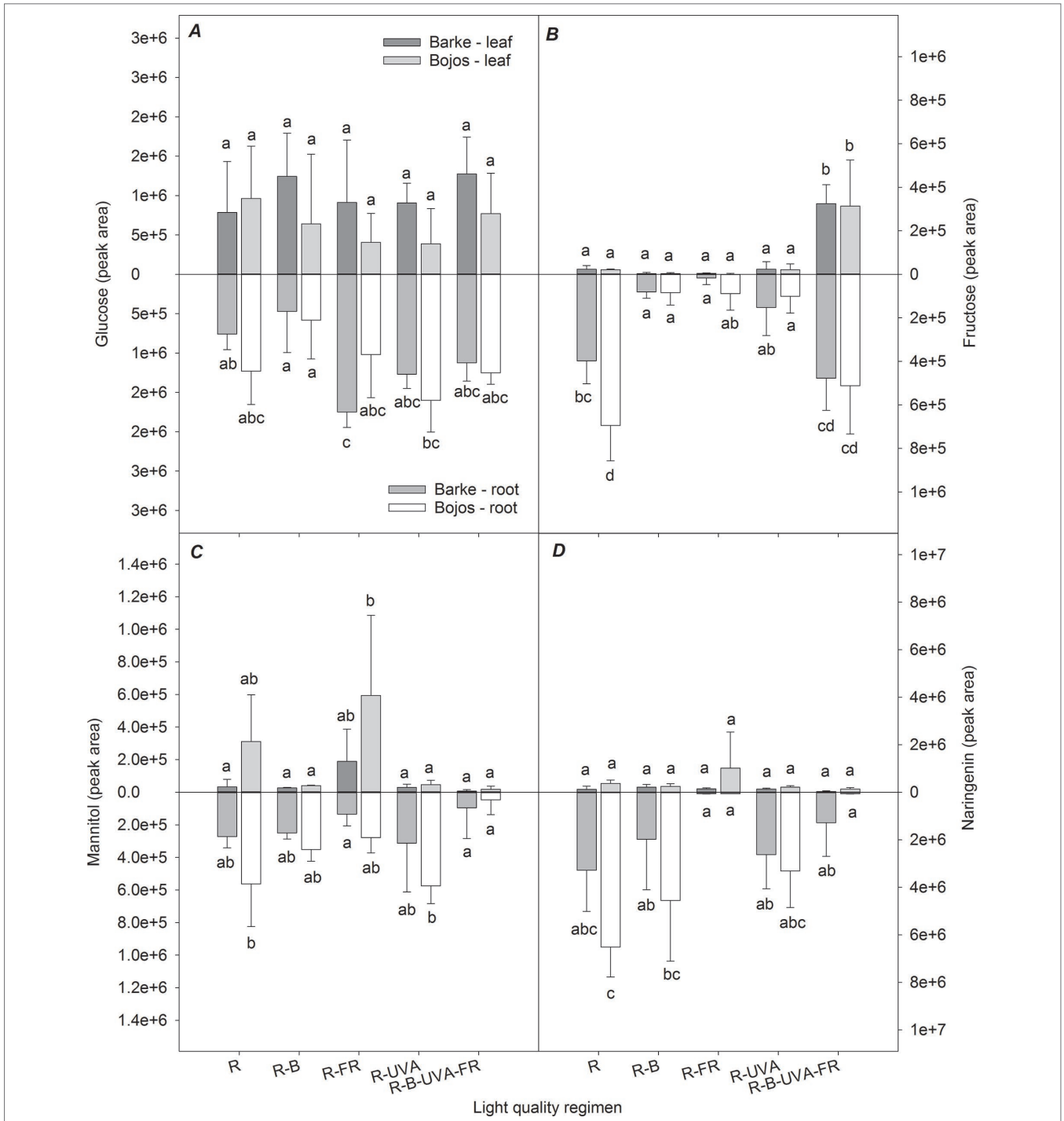


**FIGURE 10 |** Effect of 26 days exposure to different light regimens on allocation of selected sugars (glucose, **A**; fructose, **B**; mannitol, **C**) and a selected phenolic compound (naringenin, **D**) to leaves and roots of spring barley varieties Barke (dark grey) and Bojos (light grey). Additional details are in the **Figure 1** legend.

essential for the assimilation of inorganic N into amino acids, proteins, and nucleic acids and vice versa. On the other hand, N-deficiency reduces the rates of photosynthetic carbon uptake and accumulation of sugars (Wang and Ruan, 2016).

Several studies, however, reported that photosynthetic performance increased with increasing blue light intensity only in the presence of other wavelengths (Hogewoning et al., 2010; Hernández and Kubota, 2016). The opposite effects of blue light on growth and photosynthesis can be the reason for observed discrepancies in biomass formation under blue light conditions. The role of blue light signaling in RSA is still not well understood. However, under blue light, *cry* mutants of *Arabidopsis* have

substantial differences in primary root length relative to wild type (Canamero et al., 2006).

In our study, the R-B regimen (relative to the R regimen) led to a reduced content of ABA and an increased content of JA in leaves. This is in accordance with stomatal responses to the R-B regimen. Boccalandro et al. (2012) examined the roles of CRY1, CRY2, and ABA in stomatal regulation and reported that blue light led to a substantial increase of stomatal conductance and a reduced ABA content, but this did not occur in CRY1 or CRY2 mutants.

Some studies suggested a close relationship between the biosynthesis of ABA and JA (Brossa et al., 2011). However, these results may simply indicate that reduced water availability independently stimulates JA and ABA accumulation. Previous studies have examined the nature of this relationship using mutants. In particular, although the blue light–induced reduction of ABA content is mediated by CRY1 and CRY2, blue light also increases JA biosynthesis (Svyatyna and Riemann, 2012). Blue light stimulates the biosynthesis of JA by activating the expression of genes involved in JA biosynthesis, although phytochrome A signaling has a stronger effect. Although mechanistic studies with phytochrome mutants reported a crucial role of the R:FR ratio in regulation of the JA biosynthesis and resistance to fungal pathogens (Cerrudo et al., 2012), our results showed that supplementary blue light significantly increased JA accumulation, and this could provide increased resistance to environmental stressors. Blue light also induced the accumulation of several secondary metabolites in barley varieties studied, such as *p*-coumaric acid, chlorogenic acid, aucubin, and homoorientin (but had no impact on isovitexin or kaempferol), which increased in plants receiving the R-B-UVA-FR regimen. Generally, these secondary metabolites play important roles as antioxidants scavenging ROS, UV screening molecules, or anti-infection agents (reviewed by Falcone Ferreyra et al., 2012). Their role also depends on location within the leaf, having screening functions when located in the adaxial epidermis and antioxidant functions when located in the mesophyll. This is particularly true for dihydroxy B-ring–substituted flavonols such as kaempferol or quercetin (Agati et al., 2012). Soluble hydroxycinnamates such as *p*-coumaric acid or chlorogenic acid and mesophyll flavonoids are constitutively present in young leaves, but these are gradually replaced by epidermal flavonols in mature leaves acclimated to light conditions (Burchard et al., 2000; Agati et al., 2013). Walter et al. (2010) summarized the role of cell wall–associated plant secondary metabolites, such as *p*-coumaric acid and other hydroxycinnamic acids, in the inhibition of fungal growth and resistance to *Fusarium* head blight infection. Their results indicated that the blue light–induced accumulation of JA and some phenolic compounds had an important role in the blue light–induced resistance to fungal infection.

We found that blue light strongly stimulated the accumulation of the sesquiterpene sorgolactone, a strigolactone that stimulates germination of parasitic weeds. However, strigolactones also act as endogenous hormones that regulate shoot branching, secondary growth of stems, leaf senescence, primary root growth, adventitious root formation, and root hair elongation (Seto et al., 2012). Strigolactones also increase plant tolerance to drought and salinity, mainly through its effect on stomatal density and responsivity (Ha et al., 2014). Additional studies are, however, needed to further elucidate the effect of blue light on this regulatory pathway.

## Responses to UV-A Radiation

PHOTs and CRYs both percept UV-A and blue light (Gyula et al., 2003), so activation of these photoreceptors may be expected to have similar effects on hormone production. Our results, however, show that UV-A radiation did not have the same effect as the blue light on $CO_2$ assimilation and stomatal opening. Also, the R-UVA regimen had a weaker effect on TLA and root parameters than the R-B regimen.

Recently, we have also shown that UV radiation alone, and in combination with elevated atmospheric $CO_2$ concentration, alters N allocation between leaves and roots of European beech saplings, leading to changes in leaf and root C:N stoichiometry and morphological traits (Uchytilová et al., 2019). C:N stoichiometry can be considered as one of the most relevant indicators of source:sink balance and can regulate expression of several genes involved in N metabolism (Nunes-Nesi et al., 2010), secondary metabolism (Royer et al., 2013), photosynthesis (Ruiz-Vera et al., 2017; Foyer et al., 2018), and plant biomass allocation (Kruse et al., 2010).

Several studies reported that supplemental UV-A radiation increases leaf area (Biswas and Jansen, 2012; Zhang et al., 2014). However, UV-A radiation probably acts with other signaling pathways to increase the elongation of different leaf parts, suggesting the presence of intercellular signaling (Verdaguer et al., 2017). Some studies have also shown the higher allocation of resources to root biomass under UV-A radiation (Zhang et al., 2014), but others reported that UV-A radiation had a negative effect or no effect on root biomass (Cooley et al., 2001).

Although UV-B radiation has a major role in the induction of flavonoid biosynthesis, UV-A radiation also promotes the accumulation of flavonoids in many species (Morales et al., 2010). However, rather than total phenolics, UV-A radiation regulates the accumulation of specific phenolic compounds (Verdaguer et al., 2017). While UV-A radiation had only a minor effect on the accumulation of flavonoids in our study, the R-B-UVA-FR regimen induced accumulation of most flavonoids, indicating that various spectral bands may contribute to flavonoid biosynthesis. Similarly, our earlier study has proven the fundamental importance of the combined effect of PAR and UV on the accumulation of phenolics such as lutonarin and 3-feruloylquinic acid, xanthophyll cycle pigments, and subsequent tolerance to high radiation stress (Klem et al., 2015).

UV-A radiation can also ameliorate the UV-B radiation–induced damage to DNA by promoting DNA repair (Krizek, 2004). On the other hand, several studies reported that UV-A radiation damages PSII (Nawkar et al., 2013), although we observed no such effect. Under natural conditions, UV-A radiation accounts for most of the sunlight-induced damage to photosynthesis because there is much more UV-A than UV-B radiation in the solar spectrum (Verdaguer et al., 2017).

One of the compounds whose level increased the most by UV-A radiation in our study was GABA (a non-protein amino acid). This compound rapidly accumulates in plant tissues in response to biotic and abiotic stress and is a putative signaling molecule (Roberts, 2007). GABA may also have possible roles in the interfacing of C and

N metabolism (Michaeli and Fromm, 2015) and protection against oxidative stress and herbivorous pests (Bouché and Fromm, 2004). Other studies reported that increased GABA levels correlated with leaf senescence (Diaz et al., 2005) and that GABA responses depend on ethylene and ABA signaling (Lancien and Roberts, 2006). Mekonnen et al. (2016) used a GABA-depleted mutant of *Arabidopsis thaliana* to demonstrate the role of this compound in stomatal regulation and sensitivity to drought stress. Li et al. (2013) suggested that the effect of light on GABA accumulation is due to light-induced upregulation of glutamate decarboxylase or glutamic acid decarboxylase (GAD). To our best knowledge, the present study is the first to show that UV-A radiation increases the biosynthesis of GABA.

### Interactions of UV-A, Blue, and Far-Red Light

The R-B-UVA-FR regimen had the strongest effects on increasing leaf area and photosynthetic parameters. This suggests the importance of simultaneous irradiation with multiple regions of the spectrum. The effect of the R-B-UVA-FR regimen on photosynthetic parameters was comparable to the R-B regimen, suggesting that blue light had a greater effect than FR or UV-A light on this variable. Relative to the R regimen, the R-B-UVA-FR regimen strongly increased the above-ground biomass but had negligible effects on root biomass and root architecture parameters. This suggests that the addition of blue light, UV-A radiation, or both impaired the positive effect of FR light on the growth of seminal and lateral roots.

Relative to the R regimen, the R-B-UVA-FR regimen also increased the accumulation of specific amino acids (proline, valine, leucine), phenolics (isovitexin, *p*-coumaric acid, kaempferol), and saccharides (fructose) in leaves (**Figures 6**, **7**, and **9**). Moreover, such changes under the R-B-UVA-FR regimen resulted in significant increases in leaf:root ratio of saccharides (particularly fructose), which were low in other regimens. This important result indicates that light can induce changes in the transport of saccharides from the shoots to the roots.

A previous study showed that sucrose activated and promoted root elongation (Kircher and Schopfer, 2012), and coordinated root and shoot growth with light intensity and spectral quality (Wang and Ruan, 2016). Sugars also provide crosstalk with other signaling and metabolic processes to regulate local and systemic signaling pathways (Ljung et al., 2015), which is integrated *via* PIF (Stewart et al., 2011). However, as discussed earlier, the roles of individual sugars can be different as glucose and sucrose interact mainly with auxin and promote plant growth, while fructose interacts with inhibiting plant hormones such as ABA or ethylene.

It has been demonstrated by Ahanger et al. (2018) that accumulation of osmolytes, antioxidants, carotenoids, and other defense compounds under environmental stress exhibits crosstalk with the cascade of phytohormone signaling, which is mediated by brassinosteroids. Brassinosteroids can have synergistic or antagonistic interactions with other phytohormones for elicitation of stress response involving the antioxidant system, synthesis osmotic constituents, or other mechanisms. Thus, brassinosteroids play a potentially integrating role in responding to light quality and inducing plant protection mechanisms for stress.

## CONCLUSION

Our findings suggest that light quality has a different impact on the shoot and root morphology, physiology, and biochemistry, which may have major implications for plant performance under stress conditions. While the growth of above-ground biomass and photosynthetic performance were enhanced mainly by the combined action of red, blue, far-red, and UV-A light, the root growth was stimulated particularly by supplementary far-red light to red light. These findings may have significant implications for improving root development and, consequently, the drought resistance, e.g., by adjusting sowing density. Exposition of plants to the full light spectrum stimulates the accumulation of defense compounds such as proline, secondary metabolites with antioxidative functions, or JA, and reduces the accumulation of ABA, which allows to assume increased stress tolerance. In addition, blue light induced accumulation of GABA, sorgolactone, or several secondary metabolites. As these compounds play important roles as osmolytes, antioxidants, UV screening compounds, or growth regulators, the importance of light quality in the induction of protective mechanisms against abiotic and biotic stress factors is unequivocal. Application of a suitable spectrum of light wavelengths by specific plastic filters, monochromatic LED light sources, and/or crop management measures may thus provide important tools for adjusting plant tolerance to abiotic and biotic stress.

## DATA AVAILABILITY

The datasets generated for this study are available on request to the corresponding author.

## AUTHOR CONTRIBUTIONS

KK, OU, and WR designed the experiments. KK, WR, BV, and PH conducted the experiment, MO conducted the metabolomic analyses, WR conducted the root system architecture analysis, and AG-G and KK conducted the statistical analyses of data. KK, AG-G, PH, JS, JP, and OU wrote the manuscript. All authors read and approved the final manuscript.

## FUNDING

This research was supported by SustES—Adaptation strategies for sustainable ecosystem services and food security under adverse environmental conditions, project no. CZ.02.1.01/0.0/0.0/16_019/0000797.

## SUPPLEMENTARY MATERIAL

The Supplementary Material for this article can be found online at: https://www.frontiersin.org/articles/10.3389/fpls.2019.01026/full#supplementary-material

**FIGURE S1 |** Scheme of the growth unit layout (upper right), growth unit with the growing plant (upper left), and arrangement of growth units in a plastic bin with micro-irrigation pump inside.

## REFERENCES


Agati, G., Azzarello, E., Pollastri, S., and Tattini, M. (2012). Flavonoids as antioxidants in plants: location and functional significance. *Plant Sci.* 196, 67–76. doi: 10.1016/j.plantsci.2012.07.014

Agati, G., Brunetti, C., Di Ferdinando, M., Ferrini, F., Pollastri, S., and Tattini, M. (2013). Functional roles of flavonoids in photoprotection: new evidence, lessons from the past. *Plant Physiol. Biochem.* 72, 35–45. doi: 10.1016/j.plaphy.2013.03.014

Ahanger, M. A., Ashraf, M., Bajguz, A., and Ahmad, P. (2018). Brassinosteroids regulate growth in plants under stressful environments and crosstalk with other potential phytohormones. *J. Plant Growth Regul.* 37, 1007–1024. doi: 10.1007/s00344-018-9855-2

Anderson, M., Gorley, R. N., and Clarke, R. K. (2008). *Permanova+ for primer: guide to software and statistical methods*. Primer-E Limited. Lutton, UK.

Aphalo, P. J., and Lehto, T. (2001). Effect of lateral far-red light supplementation on the growth and morphology of birch seedlings and its interaction with mineral nutrition. *Trees* 15, 297–303. doi: 10.1007/s004680100100

Ballaré, C. L. (2009). Illuminated behaviour: phytochrome as a key regulator of light foraging and plant anti-herbivore defence. *Plant Cell Environ.* 32, 713–725. doi: 10.1111/j.1365-3040.2009.01958.x

Bian, Z. H., Yang, Q. C., and Liu, W. K. (2015). Effects of light quality on the accumulation of phytochemicals in vegetables produced in controlled environments: a review. *J. Sci. Food Agric.* 95, 869–877. doi: 10.1002/jsfa.6789

Biswas, D. K., and Jansen, M. A. K. (2012). Natural variation in UV-B protection amongst *Arabidopsis thaliana* accessions. *Emir. J. Food Agric.* 246, 621–631. doi: 10.9755/ejfa.v24i6.14681

Blilou, I., Xu, J., Wildwater, M., Willemsen, V., Paponov, I., Friml, J., et al. (2005). The PIN auxin efflux facilitator network controls growth and patterning in *Arabidopsis* roots. *Nature* 433, 39. doi: 10.1038/nature03184

Boccalandro, H. E., Giordano, C. V., Ploschuk, E. L., Piccoli, P. N., Bottini, R., and Casal, J. J. (2012). Phototropins but not cryptochromes mediate the blue light-specific promotion of stomatal conductance, while both enhance photosynthesis and transpiration under full sunlight. *Plant Physiol.* 158, 1475–1484. doi: 10.1104/pp.111.187237

Bolouri-Moghaddam, M. R., Roy, K. L., Xiang, L., Rolland, F., and Van den Ende, W. (2010). Sugar signalling and antioxidant network connections in plant cells. *FEBS J.* 277, 2022–2037. doi: 10.1111/j.1742-4658.2010.07633.x

Bouché, N., and Fromm, H. (2004). GABA in plants: just a metabolite? *Trends Plant Sci.* 9, 110–115. doi: 10.1016/j.tplants.2004.01.006

Brossa, R., López-Carbonell, M., Jubany-Marí, T., and Alegre, L. (2011). Interplay between abscisic acid and jasmonic acid and its role in water-oxidative stress in wild-type, ABA-deficient, JA-deficient, and ascorbate-deficient *Arabidopsis* plants. *J. Plant Growth Regul.* 30, 322–333. doi: 10.1007/s00344-011-9194-z

Burchard, P., Bilger, W., and Weissenbock, G. (2000). Contribution of hydroxycinnamates and flavonoids to epidermal shielding of UV-A and UV-B radiation in developing rye primary leaves as assessed by ultraviolet-induced chlorophyll fluorescence measurements. *Plant Cell Environ.* 2312, 1373–1380. doi: 10.1046/j.1365-3040.2000.00633.x

Campos, M. L., Yoshida, Y., Major, I. T., de Oliveira Ferreira, D., Weraduwage, S. M., Froehlich, J. E., et al. (2016). Rewiring of jasmonate and phytochrome B signalling uncouples plant growth–defense tradeoffs. *Nat. Commun.* 7, 12570. doi: 10.1038/ncomms12570

Canamero, R. C., Bakrim, N., Bouly, J.-P., Garay, A., Dudkin, E. E., Habricot, Y., et al. (2006). Cryptochrome photoreceptors cry1 and cry2 antagonistically regulate primary root elongation in *Arabidopsis thaliana*. *Planta* 224, 995–1003. doi: 10.1007/s00425-006-0280-6

Casal, J. J., Sánchez, R. A., and Botto, J. F. (1998). Modes of action of phytochromes. *J. Exp. Bot.* 49, 127–138. doi: 10.1093/jxb/49.319.127

Catalá, R., Medina, J., and Salinas, J. (2011). Integration of low temperature and light signaling during cold acclimation response in *Arabidopsis*. *Proc. Natl. Acad. Sci. U. S. A.* 108, 16475–16480. doi: 10.1073/pnas.1107161108

Cerrudo, I., Keller, M. M., Cargnel, M. D., Demkura, P. V., de Wit, M., Patitucci, M. S., et al. (2012). Low red/far-red ratios reduce *Arabidopsis* resistance to *Botrytis cinerea* and jasmonate responses *via* a COI1-JAZ10–dependent, salicylic acid–independent mechanism. *Plant Physiol.* 158, 2042–2052. doi: 10.1104/pp.112.193359

Chen, M., Chory, J., and Fankhauser, C. (2004). Light signal transduction in higher plants. *Annu. Rev. Genet.* 38, 87–117. doi: 10.1146/annurev.genet.38.072902.092259

Cho, Y.-H., and Yoo, S.-D. (2011). Signaling role of fructose mediated by FINS1/FBP in *Arabidopsis thaliana*. *PLoS Genet.* 7, e1001263. doi: 10.1371/journal.pgen.1001263

Cooley, N. M., Higgins, J. T., Holmes, M. G., and Attridge, T. H. (2001). Ecotypic differences in responses of *Arabidopsis thaliana* L. to elevated polychromatic UV-A and UV-B+A radiation in the natural environment: a positive correlation between UV-B+A inhibition and growth rate. *J. Photochem. Photobiol. B, Biol.* 60, 143–150. doi: 10.1016/S1011-1344(01)00140-3

Das, P. K., Shin, D. H., Choi, S.-B., and Park, Y.-I. (2012). Sugar-hormone cross-talk in anthocyanin biosynthesis. *Mol. Cells* 34, 501–507. doi: 10.1007/s10059-012-0151-x

de Lucas, M., and Prat, S. (2014). PIFs get BRright: PHYTOCHROME INTERACTING FACTORs as integrators of light and hormonal signals. *New Phytol.* 202, 1126–1141. doi: 10.1111/nph.12725

de Lucas, M., Davière, J.-M., Rodríguez-Falcón, M., Pontin, M., Iglesias-Pedraz, J. M., Lorrain, S., et al. (2008). A molecular framework for light and gibberellin control of cell elongation. *Nature* 451, 480–484. doi: 10.1038/nature06520

de Simone, S., Oka, Y., and Inoue, Y. (2000). Effect of light on root hair formation in *Arabidopsis thaliana* phytochrome-deficient mutants. *J. Plant Res.* 113, 63–69. doi: 10.1007/PL00013917

Demmig-Adams, B., Adams, W. W., III, Barker, D. H., Logan, B. A., Bowling, D. R., and Verhoeven, A. S. (1996). Using chlorophyll fluorescence to assess the fraction of absorbed light allocated to thermal dissipation of excess excitation. *Physiol. Plant.* 98, 253–264. doi: 10.1034/j.1399-3054.1996.980206.x

Diaz, C., Purdy, S., Christ, A., Morot-Gaudry, J.-F., Wingler, A., and Masclaux-Daubresse, C. (2005). Characterization of markers to determine the extent and variability of leaf senescence in *Arabidopsis*. A metabolic profiling approach. *Plant Physiol.* 138, 898–908. doi: 10.1104/pp.105.060764

Falcone Ferreyra, M. L., Rius, S. P., and Casati, P. (2012). Flavonoids: biosynthesis, biological functions, and biotechnological applications. *Front. Plant Sci.* 3(222), 1–15. doi: 10.3389/fpls.2012.00222

Farré, E. M. (2012). The regulation of plant growth by the circadian clock. *Plant Biol.* 14, 401–410. doi: 10.1111/j.1438-8677.2011.00548.x

Folta, K. M., and Childers, K. S. (2008). Light as a growth regulator: controlling plant biology with narrow-bandwidth solid-state lighting systems. *Hortscience* 43, 1957–1964. doi: 10.21273/HORTSCI.43.7.1957

Folta, K. M., Pontin, M. A., Karlin-Neumann, G., Bottini, R., and Spalding, E. P. (2003). Genomic and physiological studies of early cryptochrome 1 action demonstrate roles for auxin and gibberellin in the control of hypocotyl growth by blue light. *Plant J.* 36, 203–214. doi: 10.1046/j.1365-313X.2003.01870.x

Foyer, C. H., Noctor, G., and Verrier, P. (2018). Photosynthetic carbon–nitrogen interactions: modelling inter-pathway control and signalling. *Annu. Rev. Plant Biol.* 22, 325–347. doi: 10.1002/9780470988640

Franklin, K. A. (2008). Shade avoidance. *New Phytol.* 179, 930–944. doi: 10.1111/j.1469-8137.2008.02507.x

Galvão, V. C., and Fankhauser, C. (2015). Sensing the light environment in plants: photoreceptors and early signaling steps. *Curr. Opin. Neurobiol.* 34, 46–53. doi: 10.1016/j.conb.2015.01.013

Gelderen van, K., Kang, C., Paalman, R., Keuskamp, D., Hayes, S., and Pierik, R. (2018a). Far-red light detection in the shoot regulates lateral root development through the HY5 transcription factor. *Plant Cell* 30, 101–116. doi: 10.1105/tpc.17.00771

Gelderen van, K., Kang, C., and Pierik, R. (2018b). Light signaling, root development, and plasticity. *Plant Physiol.* 176, 1049–1060. doi: 10.1104/pp.17.01079

Goins, G. D., Yorio, N. C., Sanwo, M. M., and Brown, C. S. (1997). Photomorphogenesis, photosynthesis, and seed yield of wheat plants grown under red light-emitting diodes (LEDs) with and without supplemental blue lighting. *J. Exp. Bot.* 48, 1407–1413. doi: 10.1093/jxb/48.7.1407

Granot, D., and Kelly, G. (2019). Evolution of guard-cell theories: the story of sugars. *Trends Plant Sci.* 24, 507–518. doi: 10.1016/j.tplants.2019.02.009

Granot, D., Kelly, G., Stein, O., and David-Schwartz, R. (2014). Substantial roles of hexokinase and fructokinase in the effects of sugars on plant physiology and development. *J. Exp. Bot.* 65, 809–819. doi: 10.1093/jxb/ert400

Green-Tracewicz, E., Page, E. R., and Swanton, C. J. (2012). Light quality and the critical period for weed control in soybean. *Weed Sci.* 60, 86–91. doi: 10.1614/WS-D-11-00072.1

Gundel, P. E., Pierik, R., Mommer, L., and Ballaré, C. L. (2014). Competing neighbors: light perception and root function. *Oecologia* 176, 1–10. doi: 10.1007/s00442-014-2983-x

Gyula, P., Schäfer, E., and Nagy, F. (2003). Light perception and signalling in higher plants. *Curr. Opin. Plant Biol.* 6, 446–452. doi: 10.1016/S1369-5266(03)00082-7

Ha, C. V., Leyva-González, M. A., Osakabe, Y., Tran, U. T., Nishiyama, R., Watanabe, Y., et al. (2014). Positive regulatory role of strigolactone in plant responses to drought and salt stress. *Proc. Natl. Acad. Sci. U. S. A.* 111, 851–856. doi: 10.1073/pnas.1322135111

Hernández, R., and Kubota, C. (2016). Physiological responses of cucumber seedlings under different blue and red photon flux ratios using LEDs. *Environ. Exp. Bot.* 121, 66–74. doi: 10.1016/j.envexpbot.2015.04.001

Hideg, E., Jansen, M. A. K., and Strid, A. (2013). UV-B exposure, ROS, and stress: inseparable companions or loosely linked associates? *Trends Plant Sci.* 182, 107–115. doi: 10.1016/j.tplants.2012.09.003

Hogewoning, S. W., Trouwborst, G., Maljaars, H., Poorter, H., van Leperen, W., and Harbinson, J. (2010). Blue light dose–responses of leaf photosynthesis, morphology, and chemical composition of *Cucumis sativus* grown under different combinations of red and blue light. *J. Exp. Bot.* 61, 3107–3117. doi: 10.1093/jxb/erq132

Horacio, P., and Martinez-Noel, G. (2013). Sucrose signaling in plants: a world yet to be explored. *Plant Signal. Behav.* 8, e23316. doi: 10.4161/psb.23316

Horai, H., Arita, M., Kanaya, S., Nihei, Y., Ikeda, T., Suwa, K., et al. (2010). MassBank: a public repository for sharing mass spectral data for life sciences. *J. Mass Spectrom.* 45, 703–714. doi: 10.1002/jms.1777

Huché-Thélier, L., Crespel, L., Gourrierec, J. L., Morel, P., Sakr, S., and Leduc, N. (2016). Light signaling and plant responses to blue and UV radiations—perspectives for applications in horticulture. *Environ. Exp. Bot.* 121, 22–38. doi: 10.1016/j.envexpbot.2015.06.009

Kami, C., Lorrain, S., Hornitschek, P., and Fankhauser, C. (2010). "Chapter two—light-regulated plant growth and development," in *Current Topics in Developmental Biology Plant Development*. Ed. M. C. P. Timmermans (Academic Press), 29–66. doi: 10.1016/S0070-2153(10)91002-8

Kanehisa, M., and Goto, S. (2000). KEGG: Kyoto encyclopedia of genes and genomes. *Nucleic Acids Res.* 28, 27–30. doi: 10.1093/nar/28.1.27

Kang, W. H., Park, J. S., Park, K. S., and Son, J. E. (2016). Leaf photosynthetic rate, growth, and morphology of lettuce under different fractions of red, blue, and green light from light-emitting diodes (LEDs). *Hortic. Environ. Biotechnol.* 57, 573–579. doi: 10.1007/s13580-016-0093-x

Kangasjärvi, S., Neukermans, J., Li, S., Aro, E.-M., and Noctor, G. (2012). Photosynthesis, photorespiration, and light signalling in defence responses. *J. Exp. Bot.* 63, 1619–1636. doi: 10.1093/jxb/err402

Karapetyan, S., and Dong, X. (2018). Redox and the circadian clock in plant immunity: a balancing act. *Free Radic. Biol. Med.* 119, 56–61. doi: 10.1016/j.freeradbiomed.2017.12.024

Kasperbauer, M. J. (1987). Far-red light reflection from green leaves and effects on phytochrome-mediated assimilate partitioning under field conditions. *Plant Physiol.* 85, 350–354. doi: 10.1104/pp.85.2.350

Kebrom, T. H., and Brutnell, T. P. (2007). The molecular analysis of the shade avoidance syndrome in the grasses has begun. *J. Exp. Bot.* 58, 3079–3089. doi: 10.1093/jxb/erm205

Keller, M. M., Jaillais, Y., Pedmale, U. V., Moreno, J. E., Chory, J., and Ballaré, C. L. (2011). Cryptochrome 1 and phytochrome B control shade-avoidance responses in *Arabidopsis via* partially independent hormonal cascades. *Plant J.* 67, 195–207. doi: 10.1111/j.1365-313X.2011.04598.x

Kinoshita, T., Doi, M., Suetsugu, N., Kagawa, T., Wada, M., and Shimazaki, K. (2001). phot1 and phot2 mediate blue light regulation of stomatal opening. *Nature* 414, 656. doi: 10.1038/414656a

Kircher, S., and Schopfer, P. (2012). Photosynthetic sucrose acts as cotyledon-derived long-distance signal to control root growth during early seedling development in *Arabidopsis. Proc. Natl. Acad. Sci. U. S. A.* 109, 11217–11221. doi: 10.1073/pnas.1203746109

Klem, K., Ač, A., Holub, P., Kováč, D., Špunda, V., Robson, T. M., et al. (2012). Interactive effects of PAR and UV radiation on the physiology, morphology and leaf optical properties of two barley varieties. *Environ. Exp. Bot.* 75, 52–64. doi: 10.1016/j.envexpbot.2011.08.008

Klem, K., Holub, P., Štroch, M., Nezval, J., Špunda, V., Tříska, J., et al. (2015). Ultraviolet and photosynthetically active radiation can both induce photoprotective capacity allowing barley to overcome high radiation stress. *Plant Physiol. Biochem.* 93, 74–83. doi: 10.1016/j.plaphy.2015.01.001

Kopsell, D. A., and Sams, C. E. (2013). Increases in shoot tissue pigments, glucosinolates, and mineral elements in sprouting broccoli after exposure to short-duration blue light from light emitting diodes. *J. Am. Soc. Hortic. Sci.* 138, 31–37. doi: 10.21273/JASHS.138.1.31

Krizek, D. T. (2004). UV radiation effects on pathogens and insect pests of greenhouse-grown crops. *Photochem. Photobiol.* 79, 217. doi: 10.1111/j.1751-1097.2004.tb00400.x

Kruse, J., Hänsch, R., Mendel, R. R., and Rennenberg, H. (2010). The role of root nitrate reduction in the systemic control of biomass partitioning between leaves and roots in accordance to the C/N-status of tobacco plants. *Plant Soil* 332, 387–403. doi: 10.1007/s11104-010-0305-6

Kurepin, L. V., Walton, L. J., Yeung, E. C., Chinnappa, C. C., and Reid, D. M. (2010). The interaction of light irradiance with ethylene in regulating growth of *Helianthus annuus* shoot tissues. *Plant Growth Regul.* 62, 43–50. doi: 10.1007/s10725-010-9483-8

Lancien, M., and Roberts, M. R. (2006). Regulation of *Arabidopsis thaliana* 14-3-3 gene expression by γ-aminobutyric acid. *Plant Cell Environ.* 29, 1430–1436. doi: 10.1111/j.1365-3040.2006.01526.x

Lanoue, J., Leonardos, E. D., and Grodzinski, B. (2018). Effects of light quality and intensity on diurnal patterns and rates of photo-assimilate translocation and transpiration in tomato leaves. *Front. Plant Sci.* 9 (756), 1–14. doi: 10.3389/fpls.2018.00756

Lastdrager, J., Hanson, J., and Smeekens, S. (2014). Sugar signals and the control of plant growth and development. *J. Exp. Bot.* 65, 799–807. doi: 10.1093/jxb/ert474

Lau, O. S., and Deng, X. W. (2010). Plant hormone signaling lightens up: integrators of light and hormones. *Curr. Opin. Plant Biol.* 135, 571–577. doi: 10.1016/j.pbi.2010.07.001

Lavenus, J., Goh, T., Roberts, I., Guyomarc'h, S., de Lucas, M., Smet, I., et al. (2013). Lateral root development in *Arabidopsis*: fifty shades of auxin. *Trends Plant Sci.* 18, 450–458. doi: 10.1016/j.tplants.2013.04.006

Lee, M.-J., Park, S.-Y., and Oh, M.-M. (2015). Growth and cell division of lettuce plants under various ratios of red to far-red light-emitting diodes. *Hortic. Environ. Biotechnol.* 56, 186–194. doi: 10.1007/s13580-015-0130-1

Li, X., Kim, Y. B., Uddin, M. R., Lee, S., Kim, S.-J., and Park, S. U. (2013). Influence of light on the free amino acid content and γ-aminobutyric acid synthesis in *Brassica juncea* seedlings. *J. Agric. Food Chem.* 61 (36), 8624–8631. doi: 10.1021/jf401956v

Li, Y., Xin, G., Wei, M., Shi, Q., Yang, F., and Wang, X. (2017). Carbohydrate accumulation and sucrose metabolism responses in tomato seedling leaves when subjected to different light qualities. *Sci. Hortic.* 225, 490–497. doi: 10.1016/j.scienta.2017.07.053

Ljung, K., Nemhauser, J. L., and Perata, P. (2015). New mechanistic links between sugar and hormone signalling networks. *Curr. Opin. Plant Biol.* 25, 130–137. doi: 10.1016/j.pbi.2015.05.022

McLaren, J. S., and Smith, H. (1978). Phytochrome control of the growth and development of *Rumex obtusifolius* under simulated canopy light environments. *Plant Cell Environ.* 1, 61–67. doi: 10.1111/j.1365-3040.1978.tb00748.x

Mekonnen, D. W., Flügge, U.-I., and Ludewig, F. (2016). Gamma-aminobutyric acid depletion affects stomata closure and drought tolerance of *Arabidopsis thaliana. Plant Sci.* 245, 25–34. doi: 10.1016/j.plantsci.2016.01.005

Michaeli, S., and Fromm, H. (2015). Closing the loop on the GABA shunt in plants: are GABA metabolism and signaling entwined? *Front. Plant Sci.* 6 (419), 1–7. doi: 10.3389/fpls.2015.00419

Mishra, B. S., Singh, M., Aggrawal, P., and Laxmi, A. (2009). Glucose and auxin signaling interaction in controlling *Arabidopsis thaliana* seedlings root growth and development. *PLoS One* 4, e4502. doi: 10.1371/journal.pone.0004502

Morales, L. O., Tegelberg, R., Brosché, M., Keinänen, M., Lindfors, A., and Aphalo, P. J. (2010). Effects of solar UV-A and UV-B radiation on gene expression and phenolic accumulation in *Betula pendula* leaves. *Tree Physiol.* 30, 923–934. doi: 10.1093/treephys/tpq051

Murphy, G. P., and Dudley, S. A. (2009). Kin recognition: competition and cooperation in Impatiens (Balsaminaceae). *Am. J. Bot.* 96, 1990–1996. doi: 10.3732/ajb.0900006

Nawkar, G. M., Maibam, P., Park, J. H., Sahi, V. P., Lee, S. Y., and Kang, C. H. (2013). UV-induced cell death in plants. *Int. J. Mol. Sci.* 14, 1608–1628. doi: 10.3390/ijms14011608

Nunes-Nesi, A., Fernie, A. R., and Stitt, M. (2010). Metabolic and signaling aspects underpinning the regulation of plant carbon nitrogen interactions. *Mol. Plant* 36, 973–996. doi: 10.1093/mp/ssq049

Obata, T., and Fernie, A. R. (2012). The use of metabolomics to dissect plant responses to abiotic stresses. *Cell. Mol. Life Sci.* 69, 3225–3243. doi: 10.1007/s00018-012-1091-5

Ohashi-Kaneko, K., Matsuda, R., Goto, E., Fujiwara, K., and Kurata, K. (2006). Growth of rice plants under red light with or without supplemental blue light. *Soil Sci. Plant Nutr.* 52, 444–452. doi: 10.1111/j.1747-0765.2006.00063.x

Ouzounis, T., Rosenqvist, E., and Ottosen, C.-O. (2015). Spectral effects of artificial light on plant physiology and secondary metabolism: a review. *Hortscience* 50, 1128–1135. doi: 10.21273/HORTSCI.50.8.1128

Park, Y., and Runkle, E. S. (2017). Far-red radiation promotes growth of seedlings by increasing leaf expansion and whole-plant net assimilation. *Environ. Exp. Bot.* 136, 41–49. doi: 10.1016/j.envexpbot.2016.12.013

Péret, B., Larrieu, A., and Bennett, M. J. (2009). Lateral root emergence: a difficult birth. *J. Exp. Bot.* 60, 3637–3643. doi: 10.1093/jxb/erp232

Poorter, H., Niklas, K. J., Reich, P. B., Oleksyn, J., Poot, P., and Mommer, L. (2012). Biomass allocation to leaves, stems and roots: meta-analyses of interspecific variation and environmental control. *New Phytol.* 193, 30–50. doi: 10.1111/j.1469-8137.2011.03952.x

Procko, C., Crenshaw, C. M., Ljung, K., Noel, J. P., and Chory, J. (2014). Cotyledon-generated auxin is required for shade-induced hypocotyl growth in *Brassica rapa*. *Plant Physiol.* 165, 1285–1301. doi: 10.1104/pp.114.241844

Rattanapichai, W., and Klem, K. (2016). Two-dimensional root phenotyping system based on root growth on black filter paper and recirculation micro-irrigation. *Czech J. Genet. Plant Breed.* 52, 64–70. doi: 10.17221/121/2015-CJGPB

Roberts, M. R. (2007). Does GABA act as a signal in plants? Hints from molecular studies. *Plant Signal. Behav.* 2, 408–409. doi: 10.4161/psb.2.5.4335

Robson, T. M., Klem, K., Urban, O., and Jansen, M. A. K. (2015). Re-interpreting plant morphological responses to UV-B radiation. *Plant Cell Environ.* 385, 856–866. doi: 10.1111/pce.12374

Royer, M., Larbat, R., Le Bot, J., Adamowicz, S., and Robin, C. (2013). Is the C:N ratio a reliable indicator of C allocation to primary and defence-related metabolisms in tomato? *Phytochemistry* 88, 25–33. doi: 10.1016/j.phytochem.2012.12.003

Ruiz-Vera, U. M., De Souza, A. P., Long, S. P., and Ort, D. R. (2017). The role of sink strength and nitrogen availability in the down-regulation of photosynthetic capacity in field-grown *Nicotiana tabacum* L. at elevated $CO_2$ concentration. *Front. Plant Sci.* 8 (998), 1–12. doi: 10.3389/fpls.2017.00998

Sadras, V. O., Hall, A. J., Trapani, N., and Vilella, F. (1989). Dynamics of rooting and root-length: leaf-area relationships as affected by plant population in sunflower crops. *Field Crops Res.* 22, 45–57. doi: 10.1016/0378-4290(89)90088-9

Saini, S., Sharma, I., Kaur, N., and Pati, P. K. (2013). Auxin: a master regulator in plant root development. *Plant Cell Rep.* 32, 741–757. doi: 10.1007/s00299-013-1430-5

Seto, Y., Kameoka, H., Yamaguchi, S., and Kyozuka, J. (2012). Recent advances in strigolactone research: chemical and biological aspects. *Plant Cell Physiol.* 53, 1843–1853. doi: 10.1093/pcp/pcs142

Smith, C. A., Want, E. J., O'Maille, G., Abagyan, R., and Siuzdak, G. (2006). XCMS: processing mass spectrometry data for metabolite profiling using nonlinear peak alignment, matching, and identification. *Anal. Chem.* 78, 779–787. doi: 10.1021/ac051437y

Stewart, J. L., Maloof, J. N., and Nemhauser, J. L. (2011). PIF genes mediate the effect of sucrose on seedling growth dynamics. *PLoS One* 6, e19894. doi: 10.1371/journal.pone.0019894

Suzuki, A., Suriyagoda, L., Shigeyama, T., Tominaga, A., Sasaki, M., Hiratsuka, Y., et al. (2011). *Lotus japonicus* nodulation is photomorphogenetically controlled by sensing the red/far red (R/FR) ratio through jasmonic acid (JA) signaling. *Proc. Natl. Acad. Sci. U. S. A.* 108, 16837–16842. doi: 10.1073/pnas.1105892108

Svyatyna, K., and Riemann, M. (2012). Light-dependent regulation of the jasmonate pathway. *Protoplasma* 249, 137–145. doi: 10.1007/s00709-012-0409-3

Tilbrook, K., Arongaus, A. B., Binkert, M., Heijde, M., Yin, R., and Ulm, R. (2013). The UVR8 UV-B photoreceptor: perception, signaling and response. *Arabidopsis Book* 11 (e0164), 1–21. doi: 10.1199/tab.0164

Uchytilová, T., Krejza, J., Veselá, B., Holub, P., Urban, O., Horáček, P., et al. (2019). Ultraviolet radiation modulates C:N stoichiometry and biomass allocation in *Fagus sylvatica* saplings cultivated under elevated $CO_2$ concentration. *Plant Physiol. Biochem.* 134, 103–112. doi: 10.1016/j.plaphy.2018.07.038

Verdaguer, D., Jansen, M. A. K., Llorens, L., Morales, L. O., and Neugart, S. (2017). UV-A radiation effects on higher plants: exploring the known unknown. *Plant Sci.* 255, 72–81. doi: 10.1016/j.plantsci.2016.11.014

Walter, S., Nicholson, P., and Doohan, F. M. (2010). Action and reaction of host and pathogen during *Fusarium* head blight disease. *New Phytol.*, 185, 54–66. doi: 10.1111/j.1469-8137.2009.03041.x

Wang, J., Lu, W., Tong, Y., and Yang, Q. (2016). Leaf morphology, photosynthetic performance, chlorophyll fluorescence, stomatal development of lettuce (*Lactuca sativa* L.) exposed to different ratios of red light to blue light. *Front. Plant Sci.* 7 (250), 1–10 . doi: 10.3389/fpls.2016.00250

Wang, L., and Ruan, Y.-L. (2016). Shoot–root carbon allocation, sugar signalling and their coupling with nitrogen uptake and assimilation. *Funct. Plant Biol.* 43, 105–113. doi: 10.1071/FP15249

Yang, C., and Li, L. (2017). Hormonal regulation in shade avoidance. *Front. Plant Sci.* 8 (1527), 1–8. doi: 10.3389/fpls.2017.01527

Zhang, L., Allen, L. H., Vaughan, M. M., Hauser, B. A., and Boote, K. J. (2014). Solar ultraviolet radiation exclusion increases soybean internode lengths and plant height. *Agric. For. Meteorol.* 184, 170–178. doi: 10.1016/j.agrformet.2013.09.011

**Conflict of Interest Statement:** The authors declare that the research was conducted in the absence of any commercial or financial relationships that could be construed as a potential conflict of interest.

frontiers in Plant Science

ORIGINAL RESEARCH
published: 10 December 2019
doi: 10.3389/fpls.2019.01584

# Light Control of Salt-Induced Proline Accumulation Is Mediated by ELONGATED HYPOCOTYL 5 in *Arabidopsis*

*Hajnalka Kovács[1†], Dávid Aleksza[1†], Abu Imran Baba[1], Anita Hajdu[1], Anna Mária Király[1], Laura Zsigmond[1], Szilvia Z. Tóth[1], László Kozma-Bognár[1,2] and László Szabados[1]**

[1] Institute of Plant Biology, Biological Research Centre, Szeged, Hungary, [2] Department of Genetics, Faculty of Sciences and Informatics, University of Szeged, Szeged, Hungary

Plants have to adapt their metabolism to constantly changing environmental conditions, among which the availability of light and water is crucial in determining growth and development. Proline accumulation is one of the sensitive metabolic responses to extreme conditions; it is triggered by salinity or drought and is regulated by light. Here we show that red and blue but not far-red light is essential for salt-induced proline accumulation, upregulation of *Δ1-PYRROLINE-5-CARBOXYLATE SYNTHASE 1* (*P5CS1*) and downregulation of *PROLINE DEHYDROGENASE 1* (*PDH1*) genes, which control proline biosynthetic and catabolic pathways, respectively. Chromatin immunoprecipitation and electrophoretic mobility shift assays demonstrated that the transcription factor ELONGATED HYPOCOTYL 5 (HY5) binds to G-box and C-box elements of *P5CS1* and a C-box motif of *PDH1*. Salt-induced proline accumulation and *P5CS1* expression were reduced in the *hy5hyh* double mutant, suggesting that HY5 promotes proline biosynthesis through connecting light and stress signals. Our results improve our understanding on interactions between stress and light signals, confirming HY5 as a key regulator in proline metabolism.

**Keywords: ELONGATED HYPOCOTYL 5, proline accumulation, *Arabidopsis*, light signalling, gene expression regulation**

OPEN ACCESS

***Edited by:***
*Radomira Vankova, Academy of Sciences of the Czech Republic, Czechia*

***Reviewed by:***
*Sandeep Sharma, Council of Scientific and Industrial Research (CSIR), India*
*Santiago Signorelli, Universidad de la República, Uruguay*

***Correspondence:**
*László Szabados*
*szabados.laszlo@brc.hu*

*†These authors have contributed equally to this work*

***Specialty section:***
*This article was submitted to Plant Abiotic Stress, a section of the journal Frontiers in Plant Science*

***Received:*** *30 October 2018*
***Accepted:*** *12 November 2019*
***Published:*** *10 December 2019*

***Citation:***
*Kovács H, Aleksza D, Baba AI, Hajdu A, Király AM, Zsigmond L, Tóth SZ, Kozma-Bognár L and Szabados L (2019) Light Control of Salt-Induced Proline Accumulation Is Mediated by ELONGATED HYPOCOTYL 5 in Arabidopsis. Front. Plant Sci. 10:1584. doi: 10.3389/fpls.2019.01584*

## INTRODUCTION

Proline accumulates to high levels in plants at low water potential caused by drought, salinity and in response to several other abiotic and biotic stresses (Kemble and Macpherson, 1954; Schat et al., 1997; Fabro et al., 2004; Yang et al., 2009; Szabados and Savoure, 2010; Aleksza et al., 2017). Proline was suggested to act as osmoprotectant stabilizing enzymes or maintaining redox equilibrium in adverse conditions (Delauney and Verma, 1993; Székely et al., 2008; Szabados and Savoure, 2010; Verslues and Sharma, 2010; Kavi Kishor and Sreenivasulu, 2014; Per et al., 2017). Free proline content is defined by biosynthesis and degradation, and modulated by transport, protein synthesis, and degradation (Lehmann et al., 2010; Verslues and Sharma, 2010; Hildebrandt, 2018). The main biosynthetic pathway has two consecutive steps catalyzed by the rate-limiting *Δ[1]-pyrroline-carboxylate synthetase* (*P5CS*) enzyme (Hu et al., 1992) followed by P5C reductase (P5CR) (Delauney and Verma, 1990). Proline biosynthesis takes place in cytosol, although localization of P5CS1-GFP protein

in chloroplasts of salt-treated cells suggest that biosynthesis may take place in plastids under stress conditions (Székely et al., 2008). Proline degradation is a mitochondrial oxidative process, mediated by the rate-limiting proline dehydrogenase (PDH) and P5C dehydrogenase (P5CDH) enzymes (Kiyosue et al., 1996; Servet et al., 2012). In most plants P5CS is encoded by two genes. In *Arabidopsis P5CS1* (*AT2G39800*) responds to hyperosmotic stress and is regulated by ABA-dependent and independent signals, whereas *P5CS2* (*AT3G55610*) is considered to be a housekeeping gene, which can be induced by certain pathogens *via* salicylic acid-dependent signals (Savouré et al., 1997; Strizhov et al., 1997; Fabro et al., 2004; Székely et al., 2008; Sharma and Verslues, 2010). *PDH1* (*AT3G30775*) is repressed in high osmotic conditions and is induced by proline during stress recovery (Kiyosue et al., 1996). Compared to *PDH1, PDH2* has a very low expression level, which is however induced during phosphate starvation (Aleksza et al., 2017). ABA, reactive oxygen species, calcium, and lipid signals were implicated in the regulation of proline metabolism (Thiery et al., 2004; Parre et al., 2007; Ben Rejeb et al., 2015). Although important progress has been made in the last few years, transcription regulation of key genes in proline metabolism is far from well understood. A number of *cis* regulatory sequences have been identified in promoters or 5′UTRs of key metabolic genes, but direct evidence on promoter-binding transcription factors and their function is scarce (Fichman et al., 2015; Zarattini and Forlani, 2017). We have recently described that PHOSPHATE STARVATION RESPONSE 1 (PHR1) and PHOSPHATE STARVATION RESPONSE LIKE-1 (PHL1) transcription factors bind the P1BS motif in the first intron of *P5CS1,* upregulate its expression, and promote proline accumulation during phosphate starvation (Aleksza et al., 2017). A recent report showed that the transcription factor ANAC55 (*Arabidopsis* NAM, ATAF, and CUC) is a positive regulator of *P5CS1* expression and proline accumulation in high osmotic conditions, although direct binding to *P5CS1* promoter elements was not demonstrated (Fu et al., 2018). Allelic variation in the barley *P5CS1* gene was recently reported, showing that promoter mutations in the abscisic acid-responsive element (ABRE) can considerably alter *P5CS1* expression, proline accumulation, and drought tolerance (Muzammil et al., 2018). Some information is available on transcriptional regulation of *PDH1.* Basic leucine zipper (bZIP) transcription factors of the ATB2 subgroup were shown to upregulate *PDH1* expression during hypoosmolarity through binding to the ACTCAT *cis*-acting promoter element (Satoh et al., 2002; Satoh et al., 2004; Weltmeier et al., 2006). Chromatin immunoprecipitation (ChIP) analysis confirmed that bZIP1 and bZIP53 factors bind to the *PDH1* promoter and upregulate it in low energy conditions (Dietrich et al., 2011). Besides transcriptional control, epigenetic regulation and alternative splicing were shown to influence the expression of the *P5CS1* and *PDH1* genes (Kesari et al., 2012; Jimenez-Arias et al., 2015). Histone methylation was recently shown to control stress memory response of *P5CS1* in *Arabidopsis* (Feng et al., 2016).

Light was found to influence proline levels by inducing *P5CS1* and repressing *PDH1* expression (Hayashi et al., 2000; Abraham et al., 2003; Diaz et al., 2005). While considered as a housekeeping gene, *P5CS2* was identified as a target of CONSTANS (CO) and is therefore also subject to light and flowering time regulation (Samach et al., 2000). Datamining of publicly available transcript profiling data (Dubois et al., 2017) suggested reciprocal fluctuation of the expression of the *P5CS1* and *PDH1* genes in response to light and drought (**Figure S1**).

Light can influence gene expression in various ways. Light perception through photoreceptors is mediated by phytochromes (PHYA-E) absorbing red/far-red light, cryptochromes (CRY1-2) sensing blue light and phototropins (PHOT1-2), which absorb blue and additionally UV-A light (Briggs and Christie, 2002; Franklin and Quail, 2010; Kami et al., 2010; Chaves et al., 2011). bHLH-type phytochrome-interacting factors repress photomorphogenic development and promote the expression of light-repressed genes, but are degraded upon interaction with the active forms of phytochrome receptors (Leivar and Monte, 2014). The bZIP-type transcription factor ELONGATED HYPOCOTYL 5 (HY5) is a phytochrome-interacting factor antagonist that acts downstream of virtually all classes of photoreceptors, and promotes photomorphogenesis and the expression of light-induced genes (Cluis et al., 2004; Toledo-Ortiz et al., 2014). Crosstalk between light and several other signaling pathways has been demonstrated, in which HY5 can function as a signaling hub. HY5 directly interacts with ACGT-containing (ACE) Light-Responsive Elements in the promoters of light-induced genes and upregulates their transcription (Chattopadhyay et al., 1998). Signals from photoreceptors promote accumulation of HY5 at transcriptional and posttranscriptional levels (Binkert et al., 2014; Sheerin et al., 2015), but apparently do not affect the DNA-binding affinity or specificity of the HY5 protein (Hajdu et al., 2018). HY5 lacks any domains with transcriptional regulator function, thus it requires co-factors to control gene expression (Li et al., 2010) and is supposed to act as a component of multiprotein complexes. More recently the role of HY5 in multiple signaling systems was uncovered, showing that, together with the closely related HY5-HOMOLOG (HYH) factor, it integrates light, hormonal, and developmental regulation through multiple interactions with other transcription factors and regulatory proteins (Gangappa and Botto, 2016). A recent paper described that the stress-induced transcription memory of *P5CS1* is influenced by light and is mediated by HY5, able to bind to C/A-box sequence elements in the *P5CS1* promoter and 5′ UTR region (Feng et al., 2016). HY5 was also shown to modulate ABA signaling by promoting *ABI5* expression through binding to its promoter (Chen et al., 2008). Light and ABA regulation is influenced by the C2H2-type zinc finger protein ZFP3, which represses ABA signals and promotes photomorphogenesis (Joseph et al., 2014). Responses to light signals can be fine-tuned by the EREBP-type ABI4 which is implicated in ABA and sugar signaling (Wind et al., 2012). Interacting light, ABA and stress signals are therefore influenced by different sets of transcription factors such as the bZIP-type HY5 and ABI5, the C2H2-type ZFP3, or the EREBP-type ABI4.

In addition to perception through photoreceptors, light also affects the expression of a set of nuclear genes by chloroplast retrograde signaling which depends on light reactions of photosynthesis (Gollan et al., 2015). In this regulatory system chloroplasts acts as sensors and signaling components include

sugar and carotenoid metabolites, reactive oxygen species, plastoquinone pool redox state, and various classes of regulatory proteins such as protein kinases and transcription factors. Chloroplast-derived signals control chloroplast development and responses to environmetal stresses (Fey et al., 2005; Fernandez and Strand, 2008; Gollan et al., 2015; Kleine and Leister, 2016; D'Alessandro et al., 2018).

This communication focuses on the light-dependent control of proline metabolism. We show that HY5 binds to conserved sequence elements of the *P5CS1* and *PDH1* genes and can positively contribute to salt-induced proline accumulation. HY5 seems to function as a regulatory hub that integrates light and stress signals in the control of proline metabolism. We conclude that proline metabolism is controlled by multiple regulatory pathways and is influenced by interacting stress and light signals.

## RESULTS

### Proline Accumulation Is Influenced by Light

To characterize light-dependent proline accumulation in *Arabidopsis*, an *in vitro* experimental system was designed: Fourteen-day-old plantlets were treated with high intensity light (550 μE $m^{-2}$ $s^{-1}$) or deprived of light for up to 5 days, and subsequently salt or ABA-triggered proline accumulation was monitored periodically (**Figure 1A**). When plants were irradiated with strong light for several days, proline levels accumulated up to three times higher as compared to plants kept under standard light conditions (**Figure 1B**). Proline accumulation was compromised in the *p5cs1-1* mutant (Székely et al., 2008), suggesting that the *P5CS1* gene controls the rate-limiting step in proline accumulation in these conditions. In standard light conditions 1-day 10 μM ABA and 150 mM NaCl treatments lead to two or five times higher proline contents, respectively. When plants were deprived of light, proline accumulation was considerably smaller: 1 day of dark adaptation reduced proline levels from 40% to 60% of light cultured plants, whereas 5 days in darkness prevented the enhancement of proline content (**Figure 1C**). The negative effect of dark on proline accumulation may derive from the lack of adequate light or photoreceptor-derived signals reducing proline biosynthesis and/or inducing catabolism. Alternatively, if energy shortage prevents proline accumulation in dark, then externally added sugar should compensate for the absence of light. To test energy dependence, proline concentrations were measured in dark-adapted plants in the presence of various concentrations of sucrose. Proline contents in dark-adapted plants were similar in the presence of 0% and 2% (W/V) sucrose in the culture medium, whereas 4% (W/V) sucrose significantly enhanced proline accumulation. Proline levels in these conditions were, however, still far inferior to those in illuminated plants, which accumulated five to ten times more proline (**Figure 1D**). When proline content was compared in plants treated with sucrose, glucose, or mannitol, only minor differences were observed (**Figure S2**). These results suggest that sugar-dependent glycolysis cannot

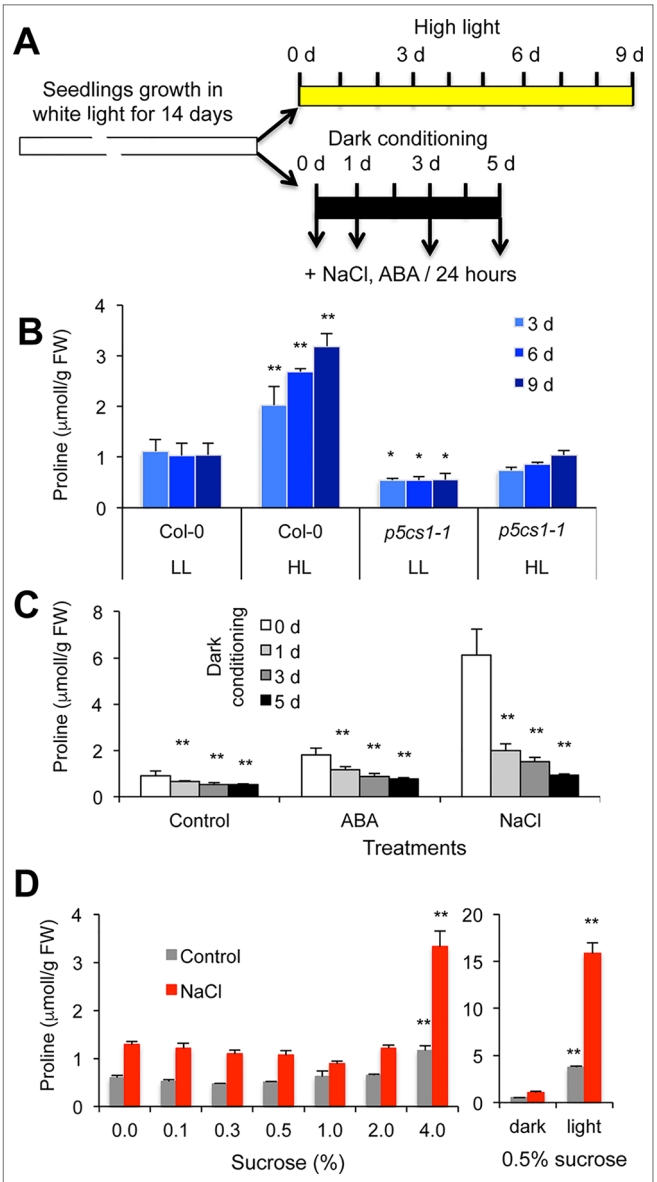


**FIGURE 1 |** Light-dependent proline accumulation in wild-type *Arabidopsis* plants. **(A)** Experimental design. **(B)** Proline accumulation in plants after high-intensity light treatment. Plants were grown *in vitro* under standard conditions for 14 days, then transferred to high-intensity light (white light, 550 μE $m^{-2}$ $s^{-1}$, 8/16 h light/dark cycle) for up to 9 days. LL: low light condition, HL: high-intensity light. **(C)** Proline accumulation in dark-conditioned plants. Fourteen-day-old plantlets were transferred to dark for 1, 3, and 5 days, then subjected to salt (150 mM NaCl) or ABA (10 μM ABA) treatment in darkness for 24 h. 0 d, 1 d, 3 d, and 5 d indicates the number of days in dark. **(D)** Effect of different sugar concentrations on proline levels in dark-conditioned plants. Fourteen-day-old plants were transferred to media with different sucrose concentrations [0 to 4% (W/V)] and placed to dark for 5 days. Plants were subsequently treated with or without 150 mM NaCl and the same sugar concentrations, for 48 h. The right diagram shows proline accumulation in dark-conditioned and light-grown plants cultured on standard culture medium containing 0.5% (W/V) sucrose. Error bars indicate SD (N = 5). Significant differences compared to Col-0 plants in low light conditions **(B)**, 0 day of dark treatment **(C)** or plants cultured on standard 0.5% (W/V) sucrose **(D)** are shown: * $p < 0.05$, ** $p < 0.01$, (one-way ANOVA, Tukey test).

compensate for the lack of light signals or other photosynthesis-derived metabolites such as NADPH.

Light generates specific signals, which can trigger biosynthetic and/or repress catabolic pathways. Light signals are perceived by specific photoreceptors, each of them possessing well-defined sensitivity to a particular spectrum of light (Franklin and Quail, 2010; Chaves et al., 2011). To test the effect of light quality on proline metabolism, dark-conditioned plants were transferred to white or monochromatic red, far-red or blue lights with or without simultaneous salt stress (**Figure 2A**). The light intensities for each light qualities (white light: fluorescent cool white, 4200 K, 60 μE $m^{-2}$ $s^{-1}$, monochromatic blue: 470 nm, 15 μE $m^{-2}$ $s^{-1}$, red: 660 nm, 15 μE $m^{-2}$ $s^{-1}$, or far-red: 730 nm, 5 μE $m^{-2}$ $s^{-1}$ light), were sufficient to saturate photoreceptors and light signaling cascades but not the photosynthetic electron transport (Wolf et al., 2011; Adam et al., 2013). In the absence of salt stress, proline levels increased under white, red and blue light, but remained unchanged in darkness or under far-red light (**Figure 2B**). Proline concentrations increased more than 10-fold in salt-treated plants under white or red light, whereas under blue light 5-fold enhancement was measured. Salt stress could only slightly augment free proline content in plants kept in dark or illuminated by monochromatic far-red light (**Figure 2B**). The effect of white and monochromatic light on proline accumulation was similar in Columbia 0 (Col-0) and Wassilewskija (WS) ecotypes (**Figure S3**). These results suggest that to promote proline accumulation, red is the most efficient component of the light spectrum followed by blue, whereas far-red light is insufficient.

To investigate the molecular background of light-dependent proline accumulation, expression patterns of the key metabolic genes *P5CS1* and *PDH1* were monitored under different light regimes with or without salt treatment. Transcript levels of *P5CS1* were significantly higher in plants illuminated with white, red, and blue light than in plants kept in dark or illuminated by far-red light. Salt treatment enhanced *P5CS1* expression in all light conditions, and transcript levels were highest under white and red lights followed by blue, but were moderately enhanced in far-red light or in darkness (**Figure 2C**, **Figure S4**). *PDH1* expression was downregulated by white, red, and blue light and not affected significantly under far-red light. Salt treatment repressed *PDH1* expression even more in most light conditions, including in darkness (**Figure 2C**, **Figure S4**). These results suggest that besides white light, red, and blue monochromatic lights are efficient in promoting *P5CS1* and suppressing *PDH1* expression, which ultimately leads to high levels of proline accumulation when plants are exposed to salt stress.

In order to investigate whether photosynthetic electron transport is required for proline accumulation, leaves were treated with 3-(3′,4′-dichlorophenyl)-1,1-dimethylurea (DCMU) in combination with salt (**Figure S5**). DCMU binds irreversibly to the acceptor side of photosystem II thereby inhibiting linear electron transport, which results in altered fast chlorophyll *a* fluorescence (OJIP) kinetics. Upon full inhibition, the J ($F_{2ms}$) step equals the maximum fluorescence ($F_M$ or P) intensity (Tóth et al., 2007), as seen also in **Figure S5C**. The DCMU treatment alone had no effect on proline levels, whereas NaCl-induced proline accumulation was significantly reduced (**Figure S5A**). In the presence of DCMU *P5CS1* induction was slightly reduced in salt-treated plants, whereas *PDH1* was upregulated in both salt-treated and control plants (**Figure S5B**).

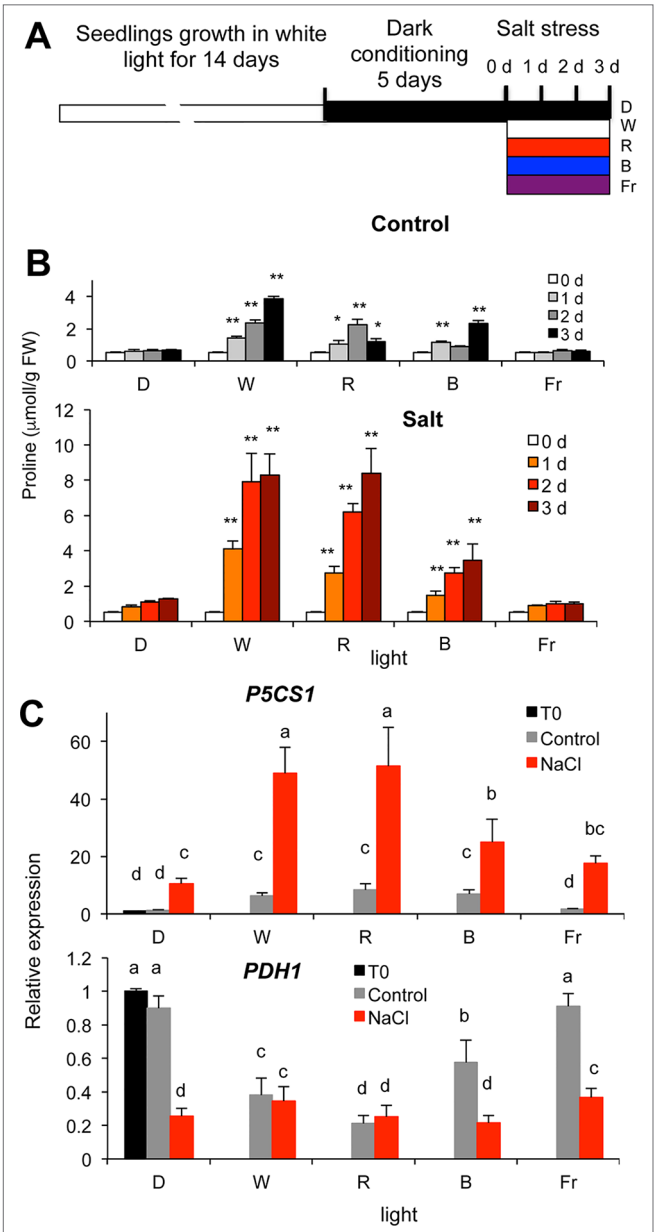


**FIGURE 2 |** Proline accumulation in salt-treated wild-type *Arabidopsis* plants under different light regimes. **(A)** Experimental design. **(B)** Proline accumulation in dark-conditioned plants, which were subsequently kept in dark (D), illuminated by white (W), monochromatic blue (B), red (R), or far red (Fr) light, with or without salt treatment (150 mM NaCl) for up to 3 days. Significant differences to dark samples are shown (N = 6): * $p < 0.05$, ** $p < 0.01$ (one-way ANOVA, Tukey test). **(C)** Expression of the *P5CS1* and *PDH1* genes in dark-conditioned plants treated with or without 150 mM NaCl for 1 day, under different light conditions (see above). Relative transcript levels are shown, normalized to *ACT2* and *UBQ1* as well as to dark-conditioned plants, where 1 corresponds to transcript level at 0 day (T0). Error bars indicate SD (N = 3). Significant differences between means are shown by different letters ($p < 0.05$, one-way ANOVA, Tukey test).

## HY5 Binds to Promoter Elements of the *P5CS1* and *PDH1* Genes

The bZIP-type transcription factor HY5 is a key positive regulator of light-dependent gene expression that controls transcription of thousands of light-induced genes (Cluis et al., 2004; Toledo-Ortiz et al., 2014). A recent ChIP-seq analysis of HY5 binding sites revealed that this transcription factor recognizes conserved *cis*-acting elements in more than three thousand genes, both under red and blue light (Hajdu et al., 2018). Genome-wide mapping of HY5 binding sites revealed that this TF can recognize the promoter regions of the *P5CS1* and *PDH1* genes (**Figures S6**, **S7**). While peak of the reads were mapped close to the transcription initiation site of *P5CS1*, maximum reads were localized to 0.5 kb upstream of the *PDH1* transcription initiation site. Another recent study revealed binding of HY5 to the 5′ UTR and a distal upstream region of *P5CS1* (Feng et al., 2016). Promoter and 5′ UTR regions of *P5CS1* contain a number of predicted regulatory sequence motifs, including a G-box (CACGTG) at +172 bp in the 5′ UTR and a C-box (GACGTC) in the promoter, at −59 bp distance from the transcription start site, which can serve as binding sites of HY5 (**Figure 3A**) (Fichman et al., 2015). The *PDH1* promoter contains one conserved C-box motif in the promoter, at −553 bp distance from the transcription start site (**Figure 3A**).

To verify HY5 binding in the identified regulatory regions, ChIP followed by quantitative PCR (ChIP-qPCR) assays were performed on *P5CS1* and *PDH1* promoter fragments containing the predicted G-box and C-box sequence motifs. When compared to intergenic regions, specific enrichment in qPCR-amplified C-box- and G-box-containing *P5CS1* and *PDH1* promoter fragments was detected in the HY5-YFP-immunoprecipitated DNA samples (**Figure 3B**). Enrichment of HY5 binding to *P5CS1* G-box and C-box regions was around 14 to 16 times higher while it was 5 times higher on C-box region of the *PDH1* promoter than on a control intergenic region (**Figure 3B**). ChIP-qPCR experiments therefore confirmed that HY5 interacts *in vivo* with the selected 5′ UTR and promoter regions of both the *P5CS1* and the *PDH1* genes. To compare our results with previously reported HY5 assays, ChIP assay was performed with primers used to amplify Region 2 and Region 5 of *P5CS1*, as defined by Feng et al. (2016). Region 2 is a 140 bp fragment, in the 5′ UTR (from −5 to +135 bp), flanked by C-box and G-box sequences. Region 5 is a 147 bp fragment in the upstream region (from −2129 to −2276 bp), which corresponds the previously described "Essential for Memory Fragment" (EMF) (Feng et al., 2016). In our experimental conditions enrichment of Region 2 in ChIP assay was similar to fragments containing G-box and C-box elements, whereas enrichment was a magnitude lower when HY5 binding was tested for Region 5, corresponding to EMF (**Figure 3B**).

To verify that the conserved C-box and G-box motifs are indeed the targets of HY5, electrophoretic mobility shift assays (EMSA) were performed using 56 bp dsDNA fragments containing the native regulatory sequences or their mutated forms in which the conserved CACGTG or GACGTC sequence motifs were altered, eliminating the core ACGT sequence (**Figure 4A**). Complex formation of HY5 with ds oligonucleotides corresponding to wild-type *P5CS1* and *PDH1* promoter fragments was observed in the EMSA assays. Complexes between HY5 and oligoes carrying the mutated G-box or C-box sequences were, however, not formed or were detected at much lower level (**Figure 4B**). These experiments confirmed that the C-box and G-box sequences are indeed responsible for HY5 binding to the *P5CS1* promoter (−59 bp) or the 5′ UTR (+172 bp) regions as well as binding of the *PDH1* promoter (−553 bp) region.

## HY5 Regulates Proline Accumulation and Expression of the *P5CS1* and *PDH1* Genes

To study the function of HY5 in proline metabolism, free proline contents and transcript levels of *P5CS1* and *PDH1* genes were compared in wild-type (WS) and *hy5hyh* mutant plants carrying knockout mutations for both *HY5* and the closely related *HYH* genes (Hajdu et al., 2018). Wild-type and *hy5hyh* double mutant plants were conditioned to dark as described above, and were subsequently treated by salt under white and monochromatic red or blue light (**Figure 5A**). Compared to plants kept in darkness, proline levels were enhanced by illumination with both white and red or blue monochromatic lights. When compared to wild type, proline levels were not affected or were slightly lower in illuminated *hy5hyh* mutants without salt treatment (**Figures 5B**, **S8**). Salt stress enhanced proline contents three to six times in illuminated plants, while proline accumulation was around 50% lower in the *hy5hyh* mutant when compared to wild-type plants in the same conditions (**Figures 5B**, **S8**). When plants were kept in darkness, proline levels were only slightly increased by salt treatment, and enhancement was similar in both genotypes.

*P5CS1* transcript levels were low in both wild-type and *hy5hyh* mutants without salt treatment with minor induction by illumination. *P5CS1* expression was clearly induced by 6 h of salt treatment in illuminated plants, reaching approximately 50% lower transcripts in the *hy5hyh* mutant than in wild-type plants (**Figures 5C**, **S9B**). In all light conditions transcript levels were higher after 6 h of stress than after 24 h (**Figure 5C**). *PDH1* expression was reduced by illumination and by salt stress in all light conditions. Genotype-dependent differences in *PDH1* transcript levels were however less pronounced and downregulation was more variable (**Figures 5D**, **S9C**). The *P5CS1* transcription pattern positively correlated with changes in proline levels, indicating that biosynthesis is essential in defining proline accumulation in these conditions, while *PDH1*-controlled catabolism can fine-tune proline levels. These data indicate that HY5 (and possibly HYH) is a positive regulator of proline accumulation by contributing to the expression of the *P5CS1* gene with a minor role in the control of *PDH1* expression.

# DISCUSSION

In this study we investigated the importance of light in salt-dependent proline accumulation, focusing on HY5-mediated light signals. A model summarizes our results integrating it with previous studies (**Figure 6**). Light was previously shown to

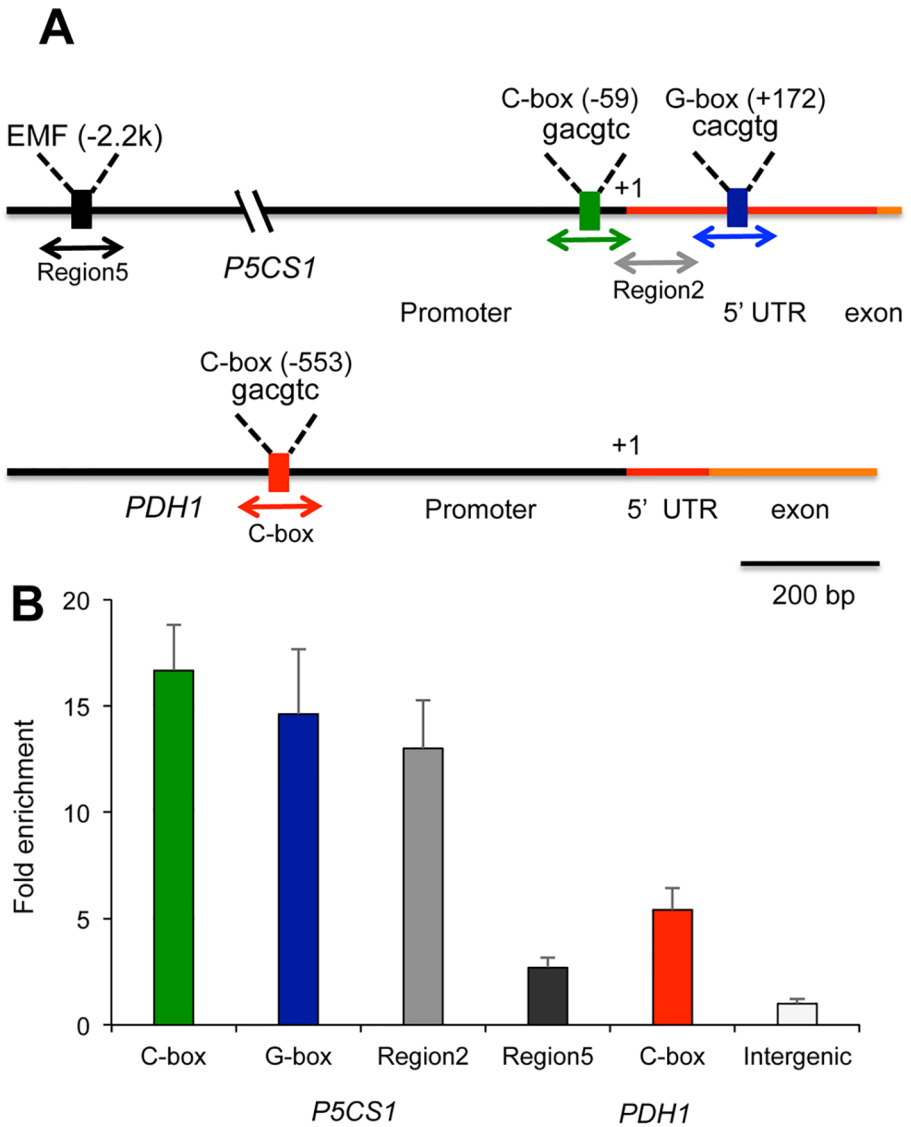


**FIGURE 3 |** Binding of HY5 on promoter regions of the *P5CS1* and *PDH1* genes. **(A)** Schematic structure of the *P5CS1* and *PDH1* promoters indicating the positions of conserved G and C box elements and Region 2 and Region 5, according to (Feng et al., 2016). Color code: black line: promoter, red line: 5′UTR region, yellow line: exon. Boxes indicate the positions of predicted basic leucine zipper (bZIP) binding sites: black: "Essential for Memory Fragment" (EMF) (Feng et al., 2016), green: C-box, blue: G-box (*P5CS1* promoter), red box on *PDH1* promoter indicate C-box (AthaMap, http://www.athamap.de). Positions indicate distance from transcription start site (+1). Double arrows indicate the regions amplified by quantitative PCR (qPCR) after chromatin immunoprecipitation. **(B)** Result of chromatin immunoprecipitation followed by quantitative PCR (ChIP-qPCR) tests on two *P5CS1* and one *PDH1* promoter region. An intergenic region with no C or G-box sequences was used as reference (= 1). Error bars on diagrams indicate SD (N = 3).

promote proline accumulation and inversely influence *P5CS1* and *PDH1* expression in *Arabidopsis* plants (**Figure S1**, Hayashi et al., 2000; Abraham et al., 2003). Here we showed that high light enhances, while extended darkness reduces proline levels, and absence of light cannot be compensated by externally supplied sugar as energy source (**Figures 1**, **S2**). Proline metabolism in *Arabidopsis* was found to be controlled by red and blue lights but is less influenced by far red light (**Figures 2**, **S3**). We showed that light-dependent proline accumulation is regulated by HY5, a key bZIP-type transcription factor in light signaling which is known to be a positive regulator of photomorphogenesis (**Figures 5**, **S8**, **S9**, Holm et al., 2002; Toledo-Ortiz et al., 2014). Genome-wide ChIP-chip or ChIP-seq experiments revealed that HY5 directly controls around 10% of the *Arabidopsis* genes through binding to their promoters (Lee et al., 2007; Zhang et al., 2011; Hajdu et al., 2018). Datamining of the ChIP-seq supplementary datasets revealed that HY5 recognizes the 5′ regions of the *P5CS1* and *PDH1* genes, suggesting that these genes are direct targets of this bZIP factor (Hajdu et al., 2018) (**Figures S6**, **S7**). HY5 was found to bind directly to the promoter or 5′ UTR regions of the key metabolic genes *P5CS1* and *PDH1*, which modulate rate-limiting steps in proline biosynthesis and degradation. The 5′ regulatory region

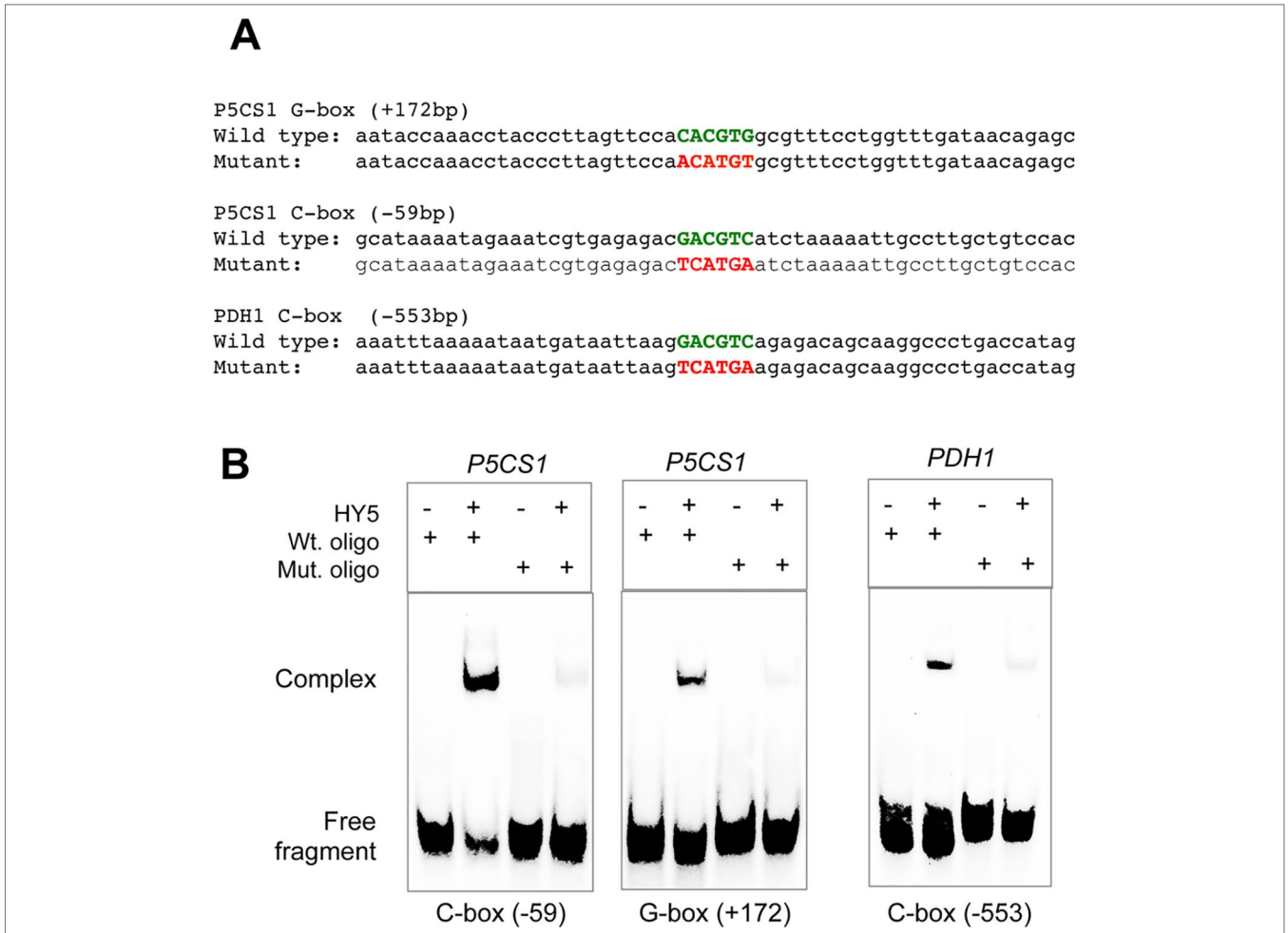


**FIGURE 4 |** Confirmation of TF binding sequence motifs with electrophoretic mobility assay (EMSA). **(A)** Sequences of the oligonucleotides containing wild-type and mutated G-box and C-box sequences of the *P5CS1* and *PDH1* promoters. **(B)** EMSA assays with wild-type (Wt. oligo) and mutant (Mut. oligo) double stranded oligonucleotides and purified HY5 protein. Note complex formation of HY5 protein with wild-type oligonucleotides, which is almost invisible with mutant ones with altered ACGT core sequences.

of *P5CS1* contains various *cis*-regulatory elements including a well-defined G-box in the 5′UTR region and a C-box motif in the promoter, which are conserved in *P5CS1* promoters of closely-related Brassicaceae species (Fichman et al., 2015). Sequence analysis revealed one C-box motif in the *PDH1* promoter. ChIP-qPCR experiments demonstrated *in vivo* binding of HY5 to at least three promoter regions of *P5CS1*, and one region of *PDH1*, which contained G-box or C-box sequence elements (**Figure 3**). EMSA experiments demonstrated that HY5 can directly and specifically bind to these sequence motifs *in vitro* (**Figure 4**). Promoter binding therefore strongly suggest that HY5 is directly involved in the control of *P5CS1* and *PDH1* transcription. G-box and C-box sequence motifs have an ACGT core, which is essential for binding of bZIP transcription factors, whereas nucleotides flanking the core sequence define the specificity of sequence recognition (Williams et al., 1992; Izawa et al., 1993). Mutations eliminating the ACGT core in the *P5CS1* and *PDH1* G-box and C-box motifs weakened or abolished HY5 binding to these DNA fragments, confirming that these promoter elements are indeed critical for the complex formation with this transcription factor (**Figure 4**). ACGT-containing sequence motifs are present in ABA Response Elements (ABRE), binding sites of bZIP-type AREB/ABF type transcription factors, which are key regulators of ABA-induced gene activation (Hobo et al., 1999; Fujita et al., 2005; Yoshida et al., 2010). Polymorphism in ABRE or adjacent CE motifs were recently shown to influence *P5CS1* expression and proline accumulation in barley, although TF binding to these motifs was not reported (Muzammil et al., 2018).

Two other HY5 binding regions were previously identified in the *Arabidopsis P5CS1* promoter, which were implicated in maintaining stress memory (Feng et al., 2016). Enhanced H3K4me3 levels near the *P5CS1* transcription start site were associated with light exposure and shown to correlate with transcript levels in repeated stresses. The distal EMF (Region 5 in **Figure 3**) is located 2.2 kb upstream of the transcription start site, and contains a C/A box, which can bind HY5 (Feng et al., 2016). Region 2 is located in 5′ UTR, which however has no recognizable sequence element for HY5 binding, but is flanked

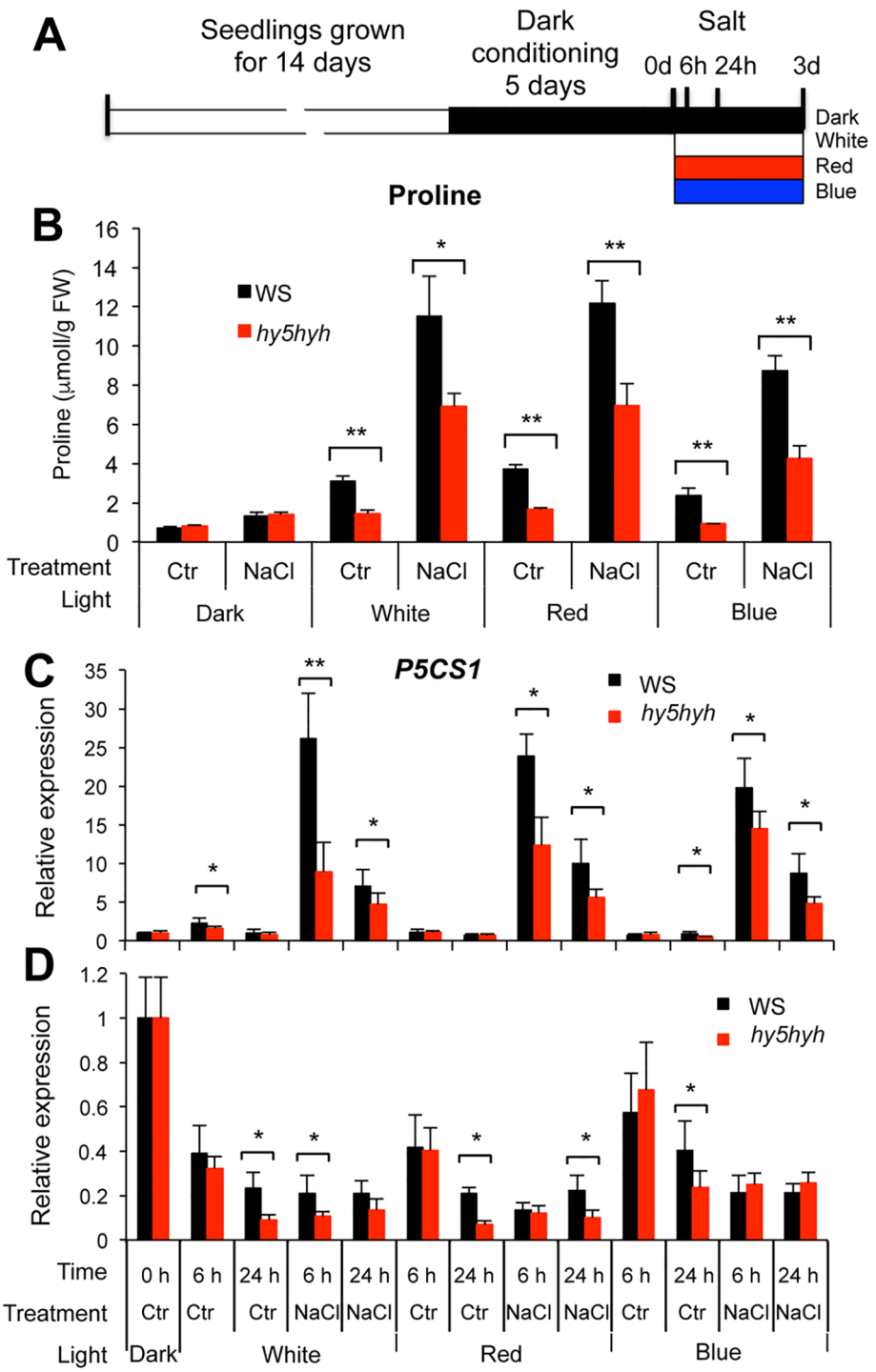


**FIGURE 5 |** Proline accumulation and expression of the *P5CS1* and *PDH1* genes in salt-treated wild-type and *hy5hyh* double mutant plants. **(A)** Experimental design: 14-day-old *in vitro*-grown plants were conditioned by dark treatment for 5 days and subsequently treated with or without 150 mM NaCl and illuminated with white or monochromatic red or blue light. **(B)** Proline accumulation in Wassilewskija (WS) wild-type and *hy5hyh* mutant plants after 3 days of salt treatment. Error bars indicate SD (N = 5). **(C, D)** Transcript levels of the *P5CS1* **(C)** and *PDH1* **(D)** genes after 6 and 24 h of salt treatment. Relative transcript levels are shown, which were normalized to *ACT2* and *UBQ1* reference genes as well as to dark-conditioned plants. Abbreviations: Ctr: control, NaCl: salt treatment. Error bars indicate SD (N = 3). Significant differences between wild type and mutant values are: * $p < 0.05$, ** $p < 0.01$ (two-way ANOVA, Tukey test, fixed parameters were genotypes and treatments).

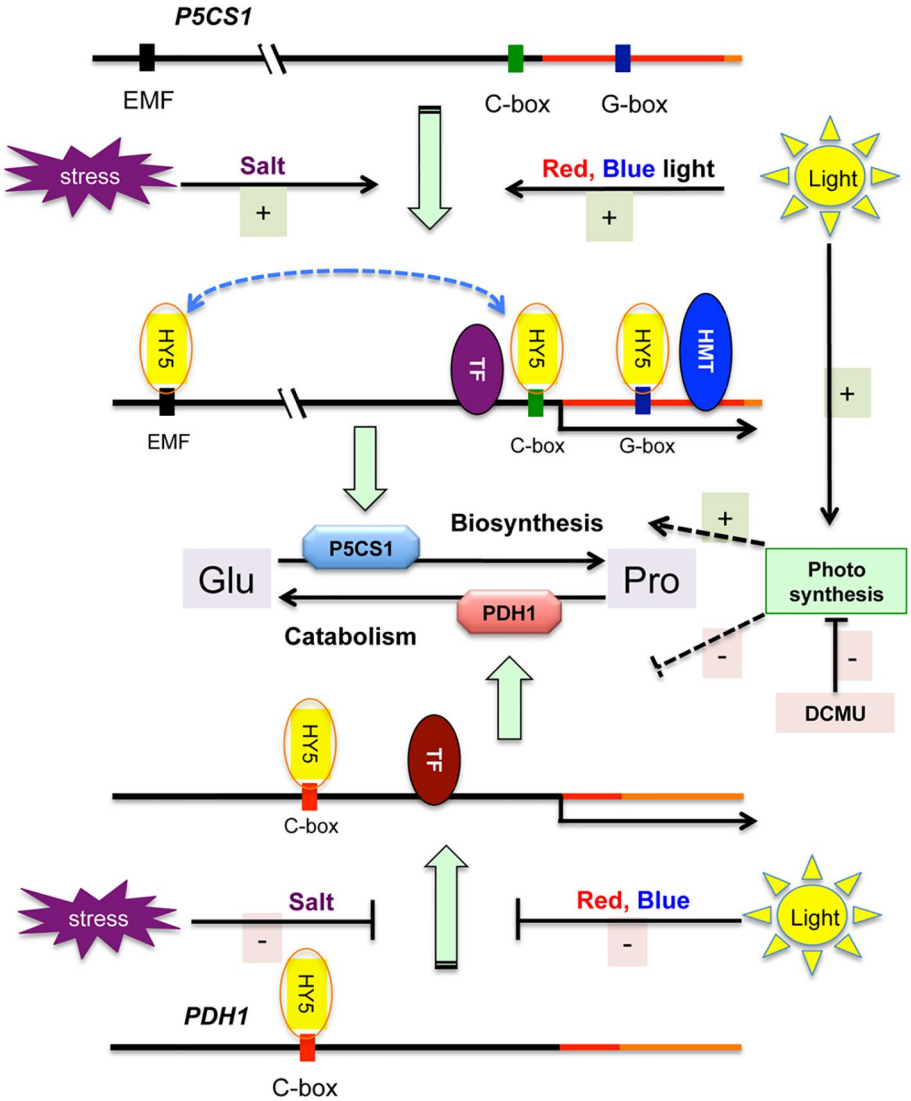


**FIGURE 6 |** Model of stress and light regulation of proline metabolism in *Arabidopsis*. Salt stress and light induces *P5CS1* and inhibits *PDH1* expression, promoting proline biosynthesis and reducing catabolism. Schematic maps of *P5CS1* (upper line) and *PDH1* (lower line) promoter and 5′ UTR regions are shown. Only HY5 binding sites are indicated in the schematic maps. HMT corresponds to histone merthyltransferase and TF indicates other transcription factors which can regulate transcription of *P5CS1* (Feng et al., 2016; Aleksza et al., 2017; Fu et al., 2018) or *PDH1* (Satoh et al., 2004; Weltmeier et al., 2006; Dietrich et al., 2011). Light-controlled HY5 binds to the promoters of both genes and contributes to *P5CS1* activation, but has only a minor effect on *PDH1* expression. Stress conditions as well as red and blue light activate *P5CS1* transcription (upper scheme), and inhibits *PDH1* activation (lower segment of the scheme). Photosynthesis can promote proline accumulation (probably enhancing biosynthesis and reducing catabolism) *via* an unknown mechanism, which is inhibited by 3-(3′,4′-dichlorophenyl)-1,1-dimethylurea (DCMU). Solid lines indicate confirmed, dashed lines show unknown/predicted interaction or regulation.

by the G-box and C-box sequence motifs, reported in this study. In our ChIP-qPCR assay similar degrees of enrichments were detected for G-box, C-box motifs and Region 2 of Feng et al. (2016) (**Figure 3**). ChIP technology has 300 to 400 bp resolution which can cover Region 2 and the flanking G-box and C-box motifs. ChIP-qPCR with primers in Region 2 could therefore detect chromatin fragments which were immunoprecipitated by the flanking G-box or C-box elements. Similar degrees of ChIP-qPCR enrichment were reported earlier for both Region 2 and Region 5 (Feng et al., 2016). In our ChIP assay binding efficiency of HY5 to Region 5 was however a magnitude lower than binding to C- or G-boxes (**Figure 3**). We used functional YFP-tagged HY5 and GFP-trap agarose beads for ChIP, whereas Feng et al. (2016) employed anti-HY5, which may explain the differences.

One of the key steps in the regulation of light-dependent gene expression is the photoreceptor-induced accumulation of the HY5 protein. Since this process is affected by virtually all photoreceptors, *hy5* mutants show photomorphogenic phenotypes, such as elongated hypocotyls not only in blue or red, but in far-red light as well (Abbas et al., 2014). Our data demonstrated that stress-induced proline accumulation did not occur in far-red light. One possibility is that far-red-derived

signals are insufficient for *P5CS1* induction and proline accumulation during salt stress. PHYA is the sole light receptor in *Arabidopsis* that can be activated by far-red light (Casal et al., 2014). Although PHYA signaling promotes the accumulation of HY5, apparently alone it cannot activate *P5CS1* transcription. Alternatively, low photosynthetic activity under far red light might prevent proline biosynthesis and promote catabolism *via* metabolic regulation (eg. due to low NAPDH pools) (Thapper et al., 2009; Pavlou et al., 2018).

Heterodimerization of bZIP transcription factors allows combinatorial control of target gene expression (Ehlert et al., 2006; Yoshida et al., 2010; Dietrich et al., 2011). HY5 and the related HYH factors were shown to form homo and heterodimers and promote light-induced expression of target genes (Holm et al., 2002). Formation of G-box-binding heteromers of HY5 with other bZIP factors was reported, suggesting that this transcription factor may cooperatively regulate transcription of ABA-induced target genes with other bZIP factors such as ABFs (Yoshida et al., 2010; Singh et al., 2012). Whether HY5 interacts with ABFs or other TFs on *P5CS1* and/or *PDH1* promoters remains to be elucidated.

The functionality of promoter binding by HY5 was tested by comparing transcript levels of the *P5CS1* and *PDH1* genes and proline accumulation in *hy5hyh* double mutant with those in wild-type plants under different light regimes (**Figures 5**, **S8**, **S9**). HY5 and HYH transcription factors are partially redundant, therefore the double knockout *hy5hyh* mutant was used in these studies. *P5CS1* transcript levels were lower in the salt-treated *hy5hyh* double mutant, suggesting that HY5 and perhaps the closely related HYH indeed contribute to high-level *P5CS1* induction in salt-stressed plants. Lower proline levels in salt-treated *hy5hyh* plants correlated with reduced transcript levels of *P5CS1*. Expression of *PDH1* was less influenced in the *hy5hyh* mutant, although minor differences could be detected during illumination with monochromatic light. These results confirm the positive role of HY5 in proline accumulation, which mediates light signals and modulates transcriptional activities of key metabolic genes. Complex formation of HY5 with the distal EMF region (Feng et al., 2016) and 5′ UTR sequences of *P5CS1* promoter was required for the retention of H3K4me3 levels and the maintenance of stress memory (Feng et al., 2016). HY5 seems to functions as a regulatory hub, which transmits light signals and connects them to stress and/or ABA signals and histone methylation and regulates the transcription of key metabolic genes by directly binding to conserved *cis* regulatory elements of their promoters (**Figure 6**).

In addition to photoreceptor-mediated signaling, light may modulate proline biosynthesis in other ways. Light can provide energy and reducing agents such as NADPH through photosynthesis, and light can modulate gene expression by specific signals, such as the redox state of the plastoquinone pool. The decline of proline levels in darkness could not be compensated by externally added sugars, suggesting that energy limitation is not a principal reason of light dependency (**Figures 1**, **S2**). Inhibition of photosynthetic electron transport with DCMU, however, reduced salt-dependent proline accumulation, *P5CS1* activation, and considerably promoted *PDH1* expression, demonstrating that photosynthesis itself can influence proline metabolism (**Figure S5**). Previously P5CS1-GFP was localized in chloroplasts in salt-treated cells, supporting the assumption that proline biosynthesis can be associated with photosynthesis in stress conditions (Székely et al., 2008; Szabados and Savoure, 2010; Sharma et al., 2011). Glutamate-derived proline biosynthesis is a reductive metabolic pathway, which could be stimulated by photosynthetic NADPH in osmotically stressed *Lotus corniculatus* leaves (Diaz et al., 2005). Alternatively, chloroplast to nucleus retrograde signaling could be implicated in light control of *P5CS1* and *PDH1* genes (Gollan et al., 2015; Kleine and Leister, 2016). Deciphering the exact mechanism how light and photosynthesis regulates proline metabolism, however needs further investigation.

# MATERIALS AND METHODS

## Plant Material and Growth Conditions

*Arabidopsis thaliana* plants were either Col-0 or WS ecotype. The *hy5hyh* double mutant (Holm et al., 2002) has WS background. Basic conditions of plant growth were described before (Aleksza et al., 2017). Briefly: seeds were surface sterilized and germinated on 1/2MS culture medium containing 0.5% (W/V) sucrose. Plants were grown *in vitro* in growth chambers under 120 μE $m^{-2}$ $s^{-1}$ illumination (white light) using a 8 h light/16 h dark cycle, and 22°C/18°C temperature cycle for 14 days.

For high-intensity light treatment 14-day-old plants were illuminated with white light with 550 μE $m^{-2}$ $s^{-1}$ light intensity in growth chambers. For dark conditioning, 14-day-old plantlets were transferred to dark, and incubated in the absence of light for up to 5 days in the same conditions (medium, temperature). For subsequent light induction, plants were transferred to either white light (fluorescent cool white, 4200 K, 60 μE $m^{-2}$ $s^{-1}$), or monochromatic blue (470 nm, 15 μE $m^{-2}$ $s^{-1}$), red (660 nm, 15 μE $m^{-2}$ $s^{-1}$), or far-red (730 nm, 5 μE $m^{-2}$ $s^{-1}$) light, or kept in dark for up to three further days. The primary criteria for setting the fluence rate of light was to reach saturation of signaling cascades triggered by phytochrome and cryptochrome photoreceptors. The most studied light responses are saturated at the light intensities described above (Wolf et al., 2011; Adam et al., 2013). Dark-conditioned plants (including those kept in constant darkness) were transferred and handled under green light.

To induce proline accumulation, plants were cultured on the surface of thin-layer liquid culture medium (10 ml medium/13 cm diameter Petri dish), using nylon mesh to prevent submergence. For stress, liquid media were supplemented with 150 mM NaCl or treated with 10 μM ABA. Proline levels were determined in plants for up to 3 days as described.

## Proline Measurements

Proline content was determined by the ninhydrin-based coloritmetric method as described (Abraham et al., 2010). Alternatively, a microtiter-scale colorimetric reaction was used, which was based on a recent paper (Lee et al., 2018) with some modifications. Plant material (approximately 50 mg fresh

weight/sample) was ground and 20 µl of 1% (W/V) sulfosalicylic acid was added per mg FW tissue. After centrifugation at top speed (15.000 rpm) for 5 min at 4°C in a microcentrifuge, the supernatant was removed and mixed with acidic ninhydrin [1,25% (W/V) ninhydrin in 80% (V/V) acetic acid] in 1:2 ratio, and incubated at 95°C for 30 min. The reaction was terminated on ice, and absorbance was measured at 510 nm in a plate reader (MULTISKAN GO, Thermo Scientific) using a 1:2 mixture of sulfosalicylic acid and acidic ninhydrin as reference. The system was calibrated with standard curves with known concentrations of proline. Anthocyanine accumulation was not visible in the plants after these treatments. Experiments were repeated three times and four to six replicates were used to determine proline levels in a treatment.

## Fast Chl A Fluorescence (OJIP) Measurements

Fluorescence measurements were carried out at room temperature with a Handy-PEA instrument (Hansatech Instruments Ltd, UK). Plants were dark-adapted for 30 min and detached leaves were then placed in a modified Handy-PEA leaf clip. The leaf sample was illuminated with continuous red light (3500 µE $m^{-2}$ $s^{-1}$, 650 nm peak wavelength; the spectral half-width was 22 nm; the light emitted by the LEDs is cut off at 700 nm by a NIR short-pass filter). The light was provided by an array of three light-emitting diodes focused on the sample surface. The first reliably measured point of the fluorescence transient is at 20 µs, which can be taken as $F_0$ (O). The length of the measurements was 1 s.

## DCMU Treatment

Fourteen-day-old *in vitro*-grown plants (Col-0 ecotype) were transferred to 150 mM NaCl and/or sprayed with 50 µM DCMU solution. OJIP fluorescence was measured 3 and 24 h after DCMU and salt treatments. Proline accumulation was measured 24, 48, and 72 h after DCMU treatment, whereas gene expression was measured after 24 h.

## Gene Expression Studies

To test transcript levels of selected genes, quantitative RT-PCR (qRT-PCR) was performed on cDNA templates obtained from total RNA samples. RNA isolation was performed with Nucleo Spin RNA isolation kit (Macherei-Nagel). Total RNA was DNase treated with TURBO DNA-free™ Kit (Invitrogen by Thermo Fisher Scientific). First-strand cDNA synthesis of 1.5 µg of total RNA was carried out with RevertAid M-MuLV Reverse Transcriptase (Fermentas), using random hexamers. Real-time PCR was carried out with the ABI 7900 Fast Real Time System (Applied Biosystems). The protocol in 45 cycles was 15 s at 95°C, followed by 1 min at 60°C. The specificity of the amplifications was verified using the ABI SDS software. Expression of the *P5CS1 (AT2G39800)* and *PDH1 (AT3G30775)* genes was monitored by qRT-PCR as described (Aleksza et al., 2017). Normalized transcript levels were calculated by the modified $2^{-\Delta\Delta Ct}$ method using averages of *actin2 (AT2G37620)* and *UBQ1* (*AT3G52590*) Ct values as reference (Livak and Schmittgen, 2001; Vandesompele et al., 2002). In relative expression data of the figures, reference was obtained on non-treated plants at the start of the experiment (*e.g.* dark-adapted plants, just before light and stress treatments). Statistical analysis was made on $2^{-\Delta\Delta Ct}$ values of three replicates corresponding to cDNA templates and RNA samples isolated from three different Petri plates. Experiments were repeated at least twice. Primers used in qRT-PCR experiments are listed in **Table S1**.

The average amplification efficiencies of each primer pair used in the qRT-PCR experiments were derived from the slope of the amplification curve in the exponential phase of three different reactions from three different samples. The corresponding PCR efficiency was calculated according to the formula: E = 10 (1/slope) (Svec et al., 2015). Each primer showed high amplification efficiency from 1.99 to 2.03. Sequences of the PCR primers are available in **Table S1**.

## Chip Followed by Quantitative PCR

The ChIP protocol by Werner Aufsatz (http://www.epigenome-noe.net/researchtools/protocol.php?protid=13) was applied with the following modifications. Fourteen-day-old *hy5* mutant plants expressing HY5-YFP fusion proteins from the *HY5* promoter (Hajdu et al., 2018) were fixed in 1% (V/V) formaldehyde solution. Chromatin samples were sonicated on ice six times for 10 s using a Vibra Cell sonicator (SONICS & MATERIALS Inc., Danbury, CT, USA) at 10% power. Sonicated and diluted chromatin samples were pre-cleared by 20 µl (bed volume) of binding control agarose beads (Chromotek GmbH, Germany) for 1 h at 4°C. An aliquot of the pre-cleared chromatin solution was saved for the input sample and the rest of the material was precipitated using 12.5 µl (bed volume) of GFP-Trap agarose beads (Chromotek GmbH, Germany) for 16 h at 4°C. Precipitated chromatin was eluted from the beads, and along with the input sample, it was de-crosslinked and DNA was extracted using the Silica Bead DNA Gel Extraction Kit (Thermo Scientific). The final volume of purified DNA samples was about 45 µl. 1.5 µl of the eluate was analyzed in qPCR reactions. Primers were designed to amplify genomic regions around the putative HY5 binding sites. Standard series were prepared from 10-fold dilutions of the input DNA samples. ChIP-related qPCR primers are listed in . ChIP data were analyzed and presented according to the "percent of input" method (Haring et al., 2007). Experiments were repeated three times.

## Electrophoretic Mobility Assay

The pET28a vector carrying the full-length HY5 cDNA fragment (Hajdu et al., 2018) was introduced into *Escherichia coli* BL21 DE3 Rosetta cells (New England 513 Biolabs). Proteins were purified on His-Select Nickel affinity gel (SIGMA). 2 µg of purified protein was incubated for 30 min with 2 pmol biotin-labeled DNA (respective P5CS1 and PDH1 oligonucleotide sequences are available in ). DNA fragments and complexes were separated in 4% (W/V) native polyacrylamide gel, then blotted to HyBond-$N^+$ nucleic acid transfer membrane (Amersham). DNA fragments were crosslinked to the membrane with UV light (UV Stratalinker,

Stratagene). DNA fragments were detected by an immune reaction with Streptavidin-conjugated horseradish-peroxidase (Thermo Scientific) using the LightShift Chemiluminescent EMSA Kit (Thermo Scientific). Signals were developed with a chemiluminescent substrate (Supersignal West-Thermo Scientific) and detected in Fusion FX western blot and *gel documentation* imaging device (Vilber). Experiments were repeated twice.

### Informatics, Statistical Analysis

Promoter sequence analysis was performed with AthaMap tool (http://www.athamap.de). Oligonucleotides were designed and analyzed by IDT OligoAnalyzer (https://eu.idtdna.com/calc/analyzer). Oligonucleotides used in this study are listed in Table S1.

Statistical analyses (one-way and two-way ANOVA, means comparisons by Tukey tests) were performed using the OriginPro 2018 software version 9.5 (OriginLab Corporation, Northampton, MA, USA). In case of one-way ANOVA the differences between means were determined Tukey test or by Duncan's multiple range test and labeled in all diagrams by different letters. When two-way ANOVA was used, the means comparison were made with Tukey test. Data were processed and in some experiments Diagrams were prepared with MS Excel 14.7.7, and figures were assembled with MS Powerpoint 14.7.7 and Adobe Photoshop CS5.1.

## AUTHOR CONTRIBUTIONS

HK, DA, AIB, AH, AK, LZ, and ST performed the experiments. LK-B evaluated the results and corrected the manuscript. LS directed the research and wrote the manuscript.

## FUNDING

This research was supported by NKFI Grants K128728, NN118089, and GINOP Project nos. 2.3.2-15-2016-00001 and 2.3.2-15-2016-00023. HK was supported by the Young Scientist Fellowship of the Hungarian Academy of Sciences.

## ACKNOWLEDGMENTS

The authors are indebted to Erzsébet Fejes for reading and correcting the manuscript.

## SUPPLEMENTARY MATERIAL

The Supplementary Material for this article can be found online at: https://www.frontiersin.org/articles/10.3389/fpls.2019.01584/full#supplementary-material

## REFERENCES

Abbas, N., Maurya, J. P., Senapati, D., Gangappa, S. N., and Chattopadhyay, S. (2014). Arabidopsis CAM7 and HY5 physically interact and directly bind to the HY5 promoter to regulate its expression and thereby promote photomorphogenesis. *Plant Cell* 26, 1036–1052. doi: 10.1105/tpc.113.122515

Abraham, E., Rigo, G., Szekely, G., Nagy, R., Koncz, C., and Szabados, L. (2003). Light-dependent induction of proline biosynthesis by abscisic acid and salt stress is inhibited by brassinosteroid in Arabidopsis. *Plant Mol. Biol.* 51, 363–372. doi: 10.1023/A:1022043000516

Abraham, E., Hourton-Cabassa, C., Erdei, L., and Szabados, L. (2010). Methods for determination of proline in plants. *Methods Mol. Biol.* 639, 317–331. doi: 10.1007/978-1-60761-702-0_20

Adam, E., Kircher, S., Liu, P., Merai, Z., Gonzalez-Schain, N., Horner, M., et al. (2013). Comparative functional analysis of full-length and N-terminal fragments of phytochrome C, D and E in red light-induced signaling. *New Phytol.* 200, 86–96. doi: 10.1111/nph.12364

Aleksza, D., Horvath, G. V., Sandor, G., and Szabados, L. (2017). Proline Accumulation Is Regulated by Transcription Factors Associated with Phosphate Starvation. *Plant Physiol.* 175, 555–567. doi: 10.1104/pp.17.00791

Ben Rejeb, K., Lefebvre-De Vos, D., Le Disquet, I., Leprince, A. S., Bordenave, M., Maldiney, R., et al. (2015). Hydrogen peroxide produced by NADPH oxidases increases proline accumulation during salt or mannitol stress in *Arabidopsis thaliana*. *New Phytol.* 208, 1138–1148. doi: 10.1111/nph.13550

Binkert, M., Kozma-Bognar, L., Terecskei, K., De Veylder, L., Nagy, F., and Ulm, R. (2014). UV-B-responsive association of the Arabidopsis bZIP transcription factor ELONGATED HYPOCOTYL5 with target genes, including its own promoter. *Plant Cell* 26, 4200–4213. doi: 10.1105/tpc.114.130716

Briggs, W. R., and Christie, J. M. (2002). Phototropins 1 and 2: versatile plant blue-light receptors. *Trends Plant Sci.* 7, 204–210. doi: 10.1016/S1360-1385(02)02245-8

Casal, J. J., Candia, A. N., and Sellaro, R. (2014). Light perception and signalling by phytochrome A. *J. Exp. Bot.* 65, 2835–2845. doi: 10.1093/jxb/ert379

Chattopadhyay, S., Ang, L. H., Puente, P., Deng, X. W., and Wei, N. (1998). Arabidopsis bZIP protein HY5 directly interacts with light-responsive promoters in mediating light control of gene expression. *Plant Cell* 10, 673–683. doi: 10.1105/tpc.10.5.673

Chaves, I., Pokorny, R., Byrdin, M., Hoang, N., Ritz, T., Brettel, K., et al. (2011). The cryptochromes: blue light photoreceptors in plants and animals. *Annu. Rev. Plant Biol.* 62, 335–364. doi: 10.1146/annurev-arplant-042110-103759

Chen, H., Zhang, J., Neff, M. M., Hong, S. W., Zhang, H., Deng, X. W., et al. (2008). Integration of light and abscisic acid signaling during seed germination and early seedling development. *Proc. Natl. Acad. Sci. U.S.A.* 105, 4495–4500. doi: 10.1073/pnas.0710778105

Cluis, C. P., Mouchel, C. F., and Hardtke, C. S. (2004). The Arabidopsis transcription factor HY5 integrates light and hormone signaling pathways. *Plant J.* 38, 332–347. doi: 10.1111/j.1365-313X.2004.02052.x

D'alessandro, S., Ksas, B., and Havaux, M. (2018). Decoding beta-Cyclocitral-Mediated Retrograde Signaling Reveals the Role of a Detoxification Response in Plant Tolerance to Photooxidative Stress. *Plant Cell* 30, 2495–2511. doi: 10.1105/tpc.18.00578

Delauney, A. J., and Verma, D. P. (1990). A soybean gene encoding delta 1-pyrroline-5-carboxylate reductase was isolated by functional complementation in Escherichia coli and is found to be osmoregulated. *Mol. Gen. Genet.* 221, 299–305. doi: 10.1007/BF00259392

Delauney, A. J., and Verma, D. P. S. (1993). Proline biosynthesis and osmoregulation in plants. *Plant J.* 4, 215–223. doi: 10.1046/j.1365-313X.1993.04020215.x

Diaz, P., Borsani, O., Marquez, A., and Monza, J. (2005). Osmotically induced proline accumulation in *Lotus corniculatus* leaves is affected by light and nitrogen source. *Plant Growth Regul.* 46, 223–232. doi: 10.1007/s10725-005-0860-7

Dietrich, K., Weltmeier, F., Ehlert, A., Weiste, C., Stahl, M., Harter, K., et al. (2011). Heterodimers of the Arabidopsis transcription factors bZIP1 and bZIP53 reprogram amino acid metabolism during low energy stress. *Plant Cell* 23, 381–395. doi: 10.1105/tpc.110.075390

Dubois, M., Claeys, H., Van Den Broeck, L., and Inze, D. (2017). Time of day determines Arabidopsis transcriptome and growth dynamics under mild drought. *Plant Cell Environ.* 40, 180–189. doi: 10.1111/pce.12809

Ehlert, A., Weltmeier, F., Wang, X., Mayer, C. S., Smeekens, S., Vicente-Carbajosa, J., et al. (2006). Two-hybrid protein-protein interaction analysis in Arabidopsis protoplasts: establishment of a heterodimerization map of group C and group S bZIP transcription factors. *Plant J.* 46, 890–900. doi: 10.1111/j.1365-313X.2006.02731.x

Fabro, G., Kovacs, I., Pavet, V., Szabados, L., and Alvarez, M. E. (2004). Proline accumulation and AtP5CS2 gene activation are induced by plant-pathogen

incompatible interactions in Arabidopsis. *Mol. Plant Microbe Interact.* 17, 343–350. doi: 10.1094/MPMI.2004.17.4.343

Feng, X. J., Li, J. R., Qi, S. L., Lin, Q. F., Jin, J. B., and Hua, X. J. (2016). Light affects salt stress-induced transcriptional memory of *P5CS1* in Arabidopsis. *Proc. Natl. Acad. Sci. U.S.A.* 113, E8335–E8343. doi: 10.1073/pnas.1610670114

Fernandez, A. P., and Strand, A. (2008). Retrograde signaling and plant stress: plastid signals initiate cellular stress responses. *Curr. Opin. Plant Biol.* 11, 509–513. doi: 10.1016/j.pbi.2008.06.002

Fey, V., Wagner, R., Brautigam, K., Wirtz, M., Hell, R., Dietzmann, A., et al. (2005). Retrograde plastid redox signals in the expression of nuclear genes for chloroplast proteins of *Arabidopsis thaliana*. *J. Biol. Chem.* 280, 5318–5328. doi: 10.1074/jbc.M406358200

Fichman, Y., Gerdes, S. Y., Kovacs, H., Szabados, L., Zilberstein, A., and Csonka, L. N. (2015). Evolution of proline biosynthesis: enzymology, bioinformatics, genetics, and transcriptional regulation. *Biol. Rev. Camb. Philos. Soc.* 90, 1065–1099. doi: 10.1111/brv.12146

Franklin, K. A., and Quail, P. H. (2010). Phytochrome functions in Arabidopsis development. *J. Exp. Bot.* 61, 11–24. doi: 10.1093/jxb/erp304

Fu, Y., Ma, H., Chen, S., Gu, T., and Gong, J. (2018). Control of proline accumulation under drought via a novel pathway comprising the histone methylase CAU1 and the transcription factor ANAC055. *J. Exp. Bot.* 69, 579–588. doi: 10.1093/jxb/erx419

Fujita, Y., Fujita, M., Satoh, R., Maruyama, K., Parvez, M. M., Seki, M., et al. (2005). AREB1 Is a transcription activator of novel ABRE-dependent ABA signaling that enhances drought stress tolerance in Arabidopsis. *Plant Cell* 17, 3470–3488. doi: 10.1105/tpc.105.035659

Gangappa, S. N., and Botto, J. F. (2016). The Multifaceted Roles of HY5 in Plant Growth and Development. *Mol. Plant* 9, 1353–1365. doi: 10.1016/j.molp.2016.07.002

Gollan, P. J., Tikkanen, M., and Aro, E. M. (2015). Photosynthetic light reactions: integral to chloroplast retrograde signalling. *Curr. Opin. Plant Biol.* 27, 180–191. doi: 10.1016/j.pbi.2015.07.006

Hajdu, A., Dobos, O., Domijan, M., Balint, B., Nagy, I., Nagy, F., et al. (2018). ELONGATED HYPOCOTYL 5 mediates blue light signalling to the Arabidopsis circadian clock. *Plant J.* 96, 1242–1254. doi: 10.1111/tpj.14106

Haring, M., Offermann, S., Danker, T., Horst, I., Peterhansel, C., and Stam, M. (2007). Chromatin immunoprecipitation: optimization, quantitative analysis and data normalization. *Plant Methods* 3, 11. doi: 10.1186/1746-4811-3-11

Hayashi, F., Ichino, T., Osanai, M., and Wada, K. (2000). Oscillation and regulation of proline content by P5CS and ProDH gene expressions in the light/dark cycles in *Arabidopsis thaliana* L. *Plant Cell Physiol.* 41, 1096–1101. doi: 10.1093/pcp/pcd036

Hildebrandt, T. M. (2018). Synthesis versus degradation: directions of amino acid metabolism during Arabidopsis abiotic stress response. *Plant Mol. Biol.* 98, 121–135. doi: 10.1007/s11103-018-0767-0

Hobo, T., Asada, M., Kowyama, Y., and Hattori, T. (1999). ACGT-containing abscisic acid response element (ABRE) and coupling element 3 (CE3) are functionally equivalent. *Plant J.* 19, 679–689. doi: 10.1046/j.1365-313x.1999.00565.x

Holm, M., Ma, L. G., Qu, L. J., and Deng, X. W. (2002). Two interacting bZIP proteins are direct targets of COP1-mediated control of light-dependent gene expression in Arabidopsis. *Genes Dev.* 16, 1247–1259. doi: 10.1101/gad.969702

Hu, C. A., Delauney, A. J., and Verma, D. P. (1992). A bifunctional enzyme (delta 1-pyrroline-5-carboxylate synthetase) catalyzes the first two steps in proline biosynthesis in plants. *Proc. Natl. Acad. Sci. U.S.A.* 89, 9354–9358. doi: 10.1073/pnas.89.19.9354

Izawa, T., Foster, R., and Chua, N. H. (1993). Plant bZIP protein DNA binding specificity. *J. Mol. Biol.* 230, 1131–1144. doi: 10.1006/jmbi.1993.1230

Jimenez-Arias, D., Borges, A. A., Luis, J. C., Valdes, F., Sandalio, L. M., and Perez, J. A. (2015). Priming effect of menadione sodium bisulphite against salinity stress in Arabidopsis involves epigenetic changes in genes controlling proline metabolism. *Environ. Exp. Bot.* 120, 23–30. doi: 10.1016/j.envexpbot.2015.07.003

Joseph, M. P., Papdi, C., Kozma-Bognar, L., Nagy, I., Lopez-Carbonell, M., Rigo, G., et al. (2014). The Arabidopsis ZINC FINGER PROTEIN3 Interferes with Abscisic Acid and Light Signaling in Seed Germination and Plant Development. *Plant Physiol.* 165, 1203–1220. doi: 10.1104/pp.113.234294

Kami, C., Lorrain, S., Hornitschek, P., and Fankhauser, C. (2010). Light-regulated plant growth and development. *Curr. Top. Dev. Biol.* 91, 29–66. doi: 10.1016/S0070-2153(10)91002-8

Kavi Kishor, P. B., and Sreenivasulu, N. (2014). Is proline accumulation per se correlated with stress tolerance or is proline homeostasis a more critical issue? *Plant Cell Environ.* 37, 300–311. doi: 10.1111/pce.12157

Kemble, A. R., and Macpherson, H. T. (1954). Liberation of amino acids in perennial ray grass during wilting. *Biochem. J.* 58, 46–59. doi: 10.1042/bj0580046

Kesari, R., Lasky, J. R., Villamor, J. G., Des Marais, D. L., Chen, Y. J., Liu, T. W., et al. (2012). Intron-mediated alternative splicing of Arabidopsis *P5CS1* and its association with natural variation in proline and climate adaptation. *Proc. Natl. Acad. Sci. U.S.A.* 109, 9197–9202. doi: 10.1073/pnas.1203433109

Kiyosue, T., Yoshiba, Y., Yamaguchi-Shinozaki, K., and Shinozaki, K. (1996). A nuclear gene encoding mitochondrial proline dehydrogenase, an enzyme involved in proline metabolism, is upregulated by proline but downregulated by dehydration in Arabidopsis. *Plant Cell* 8, 1323–1335. doi: 10.1105/tpc.8.8.1323

Kleine, T., and Leister, D. (2016). Retrograde signaling: Organelles go networking. *Biochim. Biophys. Acta* 1857, 1313–1325. doi: 10.1016/j.bbabio.2016.03.017

Lee, J., He, K., Stolc, V., Lee, H., Figueroa, P., Gao, Y., et al. (2007). Analysis of transcription factor HY5 genomic binding sites revealed its hierarchical role in light regulation of development. *Plant Cell* 19, 731–749. doi: 10.1105/tpc.106.047688

Lee, M. R., Kim, C. S., Park, T., Choi, Y. S., and Lee, K. H. (2018). Optimization of the ninhydrin reaction and development of a multiwell plate-based high-throughput proline detection assay. *Anal. Biochem.* 556, 57–62. doi: 10.1016/j.ab.2018.06.022

Lehmann, S., Funck, D., Szabados, L., and Rentsch, D. (2010). Proline metabolism and transport in plant development. *Amino Acids* 39, 949–962. doi: 10.1007/s00726-010-0525-3

Leivar, P., and Monte, E. (2014). PIFs: systems integrators in plant development. *Plant Cell* 26, 56–78. doi: 10.1105/tpc.113.120857

Li, J., Li, G., Gao, S., Martinez, C., He, G., Zhou, Z., et al. (2010). Arabidopsis transcription factor ELONGATED HYPOCOTYL5 plays a role in the feedback regulation of phytochrome A signaling. *Plant Cell* 22, 3634–3649. doi: 10.1105/tpc.110.075788

Livak, K. J., and Schmittgen, T. D. (2001). Analysis of relative gene expression data using real-time quantitative PCR and the 2(-Delta Delta C(T)) Method. *Methods* 25, 402–408. doi: 10.1006/meth.2001.1262

Muzammil, S., Shrestha, A., Dadshani, S., Pillen, K., Siddique, S., Leon, J., et al. (2018). An Ancestral Allele of Pyrroline-5-carboxylate synthase1 Promotes Proline Accumulation and Drought Adaptation in Cultivated Barley. *Plant Physiol.* 178, 771–782. doi: 10.1104/pp.18.00169

Parre, E., Ghars, M. A., Leprince, A. S., Thiery, L., Lefebvre, D., Bordenave, M., et al. (2007). Calcium signaling via phospholipase C is essential for proline accumulation upon ionic but not nonionic hyperosmotic stresses in Arabidopsis. *Plant Physiol.* 144, 503–512. doi: 10.1104/pp.106.095281

Pavlou, A., Jacques, J., Ahmadova, N., Mamedov, F., and Styring, S. (2018). The wavelength of the incident light determines the primary charge separation pathway in Photosystem II. *Sci. Rep.* 8, 2837. doi: 10.1038/s41598-018-21101-w

Per, T. S., Khan, N. A., Reddy, P. S., Masood, A., Hasanuzzaman, M., Khan, M. I. R., et al. (2017). Approaches in modulating proline metabolism in plants for salt and drought stress tolerance: Phytohormones, mineral nutrients and transgenics. *Plant Physiol. Biochem.* 115, 126–140. doi: 10.1016/j.plaphy.2017.03.018

Samach, A., Onouchi, H., Gold, S. E., Ditta, G. S., Schwarz-Sommer, Z., Yanofsky, M. F., et al. (2000). Distinct roles of CONSTANS target genes in reproductive development of Arabidopsis. *Science* 288, 1613–1616. doi: 10.1126/science.288.5471.1613

Satoh, R., Nakashima, K., Seki, M., Shinozaki, K., and Yamaguchi-Shinozaki, K. (2002). ACTCAT, a novel *cis*-acting element for proline- and hypoosmolarity-responsive expression of the ProDH gene encoding proline dehydrogenase in Arabidopsis. *Plant Physiol.* 130, 709–719. doi: 10.1104/pp.009993

Satoh, R., Fujita, Y., Nakashima, K., Shinozaki, K., and Yamaguchi-Shinozaki, K. (2004). A novel subgroup of bZIP proteins functions as transcriptional activators in hypoosmolarity-responsive expression of the ProDH gene in Arabidopsis. *Plant Cell Physiol.* 45, 309–317. doi: 10.1093/pcp/pch036

Savouré, A., Hua, X. J., Bertauche, N., Van Montagu, M., and Verbruggen, N. (1997). Abscisic acid-independent and abscisic acid-dependent regulation of proline biosynthesis following cold and osmotic stresses in *Arabidopsis thaliana*. *Mol. Gen. Genet.* 254, 104–109. doi: 10.1007/s004380050397

Schat, H., Sharma, S. S., and Vooijs, R. (1997). Heavy metal-induced accumulation of free proline in a metal-tolerant and a nontolerant ecotype of *Silene vulgaris*. *Physiol. Plant* 101, 477–482. doi: 10.1111/j.1399-3054.1997.tb01026.x

Servet, C., Ghelis, T., Richard, L., Zilberstein, A., and Savoure, A. (2012). Proline dehydrogenase: a key enzyme in controlling cellular homeostasis. *Front. Biosci. (Landmark Ed)* 17, 607–620. doi: 10.2741/3947

Sharma, S., and Verslues, P. E. (2010). Mechanisms independent of abscisic acid (ABA) or proline feedback have a predominant role in transcriptional regulation of proline metabolism during low water potential and stress recovery. *Plant Cell Environ.* 33, 1838–1851. doi: 10.1111/j.1365-3040.2010.02188.x

Sharma, S., Villamor, J. G., and Verslues, P. E. (2011). Essential role of tissue-specific proline synthesis and catabolism in growth and redox balance at low water potential. *Plant Physiol.* 157, 292–304. doi: 10.1104/pp.111.183210

Sheerin, D. J., Menon, C., Zur Oven-Krockhaus, S., Enderle, B., Zhu, L., Johnen, P., et al. (2015). Light-activated phytochrome A and B interact with members of the SPA family to promote photomorphogenesis in Arabidopsis by reorganizing the COP1/SPA complex. *Plant Cell* 27, 189–201. doi: 10.1105/tpc.114.134775

Singh, A., Ram, H., Abbas, N., and Chattopadhyay, S. (2012). Molecular interactions of GBF1 with HY5 and HYH proteins during light-mediated seedling development in *Arabidopsis thaliana*. *J. Biol. Chem.* 287, 25995–26009. doi: 10.1074/jbc.M111.333906

Strizhov, N., Abraham, E., Okresz, L., Blickling, S., Zilberstein, A., Schell, J., et al. (1997). Differential expression of two P5CS genes controlling proline accumulation during salt-stress requires ABA and is regulated by ABA1, ABI1 and AXR2 in Arabidopsis. *Plant J.* 12, 557–569. doi: 10.1046/j.1365-313X.1997.00537.x

Svec, D., Tichopad, A., Novosadova, V., Pfaffl, M. W., and Kubista, M. (2015). How good is a PCR efficiency estimate: Recommendations for precise and robust qPCR efficiency assessments. *Biomol. Detect. Quantif.* 3, 9–16. doi: 10.1016/j.bdq.2015.01.005

Szabados, L., and Savoure, A. (2010). Proline: a multifunctional amino acid. *Trends Plant Sci.* 15, 89–97. doi: 10.1016/j.tplants.2009.11.009

Székely, G., Ábrahám, E., Cséplö, A., Rigó, G., Zsigmond, L., Csiszár, J., et al. (2008). Duplicated P5CS genes of Arabidopsis play distinct roles in stress regulation and developmental control of proline biosynthesis. *Plant J.* 53, 11–28. doi: 10.1111/j.1365-313X.2007.03318.x

Thapper, A., Mamedov, F., Mokvist, F., Hammarstrom, L., and Styring, S. (2009). Defining the far-red limit of photosystem II in spinach. *Plant Cell* 21, 2391–2401. doi: 10.1105/tpc.108.064154

Thiery, L., Leprince, A. S., Lefebvre, D., Ghars, M. A., Debarbieux, E., and Savoure, A. (2004). Phospholipase D is a negative regulator of proline biosynthesis in *Arabidopsis thaliana*. *J. Biol. Chem.* 279, 14812–14818. doi: 10.1074/jbc.M308456200

Toledo-Ortiz, G., Johansson, H., Lee, K. P., Bou-Torrent, J., Stewart, K., Steel, G., et al. (2014). The HY5-PIF regulatory module coordinates light and temperature control of photosynthetic gene transcription. *PloS Genet.* 10, e1004416. doi: 10.1371/journal.pgen.1004416

Tóth, S. Z., Schansker, G., and Strasser, R. J. (2007). A non-invasive method for the determination of the redox state of the PQ-pool. *Photosynthesis Res.* 93, 193–203. doi: 10.1007/s11120-007-9179-8

Vandesompele, J., De Preter, K., Pattyn, F., Poppe, B., Van Roy, N., De Paepe, A., et al. (2002). Accurate normalization of real-time quantitative RT-PCR data by geometric averaging of multiple internal control genes. *Genome Biol.* 3, RESEARCH0034. doi: 10.1186/gb-2002-3-7-research0034

Verslues, P. E., and Sharma, S. (2010). Proline metabolism and its implications for plant-environment interaction. *Arabidopsis Book* 8, e0140. doi: 10.1199/tab.0140

Weltmeier, F., Ehlert, A., Mayer, C. S., Dietrich, K., Wang, X., Schutze, K., et al. (2006). Combinatorial control of Arabidopsis proline dehydrogenase transcription by specific heterodimerisation of bZIP transcription factors. *EMBO J.* 25, 3133–3143. doi: 10.1038/sj.emboj.7601206

Williams, M. E., Foster, R., and Chua, N. H. (1992). Sequences flanking the hexameric G-box core CACGTG affect the specificity of protein binding. *Plant Cell* 4, 485–496. doi: 10.1105/tpc.4.4.485

Wind, J. J., Peviani, A., Snel, B., Hanson, J., and Smeekens, S. C. (2012). ABI4: versatile activator and repressor. *Trends Plant Sci.* 18, 125–132. doi: 10.1016/j.tplants.2012.10.004

Wolf, I., Kircher, S., Fejes, E., Kozma-Bognar, L., Schafer, E., Nagy, F., et al. (2011). Light-regulated nuclear import and degradation of Arabidopsis phytochrome-A N-terminal fragments. *Plant Cell Physiol.* 52, 361–372. doi: 10.1093/pcp/pcq194

Yang, S. L., Lan, S. S., and Gong, M. (2009). Hydrogen peroxide-induced proline and metabolic pathway of its accumulation in maize seedlings. *J. Plant Physiol.* 166, 1694–1699. doi: 10.1016/j.jplph.2009.04.006

Yoshida, T., Fujita, Y., Sayama, H., Kidokoro, S., Maruyama, K., Mizoi, J., et al. (2010). AREB1, AREB2, and ABF3 are master transcription factors that cooperatively regulate ABRE-dependent ABA signaling involved in drought stress tolerance and require ABA for full activation. *Plant J.* 61, 672–685. doi: 10.1111/j.1365-313X.2009.04092.x

Zarattini, M., and Forlani, G. (2017). Toward Unveiling the Mechanisms for Transcriptional Regulation of Proline Biosynthesis in the Plant Cell Response to Biotic and Abiotic Stress Conditions. *Front. Plant Sci.* 8, 927. doi: 10.3389/fpls.2017.00927

Zhang, H., He, H., Wang, X., Wang, X., Yang, X., Li, L., et al. (2011). Genome-wide mapping of the HY5-mediated gene networks in Arabidopsis that involve both transcriptional and post-transcriptional regulation. *Plant J.* 65, 346–358. doi: 10.1111/j.1365-313X.2010.04426.x

**Conflict of Interest:** The authors declare that the research was conducted in the absence of any commercial or financial relationships that could be construed as a potential conflict of interest.

# Advantages of publishing in Frontiers

**OPEN ACCESS**
Articles are free to read for greatest visibility and readership

**FAST PUBLICATION**
Around 90 days from submission to decision

**HIGH QUALITY PEER-REVIEW**
Rigorous, collaborative, and constructive peer-review

**TRANSPARENT PEER-REVIEW**
Editors and reviewers acknowledged by name on published articles

**Frontiers**
Avenue du Tribunal-Fédéral 34
1005 Lausanne | Switzerland

**Visit us:** www.frontiersin.org
**Contact us:** info@frontiersin.org | +41 21 510 17 00

**REPRODUCIBILITY OF RESEARCH**
Support open data and methods to enhance research reproducibility

**DIGITAL PUBLISHING**
Articles designed for optimal readership across devices

**FOLLOW US**
@frontiersin

**IMPACT METRICS**
Advanced article metrics track visibility across digital media

**EXTENSIVE PROMOTION**
Marketing and promotion of impactful research

**LOOP RESEARCH NETWORK**
Our network increases your article's readership